MULTIDIMENSIONAL SEPARATIONS WITH ULTRAHIGH PRESSURE LIQUID CHROMATOGRAPHY – MASS SPECTROMETRY FOR THE PROTEOMICS ANALYSIS OF *SACCHAROMYCES CEREVISIAE*

Kaitlin Michelle Fague

A dissertation submitted to the faculty of the University of North Carolina at Chapel Hill in partial fulfillment of the requirements for the degree of Doctor of Philosophy in the Department of Chemistry.

Chapel Hill
2014

Approved by:

James W. Jorgenson

Gary L. Glish

R. Mark Wightman

Dorothy A. Erie

Bo Li

ABSTRACT

Kaitlin Michelle Fague: Multidimensional Separations with Ultrahigh Pressure Liquid Chromatography – Mass Spectrometry for the Proteomics Analysis of *Saccharomyces cerevisiae*
(Under the direction of James W. Jorgenson)

Many biological pathways are controlled by proteins. For proteomics analysis, the peak capacity of one-dimensional separations is routinely inadequate for the number of components in a sample. Advances in mass spectrometry (MS) and liquid chromatography (LC) have improved the limits of detection and sensitivity problems associated with co-elution. However, the pressure capabilities of the pump on a standard ultrahigh performance LC (UPLC) limit the dimensions of commercial columns resulting in a maximum peak capacity of 200 in 90 minutes. Various multidimensional strategies have been developed to further increase the peak capacity.

This dissertation will show the effects of 2DLC prefractionation method and frequency on proteome coverage. New ultrahigh pressure LC instrumentation with a constant pressure, high temperature approach for peptide separations is introduced. The system modified a standard UPLC with a pneumatic amplifier through a configuration of tubing and valves for separations up to 45000 psi. The modified UHPLC, coupled to a qTOF Premier, produced a peak capacity of 500 in 90 minutes on a meter-long microcapillary column packed with sub-2 micron particles. Peak capacity plateaued above 800 in 12 hours. The improved prefractionation methodology and modified UHPLC were coupled for the separation of a model proteome, *S. cerevisiae*. The number of protein identifications and coverage improved two-fold as compared to an analogous separation on the standard UPLC with a commercial column.

ACKNOWLEDGEMENTS

"The most incomprehensible thing about the world is that it is comprehensible."

-Einstein

Paramount in its incomprehensibility is the amount of love that I've received to reach this milestone in my life. Not by luck or anything of my own doing, it is the generosity of my family and friends that made finishing this experiment in human resilience even possible. First, I would like to thank my parents and my favorite brother for their encouragement. Constantly introducing me to new experiences, my parents taught me that there is more to this world than what we see around us. You encouraged me to venture out on my own. With your support, I knew I was never truly alone.

To my ever growing family, I thank you all. I come from a long line of hard workers: My great grandfather travelled to work in intercity Baltimore; my great grandmother canned her own vegetables to save money; my nanny worked at the A&P; and my pappy loaded trucks at Westinghouse and Schindler. Their sacrifices and savings have afforded me the opportunity to pursue my academic aspirations. Their lessons in steadfastness helped me achieve my goals.

These acknowledgements would be incomplete without mentioning the original Doc Fague (aka JW aka Grandpa) and my wonderful grandma. You have taught me the value of education. I am honored to earn the title of doctor but will never live up to the original. Cheers!

There are no words worthy of describing my advisor, James W. Jorgenson, and the amount of support he has given me. I am constantly in awe of your genius. It has been a pleasure to have you as a mentor. Thank you for your brood of graduate students that have helped me

along the way, especially: Laura, Ed, Jordan, Brian, Treadway, Stephanie, Justin and Dan. Thank you, JJ, for strongly encouraging us to do the things we do not always want to do. Especially, thank you for demanding that the brightest star of all, Jim Grinias, dance with me. JJ, I can now leave Carolina with my priceless gem, receive all praises thine.

My many years of scientific education would have meant nothing if it wasn't for the great teachers I had in the Shippensburg School District, the Carnegie Mellon University, and the University of North Carolina. Also, thank you to my mentors at GlaxoSmithKline for the practical analytical chemistry training and for pulling me when I was struggling. Thank you to my fellow classmates and coworkers. Your pursuit of excellence made me strive for more.

The business of science could not be completed without my helpful collaborators. This work has been supported by the Water Corporation. I'd like to thank Theodore Dourdeville for building the freeze/thaw valve, and Derek Wolfe for designing the switch control circuit mentioned in Chapter 3. Another thank you goes to Keith Fadgen and Martin Gilar for useful conversations regarding this work. An analytical chemist is nothing without her working instrument so thank you to our service engineer, Jim Lekander.

I will conclude with a refrain from one of my favorite musicals, Bob Fosse's Chicago. Hopefully, the reader will be singing along after finishing this manuscript:

"Understandable, understandable

Yes it's perfectly understandable

Comprehensible, Comprehensible

Not a bit reprehensible"

It's so defensible."

TABLE OF CONTENTS

LIST OF TABLES

LIST OF FIGURES

LIST OF APPENDED FIGURES

LIST OF ABBREVIATIONS AND SYMBOLS

%A	percent mobile phase A
%B	percent mobile phase B
∫TIC	integrated total ion current
°C	degrees Celsius
2D	two dimensional
2DLC	two-dimensional liquid chromatography
2D-PAGE	two-dimensional polyacrylamide gel electrophoresis
A	absorbance
Å	angstrom
ACN	acetonitrile
ACS	American chemical society
BEH	bridged ethyl hybrid
BPI	base peak intensity
BSA	bovine serum albumin
cm	centimeter
d_c	column diameter
D_m	diffusion in the mobile phase
ESI	electrospray ionization
F	flow rate
FTICR	Fourier transform ion cyclotron resonance
g	gram
H_2O	water

H_{cm}	height equivalent of a theoretical plate (resistance to mass transfer in the mobile phase)
ID	internal diameter
IDs	identifications
IEX	ion-exchange chromatography
IPA	2-propanol
iTRAQ	isobaric-tag-for-relative-and-absolute-quantification
kDa	kiloDalton
kpsi	kilo pounds per square inch
kV	kilovolts
L	liter
L	length
LC	liquid chromatography
LIFO	last in first out
M	molar
m	meter
m/z	mass to charge ratio
MALDI	matrix assisted laser desorption ionization
mg	milligram
min	minute
mL	milliliter
mM	millimolar
mm	millimeter
MRM	multiple reaction monitoring

MS	mass spectrometry
MS^E	mass spectrometry expression
N	number of theoretical plates
n_c	peak capacity
NDPC	normalized difference protein coverage
ng	nanogram
nL	nanoliter
nm	nanometer
n_p	practical peak capacity
O.D.	optical density
pI	isoelectric point
PLGS	ProteinLynx Global Server
PLRP-S	polystyrene-divinylbenzene reversed-phase HPLC column
P_{max}	maximum peak capacity
pmol	picomole
PPP	pentose phosphate pathway
psi	pounds per square inch
qTOF	quadrapole time-of-flight
Rep	replicate
RPLC	reversed-phase liquid chromatography
SEC	size exclusion chromatography
sec	second
SF	surfactant

SILAC	stable-isotope-labeling-by-amino-acids-in-cell-culture
t	time
TCA	the citric acid cycle
TCPK	tosyl phenylalanyl chloromethyl ketone, chymotrypsin inhibitor
t_d	dead time
TFA	trifluoroacetic acid
t_g	gradient time
TIC	total ion current
t_m	mobile phase time
u	linear velocity
UHPLC	ultrahigh pressure liquid chromatography
UPLC	ultrahigh performance liquid chromatography
UV	ultraviolet
V	volts
V	volume
v/v	volume per volume
v:v:v	volume to volume to volume ratio
Vis	visible
w/w	weight per weight
Xg	times gravity
YAPG	yeast agar peptone glycerol
µg	microgram
µL	microliter

μm	micrometer
Σ∫TIC	summed integrated total ion current
ΣA	summed absorbance

CHAPTER 1. An Introduction to Differential Proteomics by Multidimensional Liquid Chromatography-Mass Spectrometry

1.1 Introduction

Protein regulation has long been studied to better understand biological processes.[1] Analyses of proteins are complicated because there are thousands of proteins in a cell spanning a large range of abundances (upwards of 10^{10}).[2] A common approach to study protein regulation is by differential proteomics using multidimensional chromatography to separate the complex mixture followed by detection with mass spectrometry (MS).[3,4] In this introductory chapter, the need for studying differential protein regulation by multidimensional chromatography-MS will be explained.[5] Several accomplishments made in this field will be reviewed. Building on the ideas discussed in this introduction, the aim of this dissertation will be to improve the coverage of a model proteome, *Saccharomyces cerevisiae*, through the development of separation methods and instrumentation.

1.2 Why study proteomics?

For many years, scientists have been trying to understand why certain phenotypes are observed in nature.[6,7,8] For example, why do certain populations of people develop diabetes or heart disease while others do not? Some causes are environmental, such as diet and exercise, but other causes are inherently biological.[9,10] The central dogma (Figure 1.1) is described as the flow of genetic information through the biological system.[11] As the central dogma progresses from DNA, to RNA, to proteins, and finally metabolites, the complexity increases in both number of molecules and variety.[12] DNA and RNA are made of four nucleotides,[13] proteins are made from

20 endogenous amino acids,[11] and metabolites can be a variety of small molecules including carbohydrates, lipids, etc.[14] As complexity of the biological sample increases, the burden on the analytical method to study these molecules also increases.[15,16,17]

Scientists believed that unlocking the genomic code would demystify the existence of certain phenotypes.[18] In the 1990s, the United States government funded the completion of the human genome.[19,20] However, scientists soon learned that not all of the genome is transcribed into RNA,[21] and not all RNA is translated into proteins. Proteins control cellular pathways, and the metabolites, involved in these pathways actually, account for the phenotype. After translation, the protein can be further modified with functional groups such as acetate, phosphate, lipids and carbohydrates. These post-translational modifications (PTMs) extend the function of the protein.[11] For the regulatory role that proteins play in biological pathways, the field of proteomics emerged.[22, 23,24]

1.2.1 Differential proteomics

Consider two cell types, with different genetic variants or observed phenotypes. Determining which proteins are up and down regulated between the two samples can shed light onto what biological pathways are active. This study of relative protein abundance became known as differential proteomics.[5,25] For example, Figure 1.2. shows a portion of the regulatory pathways involved in *S. cerevisiae* (yeast) metabolism.[26] Proteins in red were up-regulated in yeast grown on glycerol, and proteins in blue were up-regulated in yeast grown on dextrose. From this differential study, it is evident that the citric acid (TCA) and glyoxylate cycles are more active when metabolizing glycerol, and fermentation is preferred for dextrose metabolism. Figure 1.2. also shows how many molecules are involved in just a simple biological pathway. In a simple proteome, such a yeast, there are thousands of proteins to identify spanning a large

range of expression levels.[27] To tackle these experimental challenges, a need arises to have better resolution, a large dynamic range and global yet specific detection.[28]

1.2.2 Differential proteomic tools

Many tools and methods have been developed to study differential proteomics.[28] This chapter aims to highlight some common practices and fundamentally ground breaking techniques. A generic workflow is outlined in Figure 1.3. The experiment starts with a cell lysate. The analyte either contains intact proteins or peptides from the digested proteins. The sample is separated, commonly by liquid chromatography (LC), because it has a large loading capacity and high resolution.[4] Loading capacity is necessary because analysis of a large amount of total protein may be required to detect a single analyte of low abundance. LC is also easily coupled to a mass spectrometer. Through electrospray, the ionization of peptides and proteins is possible making MS the near global detector for proteomics. Specificity of the MS, based on mass-to-charge, adds another level of separation.[4] The fragmentation data, from MS/MS experiments, are useful in identifying the protein.[29,30] The spectral data is compared to a genomic database, using complex computer algorithms, to identify peptides and proteins.[31,32] The relative abundance, usually in terms of a ratio of spectral counts, is calculated to give the fold change in expression of a protein in two differential proteomic samples.[33]

To help with the quantitative analysis of mass spectral data, several common strategies can be executed such as isobaric-tag-for-relative-and-absolute-quantification (iTRAQ), stable-isotope-labeling-by-amino-acids-in-cell-culture (SILAC), and label-free.[25,34] iTRAQ allows for absolute quantification by adding an isobaric label to the N-terminus and amine side chains of peptides. It is used for protein digests of samples collected from biological specimens.[35,36] SILAC requires growth of the cells on normal medium for one sample and on an isotopically

enriched medium for the other sample. Commonly, arginine labeled with ^{12}C and ^{13}C atoms are used for the normal and enriched media, respectively.[37,38] Both iTRAQ and SILAC label the sample, which greatly reduces analysis time, because differential samples can be pooled prior to the separation. The spectral data for each sample is deconvoluted by the mass shift due to the label. Analyzing both samples simultaneously reduces the day-to-day variability that can occur from temperature changes in the laboratory. The major advantages of label-free relative quantification are lower cost and a reduced risk of modifying the sample in the labeling process. Also, the spectra are not busy with isobaric and isotopic data. The validity of quantification based on spectral counts with the label-free method has been demonstrated in the literature.[39,40,41]

1.3 Choice of strategy: top-down versus bottom-up

1.3.1 Sample preparation and separation

The first step in analyzing proteomics samples is to decide between a top-down (protein) or bottom-up (peptide) strategy.[30] Typical work flows with considerations for each step are shown in Figure 1.4. The top-down experiment begins with the separation of intact proteins. A single protein may exist in many different isoforms and have different post-translational modifications which would contribute to band broadening.[42] Maintaining the solubility of proteins outside of the cell is difficult.[43] Low solubility has limited the development of new technology for the separation of intact proteins.[44] For this reason, many scientists prefer to do a bottom-up experiment in which the proteins are enzymatically digested, into peptides prior to analysis.[39] Trypsin, the most commonly used digest enzyme, cleaves proteins on the C-terminal side of arginine and lysine residues creating peptides about 20 amino acids in length.[45] Proteins come in a variety of masses but an average protein sequence would have around 400 amino acids, and roughly 20 predicted peptides.[46] The sample is now soluble but more complex.

1.3.2 Mass spectral detection

After the separation, the analytes are introduced into the mass spectrometer. Mass spectrometry of large biological molecules remained elusive until the invention of matrix assisted laser desorption ionization (MALDI) and electrospray ionization (ESI). For MALDI, the matrix is ablated with a laser initiating desorption and ionization of the analyte. The resulting spectrum, obtained with a time-of-flight (TOF) mass analyzer, contains predominantly singly charged ions with large peak widths contributing to low resolution ($R=\frac{m}{\Delta m}$, typically 300-400 for proteins).[47,48] ESI has become the preferred source due to its easy coupling with LC where a high voltage electric field is applied to a narrow capillary. The liquid becomes a fine aerosol, and ions are completely desolvated before entering the MS.[49] The spectrum, from an ESI-TOF-MS, contains multiply charged ions and has a higher resolution than MALDI (R=50000).[50] With the ability to analyze peptides and proteins by MS, the sample components don't have to be completely separated by LC because the MS can detect many species in a single scan. Furthermore, the development of gas phase ion mobility adds the option of a post-ionization separation without adding to the total analysis time.[51] However, ionization suppression and matrix effects still plague mass spectrometric techniques, necessitating separation prior to analysis.[52,53]

The ESI spectral data from top-down experiments are complex due to the many charge states of intact proteins.[54] Example spectra, drawn on the same intensity scale, are shown in Figure 1.5. Myoglobin and bovine serum albumin (BSA) were infused in similar amounts. Bovine serum albumin (a) is 66 kDa and much larger than 17 kDa myoglobin (b). The BSA molecules are distributed over more charge states than myoglobin making it less intense and

more difficult to detect. In contrast, the spectra are less convoluted for a bottom-up experiment because peptides are generally only detected in the +2 charge state.[51]

In the MS, it is useful to fragment the parent ion into a series of y- and b- product ions to identify the protein, as was pioneered by the McLafferty group.[29] Due to the size of the analyte, the fragmentation efficiency is not as great for proteins as it is for peptides.[55] For top-down experiments, higher energy fragmentation, such as collision-induced dissociation (CID) is popular. For bottom-up experiments, electron-capture dissociation (ECD) or electron-transfer dissociation (ETD) can provide a more complete fragmentation of the peptide backbone and tend to retain labile post-translational modifications (PTMs).[56] High resolution instruments, such as orbitraps and FTICR, are required for many top-down experiments.[57,58] Until recently, the acquisition of these mass spectrometers was cost prohibited in many laboratories making the time of flights instruments, used in bottom-up experiments, more common.[59]

1.3.3 Processing proteomics data

Finally, the spectral data is processed on a high-performance computer to identify the proteins. For top-down experiments, the native mass, as it existed in the cell, is deconvoluted from the parent ion scan.[60] For bottom-up experiments, the protein mass is calculated from the amino acid sequence listed in a genomic database. [31,32,61] An inference problem occurs with the rebuilding of a protein from the fragmentation data.[62] The same peptide sequence may exist in two different proteins, and it is difficult to determine to which protein the peptide should be assigned. This is particularly troublesome when the peptide has a PTM. The assignment of a PTM to a particular protein can be unclear. The inference problem is greater for bottom-up experiments because peptides from a single protein are spread throughout the entire

chromatogram. For a top-down experiment, the protein is fragmented in the MS so all data pertaining to that protein is contained in a single spectrum.[58]

Even with these challenges in data processing, the bottom-up approach is a more common practice largely due to the greater solubility of protein digests.[63] It is reported that more proteins are identified in bottom-up experiments than top-down experiments. For example, the Coon Lab recently reported the identification of 3,977 yeast proteins in a one hour bottom-up analysis.[41] Larger mass proteins are also identified by bottom-up methods. Based on the amount of data garnered, a bottom-up approach may be a better option with today's technology. However, some scientists argue that a top-down experiment gives a clearer picture of proteins as they exist in the cell. Improvements to separation science and mass spectrometry are necessary to make the top-down approach a more common laboratory practice.[58]

1.4 Peak capacity

1.4.1 Theory

Due to the complexity of proteomics samples, separation of the components is necessary before identification and quantification of individual proteins. A common way to describe the quality of a separation is through peak capacity (n_c), which is the number of peaks that can be resolved in a defined separation window.[64,65] Throughout this dissertation, the peak width refers to the width at 4σ. The separation time refers to gradient time (t_g) or the time between the first and last eluting peak. The formula for peak capacity is as follows:

$$n_c = \frac{\text{Gradient Time } (t_g)}{\text{Peak Width } (4\sigma)} + 1 \qquad (1\text{-}1)$$

The 4σ peak width refers to the width of the peak at about 11% of the maximum peak height. If two adjacent peaks, with retention times t_{r1} and t_{r2}, overlap at 11% of the maximum height, they have a resolution of 1.[66] A formula for resolution (R_s) is shown below:

$$R_s = \frac{t_{r2}-t_{r1}}{2(\sigma_1+\sigma_2)} \quad (1\text{-}2)$$

Now, let *t* be the point of overlap. If the full peak width is 4σ at the point of overlap, the mean-retention-time (t_r) for each peak is shifted from *t* by 2σ i.e. half the peak width. A diagram of this relationship can be found in Figure 1.6. The derivation proving unity resolution is as follows:

$$t_{r,1} = t-2\sigma \quad (1\text{-}3)$$

$$t_{r,2} = t+2\sigma \quad (1\text{-}4)$$

$$R_s = \frac{(t+2\sigma)-(t-2\sigma)}{2(\sigma_1+\sigma_2)} = \frac{4\sigma}{2(\sigma_1+\sigma_2)} \quad (1\text{-}5)$$

Assuming $\sigma_1 = \sigma_2$, (1-6)

$$R_s = \frac{4\sigma}{4\sigma} = 1 \quad (1\text{-}7)$$

An example separation of a standard enolase protein digest is shown in Figure 1.7. This separation had a peak capacity of 100 which is typical for a 30 minute gradient on a standard UPLC with a commercial column. A peak capacity of 100 is sufficient for the separation of peptides from the digest of a single protein.

1.4.2 The coelution problem

Now, consider the same separation method for a bottom-up proteomics sample, such as the *Escherichia coli* digest, in Figure 1.8. As evident from the many overlapping peaks, a larger peak capacity than 100 is necessary. Davis and Giddings[67] derived a formula relating the peak capacity to the percentage of resolved peaks (α):

$$\alpha = -\frac{1}{2}\ln\left(\frac{s}{\bar{m}}\right) \quad (1\text{-}8)$$

where $\bar{m}$ is the number of detectable components in a sample, s is the number of component peaks separated with a resolution of one or greater, and α is the saturation factor which is $\bar{m}$ divided by n_c.

To apply this relationship to the *E. coli* digest, the number of detectable components is related to the 4,000 proteins encoded in its genomic sequence.[68] While it is true that not every protein encoded in the genome is expressed, *E. coli* is a simple organism so 4,000 proteins is a conservative value. For example, *Homo sapiens* (human) has more than 20,000 genes that encode proteins, and *Mus musculus* (laboratory mouse) has 30,000 protein encoding genes.[69] For a bottom-up experiment, the proteins would be digested by trypsin into peptides. As mentioned earlier, the number of digestion sites and peptides varies from protein to protein.[46] To make a very conservative generalization, the number will be estimated at 10 digest peptides per protein. Therefore, the number of detectable components in a bottom-up sample of *E. coli* would be 40,000 peptides. Also, assume that the analyst wants 90% of the peaks to have a resolution of one, i.e.:

$$\frac{s}{\bar{m}} = 0.9 \tag{1-9}$$

To calculate the peak capacity necessary for a bottom-up separation of *E. coli*, these values are plugged into Equation 1-8.

$$\alpha = \frac{\bar{m}}{n_c} = \frac{40000}{n_c} \tag{1-10}$$

$$\alpha = -\frac{1}{2}\ln(0.9) \tag{1-11}$$

$$\frac{40000}{n_c} = -\frac{1}{2}\ln(0.9) \tag{1-12}$$

$$n_c = 760{,}000 \tag{1-13}$$

There is no single separation that exists with the peak capacity necessary to separate 90% of the components in an *E. coli* proteome digest with the resolution of one.

1.4.3 Advent of Ultrahigh Pressure Liquid Chromatography

A major improvement to the separation of proteomic samples has been the invention of the UHPLC by the Jorgenson group.[70] At the time of publishing, the Jorgenson lab reported a peak capacity of 300 in 30 minutes which more than doubled the peak capacity achieved with a HPLC.[71] This technology was commercialized (as UPLC) 10 years ago and has become a common instrument in proteomics laboratories. UHPLC enabled the use of microcapillary columns with sub-2 micron particles which have greater peak capacity than standard bore columns. Other labs have since reported higher peak capacities through the use of longer columns.[72,73] Chapter 3 of this dissertation has a more in-depth discussion on the benefits of long microcapillary columns and details a modified UHPLC that produces peak capacities greater than those previously reported in the literature.

1.5 Multidimensional separations

Even with the highest performing UHPLC, the peak capacity is still not sufficient for proteomics samples.[74] A solution for providing more peak capacity has been multidimensional separations. Giddings wrote that the peak capacity of a two-dimensional separation is the product of the two individual peak capacities:

$$n_{c,total} = n_{c,1} \times n_{c,2} \quad (1\text{-}14)$$

if (1) the separations are orthogonal and (2) resolution is not lost in coupling the separations.[64]

1.5.1 2D-PAGE

Traditionally, 2D separations of intact proteins were completed in space via polyacrylamide gel electrophoresis (2D-PAGE).[75,76] In this technique, the sample is first separated by isoelectric point (pI) and then by molecular weight. The spots are then excised, digested, and analyzed by MALDI-MS. Both of Giddings' rules are preserved and thousands of proteins can be separated by this technique, but several limitations exist. (1) Hydrophobic proteins may not enter the gel. (2) It is labor intensive to excise and digest spots. (3) Resolution is not as great for proteins with acidic or basic pI as it is for proteins with intermediate pI. (4) Proteins of low abundance are not easily detected with most staining techniques.[77,78]

The limitations with 2D-PAGE have led to the development of 2D separations in time via liquid chromatography (2DLC). Going back to Giddings' second rule for 2D separations, the multiplicative peak capacity is only achieved if the resolution is preserved from the first to second dimension.[79] For resolution to be preserved, the second dimension would have to be faster than practically possible in LC, or the first dimension would have to be extremely slowed down. Therefore, fractionation of the first dimension is often necessary when coupling two columns. The peak capacity of the first dimension then becomes the number of fractions. In order to reduce the loss of peak capacity caused by fractionation, the second dimension should have the greater peak capacity of the two separations.[80,81]

1.5.2 MudPIT

A common 2DLC method developed by Yates and colleagues is called multidimensional protein identification in time (MudPIT). This method utilizes a biphasic column in which the stationary phase for each dimension is packed sequentially into a single column. A step gradient associated with the first dimension separation mode is run through the column. Between each

step, a linear gradient associated with the second dimension separation mode is run. The column effluent is sent to the MS/MS for detection. Usually, the first mode of separation is strong cation exchange followed by a second dimension reversed-phase separation.[82,83] This method was developed for protein digests from cell lysates.

1.5.3 Top-down proteomics

The multidimensional separation of intact proteins has occurred online and offline. Figure 1.9.a. shows the instrument schematic for an online approach. There are two identical columns (A and B) in the second dimension. The effluent from the first separation is loaded onto the head of column A. Using two 4-port valves, the effluent is then switched to column B, and a gradient is pumped through column A to complete the second-dimension separation. This cycle continues until the desired number of fractions from the first dimension is obtained.[84] Alternatively, this can be completed with one second-dimension column using two storage loops between the dimensions as shown in Figure 1.9.b.[80,85]

More recent work, associated with the Human Genome Project, focused on an offline separation of intact proteins by three modes before analysis by ESI-FTICR-MS. The first two separations were similar to 2D-PAGE because they involved electrophoretic separations by size and isoelectric focusing. This modern technique used Gel-Eluted Liquid Fraction Entrapment Electrophoresis (GELFrEE). The proteins are separated on a gel cartridge, migrated off the gel, and fractionated into a gel-free sample-well. The fraction is isolated in-solution which is easier than the manual excision required by its slab-gel ancestor. The third mode of separation was reversed-phase LC. The multidimensional separation took more than 45 hours and identified 1,043 gene products from human cells.[55,58]

1.5.4 Practical peak capacity of 2DLC

In reality, Giddings' rules, for two dimensional peak capacities, are never fully met. The practical peak capacity is calculated by modifying Giddings' rule with factors that describe the lack of orthogonality and loss of resolution in the coupling of two separations.[86,87] To demonstrate the practical peak capacity of a real separation, consider the top-down 2D chromatogram in Figure 1.10. of *S. cerevisiae*.[88] The sample was separated on a strong anion-exchange column in the first dimension and reversed-phase column in the second dimension. Resolution is lost in the coupling of the two dimensions. Due to online fractionation, the peak capacity of the first dimension is reduced to 30. Also, the 2D space is not completely utilized. The top left of the chromatographic space contains few peaks. This chromatogram also demonstrates the difficulty of separating intact proteins. The peaks are several minutes wide and "ghost" as evident from the feature that appears at 17 minutes in fractions 12-25. "Ghosting" describes an analyte that partially remains on the column after the separation method is complete. The analyte slowly bleeds off the column creating "ghost" peaks in subsequent chromatograms. In practice, only a portion of the multiplicative peak capacity, described by Giddings, is realized.

Now, consider the practical peak capacity of the bottom-up 2D chromatogram in Figure 1.11. of *S. cerevisiae*.[88] A step gradient is implemented for the first dimension separation. There are five steps dictating the peak capacity of the first dimension. A reversed-phase column is used in both dimensions. The separation attempts to be orthogonal by modifying the sample with high-pH mobile phase in the first dimension and low-pH mobile phase in the second dimension. Stapels and Fadgen have demonstrated that this technique has some orthogonal attributes.[89] However, the orthogonality leaves a lot to be desired, as evident by the chromatograms in Figure

1.11. There are few late eluting peaks in the first fraction (red) and few early eluting peaks in the last fraction (pink).

1.5.5 Prefractionation

Another offline multidimensional separation has been growing in popularity. This prefractionation method takes advantage of both top-down and bottom-up experiments.[90,91] The first dimension is an intact protein separation. Fractions of the effluent are collected, enzymatically digested, and analyzed by reversed-phase UPLC-MS/MS. By changing the sample from protein to peptide via digestion between the two dimensions, the separations are orthogonal even if the same separation mode is used in both dimensions. The prefractionation separations are more orthogonal than the example top-down and bottom-up 2D chromatograms in Figure 1.10 and Figure 1.11. To see example prefractionation chromatograms, refer to Figure 2.7. in Chapter 2.

1.6 Scope of dissertation

The scope of this dissertation is to improve the separation of proteomic samples through the development of new liquid chromatography methods and instrumentation. Chapter 2 has a deeper discussion on the benefits of the protein prefractionation method. It studies how different prefractionation techniques and frequencies affect the number of protein identifications. Chapter 3 and 4 demonstrate the peak capacity gained by modifying a UHPLC for separations at elevated temperatures and pressures. The modified UHPLC is used to improve the productivity (protein identifications / time) of a prefractionation experiment in Chapter 5. The final chapter applies the methods developed in the previous chapters to conduct a differential analysis of *S. cerevisiae* grown on two different carbon sources. The benefits of these studies are demonstrated by the improved proteome coverage as compared to previous analyses.

The ideas presented in this dissertation can be used, in the future, to analyze other complex biological samples. As more is discovered about the transmission of biological information through the central dogma, an interest is metabolomics has grown.[92] The instrumentation described in this dissertation has the potential for metabolomic applications. In reality, a panomics approach, covering genomics, transcriptomics, proteomics, and metabolomics, will likely be necessary to fully understand the regulation of biological pathways.[93]

1.7 FIGURES

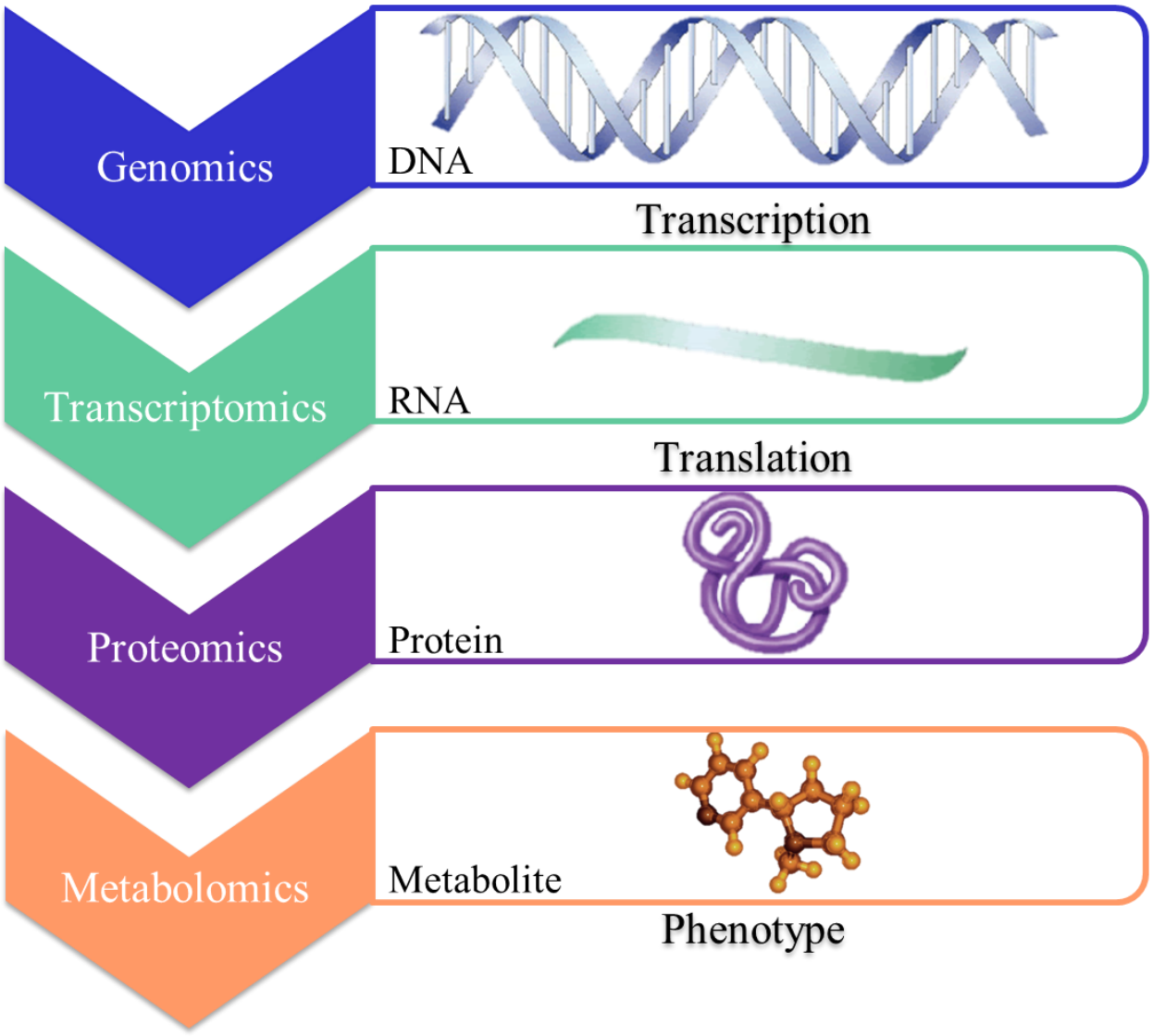

Figure 1.1. The explanation for the flow of genetic information through the biological system is referred to as the central dogma. DNA is transcribed into RNA which is translated into proteins. The proteins regulate metabolites which result in the observed phenotype.

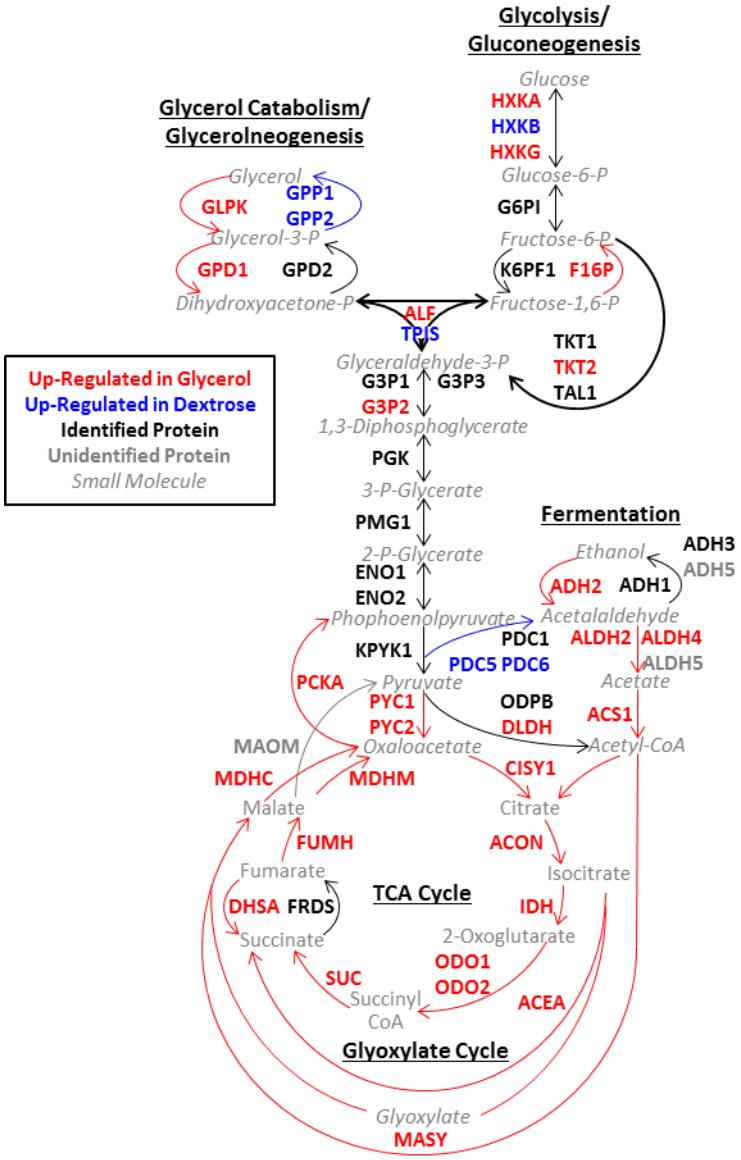

Figure 1.2. A small portion of the regulatory pathways involved in *S. cerevisiae* metabolism is shown. Proteins in red were up-regulated in yeast grown on glycerol, and proteins in blue were up-regulated in yeast grown on dextrose. Small molecules involved in the pathway are in italics. For this differential study, it is evident that glycerol catabolism, TCA, glyoxylate cycles are more active for metabolizing glycerol while fermentation and glycerolneogenesis occurs in dextrose metabolism.[26]

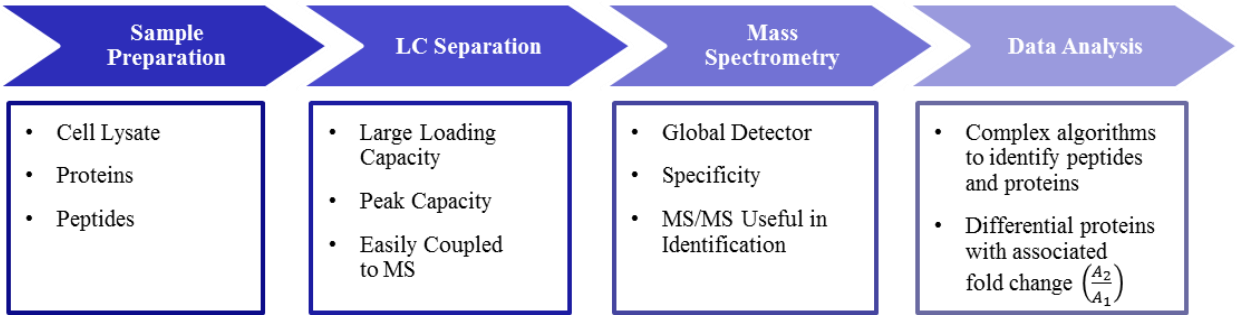

Figure 1.3. A workflow is outlined for a generic proteomics experiment. The experiment starts with a cell lysate. The analyte is either proteins or peptides. The sample is separated, commonly by liquid chromatography (LC), because it has a large loading capacity and peak capacity. LC is easily coupled to a mass spectrometer. Through electrospray, the ionization of peptides and proteins is possible making MS a near global detector. Specificity of MS, based on mass-to-charge, adds another level of separation. The fragmentation data associated from MS/MS experiments is useful in identifying the protein. Complex algorithms process the spectral data to identify peptides and proteins. The relative abundance, usually in terms of spectral counts, is calculated to give the fold change in expression of a protein in two differential proteomic samples.

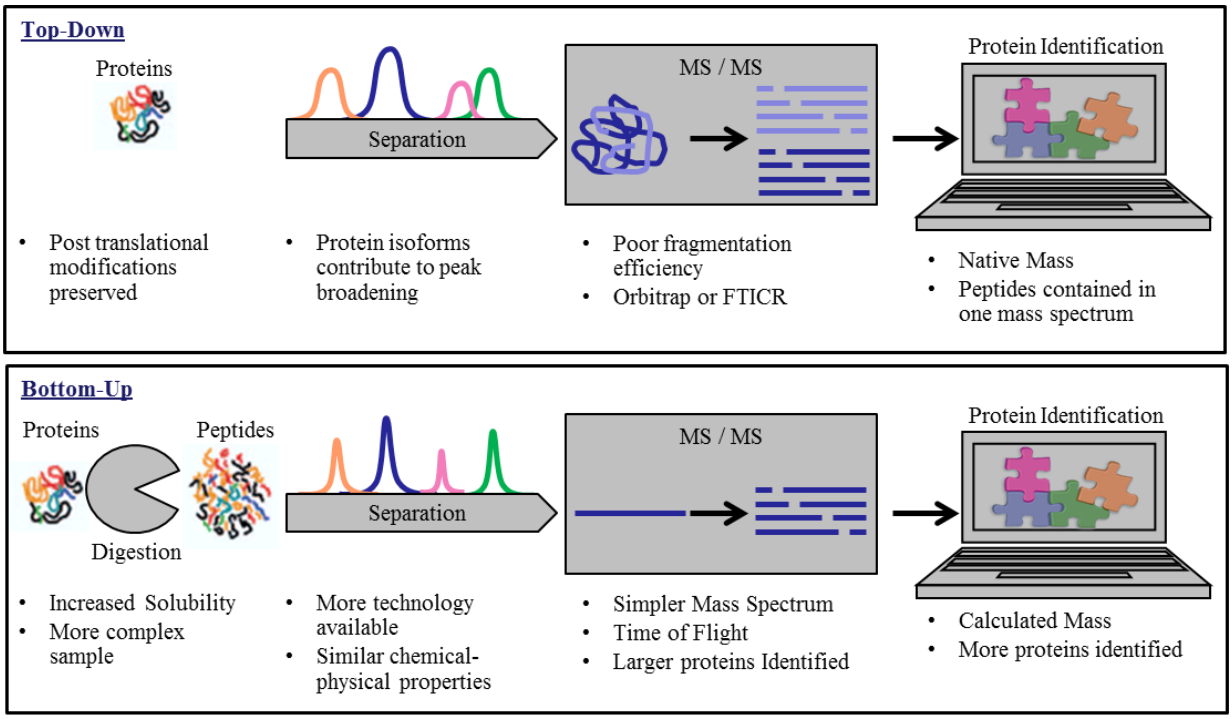

Figure 1.4. Typical work flows for top-down and bottom-up experiments with considerations for each step are shown.

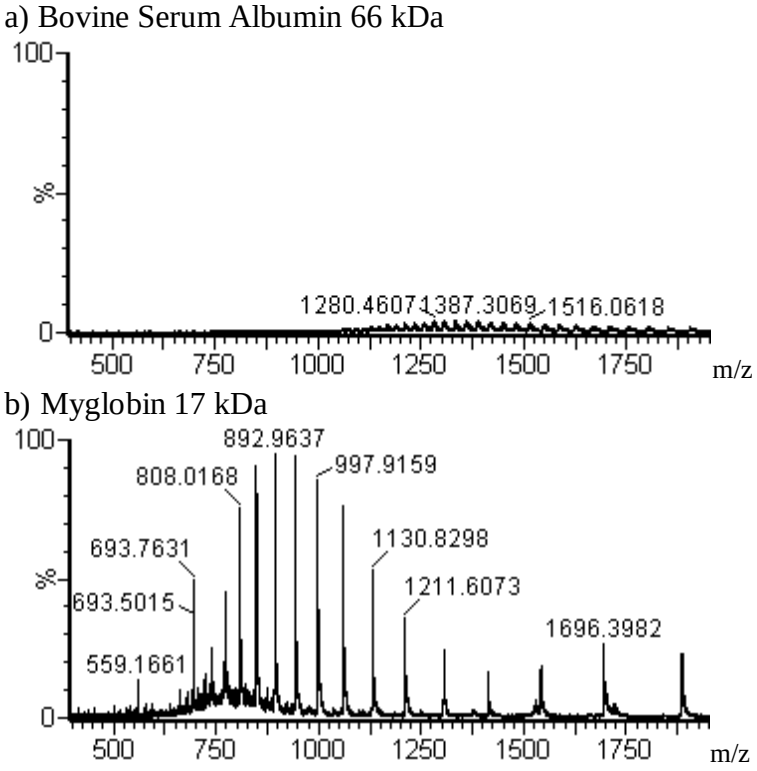

Figure 1.5. Example spectra of protein envelops acquired by ESI-TOF-MS are shown drawn to the same intensity scale. Myoglobin and bovine serum albumin (BSA) were infused in similar amounts. Bovine serum albumin (a) is 66 kDa and much larger than 17 kDa myoglobin (b). The BSA molecules are split over more charge states than myoglobin making it less intense and more difficult to detect.

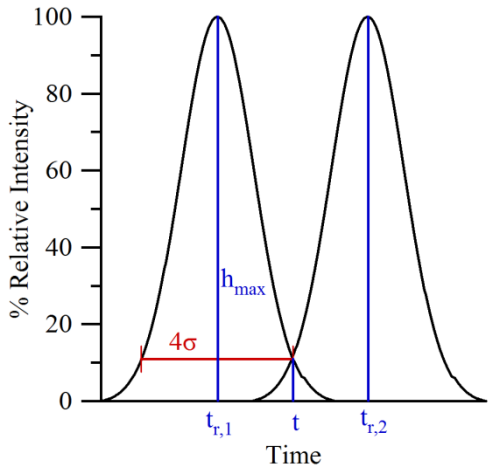

Figure 1.6. This diagram shows two adjacent peaks, with retention times $t_{r,1}$ and $t_{r,1}$ and peak widths of 4σ at 11% of the maximum height. The two peaks have a resolution of 1.

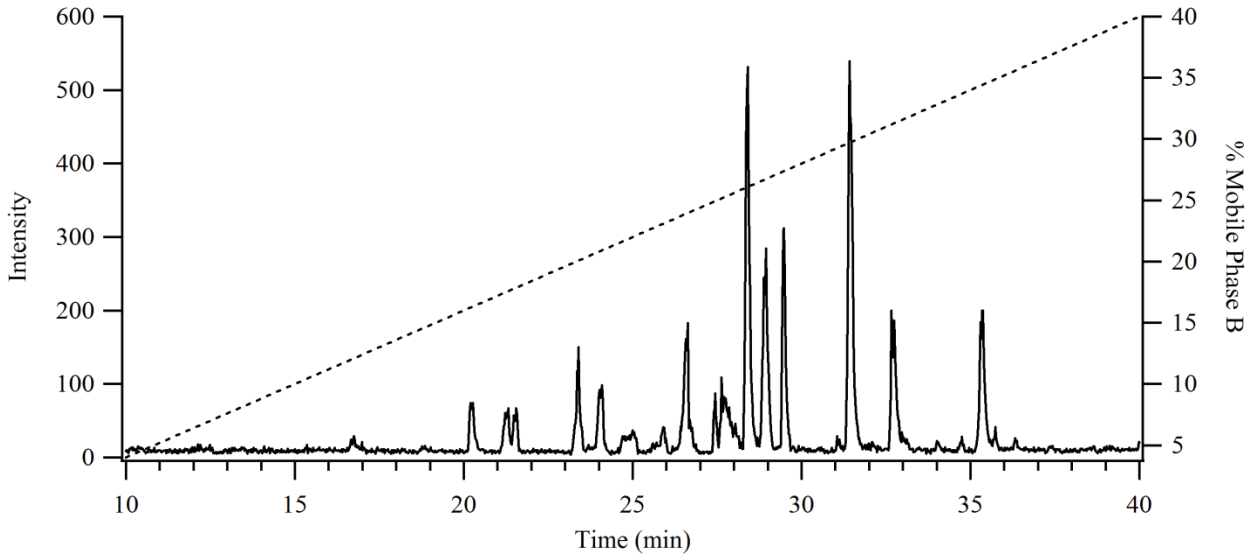

Figure 1.7. This example separation is of a standard enolase protein digest. This separation has a peak capacity of 100 which is typical for a 30 minute gradient on a standard UPLC with a commercial column. A peak capacity of 100 is sufficient for the separation of a single protein digest.

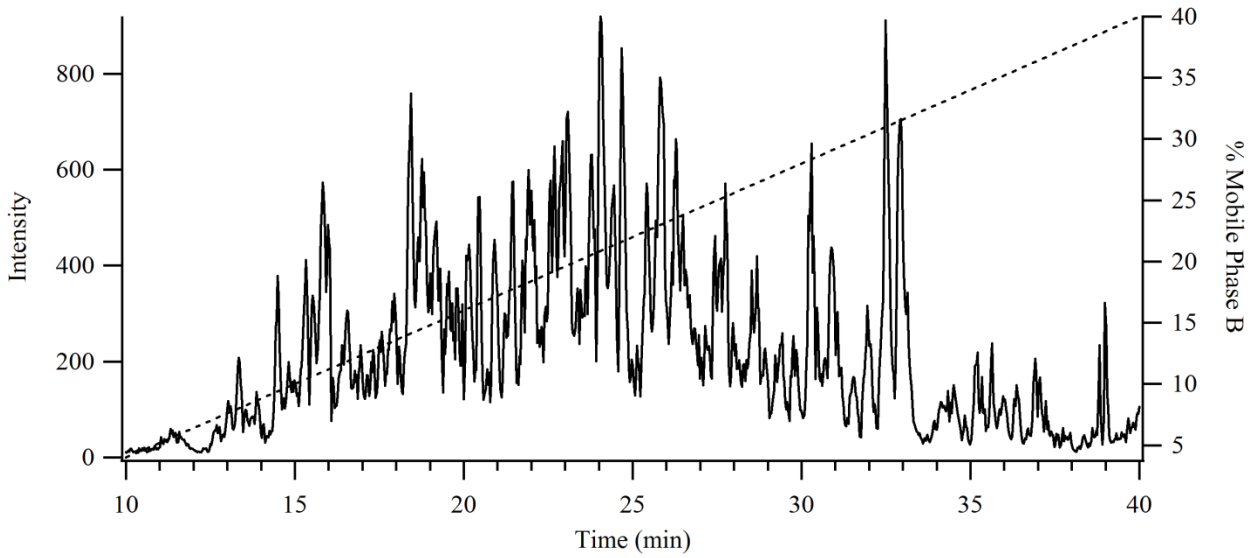

Figure 1.8. An example separation (n_c=100) of an *E. coli* digest shows many overlapping peaks.

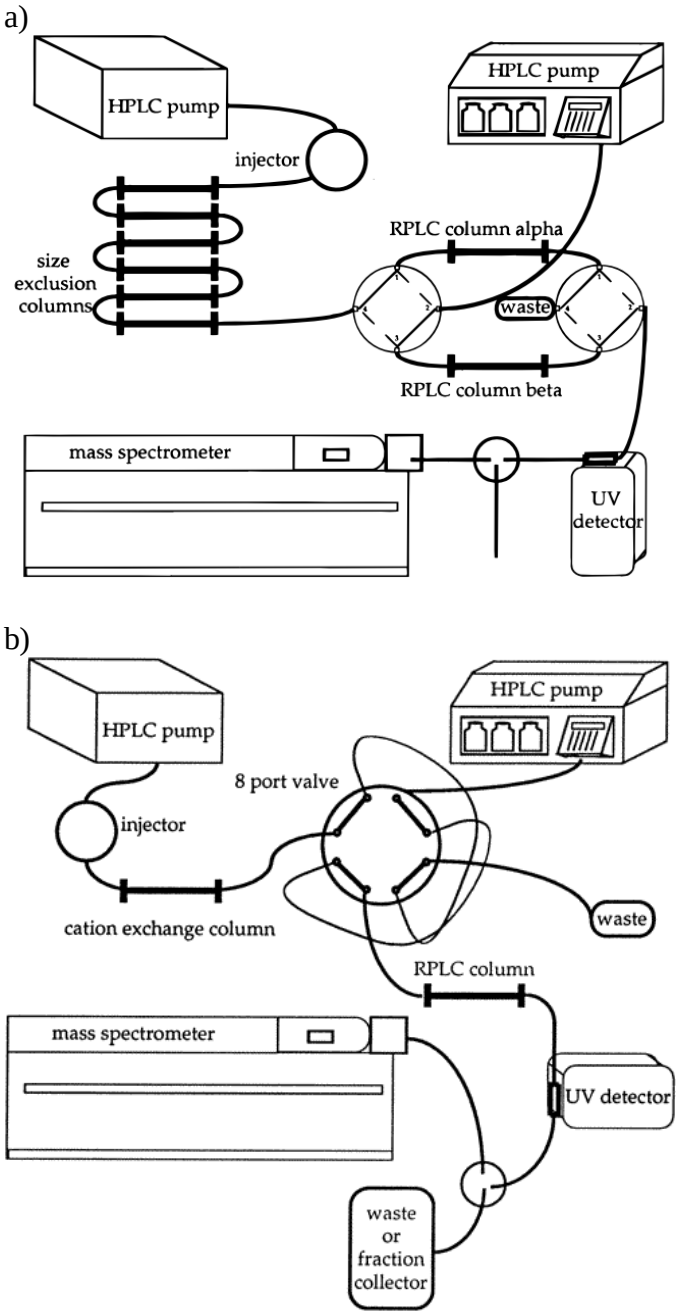

Figure 1.9. Two instrument schematics are shown for an online multidimensional separation. In part (a), there are two identical columns (A and B) in the second dimension. The effluent from the first separation is loaded onto the head of column A. Using two 4-port valves, the effluent is then switched to column B, and a gradient is pumped through column A to complete the second-dimension separation. This cycle continues until the desired number of fractions from the first dimension is obtained.[84] Alternatively, this can be completed with one second-dimension column using two storage loops between the dimensions as shown in part (b).[80,85]

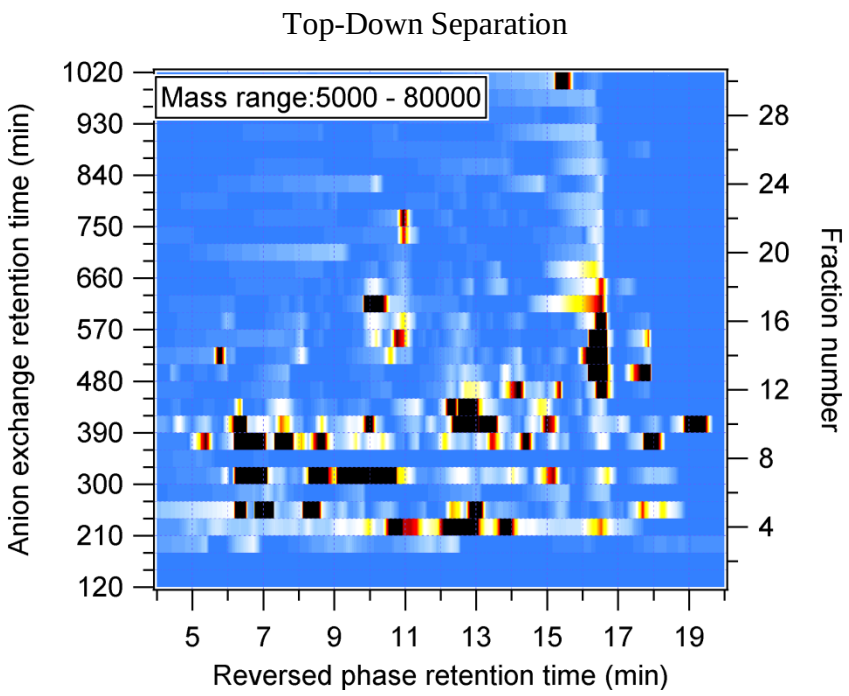

Figure 1.10. The top-down 2D chromatogram shows *S. cerevisiae* separated on a strong anion-exchange column in the first dimension and reversed-phase column in the second dimension.[88]

Bottom-Up Separation Nano2D Hi-Low pH

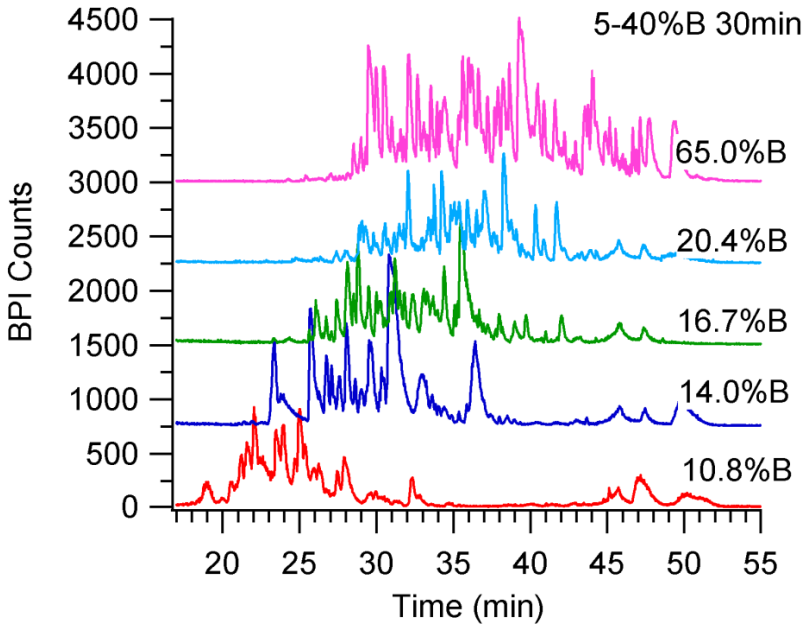

Figure 1.11. The 2D chromatogram shows the bottom-up separation of *S. cerevisiae*. A step gradient is implemented for the first dimension separation. There were five steps dictating the peak capacity of the first dimension. A reversed-phase column is used in both dimensions. The separation attempts to be orthogonal by modifying the sample with high-pH mobile phase in the first dimension and low-pH mobile phase in the second dimension.[88]

1.8 REFERENCES

1. Pandey, A.; Mann, M., Proteomics to study genes and genomes. *Nature* 2000, *405* (6788), 837-846.

2. Anderson, N. L.; Anderson, N. G., The Human Plasma Proteome: History, Character, and Diagnostic Prospects. *Molecular & Cellular Proteomics* 2003, *2* (1), 50.

3. Monteoliva, L.; Albar, J. P., Differential proteomics: An overview of gel and non-gel based approaches. *Briefings in Functional Genomics & Proteomics* 2004, *3* (3), 220-239.

4. Righetti, P. G.; Campostrini, N.; Pascali, J.; Hamdan, M.; Astner, H., Quantitative proteomics: a review of different methodologies. *Eur J Mass Spectrom (Chichester, Eng)* 2004, *10* (3), 335-48.

5. Roy, S. M.; Anderle, M.; Lin, H.; Becker, C. H., Differential expression profiling of serum proteins and metabolites for biomarker discovery. *International Journal of Mass Spectrometry* 2004, *238* (2), 163-171.

6. Lockhart, D. J.; Winzeler, E. A., Genomics, gene expression and DNA arrays. *Nature* 2000, *405* (6788), 827-836.

7. Hieter, P.; Boguski, M., Functional genomics: it's all how you read it. *Science* 1997, *278* (5338), 601-602.

8. Ge, H.; Walhout, A. J. M.; Vidal, M., Integrating 'omic' information: a bridge between genomics and systems biology. *Trends in Genetics* 2003, *19* (10), 551-560.

9. Pate, R. R.; Pratt, M.; Blair, S. N.; et al., Physical activity and public health: A recommendation from the centers for disease control and prevention and the american college of sports medicine. *JAMA* 1995, *273* (5), 402-407.

10. Pearson, T. A.; Mensah, G. A.; Alexander, R. W.; Anderson, J. L.; Cannon, R. O.; Criqui, M.; Fadl, Y. Y.; Fortmann, S. P.; Hong, Y.; Myers, G. L., Markers of inflammation and cardiovascular disease application to clinical and public health practice: a statement for healthcare professionals from the centers for disease control and prevention and the American Heart Association. *Circulation* 2003, *107* (3), 499-511.

11. Bettelheim, F.; Brown, W.; Campbell, M.; Farrell, S.; Torres, O., *Introduction to Organic and Biochemistry*. Cengage Learning: 2012.

12. Crick, F., Central dogma of molecular biology. *Nature* 1970, *227* (5258), 561-563.

13. Watson, J. D.; Crick, F. H., Molecular structure of nucleic acids. *Nature* 1953, *171* (4356), 737-738.

14. Schreiber, S. L., Small molecules: the missing link in the central dogma. *Nature chemical biology* 2005, *1* (2), 64-66.

15. Xiayan, L.; Legido-Quigley, C., Advances in separation science applied to metabonomics. *ELECTROPHORESIS* 2008, *29* (18), 3724-3736.

16. Lay Jr, J. O.; Liyanage, R.; Borgmann, S.; Wilkins, C. L., Problems with the "omics". *TrAC Trends in Analytical Chemistry* 2006, *25* (11), 1046-1056.

17. Ryan, D.; Robards, K., Metabolomics: the greatest omics of them all? *Analytical Chemistry* 2006, *78* (23), 7954-7958.

18. Collins, F. S.; McKusick, V. A., Implications of the human genome project for medical science. *JAMA* 2001, *285* (5), 540-544.

19. Sawicki, M. P.; Samara, G.; Hurwitz, M.; Passaro Jr, E., Human Genome Project. *The American Journal of Surgery* 1993, *165* (2), 258-264.

20. Collins, F. S.; Patrinos, A.; Jordan, E.; Chakravarti, A.; Gesteland, R.; Walters, L.; DOE, t. m. o. t.; groups, N. p., New Goals for the U.S. Human Genome Project: 1998-2003. *Science* 1998, *282* (5389), 682-689.

21. Saha, S.; Sparks, A. B.; Rago, C.; Akmaev, V.; Wang, C. J.; Vogelstein, B.; Kinzler, K. W.; Velculescu, V. E., Using the transcriptome to annotate the genome. *Nature biotechnology* 2002, *20* (5), 508-512.

22. Kenyon, G. L.; DeMarini, D. M.; Fuchs, E.; Galas, D. J.; Kirsch, J. F.; Leyh, T. S.; Moos, W. H.; Petsko, G. A.; Ringe, D.; Rubin, G. M.; Sheahan, L. C., Defining the Mandate of Proteomics in the Post-Genomics Era: Workshop Report: ©2002 National Academy of Sciences, Washington, D.C., USA. Reprinted with permission from the National Academies Press for the National Academy of Sciences. All rights reserved. The original report may be viewed online at http://www.nap.edu/catalog/10209.html. *Molecular & Cellular Proteomics* 2002, *1* (10), 763-780.

23. Omenn, G. S., The Human Proteome Organization Plasma Proteome Project pilot phase: reference specimens, technology platform comparisons, and standardized data submissions and analyses. *PROTEOMICS* 2004, *4* (5), 1235-1240.

24. Paik, Y.-K.; Jeong, S.-K.; Omenn, G. S.; Uhlen, M.; Hanash, S.; Cho, S. Y.; Lee, H.-J.; Na, K.; Choi, E.-Y.; Yan, F.; Zhang, F.; Zhang, Y.; Snyder, M.; Cheng, Y.; Chen, R.; Marko-Varga, G.; Deutsch, E. W.; Kim, H.; Kwon, J.-Y.; Aebersold, R.; Bairoch, A.; Taylor, A. D.; Kim, K. Y.; Lee, E.-Y.; Hochstrasser, D.; Legrain, P.; Hancock, W. S., The Chromosome-Centric Human Proteome Project for cataloging proteins encoded in the genome. *Nat Biotech* 2012, *30* (3), 221-223.

25. Julka, S.; Regnier, F. E., Recent advancements in differential proteomics based on stable isotope coding. *Briefings in Functional Genomics & Proteomics* 2005, *4* (2), 158-177.

26. Stobaugh, J. T.; Fague, K. M.; Jorgenson, J. W., Prefractionation of Intact Proteins by Reversed-Phase and Anion-Exchange Chromatography for the Differential Proteomic

Analysis of Saccharomyces cerevisiae. *Journal of Proteome Research* 2012, *12* (2), 626-636.

27. Cherry, J. M.; Hong, E. L.; Amundsen, C.; Balakrishnan, R.; Binkley, G.; Chan, E. T.; Christie, K. R.; Costanzo, M. C.; Dwight, S. S.; Engel, S. R.; Fisk, D. G.; Hirschman, J. E.; Hitz, B. C.; Karra, K.; Krieger, C. J.; Miyasato, S. R.; Nash, R. S.; Park, J.; Skrzypek, M. S.; Simison, M.; Weng, S.; Wong, E. D., Saccharomyces Genome Database: the genomics resource of budding yeast. *Nucleic Acids Research* 2012, *40* (D1), D700-D705.

28. Yates, J. R.; Ruse, C. I.; Nakorchevsky, A., Proteomics by Mass Spectrometry: Approaches, Advances, and Applications. *Annual Review of Biomedical Engineering* 2009, *11* (1), 49-79.

29. Zubarev, R. A.; Kelleher, N. L.; McLafferty, F. W., Electron Capture Dissociation of Multiply Charged Protein Cations. A Nonergodic Process. *Journal of the American Chemical Society* 1998, *120* (13), 3265-3266.

30. Kelleher, N. L.; Lin, H. Y.; Valaskovic, G. A.; Aaserud, D. J.; Fridriksson, E. K.; McLafferty, F. W., Top Down versus Bottom Up Protein Characterization by Tandem High-Resolution Mass Spectrometry. *Journal of the American Chemical Society* 1999, *121* (4), 806-812.

31. Keller, A.; Nesvizhskii, A. I.; Kolker, E.; Aebersold, R., Empirical Statistical Model To Estimate the Accuracy of Peptide Identifications Made by MS/MS and Database Search. *Analytical Chemistry* 2002, *74* (20), 5383-5392.

32. Nesvizhskii, A. I.; Keller, A.; Kolker, E.; Aebersold, R., A Statistical Model for Identifying Proteins by Tandem Mass Spectrometry. *Analytical Chemistry* 2003, *75* (17), 4646-4658.

33. Old, W. M.; Meyer-Arendt, K.; Aveline-Wolf, L.; Pierce, K. G.; Mendoza, A.; Sevinsky, J. R.; Resing, K. A.; Ahn, N. G., Comparison of Label-free Methods for Quantifying Human Proteins by Shotgun Proteomics. *Molecular & Cellular Proteomics* 2005, *4* (10), 1487-1502.

34. Matzke, M. M.; Brown, J. N.; Gritsenko, M. A.; Metz, T. O.; Pounds, J. G.; Rodland, K. D.; Shukla, A. K.; Smith, R. D.; Waters, K. M.; McDermott, J. E.; Webb-Robertson, B.-J., A comparative analysis of computational approaches to relative protein quantification using peptide peak intensities in label-free LC-MS proteomics experiments. *PROTEOMICS* 2013, *13* (3-4), 493-503.

35. Gan, C. S.; Chong, P. K.; Pham, T. K.; Wright, P. C., Technical, Experimental, and Biological Variations in Isobaric Tags for Relative and Absolute Quantitation (iTRAQ). *Journal of Proteome Research* 2007, *6* (2), 821-827.

36. Ross, P. L.; Huang, Y. N.; Marchese, J. N.; Williamson, B.; Parker, K.; Hattan, S.; Khainovski, N.; Pillai, S.; Dey, S.; Daniels, S., Multiplexed protein quantitation in

Saccharomyces cerevisiae using amine-reactive isobaric tagging reagents. *Molecular & Cellular Proteomics* 2004, *3* (12), 1154-1169.

37. Ong, S.-E.; Blagoev, B.; Kratchmarova, I.; Kristensen, D. B.; Steen, H.; Pandey, A.; Mann, M., Stable Isotope Labeling by Amino Acids in Cell Culture, SILAC, as a Simple and Accurate Approach to Expression Proteomics. *Molecular & Cellular Proteomics* 2002, *1* (5), 376-386.

38. Mann, M., Functional and quantitative proteomics using SILAC. *Nature reviews Molecular cell biology* 2006, *7* (12), 952-958.

39. Wolters, D. A.; Washburn, M. P.; Yates, J. R., An Automated Multidimensional Protein Identification Technology for Shotgun Proteomics. *Analytical Chemistry* 2001, *73* (23), 5683-5690.

40. Washburn, M. P.; Ulaszek, R.; Deciu, C.; Schieltz, D. M.; Yates, J. R., Analysis of Quantitative Proteomic Data Generated via Multidimensional Protein Identification Technology. *Analytical Chemistry* 2002, *74* (7), 1650-1657.

41. Hebert, A. S.; Richards, A. L.; Bailey, D. J.; Ulbrich, A.; Coughlin, E. E.; Westphall, M. S.; Coon, J. J., The One Hour Yeast Proteome. *Molecular & Cellular Proteomics* 2014, *13* (1), 339-347.

42. McCormick, R. M., Capillary zone electrophoretic separation of peptides and proteins using low pH buffers in modified silica capillaries. *Analytical Chemistry* 1988, *60* (21), 2322-2328.

43. Whitelegge, J. P.; Zhang, H.; Aguilera, R.; Taylor, R. M.; Cramer, W. A., Full Subunit Coverage Liquid Chromatography Electrospray Ionization Mass Spectrometry (LCMS+) of an Oligomeric Membrane Protein Cytochrome b6f Complex From Spinach and the Cyanobacterium Mastigocladus Laminosus. *Molecular & Cellular Proteomics* 2002, *1* (10), 816-827.

44. Wang, Y.; Balgley, B. M.; Rudnick, P. A.; Lee, C. S., Effects of chromatography conditions on intact protein separations for top-down proteomics. *Journal of Chromatography A* 2005, *1073* (1–2), 35-41.

45. Steen, H.; Mann, M., The ABC's (and XYZ's) of peptide sequencing. *Nature reviews Molecular cell biology* 2004, *5* (9), 699-711.

46. Marcotte, E. M., How do shotgun proteomics algorithms identify proteins? *Nature biotechnology* 2007, *25* (7), 755-757.

47. Hillenkamp, F.; Karas, M.; Beavis, R. C.; Chait, B. T., Matrix-assisted laser desorption/ionization mass spectrometry of biopolymers. *Analytical Chemistry* 1991, *63* (24), 1193A-1203A.

48. Strupat, K.; Karas, M.; Hillenkamp, F.; Eckerskorn, C.; Lottspeich, F., Matrix-assisted laser desorption ionization mass spectrometry of proteins electroblotted after polyacrylamide gel electrophoresis. *Analytical Chemistry* 1994, *66* (4), 464-470.

49. Fenn, J. B.; Mann, M.; Meng, C. K.; Wong, S. F.; Whitehouse, C. M., Electrospray ionization for mass spectrometry of large biomolecules. *Science* 1989, *246* (4926), 64-71.

50. Lössl, P.; Snijder, J.; Heck, A. J., Boundaries of Mass Resolution in Native Mass Spectrometry. *Journal of the American Society for Mass Spectrometry* 2014, *25* (6), 906-917.

51. Fenn, L.; Kliman, M.; Mahsut, A.; Zhao, S.; McLean, J., Characterizing ion mobility-mass spectrometry conformation space for the analysis of complex biological samples. *Anal Bioanal Chem* 2009, *394* (1), 235-244.

52. Wilm, M. S.; Mann, M., Electrospray and Taylor-Cone theory, Dole's beam of macromolecules at last? *International Journal of Mass Spectrometry and Ion Processes* 1994, *136* (2–3), 167-180.

53. Wilm, M.; Mann, M., Analytical Properties of the Nanoelectrospray Ion Source. *Analytical Chemistry* 1996, *68* (1), 1-8.

54. Zubarev, R. A.; Horn, D. M.; Fridriksson, E. K.; Kelleher, N. L.; Kruger, N. A.; Lewis, M. A.; Carpenter, B. K.; McLafferty, F. W., Electron Capture Dissociation for Structural Characterization of Multiply Charged Protein Cations. *Analytical Chemistry* 2000, *72* (3), 563-573.

55. Vellaichamy, A.; Tran, J. C.; Catherman, A. D.; Lee, J. E.; Kellie, J. F.; Sweet, S. M. M.; Zamdborg, L.; Thomas, P. M.; Ahlf, D. R.; Durbin, K. R.; Valaskovic, G. A.; Kelleher, N. L., Size-Sorting Combined with Improved Nanocapillary Liquid Chromatography−Mass Spectrometry for Identification of Intact Proteins up to 80 kDa. *Analytical Chemistry* 2010, *82* (4), 1234-1244.

56. Coon, J. J.; Ueberheide, B.; Syka, J. E.; Dryhurst, D. D.; Ausio, J.; Shabanowitz, J.; Hunt, D. F., Protein identification using sequential ion/ion reactions and tandem mass spectrometry. *Proceedings of the National Academy of Sciences of the United States of America* 2005, *102* (27), 9463-9468.

57. Rose, R. J.; Damoc, E.; Denisov, E.; Makarov, A.; Heck, A. J., High-sensitivity Orbitrap mass analysis of intact macromolecular assemblies. *Nature methods* 2012, *9* (11), 1084-1086.

58. Tran, J. C.; Zamdborg, L.; Ahlf, D. R.; Lee, J. E.; Catherman, A. D.; Durbin, K. R.; Tipton, J. D.; Vellaichamy, A.; Kellie, J. F.; Li, M.; Wu, C.; Sweet, S. M. M.; Early, B. P.; Siuti, N.; LeDuc, R. D.; Compton, P. D.; Thomas, P. M.; Kelleher, N. L., Mapping intact protein isoforms in discovery mode using top-down proteomics. *Nature* 2011, *480* (7376), 254-258.

59. Doerr, A., Mass spectrometry of intact protein complexes. *Nat Meth* 2013, *10* (1), 38-38.

60. Zhang, Z.; Guan, S.; Marshall, A. G., Enhancement of the effective resolution of mass spectra of high-mass biomolecules by maximum entropy-based deconvolution to eliminate the isotopic natural abundance distribution. *Journal of the American Society for Mass Spectrometry* 1997, *8* (6), 659-670.

61. Searle, B. C., Scaffold: A bioinformatic tool for validating MS/MS-based proteomic studies. *PROTEOMICS* 2010, *10* (6), 1265-1269.

62. Nesvizhskii, A. I.; Aebersold, R., Interpretation of Shotgun Proteomic Data: The Protein Inference Problem. *Molecular & Cellular Proteomics* 2005, *4* (10), 1419-1440.

63. Di Palma, S.; Hennrich, M. L.; Heck, A. J. R.; Mohammed, S., Recent advances in peptide separation by multidimensional liquid chromatography for proteome analysis. *Journal of Proteomics* 2012, *75* (13), 3791-3813.

64. Giddings, J. C., *Unified separation science*. Wiley: 1991.

65. Neue, U. D., *HPLC Columns: Theory, Technology, and Practice*. Wiley: 1997.

66. Neue, U. D., Theory of peak capacity in gradient elution. *Journal of Chromatography A* 2005, *1079* (1–2), 153-161.

67. Davis, J. M.; Giddings, J. C., Statistical theory of component overlap in multicomponent chromatograms. *Analytical Chemistry* 1983, *55* (3), 418-424.

68. Blattner, F. R.; Plunkett, G.; Bloch, C. A.; Perna, N. T.; Burland, V.; Riley, M.; Collado-Vides, J.; Glasner, J. D.; Rode, C. K.; Mayhew, G. F.; Gregor, J.; Davis, N. W.; Kirkpatrick, H. A.; Goeden, M. A.; Rose, D. J.; Mau, B.; Shao, Y., The Complete Genome Sequence of Escherichia coli K-12. *Science* 1997, *277* (5331), 1453-1462.

69. Pray, L., Eukaryotic genome complexity. *Nature Education* 2008, *1* (1).

70. MacNair, J. E.; Patel, K. D.; Jorgenson, J. W., Ultrahigh-Pressure Reversed-Phase Capillary Liquid Chromatography: Isocratic and Gradient Elution Using Columns Packed with 1.0-μm Particles. *Analytical Chemistry* 1999, *71* (3), 700-708.

71. Stadalius, M. A.; Gold, H. S.; Snyder, L. R., Optimization model for the gradient elution separation of peptide mixtures by reversed-phase high-performance liquid chromatography : Verification of band width relationships for acetonitrile-water mobile phases. *Journal of Chromatography A* 1985, *327* (0), 27-45.

72. Shen, Y.; Zhang, R.; Moore, R. J.; Kim, J.; Metz, T. O.; Hixson, K. K.; Zhao, R.; Livesay, E. A.; Udseth, H. R.; Smith, R. D., Automated 20 kpsi RPLC-MS and MS/MS with Chromatographic Peak Capacities of 1000−1500 and Capabilities in Proteomics and Metabolomics. *Analytical Chemistry* 2005, *77* (10), 3090-3100.

73. Zhou, F.; Lu, Y.; Ficarro, S. B.; Webber, J. T.; Marto, J. A., Nanoflow Low Pressure High Peak Capacity Single Dimension LC-MS/MS Platform for High-Throughput, In-Depth Analysis of Mammalian Proteomes. *Analytical Chemistry* 2012, *84* (11), 5133-5139.

74. Gilar, M.; Olivova, P.; Daly, A. E.; Gebler, J. C., Two-dimensional separation of peptides using RP-RP-HPLC system with different pH in first and second separation dimensions. *Journal of Separation Science* 2005, *28* (14), 1694-1703.

75. Klose, J., Protein mapping by combined isoelectric focusing and electrophoresis of mouse tissues. *Humangenetik* 1975, *26* (3), 231-243.

76. O'Farrell, P. H., High resolution two-dimensional electrophoresis of proteins. *Journal of Biological Chemistry* 1975, *250* (10), 4007-4021.

77. Wang, H.; Hanash, S., Multi-dimensional liquid phase based separations in proteomics. *Journal of Chromatography B* 2003, *787* (1), 11-18.

78. Godovac-Zimmermann, J.; Brown, L. R., Perspectives for mass spectrometry and functional proteomics. *Mass Spectrometry Reviews* 2001, *20* (1), 1-57.

79. Davis, J. M.; Stoll, D. R.; Carr, P. W., Dependence of Effective Peak Capacity in Comprehensive Two-Dimensional Separations on the Distribution of Peak Capacity between the Two Dimensions. *Analytical Chemistry* 2008, *80* (21), 8122-8134.

80. Bushey, M. M.; Jorgenson, J. W., Automated instrumentation for comprehensive two-dimensional high-performance liquid chromatography of proteins. *Analytical Chemistry* 1990, *62* (2), 161-167.

81. Sandra, K.; Moshir, M.; D'hondt, F.; Tuytten, R.; Verleysen, K.; Kas, K.; François, I.; Sandra, P., Highly efficient peptide separations in proteomics: Part 2: Bi- and multidimensional liquid-based separation techniques. *Journal of Chromatography B* 2009, *877* (11–12), 1019-1039.

82. Link, A. J.; Eng, J.; Schieltz, D. M.; Carmack, E.; Mize, G. J.; Morris, D. R.; Garvik, B. M.; Yates, J. R., Direct analysis of protein complexes using mass spectrometry. *Nature biotechnology* 1999, *17* (7), 676-682.

83. Washburn, M. P.; Wolters, D.; Yates, J. R., Large-scale analysis of the yeast proteome by multidimensional protein identification technology. *Nature biotechnology* 2001, *19* (3), 242-247.

84. Opiteck, G. J.; Jorgenson, J. W.; Anderegg, R. J., Two-Dimensional SEC/RPLC Coupled to Mass Spectrometry for the Analysis of Peptides. *Analytical Chemistry* 1997, *69* (13), 2283-2291.

85. Opiteck, G. J.; Lewis, K. C.; Jorgenson, J. W.; Anderegg, R. J., Comprehensive On-Line LC/LC/MS of Proteins. *Analytical Chemistry* 1997, *69* (8), 1518-1524.

86. Rutan, S. C.; Davis, J. M.; Carr, P. W., Fractional coverage metrics based on ecological home range for calculation of the effective peak capacity in comprehensive two-dimensional separations. *Journal of Chromatography A* 2012, *1255* (0), 267-276.

87. Gu, H.; Huang, Y.; Carr, P. W., Peak capacity optimization in comprehensive two dimensional liquid chromatography: A practical approach. *Journal of Chromatography A* 2011, *1218* (1), 64-73.

88. Stobaugh, J. T. Strategies for Differential Proteomic Analysis by Liquid Chromatography-Mass Spectrometry [electronic resource]. OCLC Number: 861218087. University of North Carolina at Chapel Hill, Chapel Hill, N.C., 2012.

89. Stapels, M. a. F., Keith. A Reproducible Online 2D Reversed Phase–Reversed Phase High–Low pH Method for Qualitative and Quantitative Proteomics *LC-GC* [Online], 2009.

90. Martosella, J.; Zolotarjova, N.; Liu, H.; Nicol, G.; Boyes, B. E., Reversed-Phase High-Performance Liquid Chromatographic Prefractionation of Immunodepleted Human Serum Proteins to Enhance Mass Spectrometry Identification of Lower-Abundant Proteins. *Journal of Proteome Research* 2005, *4* (5), 1522-1537.

91. Dowell, J. A.; Frost, D. C.; Zhang, J.; Li, L., Comparison of Two-Dimensional Fractionation Techniques for Shotgun Proteomics. *Analytical Chemistry* 2008, *80* (17), 6715-6723.

92. German, J. B.; Hammock, B. D.; Watkins, S. M., Metabolomics: building on a century of biochemistry to guide human health. *Metabolomics* 2005, *1* (1), 3-9.

93. Rochfort, S., Metabolomics Reviewed: A New "Omics" Platform Technology for Systems Biology and Implications for Natural Products Research. *Journal of Natural Products* 2005, *68* (12), 1813-1820.

CHAPTER 2. An Equal-Mass versus Equal-Time Prefractionation Frequency Study of a Multidimensional Separation for *Saccharomyces cerevisiae* Proteomics Analysis

2.1 Introduction

2.1.1 Peak capacity considerations for multidimensional separations

Early in the field of proteomics, multidimensional separations have been employed to handle the complexity of the sample mixture.[1,2,3] As described in the previous chapter, peak capacity is used to determine the quality of the separation. Giddings wrote that the peak capacity of a multidimensional separation is the product of two peak capacities of each individual separation (n_c):

$$n_{c,total} = n_{c,1} \times n_{c,2} \quad (2\text{-}1)$$

if (1) the separations are orthogonal and (2) resolution is not lost in coupling the separations.[4] These two qualifiers to Giddings rule are difficult to realize. Several scientists have proposed additional terms to Giddings equation to account for the loss of resolution and lack of orthogonality between two separations.[5,6] A very practical way to assess the use of the separation space is to divide the 2D chromatogram into equally sized bins as seen in Figure 2.1. To calculate the practical peak capacity (n_p), a factor is added to Equation 2-1 that counts the number of bins containing a peak (Σ bins) divided by the maximum peak capacity (P_{max}) as demonstrated in [7,8]

$$n_P = n_{c,1} n_{c,2} \frac{\sum \text{bins}}{P_{max}} \quad (2\text{-}2)$$

When considering the methods described in this manuscript, the increase in maximum theoretical peak capacity is compared to how much of the 2D separation space actually contains a peak.

When sampling the first dimension, several factors must be considered. First, it is impractical to completely preserve the peak capacity of the first dimension. The peak capacity of the first dimension is reduced to the number of samples or fractions taken.[9] For example, more frequent sampling will increase the quality of the separation.[10] Secondly, fractionation dilutes the sample and raises the limit of detection by increasing the probability that an analyte will be split between multiple fractions.[11] Finally, analysis time should be considered during multidimensional method development. The second dimension must be fast in order to be run in-line with the first dimension, or an off-line approach must be implemented in which fractions are collected from the eluent of the first column for subsequent analysis. Frequent fractionation will add to the analysis time which is a limited resource.[12] In summary, the variables of peak capacity, sample dilution, and analysis time should be taken into account when developing a practical multidimensional separation.

Even with extensive method development, a complex mixture will not elute evenly over a linear gradient. For a bottom-up high-low pH 2D RPLC experiment, as previously reported by Martha Stapels, et al, she described a method to more evenly distribute the peptides across the first dimension separation. Briefly, the first dimension is a RPLC step gradient at high pH. Steps were taken at 2% increases in organic phase. The eluent was concentrated on a trap column and diluted with low pH mobile phase. The sample was then separated on the analytical column and coupled to MS. The total ion current (TIC) from these chromatograms was used to determine the appropriate mobile phase composition for each step of the first dimension gradient to separate the sample into even parts. The result was more appropriate loading of the second dimension column and a higher number of protein identifications.[13] In this chapter, a similar method is described for an intact protein separation.

The orthogonality requirement to Giddings rule carries with it several challenges. Different modes of liquid chromatography (LC) have different resolutions. Reverse phase LC (RPLC) is one of the higher resolution separation modes of LC as compared to ion exchange (IEX) or size exclusion chromatography (SEC).[14] Since some resolution realistically is lost when coupling two separations, it is best to have the highest resolution separation in the second dimension.[15] Commonly, RPLC followed by mass spectrometry (MS) is the final step of the multidimensional separation. Therefore, the first dimension has to be compatible with these techniques. For example, buffers used for IEX mobile phases must contain volatile salts that do not interfere with MS ionization. Also, SEC mobile phases must contain low amounts of organic to match the initial conditions of a RPLC gradient, or an auxillary pump and trap column must be used to dilute the organic composition before sample is loaded onto the RP analytical column. These restrictions are particularly challenging for intact protein samples which have poor solubility in many mobile phases suitable for LC. Furthermore, IEX and SEC are not completely orthogonal to RPLC.[16,17]

2.1.2 Top-down versus bottom-up proteomics

When developing multidimensional separations for proteomics analysis, the ongoing question is whether to do a top-down (protein) or bottom-up (peptide) separation. (The merits of both techniques are more fully explained in the first chapter.) To take advantage of the benefits from both top-down and bottom-up experiments, prefractionation methods have been growing in popularity.[18,19] The first step in sample preparation is to isolate the intact proteins from a cell lysate by centrifugation. The soluble portion of the proteome is separated by LC or electrophoresis in the first dimension. Fractions are collected, digested with trypsin, and analyzed by UPLC-MS/MS. By changing the sample from protein to peptide via digestion

between the two dimensions, the separations are orthogonal even if the same separation mode is used in both dimensions. The more difficult protein separation is required in only one dimension, and high resolution chromatography modes such as RPLC can be used in both dimensions. The prefractionation method is analogous to a mass spectrometry MRM experiment in which the precursor ion is isolated in a mass analyzer and fragmented before analysis by a tandem mass analyzer.[20] Digesting the proteins prior to introduction into the mass spectrometer simplifies the spectral data because peptides have many less charge states than proteins when ionized by electrospray.[21,22] As opposed to bottom-up 2DLC experiments where peptides from a single protein may be spread over the entire chromatogram, peptides from a single protein are confined to a single first dimension fraction easing computational requirements. This may reduce the protein inference problem in which a single peptide may be mistakenly assigned to multiple proteins.[23]

2.1.3 Prefractionation by Equal-Mass

Sampling the first dimension chromatogram usually occurs in evenly timed intervals even though the analytes do not elute as evenly spaced peaks. In RPLC, for example, most proteins are of average hydrophobicity[24] meaning most molecules will elute in the middle of the gradient with fewer at the beginning or end. For targeted analyses, a heart-cutting approach, which samples only the portions of the first dimension separation containing analytes of interest, may be employed.[25] For an -omics approach, the goal is to have the entire sample mass evenly split amongst the first dimension fractions which we will prove is poorly achieved by equal-time prefractionation. A possible method to determine equal-mass fractionation would be to collect minute-wide fractions from the first dimension separation, determine the protein concentration of

each fraction by Bradford Assay,[26] and then recombine the fractions to make the desired number of equal-mass fractions. However, this procedure would be very tedious.

Herein, we describe a method using *Saccharomyces cerevisiae* as a model proteomics sample to form equal-mass fractions based on the UV absorbance values of the first dimension chromatogram. We validate this method with a comparison of the absorbance values to the TIC chromatograms from the second dimension and to the number of proteins identified in each fraction. The equal-mass fractionation method is compared to an equal-time fractionation method to demonstrate the increase in number of protein identifications and protein coverage. We propose a newly defined metric, namely Normalized Difference Protein Converge (NDPC), which compares protein coverage between multiple methods, will be discussed. The frequency of prefractionation will also be investigated as it has not been extensively studied for a prefractionation type 2D separation. The results of the prefractionation frequency experiments compare number of protein identifications to analysis time and expose the detriment of over fractionation.

2.2 Materials and method

2.2.1 Materials

Water, acetonitrile, isopropyl alcohol and ammonium hydroxide were purchased from Fisher Scientific (Fair Lawn, NJ). Ammonium acetate, ammonium bicarbonate, formic acid, trifluoroacetic acid and iodoacetamide were purchased from Sigma-Aldrich Co. (St. Louis, MO). Rapigest^{TM} SF acid-labile surfactant and bovine serum album (BSA) was obtained from Waters Corporation (Milford, MA). Dithiothreitol was purchased from Research Products International (Mt. Prospect, IL) and TPCK-modified trypsin was purchased from Pierce (Rockford, IL). Water

and acetonitrile were Optima LC-MS grade, and all other chemicals were ACS reagent grade or higher.

2.2.2 Sample preparation

Growth media YAPG was prepared by combining 6.0 g of yeast extract, 12.0 g of peptone, 5 mL of glycerol, 60 mg adenine hemisulfate, 600 mL of water, and an additional 10 g bacto-agar for plate medium. *S. cerevisiae* (BY4741) was the cell line used for analysis. Plates of growth media were streaked with yeast and incubated for four days when sizeable colonies were obtained. A single colony was then used to inoculate a 150 mL small-scale culture. These cultures were grown to an O.D. greater than two before being used to inoculate a 2 L (in a 4 L flask) prep scale batch. The yeast cells were harvested when the O.D. was 2.0. Cells were centrifuged at 7000 Xg in a Sorvall GS-3 rotor for 30 minutes until pelleted. Cells were then stored at -80°C until processed.

Cells were resuspended by pipet in 2 volumes of 50 mM ammonium bicarbonate with protease inhibitors present (Pierce protease inhibitor tablets, 88661) prepared to manufacturer's recommendations. A homogenate was prepared by 8 passes through a chilled french press cell dropwise at 20,000 psi. The homogenate was centrifuged (Beckman JA20 rotor, 30,000 Xg, 20 min, 4°C) and a cytosolic fraction was prepared from the cleared lysate by ultracentrifugation at 120,000 Xg for 90 min, 4 °C. Cytosolic fractions determined to be between 10-13 mg/mL of total protein using the Bio-Rad (Hercules, CA) protein assay with BSA standard. Immediately prior to analysis, each fraction was diluted with formic acid (Fisher) to a final protein concentration of 7.3 mg/mL.

2.2.3 Intact protein prefractionation

The prefractionation of intact proteins, outlined in Figure 2.2, begins with a separation on a 4.6 x 250 mm PLRP-S column with 5 µm particles (Agilent, Santa Clara, CA) heated to 80 °C. Four milligrams of total protein were injected onto the column. The flow rate, mobile phase compositions and gradient profile is shown in Table 2.1. One-minute-wide fractions were collected from 2 to 42 minutes, yielding 40 fractions. Fractions were stored at -80º C until needed.

2.2.4 Protein digestion

Fractions were transferred to microcentrifuge tubes, then lyophilized and reconstituted in 25 µL of 50 mM ammonium bicarbonate, pH 8. Three microliters of 6.67% (w/v) RapiGest™ SF in buffer were added (15 min, 80 ºC) to denature the proteins. The proteins were reduced by adding 1 µL of 100 mM dithiothreitol (30 min, 60ºC), and then alkylated with 1 µL of 200 mM iodoacetamide (30 min, room temperature, protected from light). The proteins were then digested by adding 10 µL of 320 ng/µL TPCK-modified trypsin in 50 mM ammonium bicarbonate, pH 8 (overnight, 37ºC). The trypsin amount was approximated to be a 25:1 (w/w) protein to enzyme ratio if the initial protein amount was equally distributed across the 40 fractions. The digestion was quenched and the RapiGest™ SF was degraded using 44 µL of 1% (v/v) trifluoroacetic acid (2 h, 60ºC). The fractions were centrifuged for 20 minutes at 14,000 Xg to pellet the hydrolyzed surfactant, after which they were ready for analysis. The samples were transferred to LC vials and spiked with 4.21 µL of a 1 pmol/L internal standard BSA digest (Waters). This set of 40 fractions was recombined in the following configurations to investigate prefractionation frequency and the method for selecting fractions.

2.2.5 Equal-time fractionation

To vary the prefractionation frequency, 10 µL of each fraction were pooled in the following three configurations: (1) every other fraction was combined to yield 20 two-minute wide fractions, (2) every four fractions were combined to yield 10 four-minute wide fractions, and (3) every 8 fractions were combined to yield 5 eight-minute wide fractions. These samples will be referred to as equal-time fractions.

2.2.6 Peptide analysis by LC-MS/MS

Each fraction was analyzed in duplicate by capillary RPLC-MS/MS using a Waters nanoAcquity/QTOF Premier system. To normalize the concentration of each fraction, the sample injection volume was adjusted based on the width of the first dimension fractionation. For example, a 1 µL injection was used for a one-minute wide fraction, and a 4 µL injection was used for a four-minute wide fraction. While total column load varied for each injection, the amount of each peptide loaded remained constant. Mobile phase A was Optima Grade water with 0.1% formic acid (Fisher), and mobile phase B was Optima-grade acetonitrile with 0.1% formic acid (Fisher). The samples were pre-concentrated on a 180 µm x 20 mm Symmetry C18 trap column with 5 µm particles at 0.5% mobile phase B, and then separated on a 250 mm x 75 µm ID capillary column packed with 1.7 µm silica bridged-ethyl particles with a C18 stationary phase (Waters). At a flow rate of 300 nL/min, a 90 minute gradient from 5-40% B was used to separate the peptides, followed by a 5 minute column wash at 85% B, after which the mobile phase was returned to 5% B. The outlet of the RPLC column was directly connected to an uncoated fused silica nanospray emitter with a 20 µm ID and pulled to a 10 µm tip (New Objective, Woburn, MA) operated at 2.7 kV. Data-independent acquisition, or MS^E scans, was

performed and the instrument was set to acquire parent ion scans from m/z 50-1990 over 0.6 sec at 5.0 V. The collision energy was then ramped from 15-40 V over 0.6 sec.

2.2.7 Equal-mass fractionation

The TIC chromatograms were integrated for the sample set with 40 equal-timed fractions as demonstrated in Figure 2.3. For each fraction, the peak area (A) of that fraction and all previous fractions were summed as follows:

$$\text{Summed Integrated TIC } (\Sigma\int\text{TIC}) = \sum_1^n \text{Area}_n, \tag{2-3}$$

where n=fraction number and Area is the TIC chromatogram peak area.

The normalized $\int$ TIC was plotted versus the first dimension separation time in Figure 2.4. These values were documented in Table 2.2. The y-axis was annotated with hash marks in increments of 0.2, 0.1, or 0.05 which, respectively, split the axis into 5, 10 or 20 equal parts. Lines were drawn from the hash marks on the y-axis to the corresponding x-coordinate on the normalized $\int$ TIC curve. These x-coordinates were used to determine size of the equal-mass first dimension fractions. These fractions were then analyzed by LC-MS/MS as described in the previous section.

2.2.8 Peptide data processing

The peptide LC-MS/MS data were processed using ProteinLynx Global Server 2.5 (Waters). The MS^E spectra were searched against a database of known yeast proteins from the Uni-Prot protein knowledgebase (www.uniprot.org) with a 1X randomized sequence appended to the end. The false discovery rate was set to 100% to yield data compatible for further processing.

After the database search was complete, the results were imported into Scaffold 3.1.4.1 (Proteome Software, Portland, OR). The minimum protein probability and peptide probability

filters were set to a 5% false discovery rate, and the number of peptides required for protein identification was set 3. Peptides matching multiple proteins were exclusively assigned to the protein with the most evidence. The spectral counts for each peptide assigned to a protein were summed to give the quantitative value of that protein. The value was normalized by multiplying the average total number of spectra, for all yeast samples, divided by the individual sample's total number of spectra.[27,28]

2.3 Discussion

2.3.1 Equal-time versus equal-mass fractionation

Herein, the merits of increasing fractionation frequency will be discussed. A comparison will be made between two fractionation techniques, equal-time and equal-mass. The equal-time fractionation method split the first dimension in to evenly timed fractions. The first dimension LC separation attempted to evenly distribute the proteins throughout the separation window. However, few proteins eluted at the beginning and end of the chromatogram with most proteins eluting between 30 to 40% mobile phase B. The equal-mass method attempted to split the first dimension into fractions with equal amounts of protein. As described in the methods section, the first dimension separation was sampled frequently i.e. every minute. The fractions were digested and analyzed by LC-MS. Data from these fractions were used to create the $\Sigma\int$TIC plot in Figure 2.4. For many assays and in many laboratories, time may not be available for extensive method development. As an alternative, the normalized summed absorbance (ΣA) from the first dimension chromatogram was a good approximation to the number of proteins in each fraction (Figure 2.4a). The first dimension separation was followed by UV detection to give a qualitative chromatogram of the separation. The wavelength was set to 280 nm, which is the lambda max of tryptophan. This method is in no way specific for the yeast proteome but is used to monitor the

separation. Summing of the absorbance values began after the void time because the spike in absorbance due to formic acid in the injection plug did not correlate to the number of proteins identified in these fractions. This fractionation scheme was analogous to dividing the UV chromatogram into parts with equal area under the curve as seen in Figure 2.4b-d.

The first dimension separation produced 40 fractions. Analyzing all the fractions by LC-MS^E took 80 hours which was longer than most proteomics laboratories would be willing to spend on a single sample. The time requirement would be even worse when considering that a study may include 3 biological replicates and at least two sample types. Therefore, it was important to investigate the benefits, which may include protein identifications and protein coverage, of increasing prefractionation frequency.

As fractionation frequency was increased, peak capacity also increased. By coupling the separation with mass spectrometry, it was not necessary to fully resolve the peptides chromatographically because the analytes were also resolved by their mass-to-charge ratio. Increasing the fractionation frequency also diluted the analytes and at a certain frequency a protein may have been split between multiple fractions. At this point, the intensity of its peptide peaks may have dropped below the limit of detection. This trend is demonstrated in Figure 2.5. As the number of first dimension fractions increased from 5 to 10 to 20, more proteins were identified but the graph leveled off between 20 and 40 fractions. Also, the equal-mass fractionation method identified more proteins than the equal-time fractionation method at every level of fractionation frequency.

To understand the differences between the fractionation methods qualitatively, the 2D chromatograms in Figure 2.6, Figure 2.7, Figure 2.8, and Figure 2.9 should be considered. The vertical axis represented the first dimension protein separation, and the x-axis showed the second

dimension peptide separation. The peak height was represented by false color in the z-direction. For the chromatograms of the equal-time fractions, the number of peaks decreased towards the end of the chromatogram. This corresponds to fractions 30-40 in Figure 2.6, 16-20 in Figure 2.7a, 8-10 in Figure 2.8a, and fraction 5 in Figure 2.9a. In fact, the same trypsin autolysis peaks dominated the chromatograms of these fractions. In comparison, the equal-mass chromatograms appeared to have unique bands for each fraction.

2.3.2 Proteins per fraction

To confirm that more proteins were identified in the late eluting fractions of the equal-mass method, the number of protein identifications was plotted for each fraction in the bar graphs in Figure 2.10, Figure 2.11, Figure 2.12, and Figure 2.13. The light gray bars showed the total number of proteins identifications in each fraction, and the dark gray bars signified the number of unique proteins found in each fraction. Proteins found in multiple fractions were assigned to the fraction in which it was most intense. The first eluting fractions, corresponding to the injection plug, contained few protein identifications. A couple of factors may have contributed to the low number of identifications. (1) There were no proteins eluting in the injection plug. (2) The injection plug contains large proteins or agglomerated proteins that were excluded from the stationary phase. Large proteins were often difficult to digest because they did not fully denature blocking trypsin from the digestion sites. The total number of proteins identified in the late eluting fractions remained relatively constant for both the equal-time and equal-mass fractionation methods. However, the number of unique protein identifications in the late eluting fractions was greater for the equal-mass than the equal-time fractionation method. For the equal-mass fractions, the number of unique protein identifications was more even fraction to fraction. With the instrumentation used for this experiment, it seemed that a limited

maximum number of proteins could be identified per fraction. By more evenly distributing the proteins between the fractions, as achieved with the equal-mass fractionation method, the number of unique protein identifications increased. Figure 2.5 showed a 19% increase in identifications for 5 fractions, 22% for 10 fractions, and 10% for 20 fractions.

2.3.3 Venn comparison

The Venn diagram of proteins identifications in Figure 2.14a showed that most of the proteins identified in the 5 equal-time fractions were also identified in the 10 equal-time fractions. Additionally, 103 new proteins were identified with only 9 identifications lost which yielded an improvement of 40%. Similarly, when equal-time fractionation was increased to 20, 175 more identifications were made with only a loss of 8 identifications which was also a gain of 40%. A similar trend was observed for the equal-mass fractions in Figure 2.15. However, the Venn diagram in Figure 2.14b showed that while 78 new proteins were identified in the 40 equal-time fractions, 41 were lost. In doubling the analysis time, protein identifications were only improved by 9%. It was hypothesized that the loss of 41 protein identifications was due to proteins being split between multiple fractions.

2.3.4 Fractions per protein

Ideally, a protein peak should not be split between multiple fractions. The probability of peak splitting increases as fractionation frequency increases. Also, a protein may have appeared in multiple fractions due to different post translational modifications and variations in its tertiary structure. To determine the amount of peak splitting between multiple first dimension fractions, the percentage of protein identifications that were identified in only one fraction, two fractions, and three-or-more fractions were plotted in Figure 2.16. For every fractionation scheme, the majority of the proteins were identified in only one fraction. The highest percentage of proteins

being identified in only one fraction occurred when only 5 first dimension fractions were taken. This percentage decreased as fractionation frequency increased. The percentage of proteins identified in multiple fractions was similar for the 5 and 10 first dimension fraction sets. A nearly 50% increase of proteins found in multiple fractions was observed when prefractionation was increased to 20 and 40 fractions. When considering the equal-mass fractionation method, a larger portion of proteins was identified in only one fraction as compared to the equal-time fractionation method. For example, 80% of the proteins were identified in only one fraction in the 5 equal-mass fractionation set, and 70% of proteins were identified in only one fraction in the 5 equal-time fractionation set. A larger percentage of proteins were identified in 3 or more fractions by the equal-time than the equal-mass fractionation method.

2.3.5 Normalized Difference Protein Coverage

When discussing the merit of multidimensional proteomic separations, it was not merely enough to report the total number of proteins identifications without further commenting on protein coverage. To compare the methods, coverage is reported in Table 2.3. for several proteins involved in the metabolic processes of yeast. On average, coverage increased with higher fractionation frequency. For a large data set containing hundreds of proteins, comparing the coverage for each protein is not straight forward. For example, reducing protein coverage to an average can be misleading. The additional proteins identified in a separation with higher peak capacity were usually of lower abundance and had lower coverage, bringing down the average. Alternatively, comparing only proteins identified by both methods would limit the analysis to only easily detectible proteins which usually had higher coverage and, thus, mute the difference between the methods. Herein, an original method to compare protein coverage based on the mathematical concept of a normalized difference is described. We named this metric the

normalized difference protein coverage (NDPC) and define it as the difference in coverage of a protein between two methods divided by the sum of the coverage. The NDPC was calculated as follows:

$$\text{NDPC} = \frac{\text{Coverage}_{a,i} - \text{Coverage}_{a,j}}{\text{Coverage}_{a,i} + \text{Coverage}_{a,j}}, \tag{2-4}$$

where $Coverage_{a,i}$ was the percent coverage of protein a in method i, and $Coverage_{a,j}$ was the percent coverage of protein a in method j. For example, the NDPC for fumarate hydratase (FUMH), a protein involved in the citric acid cycle of *S. cerevisiae*, was calculated to compare 10 equal-time and 10 equal-mass fractions:

$$\text{NDPC} = \frac{\text{Coverage}_{\text{FUMH,10 equal-mass}} - \text{Coverage}_{\text{FUMH,10 equal-time}}}{\text{Coverage}_{\text{FUMH,10 equal-mass}} + \text{Coverage}_{\text{FUMH,10 equal-time}}}, \tag{2-5}$$

$$= \frac{52-36}{52+36} = 0.19 \tag{2-6}$$

With this example, a protein found with higher coverage in the 10 equal-mass fractions would have a positive NDPC. A negative NDPC would signify that the protein was found with higher coverage in the 10 equal-time fractions. A value of +1 meant the protein was only identified in the 10 equal-mass fractions, and a value of -1 meant the protein was only identified in the 10 equal-time fractions. The equal-time and equal-mass prefractionation methods were compared for 5 fractions in Figure 2.17, for 10 fractions in Appendix A.1. and for 20 fractions in Appendix A.2. The NDPC values were plotted with the proteins ordered from largest to smallest denominator, putting the proteins with highest coverage on the left, and the lowest coverage on the right. The absolute values of NDPC increased as the denominator (summed protein coverage) decreased. These figures were large and split amongst several pages. To better comprehend the trend, the protein identifier information was removed so the graph could fit onto a single page. The abundance of red lines in Figure 2.18.a. and Figure 2.18.b. signified higher coverage in the 5

and 10 equal-mass fractions. When fractionation increased to 20 (Figure 2.18.c.), there was little difference in coverage between the two methods.

In an attempt to further simplify the comparison of coverage between multiple methods, while maintaining the meaning of the values, we propose the Grand NDPC which is calculated by the difference between the grand total protein coverage in method one and method two normalized by the grand sum of protein coverage in both methods. An example calculation is shown in Equation 2-5:

$$\text{Grand NDPC} = \frac{(\sum \text{Coverage}_{\text{method 1}}) - (\sum \text{Coverage}_{\text{method 2}})}{\sum \text{Coverage}_{\text{method 1}} + \sum \text{Coverage}_{\text{method 2}}} \quad (2\text{-}7)$$

Perhaps a more relevant interpretative of the Grand NDPC would be to relate it to a fold-change improvement in coverage as follows:

$$\text{Fold-Change in Coverage} = \frac{\sum \text{Coverage}_{\text{method 1}}}{\sum \text{Coverage}_{\text{method 2}}} = \frac{1 + \text{Grand NDPC}}{1 - \text{Grand NDPC}} \quad (2\text{-}8)$$

If the fold-change was less than one, the negative reciprocal of the value was used as is conventional with fold-change calculations. The Grand NDPC and Fold-Change in Coverage is listed in Table 2.4 for each fractionation frequency. Positive values represented higher coverage with the equal-mass fractionation method, and negative values represented higher coverage with the equal-time fractionation method. The Grand NDPC and Fold-Change Coverage increased in favor of the equal-mass method for 5 and 10 fractions. The largest fold-change improvement was 1.4 with the 10 fraction comparison. No significant difference in coverage was observed between the two methods with 20 first dimension fractions.

2.4 Conclusion

While this was a limited study of only one organism, it can serve as a guide for multidimensional method development with prefractionation. Protein identifications increased as

fractionation frequency was increased. These benefits had diminishing returns with respect to time as prefractionation increased to more than 20 fractions. The equal-mass prefractionation method proved to be a good technique to get more information out of a sample in the same amount of time as compared to the equal-time fractionation method. Future improvements could be made to the second dimension separation. The use of a LC with higher pressure limitations could make possible the use of smaller particles and longer columns to improve peak capacity without increasing analysis time.

2.5 TABLES

Time (min)	Flow Rate (mL/min)	90:5:5 H_2O:ACN:IPA + 0.2% TFA (%A)	50:50 ACN:IPA + 0.2% TFA (%B)
0	1.0	100	0
2	1.0	100	0
5	1.0	75	25
40	1.0	50	50
45	1.0	35	65
45.1	1.0	0	100
50	1.0	0	100
50.1	1.0	100	0

Table 2.1. Chromatographic conditions for the reversed-phase prefractionation of intact proteins.

	Integrated TIC of 40 Fractions					
Fraction	Rep 1 ($x10^7$)	Rep 2 ($x10^7$)	Rep 3 ($x10^7$)	Average	Summed	Normalized
1	0.38	0.31	0.20	0.30	0.30	0.00
2	0.64	0.32	0.21	0.39	0.68	0.01
3	1.93	0.96	1.15	1.35	2.03	0.02
4	2.22	1.26	1.29	1.59	3.62	0.03
5	1.92	2.03	1.40	1.78	5.40	0.05
6	4.59	4.56	3.07	4.07	9.48	0.09
7	6.31	3.94	4.11	4.78	14.26	0.13
8	6.20	5.32	4.32	5.28	19.54	0.18
9	3.42	3.42	2.48	3.11	22.65	0.20
10	2.98	2.18	2.02	2.40	25.04	0.23
11	2.96	2.37	1.98	2.43	27.48	0.25
12	2.97	2.26	1.85	2.36	29.84	0.27
13	4.14	3.19	2.22	3.18	33.02	0.30
14	3.43	2.65	2.21	2.76	35.78	0.32
15	4.73	4.25	3.12	4.03	39.81	0.36
16	6.01	5.86	3.66	5.18	44.99	0.41
17	9.41	8.76	5.37	7.85	52.84	0.48
18	6.23	6.27	3.89	5.46	58.30	0.53
19	8.47	6.16	5.01	6.55	64.84	0.59
20	8.64	6.01	4.82	6.49	71.34	0.64
21	8.14	4.85	3.92	5.64	76.97	0.69
22	9.03	5.65	4.64	6.44	83.41	0.75
23	5.82	3.00	2.59	3.80	87.22	0.79
24	5.94	2.67	3.01	3.87	91.09	0.82
25	6.32	5.01	3.92	5.09	96.18	0.87
26	3.27	2.26	2.26	2.60	98.77	0.89
27	2.95	1.84	2.02	2.27	101.04	0.91
28	1.99	1.22	1.44	1.55	102.59	0.93
29	2.22	0.95	1.39	1.52	104.11	0.94
30	0.21	0.82	1.10	0.71	104.82	0.95
31	1.16	0.53	0.78	0.83	105.65	0.95
32	1.05	0.48	0.76	0.76	106.41	0.96
33	0.54	0.25	0.44	0.41	106.82	0.96
34	1.02	0.41	0.55	0.66	107.48	0.97
35	0.89	0.37	0.54	0.60	108.08	0.98
36	0.80	0.28	0.50	0.53	108.61	0.98
37	0.91	0.37	0.64	0.64	109.25	0.99
38	0.81	0.26	0.61	0.56	109.81	0.99
39	0.60	0.22	0.52	0.44	110.26	1.00
40	0.65	0.26	0.63	0.52	110.77	1.00

Table 2.2. Integrated TIC values, summed integrated TIC, and normalized summed integrated TIC value used to determine first dimension fractionation schemes.

		Protein Coverage (%)						
		Number of equal-time fractions				Number of equal-mass fractions		
Name	Accession	5	10	20	40	5	10	20
6-phosphogluconate dehydrogenase	6PGD1	61%	39%	76%	70%	29%	54%	63%
Isocitrate lyase	ACEA	-	-	29%	38%	3%	31%	41%
Aconitate hydratase, mito	ACON	38%	46%	47%	49%	44%	48%	40%
Acetyl-coenzyme A synthetase 1	ACS1	25%	30%	51%	49%	24%	42%	55%
Alcohol dehydrogenase 1	ADH1	60%	58%	65%	69%	62%	69%	59%
Alcohol dehydrogenase 2	ADH2	66%	72%	71%	73%	69%	73%	67%
Alcohol dehydrogenase 3, mito	ADH3	8%	-	19%	17%	-	22%	18%
Alcohol dehydrogenase 6	ADH6	-	-	3%	-	-	-	-
K-activated aldehyde dehydrogenase	ALDH4	75%	72%	81%	88%	75%	87%	83%
Aldehyde dehydrogenase 5, mito	ALDH5	-	-	-	-	-	-	-
Fructose-bisphosphate aldolase	ALF	69%	76%	69%	81%	73%	71%	75%
Citrate synthase, mito	CISY1	31%	35%	52%	57%	45%	53%	61%
Dihydrolipoyl dehydrogenase, mito	DLDH	39%	38%	77%	70%	32%	39%	72%
Enolase 1	ENO1	73%	80%	79%	83%	76%	84%	81%
Enolase 2	ENO2	76%	78%	86%	87%	83%	81%	87%
Fumarate reductase	FRDS	-	8%	21%	24%	6%	22%	25%
Fumarate hydratase, mitoc	FUMH	26%	36%	43%	53%	27%	52%	49%
Glyceraldehyde-3-P dehydrogenase 1	G3P1	71%	70%	85%	77%	74%	79%	76%
Glyceraldehyde-3-P dehydrogenase 2	G3P2	83%	71%	89%	87%	83%	84%	88%
Glyceraldehyde-3-P dehydrogenase 3	G3P3	90%	78%	92%	90%	91%	92%	91%
Glucose-6-phosphate isomerase	G6PI	61%	60%	69%	60%	52%	64%	65%
Hexokinase-1	HXKA	52%	56%	80%	75%	50%	68%	76%
Hexokinase-2	HXKB	60%	53%	84%	74%	61%	67%	69%
Glucokinase-1	HXKG	54%	40%	69%	68%	57%	72%	67%
6-phosphofructokinase subunit α	K6PF1	8%	8%	32%	28%	24%	31%	24%
Pyruvate kinase 1	KPYK1	59%	68%	85%	81%	76%	83%	81%
Malate dehydrogenase, cyto	MDHC	26%	35%	64%	44%	22%	39%	52%

		Protein Coverage (%)						
		Number of equal-time fractions				Number of equal-mass fractions		
Name	Accession	5	10	20	40	5	10	20
Malate dehydrogenase, mito	MDHM	75%	78%	74%	76%	68%	82%	76%
Pyruvate dehydrogenase E1 comp β	ODPB	-	-	17%	29%	-	9%	33%
Phosphoenolpyruvate carboxykinase	PCKA	41%	53%	59%	61%	46%	57%	59%
Pyruvate decarboxylase isozyme 1	PDC1	63%	65%	74%	74%	55%	68%	67%
Phosphoglycerate kinase	PGK	79%	70%	84%	86%	83%	88%	84%
Phosphoglycerate mutase 1	PMG1	76%	79%	76%	69%	78%	76%	54%
Pyruvate carboxylase 1	PYC1	-	-	18%	38%	-	4%	38%
Succinyl-CoA ligase subunit α	SUCA	60%	67%	84%	71%	60%	72%	69%
Succinyl-CoA ligase subunit β	SUCB	-	16%	38%	37%	13%	38%	30%
Transketolase 1	TKT1	15%	22%	43%	51%	27%	54%	49%
Transketolase 2	TKT2	-	-	6%	20%	-	14%	21%
Triosephosphate isomerase	TPIS	76%	75%	82%	89%	80%	88%	86%
Average		55%	54%	60%	62%	53%	58%	60%

Table 2.3. The protein coverage (%) was reported for some of the proteins involved in *S. cerevisiae* metabolism. Generally, protein coverage increased with fractionation frequency.

Number of Fractions	Grand NDPC	Fold-Change in Coverage
5	0.050	1.1
10	0.17	1.4
20	-0.0093	-1.0

Table 2.4. The Grand NDPC and Fold-Change in Coverage was listed in for each fractionation frequency. Positive values represented higher coverage with the equal-mass fractionation method, and negative values represented higher coverage with the equal-time fractionation method. The Grand NDPC and Fold-Change in Coverage favored of the equal-mass method for 5 and 10. The largest fold-change improvement was 1.4 with the 10 fraction comparison. No significant difference in coverage was observed between the two methods with 20 first dimension fractions.

2.6 FIGURES

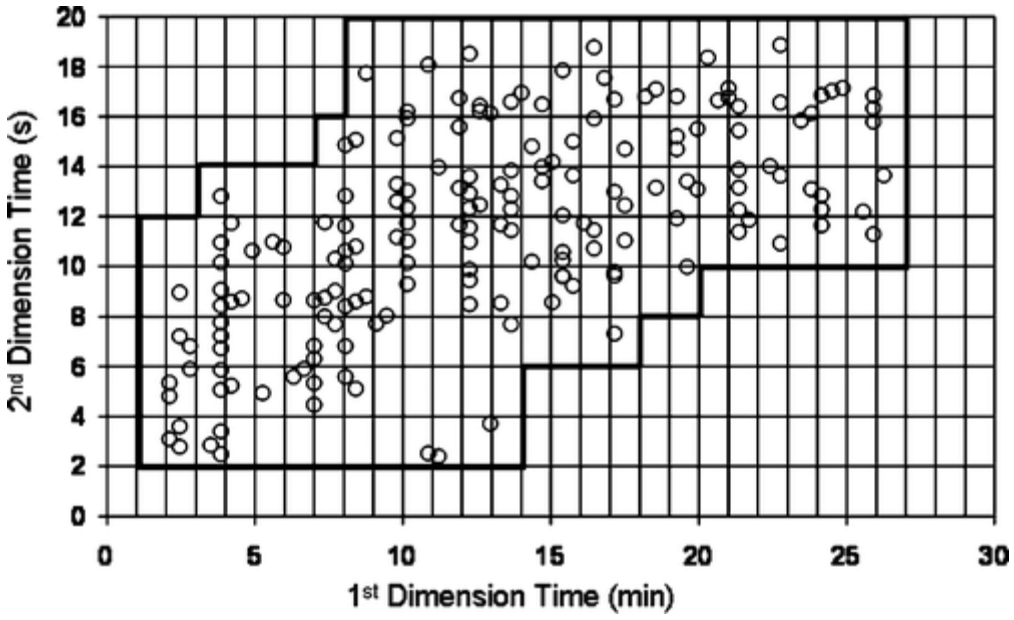

Figure 2.1. This 2D chromatogram was divided in to bins by Davis and coworkers.[7] A perimeter was drawn around the bins containing a circle, which represented a sample peak, to illustrate the orthogonality of the separation.

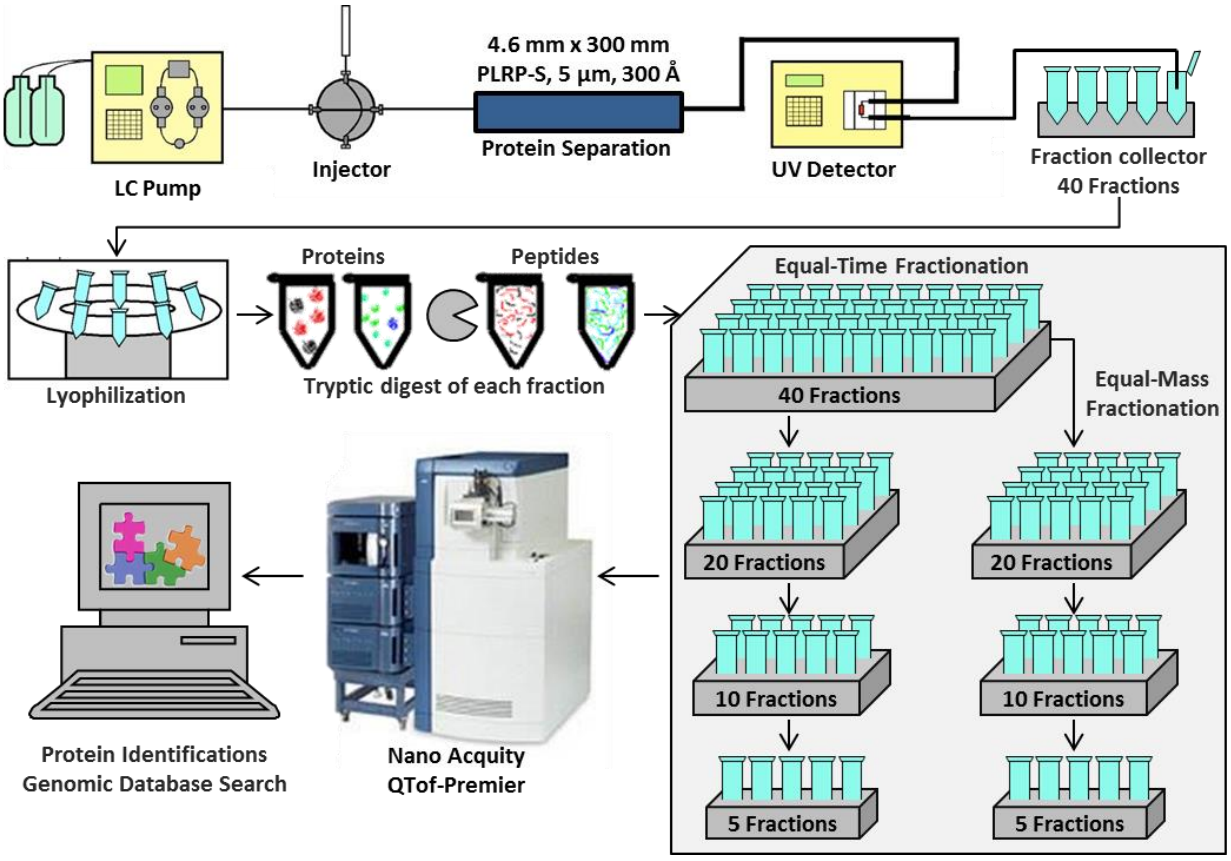

Figure 2.2. The workflow for the prefractionation method started with HPLC-UV of the intact proteins. Forty fractions were collected, lyophilized, and digested with trypsin. The forty one-minute-wide fractions were pooled into 20, 10, and 5 equal-time and equal-mass fractions before the second dimension analysis by UPLC-MS. The spectral data was searched against a genomic database to identify the proteins.

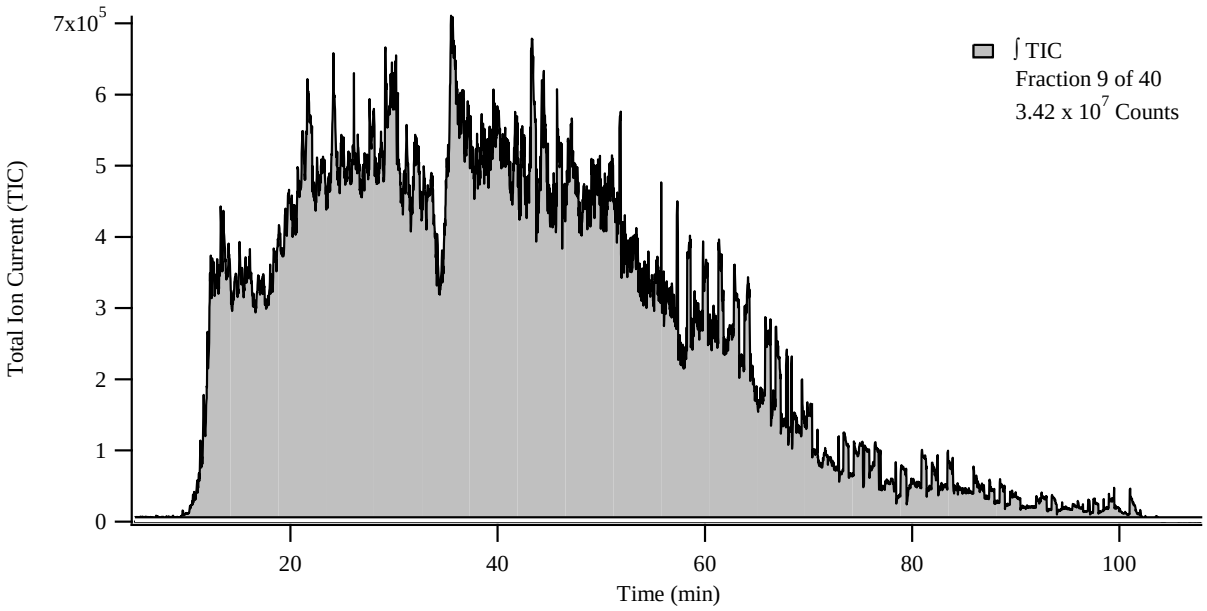

Figure 2.3. The representative TIC chromatogram from a peptide (second dimension) separation of the 40 equal-time fraction set showed an example of peak integration. The peak area was the ∫TIC value used in Table 2.2 for the determination of the equal-mass prefractionation schemes.

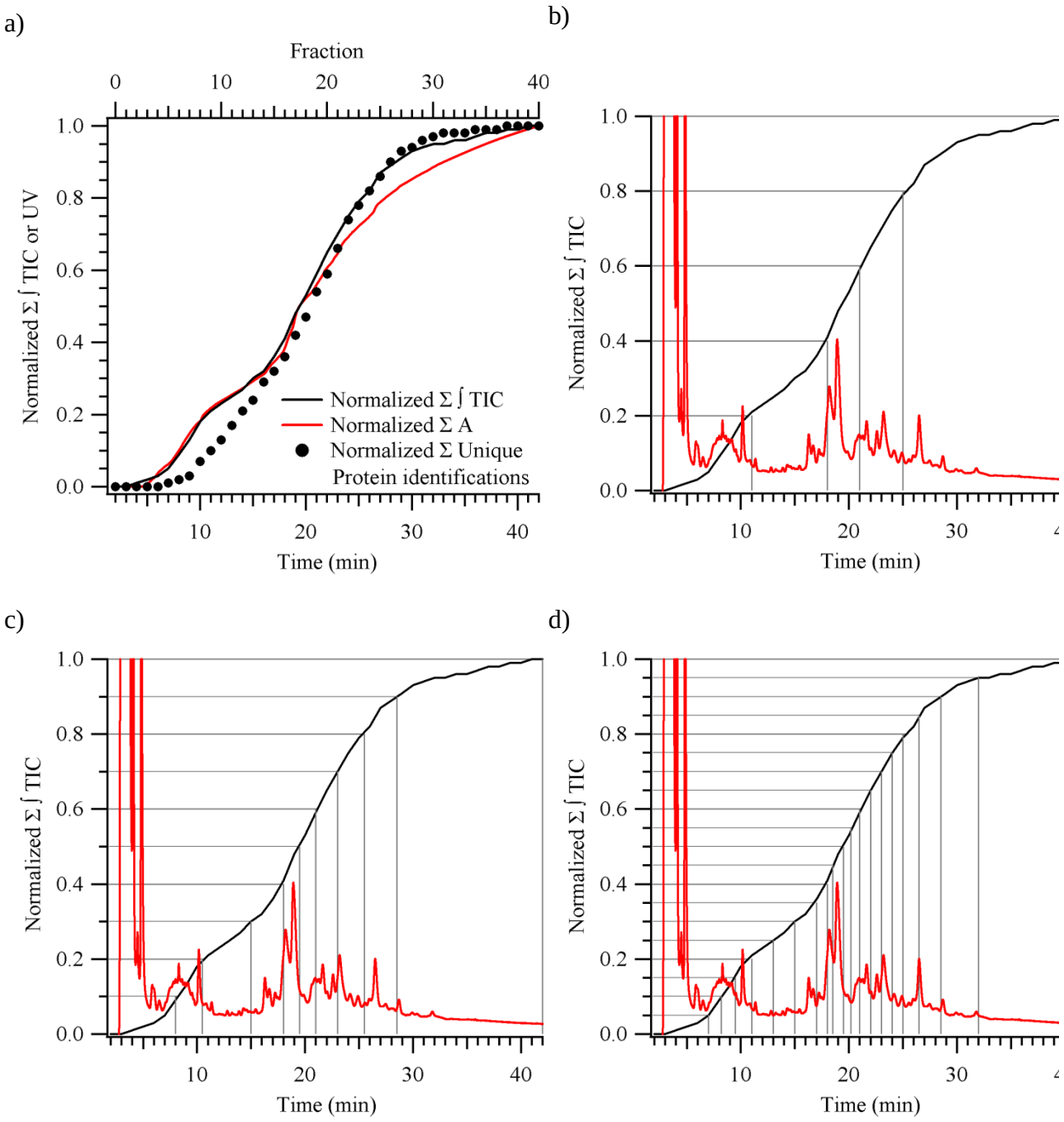

Figure 2.4. (a) The normalized Σ∫TIC, Σ absorbance, and summed unique protein count were plotted versus the first dimension separation time and fraction number. The similarity of the three traces should be noted. The y-axis was annotated with hash marks in increments of 0.2, 0.1, or 0.05, as shown in parts (b), (c), and (d), respectively. Lines were drawn from the hash marks on the y-axis to the corresponding x-coordinate on the normalized equal-mass curve. These x-coordinates were used to determine size of the first dimension fractions.

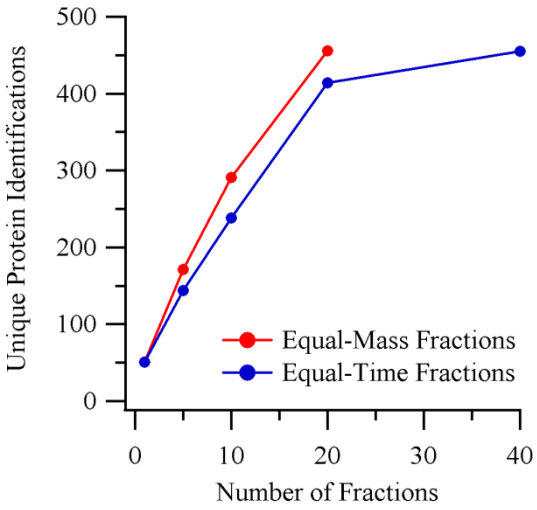

Figure 2.5. The number of protein identifications was plotted versus number of first dimension fractions. The blue and red traces were for the equal-time and equal-mass fractionation methods, respectively. The number of protein identifications increased with increased prefractionation up to 40 fractions. At all prefractionation frequencies, the equal-mass prefractionation method outperformed the equal-time prefractionation method.

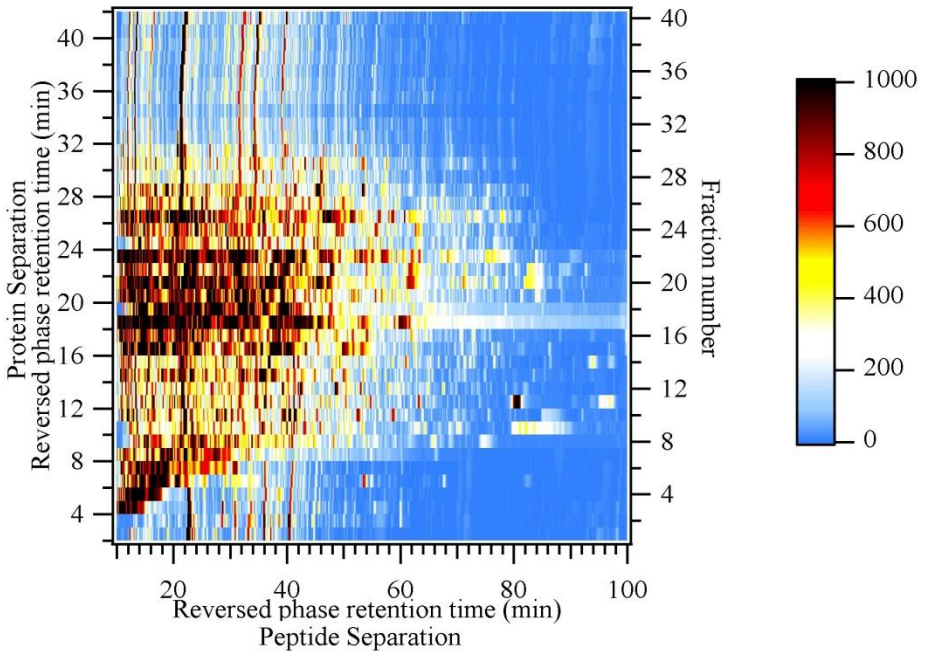

Figure 2.6. The 2D chromatogram for 40 first dimension fractions was plotted with the first dimension (protein) separation time and fraction number plotted on the vertical axes and the second dimension (peptide) separation on the bottom axis. Starting with fraction 30, the peak pattern repeated for all subsequent fractions. These peaks corresponded to peptides from trypsin autolysis.

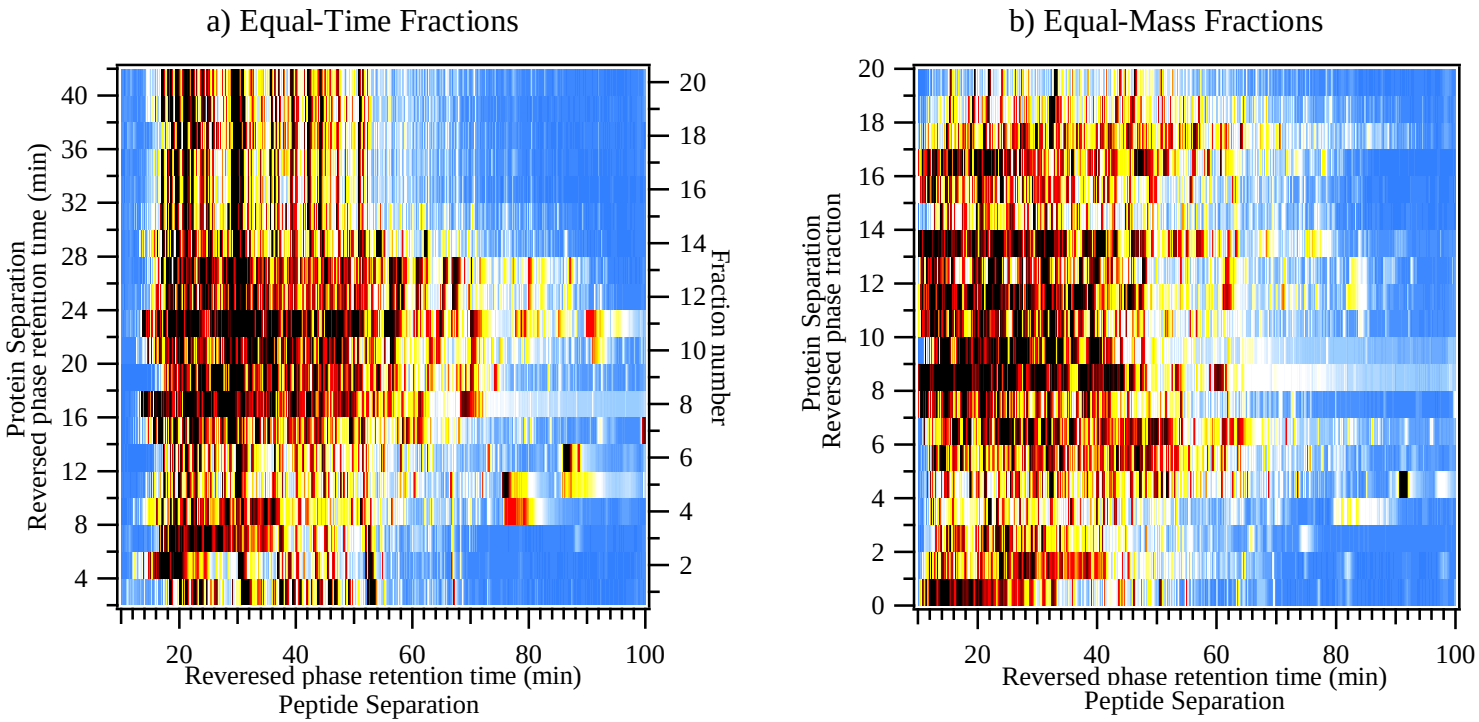

Figure 2.7. The 2D chromatograms for 20 first dimension fractions were plotted with the first dimension (protein) separation time or fraction number plotted on the vertical axes and the second dimension (peptide) separation on the bottom axis. Peak intensity was plotted in the z-direction. In the later eluting fractions, more peaks were observed in (b) the equal-mass fractionation chromatogram than in (a) the equal-time fractionation chromatogram.

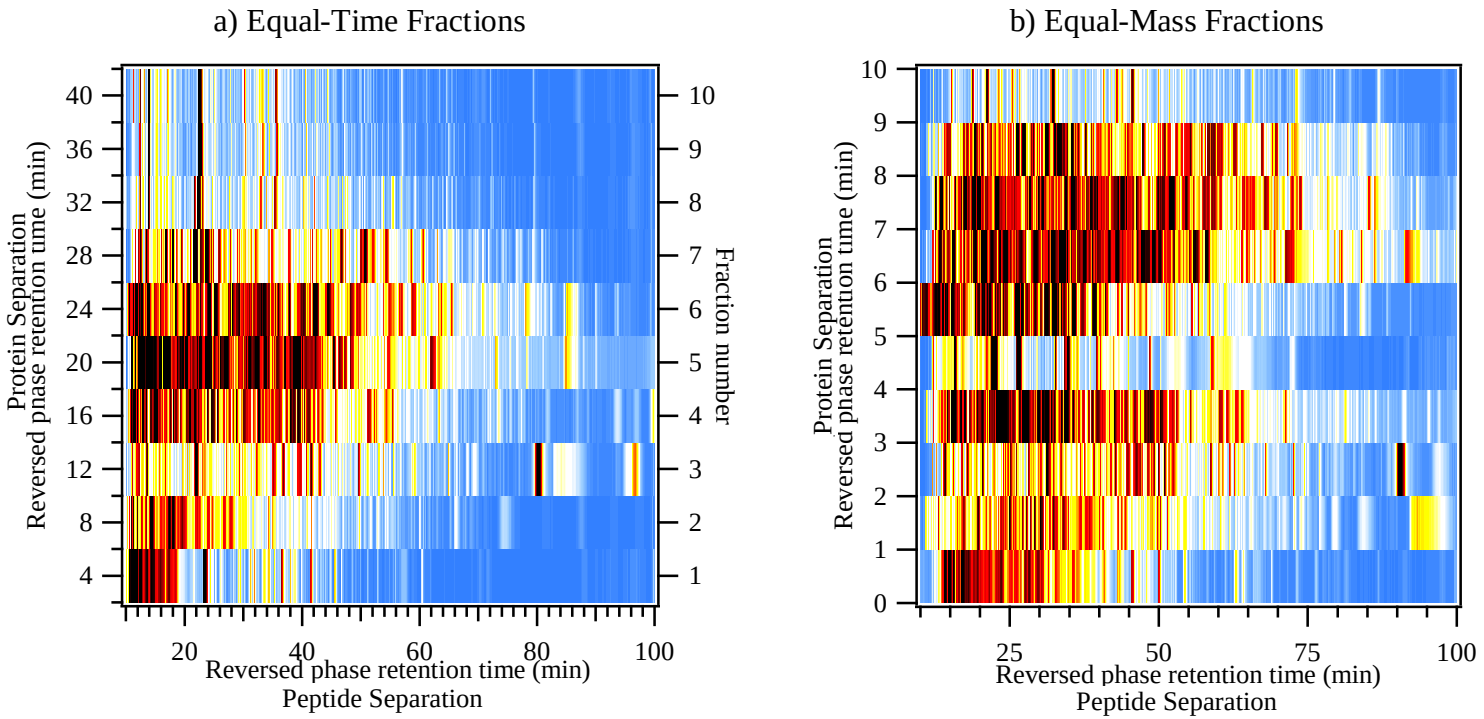

Figure 2.8. The 2D chromatograms for 10 first dimension fractions were plotted with the first dimension (protein) separation time or fraction number plotted on the vertical axes and the second dimension (peptide) separation on the bottom axis. Peak intensity was plotted in the z-direction. In the later eluting fractions, more peaks were observed in (b) the equal-mass fractionation chromatogram than in (a) the equal-time fractionation chromatogram.

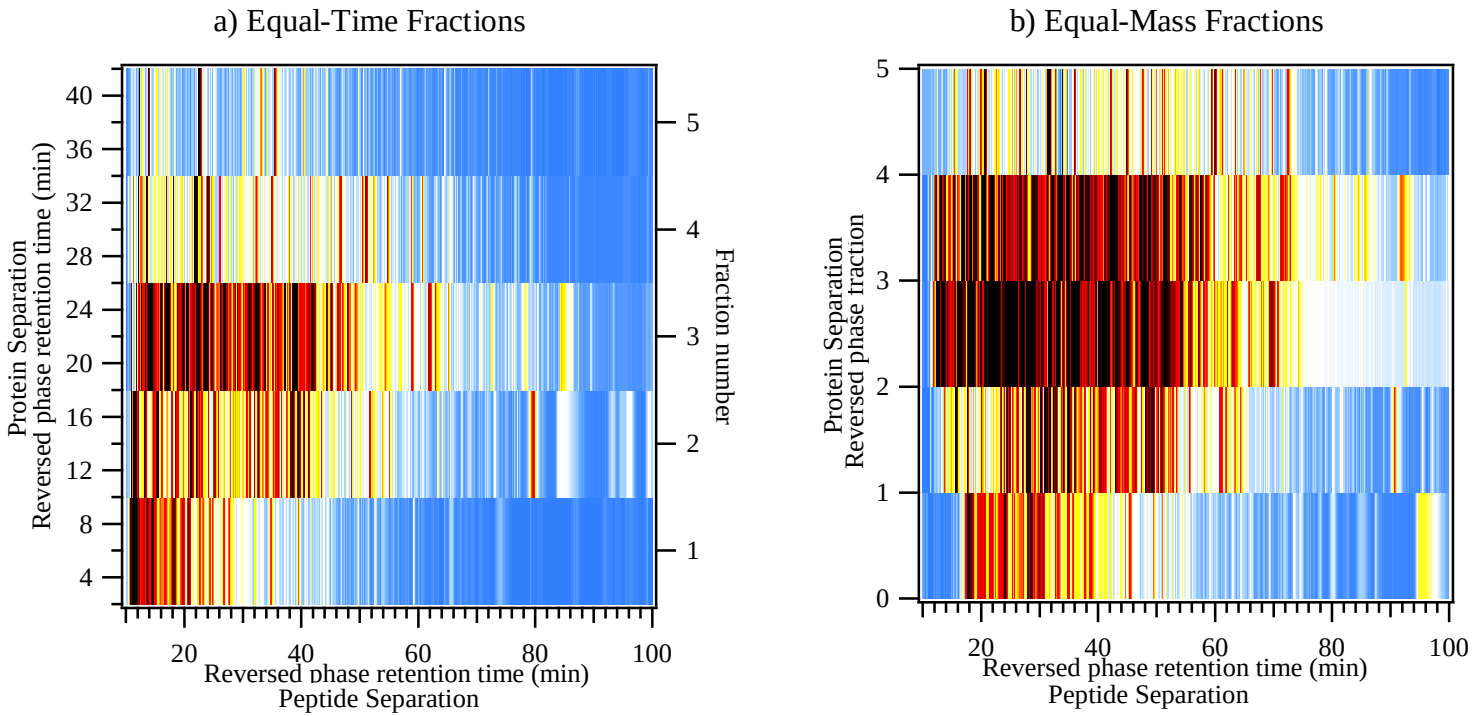

Figure 2.9. The 2D chromatograms for 5 first dimension fractions were plotted with the first dimension (protein) separation time or fraction number plotted on the vertical axes and the second dimension (peptide) separation on the bottom axis. Peak intensity was plotted in the z-direction. In the later eluting fractions, more peaks were observed in (b) the equal-mass fractionation chromatogram than in (a) the equal-time fractionation chromatogram.

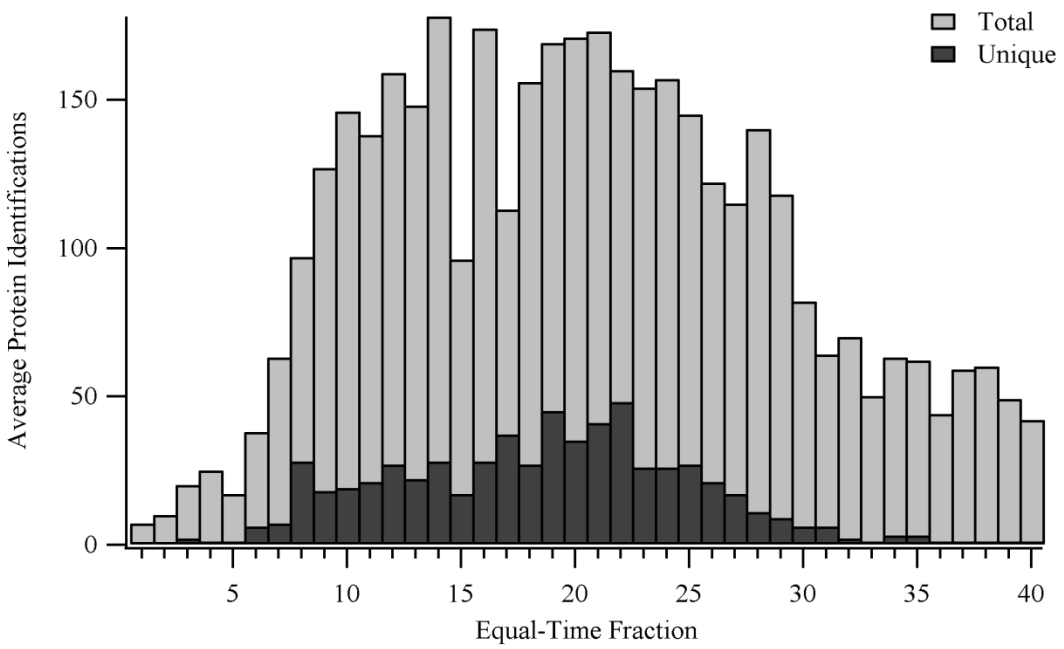

Figure 2.10. The light gray bars show the total protein identifications in each fraction, and the dark gray bars signify the unique protein identifications in each fraction for 40 first dimensional fractions. The number of unique protein identifications decreased in the last 15 fractions faster than the total protein identifications. This trend was less pronounced as prefractionation frequency decreased.

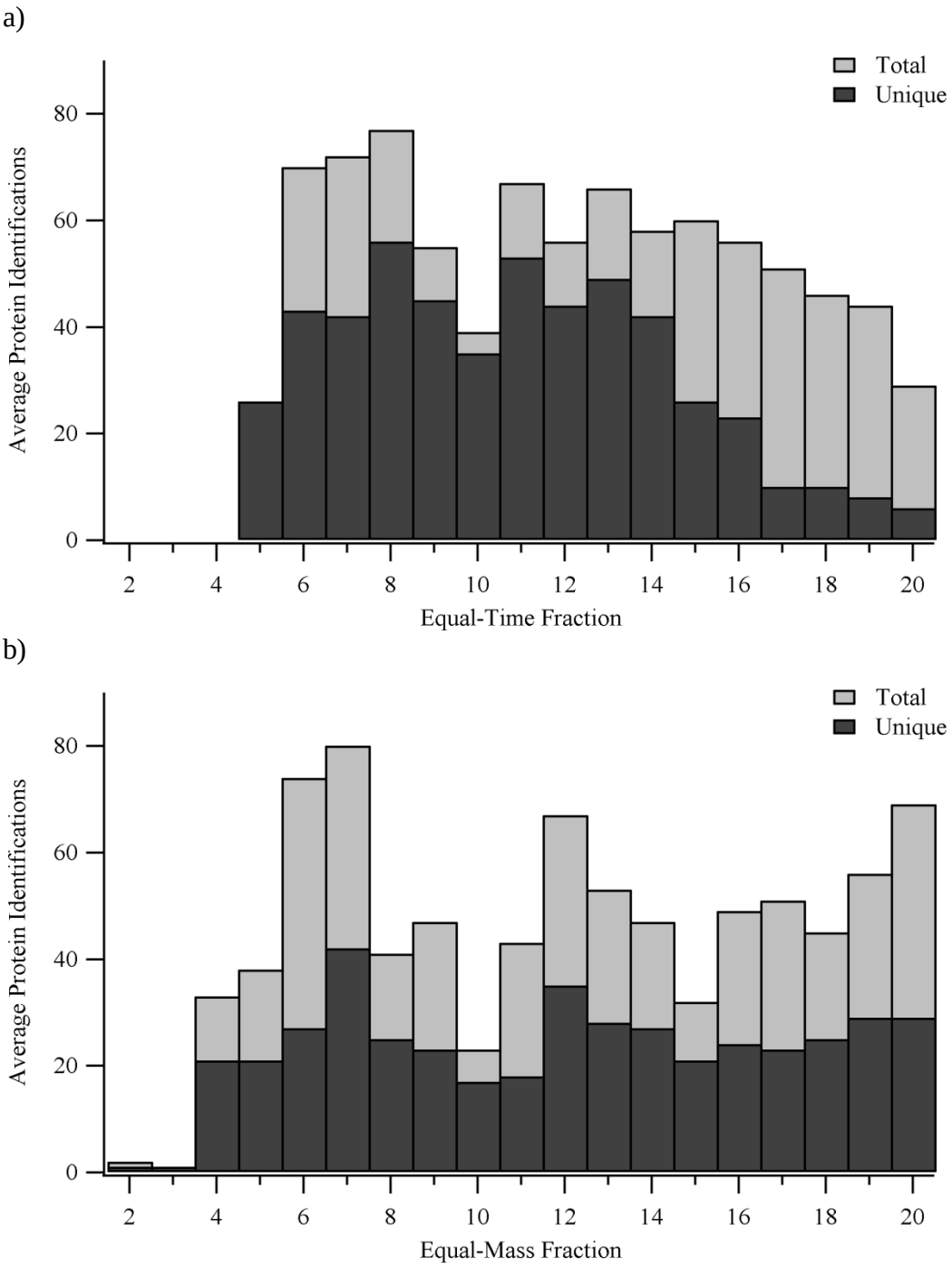

Figure 2.11. The light gray bars show the total protein identifications in each fraction, and the dark gray bars signify the unique protein identifications in each fraction for 20 first dimensional fractions. By more evenly distributing the sample mass between the fractions, as with the equal-mass fractionation method (b), the number of unique protein identifications was more even fraction to fraction and increased in the late eluting fractions as compared to the equal-time fractionation method (a).

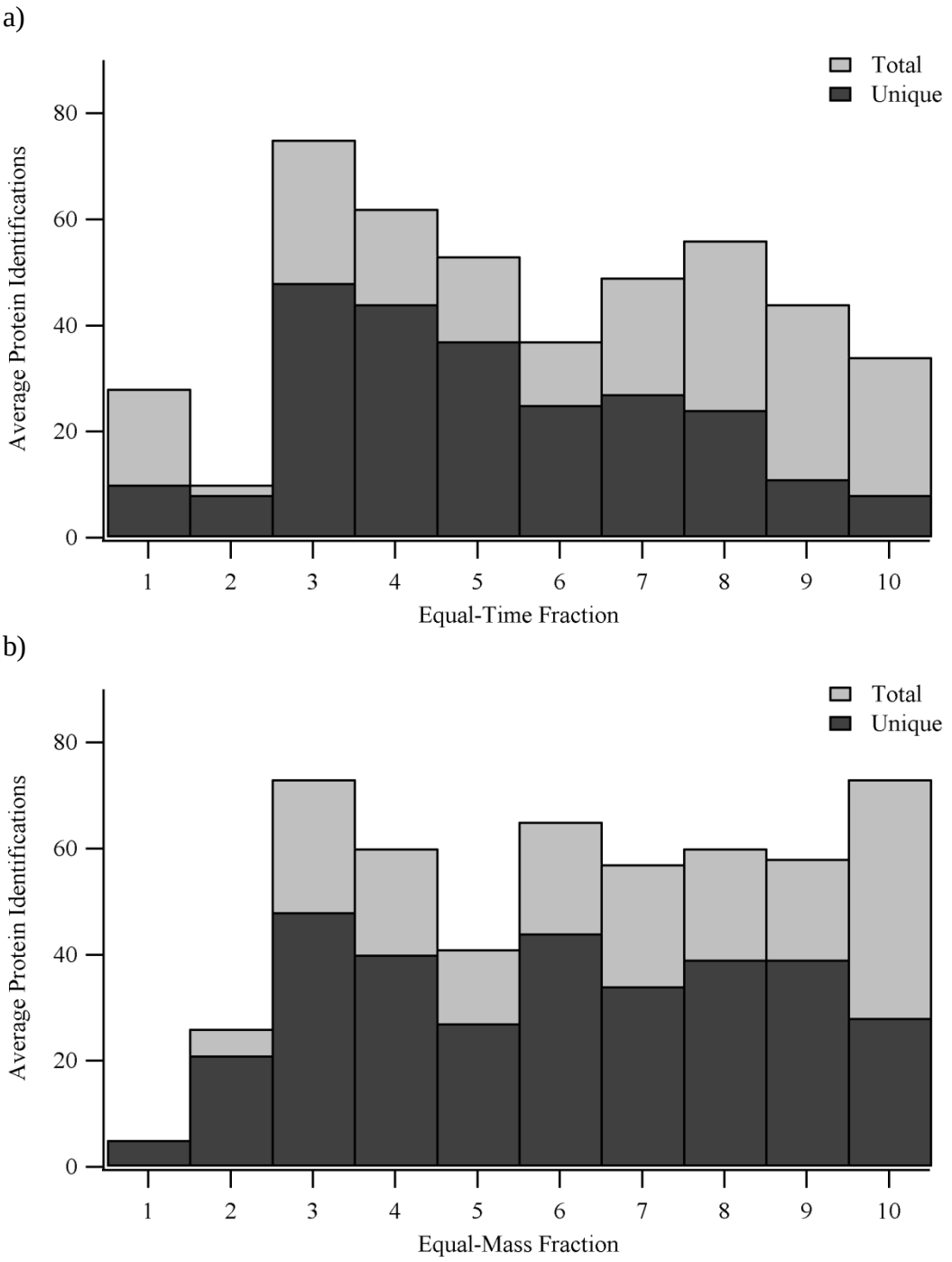

Figure 2.12. The light gray bars show the total protein identifications in each fraction, and the dark gray bars signify the unique protein identifications in each fraction for 10 first dimensional fractions. By more evenly distributing the sample mass between the fractions, as with the equal-mass fractionation method (b), the number of unique protein identifications was more even fraction to fraction and increased in the late eluting fractions as compared to the equal-time fractionation method (a).

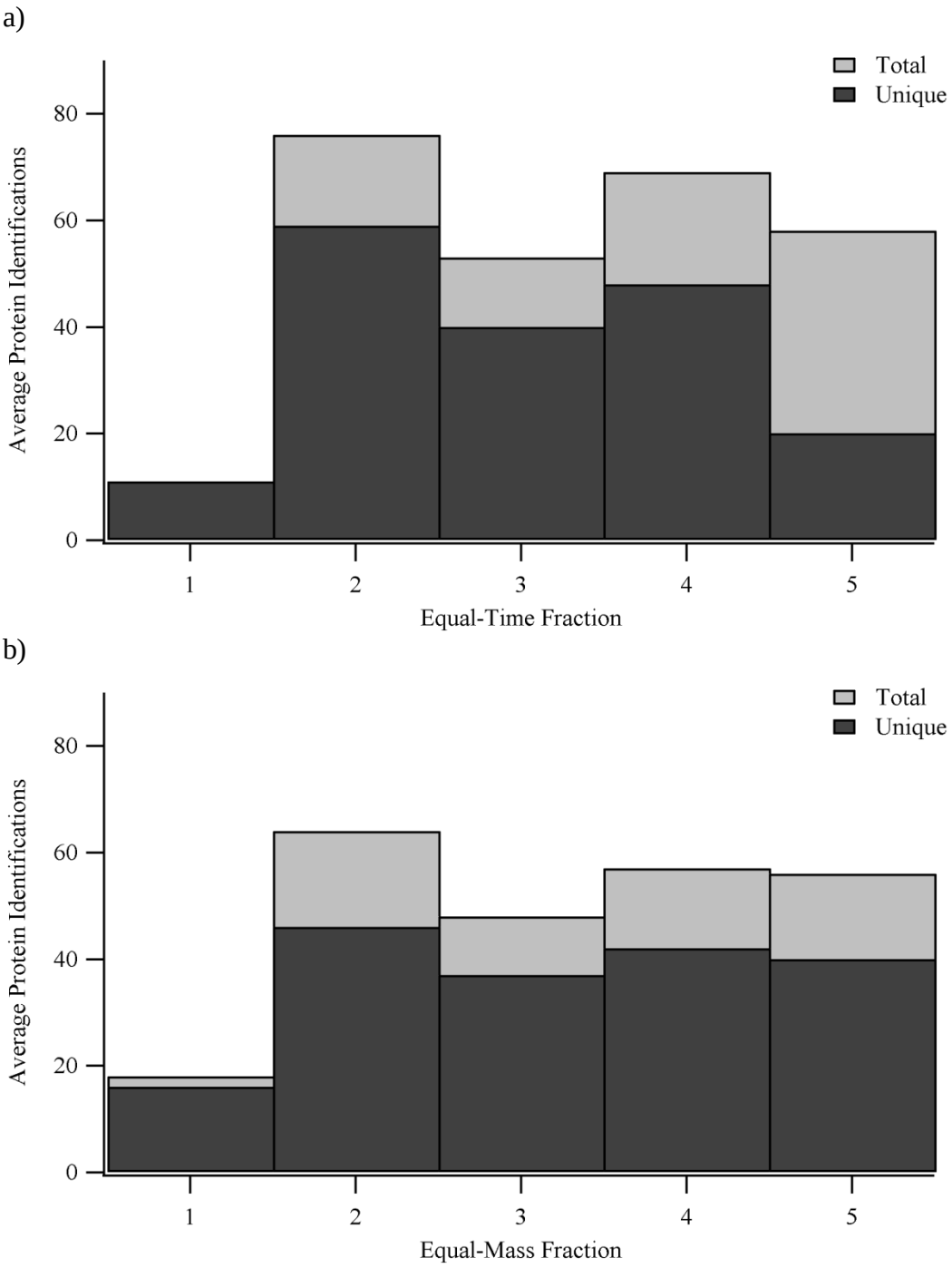

Figure 2.13. The light gray bars show the total protein identifications in each fraction, and the dark gray bars signify the unique protein identifications in each fraction for 5 first dimensional fractions. By more evenly distributing the sample mass between the fractions, as with the equal-mass fractionation method (b), the number of unique protein identifications was more even fraction to fraction and increased in the late eluting fractions as compared to the equal-time fractionation method (a).

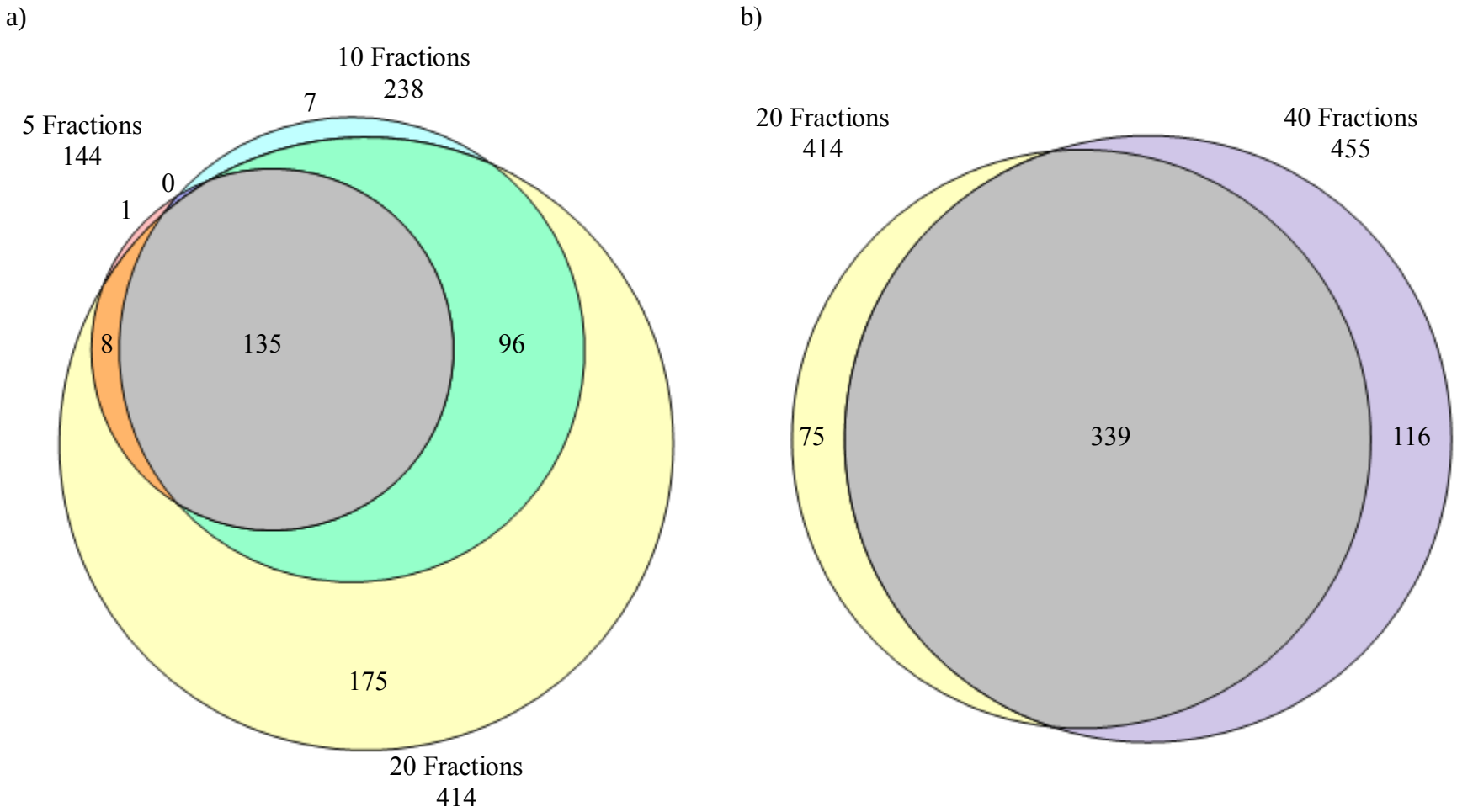

Figure 2.14. Venn diagram (a) showed the overlap in protein identifications for 5, 10, and 20 equal-time fractions. Increasing fractionation to 20 led to new protein identifications while still identifying most of the proteins identified in the five and ten fraction sets. Venn diagram (b) showed the overlap in protein identifications for 20 and 40 equal-time fractions.

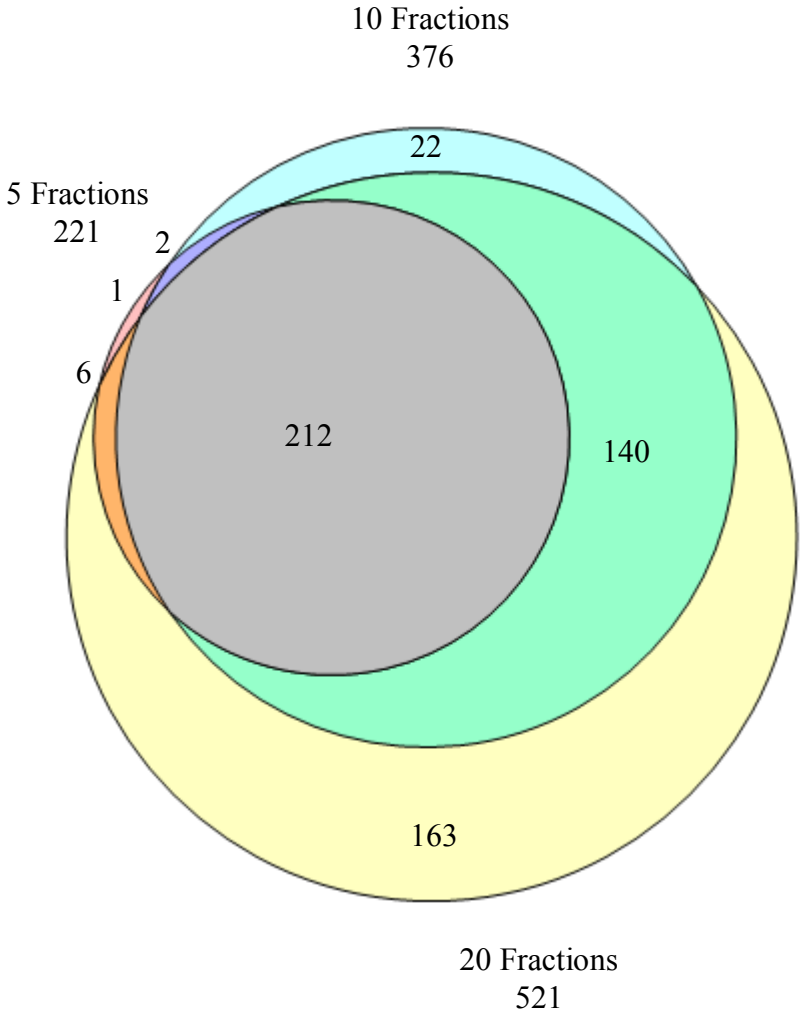

Figure 2.15. The Venn diagram showed the overlap in protein identifications for 5, 10, and 20 equal-mass fractions. Increasing fractionation to 20 led to new protein identifications while still identifying most of the proteins identified in the five and ten fraction sets.

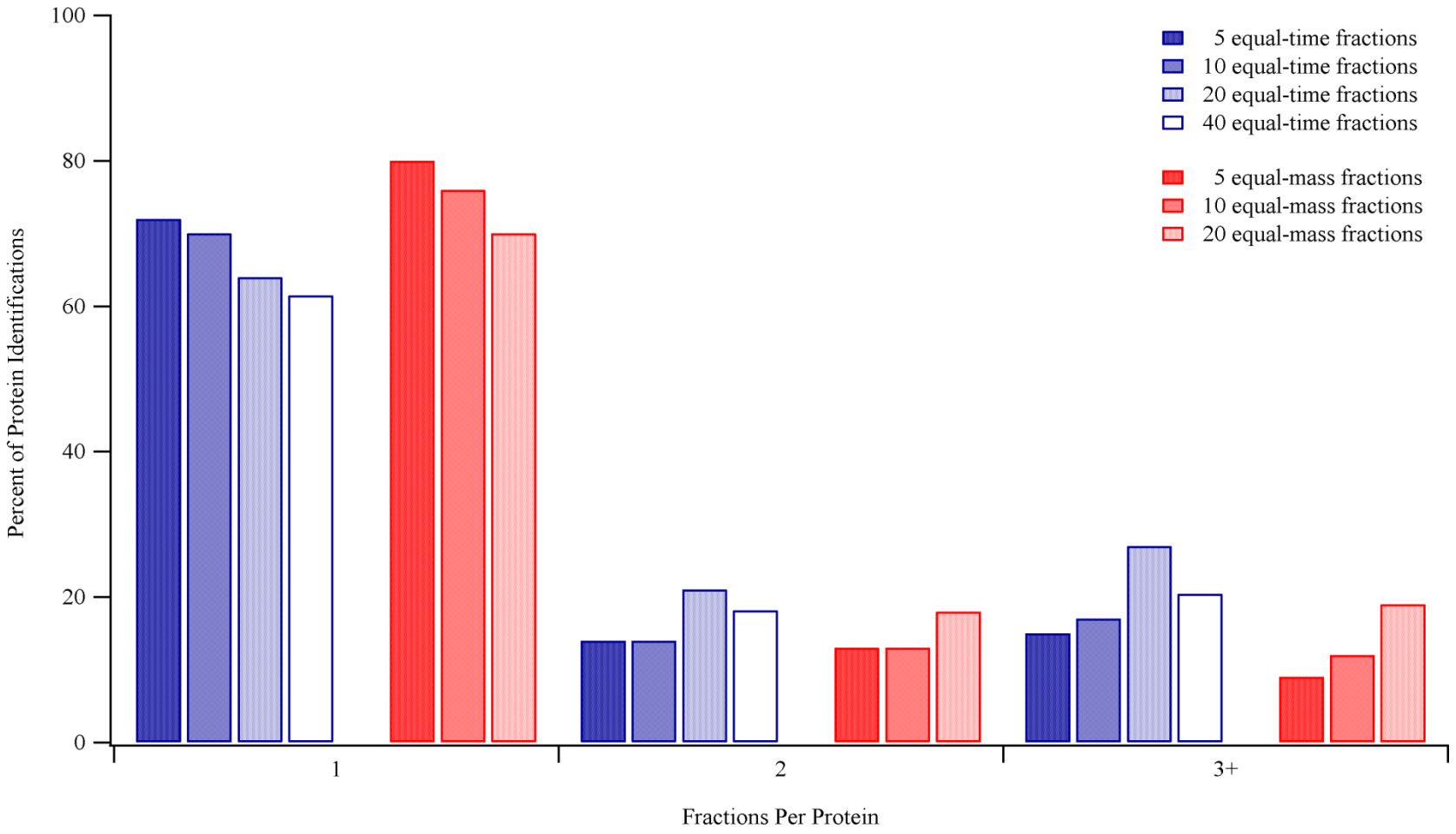

Figure 2.16. Fractions per protein described the percentage of protein identifications that were detected in one, two, or more fractions (3+). As prefractionation frequency increased, more proteins were identified in multiple fractions. This effect was heightened for the equal-time fractions (blue) as compared to the equal-mass fractions (red).

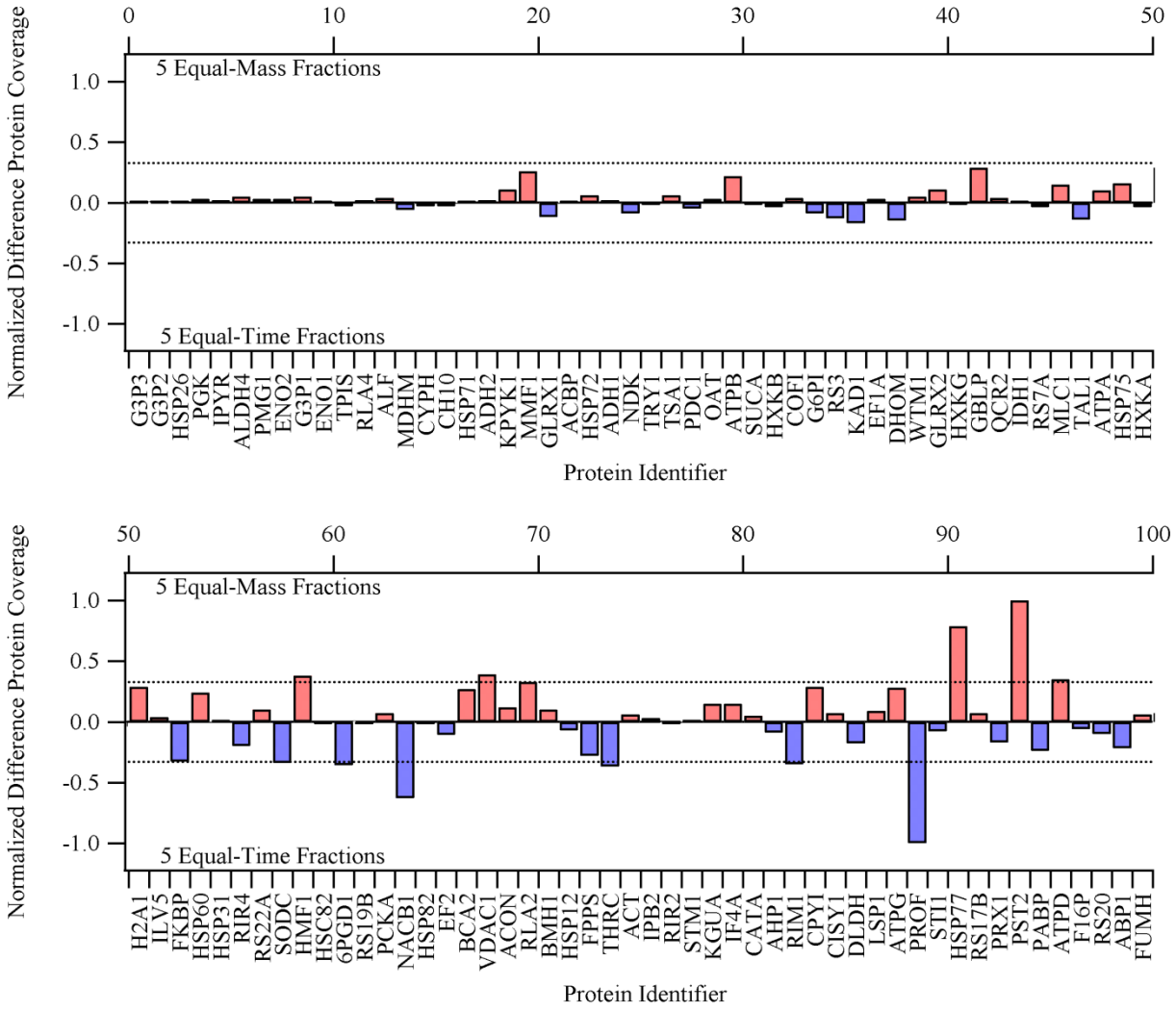

Figure 2.17. To compare the 5 equal-mass and 5 equal-time fractions, the Normalized Difference Protein Coverage (NDPC) was plotted with proteins with higher coverage on the left, and proteins with lower coverage on the right. If a protein was identified with higher sequence coverage in the 5 equal-mass fractions, its NDPC value was positive (red bars). The blue bars signified higher coverage in the 5 equal-time fractions. Differences in coverage were minimal for highly covered proteins. As protein coverage decreased, more proteins were identified with higher coverage in the equal-mass fractions. The dashed lines indicate a level of two-fold greater protein coverage.

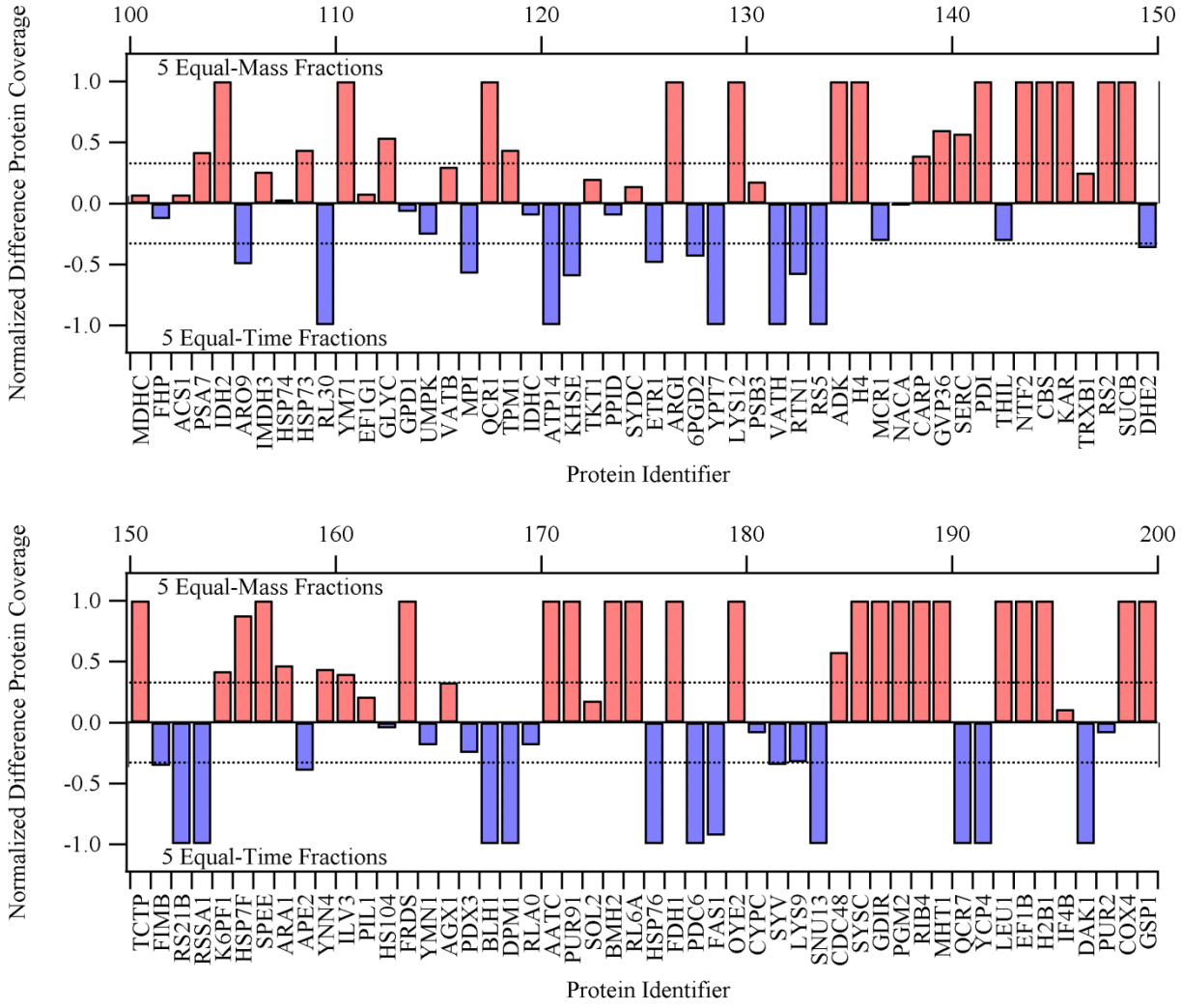

Figure 2.17. (continued)

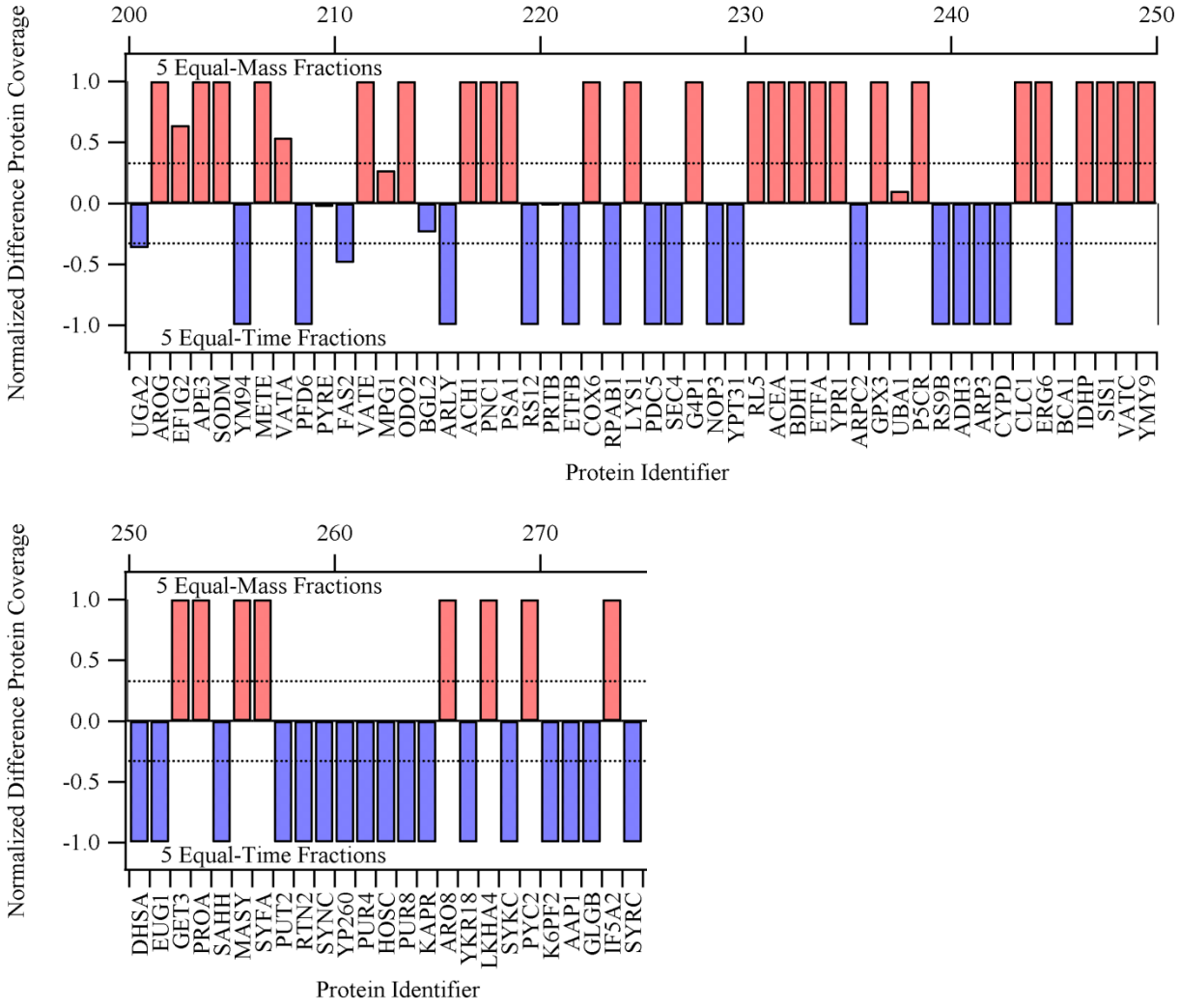

Figure 2.17. (continued)

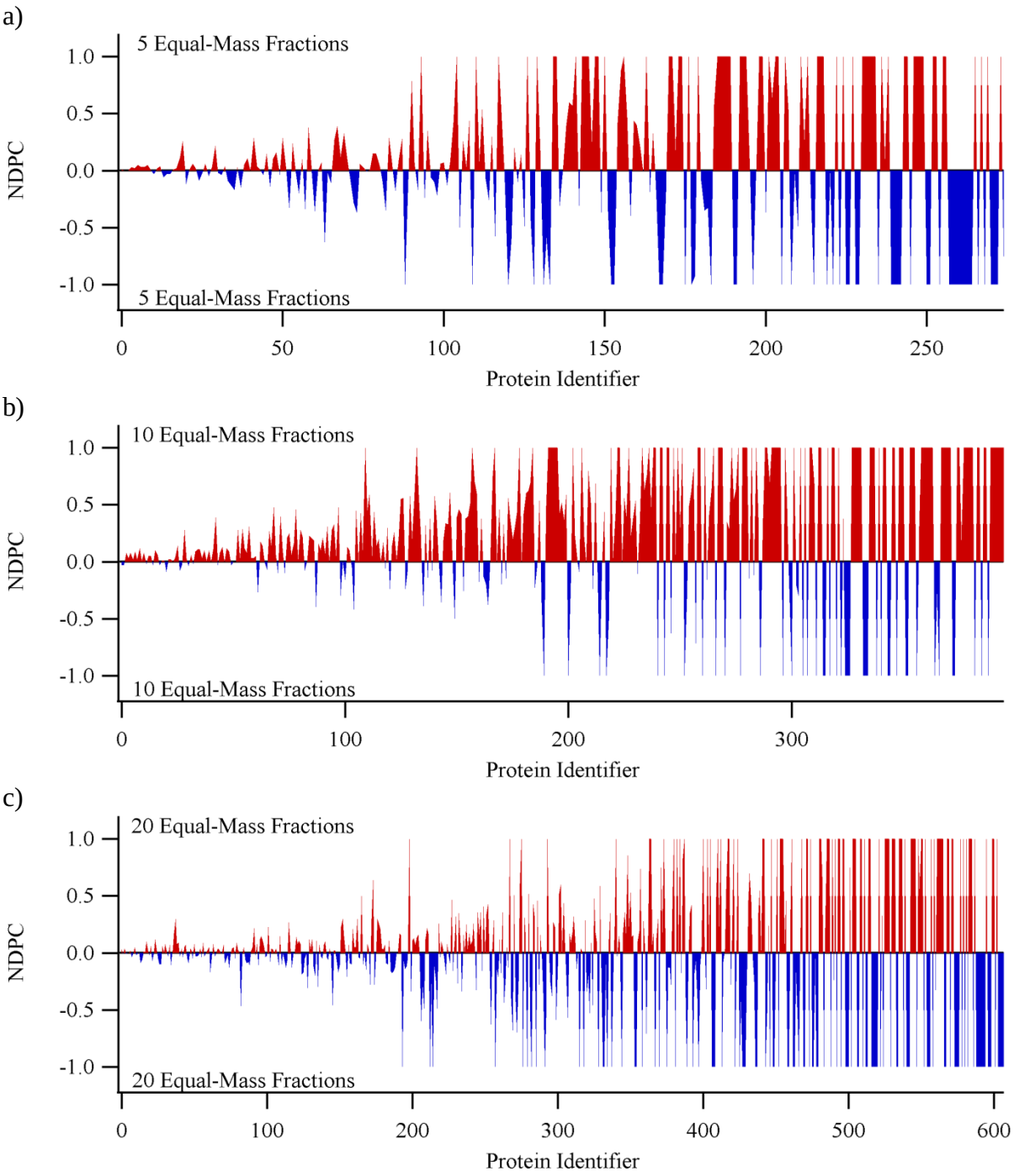

Figure 2.18. The NDPC compared the equal-mass and equal-time methods for 5 (part a), 10 (part b), and 20 (part c) first dimension fractions. If a protein was identified with higher sequence coverage in the equal-mass fractions, the NDPC value was positive (red lines). The blue lines signified higher coverage in the equal-time fractions. Proteins with higher coverage were plotted on the left, and proteins with lower coverage were on the right. Differences in coverage were minimal for highly covered proteins. As protein coverage decreased, more proteins were identified with higher coverage by the equal-mass method for 5 and 10 fractions. There was little difference in NDPC for 20 equal-mass and 20 equal-time fractions.

2.7 REFERENCES

1. Xie, F.; Smith, R. D.; Shen, Y., Advanced proteomic liquid chromatography. *Journal of Chromatography A* 2012, *1261* (0), 78-90.

2. Wolters, D. A.; Washburn, M. P.; Yates, J. R., An Automated Multidimensional Protein Identification Technology for Shotgun Proteomics. *Analytical Chemistry* 2001, *73* (23), 5683-5690.

3. Washburn, M. P.; Ulaszek, R.; Deciu, C.; Schieltz, D. M.; Yates, J. R., Analysis of Quantitative Proteomic Data Generated via Multidimensional Protein Identification Technology. *Analytical Chemistry* 2002, *74* (7), 1650-1657.

4. Giddings, J. C., *Unified separation science*. Wiley: 1991.

5. Rutan, S. C.; Davis, J. M.; Carr, P. W., Fractional coverage metrics based on ecological home range for calculation of the effective peak capacity in comprehensive two-dimensional separations. *Journal of Chromatography A* 2012, *1255* (0), 267-276.

6. Gu, H.; Huang, Y.; Carr, P. W., Peak capacity optimization in comprehensive two dimensional liquid chromatography: A practical approach. *Journal of Chromatography A* 2011, *1218* (1), 64-73.

7. Davis, J. M.; Stoll, D. R.; Carr, P. W., Dependence of Effective Peak Capacity in Comprehensive Two-Dimensional Separations on the Distribution of Peak Capacity between the Two Dimensions. *Analytical Chemistry* 2008, *80* (21), 8122-8134.

8. Gilar, M.; Olivova, P.; Daly, A. E.; Gebler, J. C., Orthogonality of Separation in Two-Dimensional Liquid Chromatography. *Analytical Chemistry* 2005, *77* (19), 6426-6434.

9. Siegler, W. C.; Fitz, B. D.; Hoggard, J. C.; Synovec, R. E., Experimental Study of the Quantitative Precision for Valve-Based Comprehensive Two-Dimensional Gas Chromatography. *Analytical Chemistry* 2011, *83* (13), 5190-5196.

10. Sheldon, E. M., Development of a LC–LC–MS complete heart-cut approach for the characterization of pharmaceutical compounds using standard instrumentation. *Journal of Pharmaceutical and Biomedical Analysis* 2003, *31* (6), 1153-1166.

11. Schure, M. R., Limit of Detection, Dilution Factors, and Technique Compatibility in Multidimensional Separations Utilizing Chromatography, Capillary Electrophoresis, and Field-Flow Fractionation. *Analytical Chemistry* 1999, *71* (8), 1645-1657.

12. Gilar, M.; Daly, A. E.; Kele, M.; Neue, U. D.; Gebler, J. C., Implications of column peak capacity on the separation of complex peptide mixtures in single- and two-dimensional high-performance liquid chromatography. *Journal of Chromatography A* 2004, *1061* (2), 183-192.

13. Stapels, M. F., Keith. A Reproducible Online 2D Reversed Phase–Reversed Phase High–Low pH Method for Qualitative and Quantitative Proteomics *Current Trends in Mass Spectrometry* [Online], 2009.

14. Issaq, H. J.; Chan, K. C.; Janini, G. M.; Conrads, T. P.; Veenstra, T. D., Multidimensional separation of peptides for effective proteomic analysis. *Journal of Chromatography B* 2005, *817* (1), 35-47.

15. Moore, A. W.; Jorgenson, J. W., Comprehensive three-dimensional separation of peptides using size exclusion chromatography/reversed phase liquid chromatography/optically gated capillary zone electrophoresis. *Analytical Chemistry* 1995, *67* (19), 3456-3463.

16. Ye, M.; Jiang, X.; Feng, S.; Tian, R.; Zou, H., Advances in chromatographic techniques and methods in shotgun proteome analysis. *TrAC Trends in Analytical Chemistry* 2007, *26* (1), 80-84.

17. Link, A. J., Multidimensional peptide separations in proteomics. *Trends in Biotechnology* 2002, *20* (12), s8-s13.

18. Martosella, J.; Zolotarjova, N.; Liu, H.; Nicol, G.; Boyes, B. E., Reversed-Phase High-Performance Liquid Chromatographic Prefractionation of Immunodepleted Human Serum Proteins to Enhance Mass Spectrometry Identification of Lower-Abundant Proteins. *Journal of Proteome Research* 2005, *4* (5), 1522-1537.

19. Dowell, J. A.; Frost, D. C.; Zhang, J.; Li, L., Comparison of Two-Dimensional Fractionation Techniques for Shotgun Proteomics. *Analytical Chemistry* 2008, *80* (17), 6715-6723.

20. Stobaugh, J. T.; Fague, K. M.; Jorgenson, J. W., Prefractionation of Intact Proteins by Reversed-Phase and Anion-Exchange Chromatography for the Differential Proteomic Analysis of Saccharomyces cerevisiae. *Journal of Proteome Research* 2012, *12* (2), 626-636.

21. Staub, A.; Guillarme, D.; Schappler, J.; Veuthey, J.-L.; Rudaz, S., Intact protein analysis in the biopharmaceutical field. *Journal of Pharmaceutical and Biomedical Analysis* 2011, *55* (4), 810-822.

22. Vellaichamy, A.; Tran, J. C.; Catherman, A. D.; Lee, J. E.; Kellie, J. F.; Sweet, S. M. M.; Zamdborg, L.; Thomas, P. M.; Ahlf, D. R.; Durbin, K. R.; Valaskovic, G. A.; Kelleher, N. L., Size-Sorting Combined with Improved Nanocapillary Liquid Chromatography−Mass Spectrometry for Identification of Intact Proteins up to 80 kDa. *Analytical Chemistry* 2010, *82* (4), 1234-1244.

23. Nesvizhskii, A. I.; Aebersold, R., Interpretation of Shotgun Proteomic Data: The Protein Inference Problem. *Molecular & Cellular Proteomics* 2005, *4* (10), 1419-1440.

24. Bigelow, C. C., On the average hydrophobicity of proteins and the relation between it and protein structure. *Journal of Theoretical Biology* 1967, *16* (2), 187-211.

25. McCoy, B. J., Multidimensional chromatography—techniques and applications. Edited by H. J. Cortes, Marcel Dekker, New York, NY, 1990, 424 pp. $99.75 (U.S. and Canada), $119.50 (all other countries). *AIChE Journal* 1990, *36* (12), 1933-1933.

26. Bradford, M. M., A rapid and sensitive method for the quantitation of microgram quantities of protein utilizing the principle of protein-dye binding. *Analytical Biochemistry* 1976, *72* (1–2), 248-254.

27. Searle, B. C., Scaffold: A bioinformatic tool for validating MS/MS-based proteomic studies. *PROTEOMICS* 2010, *10* (6), 1265-1269.

28. Eng, J. K.; Searle, B. C.; Clauser, K. R.; Tabb, D. L., A Face in the Crowd: Recognizing Peptides Through Database Search. *Molecular & Cellular Proteomics* 2011, *10* (11).

CHAPTER 3. Increasing Peak Capacities for Peptide Separations Using Long Microcapillary Columns and Sub-2 μm Particles at 30,000+ psi

3.1 Introduction

The field of proteomics is growing in popularity as understanding protein expression in biological systems is essential to elucidating the mechanism of diseases.[1] Analysis of proteins is complicated because there are thousands of proteins in a cell spanning a large range of abundances (greater than 10^{10}).[2] To reduce the complexity, many proteomic experiments include a separation by reversed phase liquid chromatography (RPLC) before introduction into the mass spectrometer.[3] Because protein separations are plagued by sample carryover, and the ionization and fragmentation efficiency of proteins are low, many experiments start with a digestion before the separation which increases the number of components in the mixture.[4,5,6,7]

3.1.1 Coupling LC with MS

To date, no single-dimension separation technique exists with the peak capacity to completely resolve an entire proteome.[8] This issue has been mitigated by the coupling of LC to MS which can detect many species in a single scan. Efforts have been made in the field of mass spectrometry to increase acquisition rates while simultaneously improving limits of detection. The invention of nanoESI resulted in higher ionization efficiency, reduced matrix effects, and facilitated the coupling of LC to MS.[9,10,11,12] Incorporating ion mobility into the mass spectrometer adds another level of analyte separation based on drift time without increasing total analysis time.[13] To handle the massive amounts of information acquired during proteomic experiments, bioinformaticians have developed several programs to mine the data for

information such as retention time, drift time, and parent and product ion mass/charge to identify proteins with higher probability and increased peptide coverage.[14] Even with these improvements, the most advanced proteomic workflows still can't cover the complete proteome in a single analysis of a simple organism such yeast.[15]

3.1.2 Peak capacity improvements

Developing more efficient liquid chromatography techniques for introducing the sample as fully resolved analytes to the mass spectrometer has potential to increase the total number of peptide and protein identifications. For example, more efficient separations reduce the problem of ion suppression by decreasing the number of peptides reaching the mass spectrometer simultaneously.[16]

The effectiveness of a separation is often described by the peak capacity, defined as the maximum number of components that can be resolved within a given separation time. The following equation is often used to calculate peak capacity:

$$n_c = \left(\frac{t_g}{4\sigma}\right) + 1 \qquad (3\text{-}1)$$

where t_g is gradient time and 4σ describes the width of the peak.[17,18]

Peak capacity can be increased by extending the gradient time but will level off as gradients become more shallow.[19] Peak capacity can also be increased by improving column performance. For instance, efficiency can be gained from the use of narrow bore columns because flow dispersion decreases.[20] An additional benefit from capillary columns is the improvement to signal intensity which is inversely proportional to the column diameter squared. Improvements to intensity are important for proteomic experiments because sample is often limited, and the analytes include proteins of low abundance.[11,12] Other column dimensions that affect efficiency are length and particle diameter.[20-21] Sub-2 µm particles reduce multipath

dispersion and the resistance to mass transfer.[22] Peak capacity is proportional to the square root of column length for a given particle diameter, and it is inversely proportional to the square root of the particle diameter at a given column length. The pressure requirement, however, increases proportionally to column length and inversely proportional to the particle diameter cubed.[23]

3.1.3 Previous UHPLC systems

Several manufacturers produce LC systems capable of delivering nanoflow gradients at pressures up to 15 kpsi. Smith and coworkers developed an automated 20 kpsi RPLC-MS to run 40-200 cm x 50 µm ID columns packed with 1.4-3 µm particles. These separations obtained peak capacities of 1000-1500 in 400-2000 minutes (calculated using peak widths at half maximum).[24] A gradient LC system capable of delivering preloaded gradients at constant pressures up to 50000 psi was previously reported from the Jorgenson group.[25,26] This system, however, was built around a now obsolete LC pump and required a splitter to deliver nanoflow to the column which resulted in the loss of sample.[27] More recently, Gritti and Guichon[28] compared gradients delivered by constant pressure and constant flow modes and found that peak capacities were similar for both modes. When comparing peak capacity to analysis time, the constant pressure mode showed a slight advantaged as the system is always running at the maximum pressure and flow rate. In flow mode, the flow rate is limited by the pressure produced when the viscosity of the mobile phase in the column is at the maximum.[29]

Herein, we describe a new constant pressure LC system capable of delivering split-less nanoflow gradients up to 45 kpsi. This automated system is built around a modified nanoAcquity and controlled by MassLynx. The peak capacities achieved with this system for a standard peptide mixture ranged from 174 in 22 minutes for fast, steep gradients and 773 in 360 minutes

for slower shallower gradients. These improved peak capacities led to an increase in protein identifications and protein coverage for an *Escherichia coli* digestion standard.

3.2 Materials and methods

3.2.1 Materials

Optima grade water + 0.1% formic acid, acetonitrile + 0.1% formic acid, L-ascorbic acid, and acetone were purchased from Fisher Scientific (Fair Lawn, NJ). MassPREP^{TM} Digestion Standard Protein Expression Mixture 2, enolase digestion standard and *E. coli* digestion standard were obtained from Waters Corporation (Milford, MA). Water and acetonitrile were Optima LC-MS grade, and all other chemicals were ACS reagent grade or higher. All hardware including valves, ferrules, nuts, connector-tees, unions and stainless steel tubing were purchased from Valco Instrument Co. (Houston, TX) unless otherwise noted. All fused silica capillary tubes were purchased from Polymicro Technologies, Inc. (Phoenix, AZ).

3.2.2 Column preparation

Analytical columns were packed in 75 µm I.D. capillaries and characterized with hydroquinone as previously described by the Jorgenson lab.[23,25] The packing material selected was a silica bridged ethyl hybrid (BEH) particle with a C18 functional group (Waters). The particle diameters evaluated were 1.1 µm, 1.4 µm and 1.9 µm. Column lengths were shortened as particle size decreased to produce nominal flow rates of 300 nL/min at the operating pressure. The final columns evaluated were as follows: 28.5 cm x 75 µm, 1.1 µm BEH C18; 39.2 cm x 75 µm, 1.4 µm BEH C18; 44.1 cm x 75 µm, 1.9 µm BEH C18; and 98.2 cm x 75 µm, 1.9 µm BEH C18;

3.2.3 Instrumentation

The chromatographic system was built around a nanoAcquity as depicted in Figure 3.1. Several 30 cm long pieces of 50 μm ID fused silica capillary tubing connected the sample manager injection valve to a nano-tee (Waters) which split flow to the vent valve (10 kpsi pin valve, Valco) and the high pressure isolation valve (40 kpsi pin valve, Valco). The vent valve was a safety measure should valves isolating the nanoAcquity from the ultrahigh pressure fail. To this point, all connections were made with a peek ferrule and a 1/32" nut. From the high pressure isolation valve, a 60 cm length of the 50 μm ID silica capillary was directed through a freeze/thaw valve and to a second nano-tee. The freeze/thaw valve, developed by Dourdeville,[30] was added to the system because the high pressure isolation valve failed to reliably block all flow at pressures above 30 kpsi. Freezing was driven by a Peltier heat pump with fans to dissipate the heat on the hot side. A dual-output linear power supply by way of a double-pole, double-throw relay drove the direction of the heating and cooling configuration. The output voltage from the power supply was adjusted for the valve to reach -55°C in the freeze state and 7°C in the thaw state. At the second nano-tee, the analytical column and gradient storage loop were joined to the high pressure isolation valve. The gradient storage loop consisted of 10 m of 50 μm ID silica capillary joined by a zero dead volume union (Valco) to 40 m of 250 μm ID stainless steel tubing (Valco). A third nano-tee connected the end of the storage loop to the gradient storage loop valve (40 kpsi pin valve, Valco) and a 903:1 pneumatic amplifier pump, with a 75 kpsi pressure maximum (Haskel International Inc., Burbank,CA). The pump was connected to the third nano-tee by 10 μm ID silica capillary connected with a polyamide cylinder capillary compression fitting previously described.[25] All other high pressure connections were made with a PEEK ferrule and PEEK tubing compressed with a 1/32" nut, collet and collar. The very narrow, 10 μm

ID, silica capillary was selected to provide a flow limiter. If a large leak were to form farther down the fluidic network, most pressure, applied by the pneumatic amplifier, would drop across this narrow ID capillary. All valves were actuated through FET gates controlled by the on/off switches on the rear panel of the nanoAcquity.

3.2.4 Operating procedure

The system operating procedure began with the vent valve closed, and the high pressure isolation valve, freeze/thaw valve, and the gradient storage loop valve opened. Mobile phase A was Optima Grade water with 0.1% formic acid, and mobile phase B was Optima-grade acetonitrile with 0.1% formic acid. The desired gradient program had a 4-40% B linear gradient followed by a 4 µL wash at 85% B and re-equilibration step at 4% B. To produce this gradient, it had to be programmed in reverse order, with the high organic content first and low organic content last, into the MassLynx (Waters) method. The gradient method was loaded onto the gradient storage loop at 5 µL/min. Next, one µL of the MassPrep digest sample was loaded with a push of 0.5% B at 5 µL/min. A total of 10 µL of mobile phase was required to push the sample out of the 1µL injection loop, through the transfer tubing and onto the storage loop. After the gradient and sample were parked on the storage loop, the vent valve was closed; and the high pressure isolation valve, the freeze/thaw valve, and gradient storage loop valve were closed. After waiting 2.5 min for the mobile phase to freeze in the Peltier device, the pneumatic amplifier pump was initiated, to begin the high pressure separation. The method as programmed into MassLynx is listed in Table 3.1

3.2.5 Gradient volume determination

Traditionally, gradient lengths are reported in time. For a constant pressure system, reporting gradient length in terms of volume is more appropriate. The gradient volume was

calculated as the time to load the gradient multiplied by the flow rate (5 µL/min). The length of the linear gradient was programmed to produce a 1, 2, or 4% change in %B per column mobile phase volume. The column mobile phase volume was determined empirically by multiplying the retention time of an unretained compound (L-ascorbic acid) by the flow rate in 50:50 acetonitrile:water with the column run at room temperature. The volumetric flow rate was determined by the time necessary to fill a 10 µL glass micropipette (Fisher) with column effluent. Flow rates and gradient volumes for every method were reported in Table 3.2.

3.2.6 Gradient linearity determination

To measure the gradient profile, mobile phase B was spiked with 10% acetone. The analytical column was replaced with a 55 cm x 5 µm ID open tubular silica capillary run at 30 kpsi with a measure flow rate of 290 nL/min. The flow from the capillary was directed to a Waters CapLC2489 UV/Vis Detector with a 75 µm bubble cell and set to acquire data at 265nm.

3.2.7 Retention time repeatability

To test the repeatability of retention time, a 1µL injection of enolase digest, prepared as per manufacturer's instructions, was run once a day for 12 days. The separation occurred on a 110 cm x 75 µm ID column packed with 1.9 µm BEH C18 particles run at 65°C and 30 kpsi. The gradient volume was 12.5 µL from 4-40% B. The retention times were tracked for 17 peptide peaks.

3.2.8 Peptide analysis

The Standard Protein Expression Digestion Mixture 2 was run in duplicate, and the *E. coli* digestion standard was run in triplicate for each chromatographic method. The outlet of the RPLC column was coupled to a qTOF Premier (Waters) via a 30 cm x 20 µm I.D. piece of silica capillary and a stainless steel nanospray emitter with a 20 µm ID and a 10 µm tip (Waters). Spray

voltage (+2.5kV) was applied via electrical contact with the zero-dead-volume union in the nanoflow sprayer. MS^E scans were performed in data-independent analysis mode. The instrument was set to acquire parent ion scans from m/z 50-1990 at 5.0 V. The collision energy was then ramped from 15-40 V. Scan times were set to 0.3 sec for analysis of sub-20 second wide chromatographic peaks and 0.6 sec for wider peaks with a 0.1 sec interscan delay in both cases.

3.2.9 Peptide data processing

The LC-MS/MS data were processed using ProteinLynx Global Server 2.5 (Waters). The Standard Protein Expression Digestion Mixture 2 data were searched against a database of alcohol dehydrogenase, bovine serum albumin, glycogen phosphorylase b, and enolase. The *E. coli* spectral data was search against a database of known *E. coli* proteins. The amino acid sequences were found from the Uni-Prot protein knowledgebase (www.uniprot.org) and appended with a 1X reversed sequence. The false discovery rate was set to 4%.

3.2.10 Calculating peak capacity

The Standard Protein Expression Digestion Mixture 2 data were used to determine peak capacity. The full width at half maximum intensity (FWHM) of each peptide peak was determined by ProteinLynx Global Server ion accounting output. The average (arithmetic mean) FWHM was multiplied by 1.7 to calculate the 4σ peak width. The peak capacity was ultimately determined by the separation widow divided by the average (arithmetic mean) 4σ peak width. The separation window was the time between the elution of the first and last peak. The sample was sufficiently complex to have peaks eluting throughout the entire gradient length.

3.3 Discussion

3.3.1 Instrumental design

Previous attempts proved the difficulty of producing linear gradients at ultrahigh pressures.[25] Two challenges included keeping dead times and mixing volumes low. To reduce mixing, narrow bore capillaries are used. The combination of narrow bore capillaries and nano-flow prior to the column can greatly increase the solvent delay and dead time. Commercially available systems, like the nanoAcquity UPLC used in these experiments, accurately and reproducibly generate linear gradients up to 10 kpsi.[31] The nanoAcquity also provides software for easy method programing and provides on/off switches used to control additional valves. For these reasons, the nanoAcquity was selected as the base for the UHPLC. The gradients were generated by the nanoAcquity at lower pressures (2-4 kpsi) and loaded onto a storage loop. Therefore, the gradient merely needs to be pushed but not formed at ultrahigh pressures. Gradient loading only adds a few minutes onto the run time because loading occurred at 5 µL/min as opposed the 0.2-0.6 µL/min playback flow rate. The gradient was loaded on to the front of the storage loop in reverse order, and played back in a last-in-first-out (LIFO) workflow. LIFO allowed the loading time to be directly proportional to the gradient volume. If the gradient was loaded in order, it would have to be loaded into the back of the storage loop causing the dead volume of the instrument to be the volume of the storage loop minus the volume of the gradient. By loading the gradient onto the end of the storage loop closest to the head of the column, the system basically had zero dead volume. The only dead volume was from the 150 µm i.d. bore through the tee that connects the storage loop to the column.

When the valves were configured for ultrahigh pressure mode, the pressure was delivered by the Haskel pneumatic amplifier pump which was capable of working at 75 kpsi. The system

was prohibited from working at this pressure by the fittings and pin-valves. The silica capillary fittings start leaking at 50 kpsi. Previously published fittings[23] compatible with pressures greater than 50 kpsi were much larger and would require the use of a larger tee to connect the gradient storage loop to the column. Larger tees have larger dead volumes allowing mixing of mobile phase in the tee and mostly likely interfere with the focusing of the injection plug onto the head of the column.

3.3.2 Gradient storage loop dimensions

When designing the system, the versatility was desired to run both long gradients for long columns and fast gradients on short columns with smaller particles. The storage loop must provide ample volume to accommodate larger gradients while having a narrow internal diameter to reduce Taylor-Aris mixing of the mobile phase.[32] Mixing of the mobile phase in the storage loop is best described by the height equivalent of a theoretical plate (H_{CM}) in an open tube. H_{CM} is proportional to the inner diameter of an open tube (d_c), where D_m is the diffusion of a molecule in the mobile phase[33] as shown in Equation 3-2.

$$H_{CM} = \frac{d_c^2 u}{96 D_m} \tag{3-2}$$

The larger volume (V) gradients occupy a longer length (L) of the storage loop as described in Equation 3-3.

$$L = \frac{4V}{\pi d_c^2} \tag{3-3}$$

Larger gradients are less affected by the inner diameter of the storage loop because the number of theoretical plates (N) is proportional to length.[34]

$$N = \frac{L}{H_{CM}} \tag{3-4}$$

The derivation comparing band broadening for different storage loops and gradient volumes can be found in table Table 3.3. For the larger, 125 µL, gradient, 2300 theoretical plates were calculated with a 0.025 cm ID storage loop. For a shorter, 5 µL, gradient, there were only 91 theoretical plates. To achieve 2300 theoretical plates for the shorter gradient, a 0.0050 cm storage loop had to be used. A balance must be made, however, between the internal diameter and the practicality of the length of the storage loop. To provide storage of larger gradients without compromising the integrity of shorter gradients two storage loops were used in tandem. The first section was 10 m of 50 µm I.D. silica capillary, which stored 20 µL. The second section was 10 m of 250 µm ID stainless steel tubing capable of storing 0.5 mL. As shown in Figure 3.2, a linear gradient was not delivered with only the 250 µm ID storage loop installed. The 17 µL gradient should produce a 56-min-long linear section from 4-40%B followed by a ramp to a 85%B wash. The red trace shows mixing of the gradient when it was loaded at 10 µL/min into the 250 µm ID storage loop. The loading flow rate was reduced to 5 µL/min which slightly improved the linearity of the delivered gradient (blue trace). The addition of the 50 µm ID silica capillary produced a very linear, 56-minute-long gradient that was not mixed with the 85%B wash (green trace). With the narrow ID storage loop inline, the desired gradient profiles were delivered after storage in the loop.

3.3.3 Selecting the flow rate for gradient loading

The H_{cm}-term is also proportional to the linear velocity (u) making the flow rate (F)[34] at which the gradient was loaded an important parameter to study. The relationship is as follows:

$$u = \frac{4F}{\pi d_c^2} \tag{3-5}$$

The effect of gradient loading flow rate is shown in Figure 3.2. When the gradient is loaded at 10 µL/min, the playback of the gradient is not as desired. Reducing the gradient loading flow rate to

5 µL/min improved the gradient profile as depicted in Figure 3.3.a. with the playback of gradients of varying volumes. The time of the linear portion of the gradient profile was plotted versus the gradient volume in Figure 3.3.b. The linear fit of the data produced an R^2 value of 0.999. The equation of the line was y = 3.33x +4.19. The inverse slope was 0.300 µL/min and corresponded to the playback flow rate.

3.3.4 Repeatability

The repeatability was accessed for a 12.5 µL gradient run at 30 kpsi and 65°C on a 110 cm x 75 µm ID column packed with 1.9 µm BEH C18 particles. Enolase was separated by this method on twelve different days. The retention times are listed in Table 3.4 for peptides identified in all the analyses. The mean ($\bar{x}$), standard deviation (s), and relative standard deviations (%RSD) were calculated from these results. All peptides had retention times with a 4.5%RSD or less. The retention time residual for each peptide was calculated as the retention time on a given day minus the average retention time. The residuals were plotted versus day of analysis in Figure 3.4. On most days (replicates 1-6, 10 and 12), retention times vary by less than two minutes from the mean. As evident from the tight clusters of data (except for replicates 1, 7 and 11), the retention time shifts were similar for all peaks on any given day. Since this is a constant pressure system, longer retention times, for replicated 9 and 10, may be attributed to partial clogging of the pigtail or spray tip after the column.

3.3.5 Elevated temperature separations

Though not a requirement for operating the system, there were several motivations to heat the column to 65°C. Higher temperatures reduce the viscosity of the mobile phase. Therefore, longer columns can be used without reducing flow rate and increasing analysis time at a given pressure. The higher temperatures also reduced the change in mobile phase viscosity.

The gradient varied from 4-40% acetonitrile in water. Through the gradient, the viscosity and flow rate would fluctuate by nearly 10% at 25°C but only 5% at 65°C.[35,36,37] The resistance to mass transfer is reduced at high temperatures which flattens the C-term portion of a Van Deemter plot and consequently shifts optimal velocity to a higher value. Analysis time can then be reduced because a separation with a higher flow rate will not suffer as great a loss of theoretical plates when run at 65°C versus 25°C.[34]

3.3.6 Column selection

To test the performance capabilities of the UHPLC, columns of varying length with several different particle diameters were selected. The internal column diameter was kept constant at 75 µm to be compatible with the volume necessary for nanoESI. Before use the column performance was evaluated by isocratic elution to confirm that all columns had similar reduced Van Deemter terms which is evident in Figure 3.5. The h-min of the 28.5 cm x 75 µm ID column with 1.1 µm BEH C18 stationary phase was slightly higher than the other columns evaluated. However, 1.1 µm particles were difficult to pack, especially to a length of 28.5 cm, and an h-min around 2.5 was very acceptable.

3.3.7 Separations at ultrahigh pressures

Once it was determined that the system delivered gradients as desired, separations were conducted at a variety of gradient volumes as shown in Figure 3.6. Resolving power increased as gradient volume increased for separations at 15 kpsi of the standard protein digest on a 44.1 cm x 75 µm, 1.4 µm BEH C18 column. From each of the chromatograms, a representative peak, selected for its average intensity and retention time, was extracted and plotted in the insert of Figure 3.6. As gradient volume increased, peak width increased and peak height decreased. This same experiment was carried out at 15, 30 and 45 kpsi. Example chromatograms in Figure 3.7 of

a 56 µL gradient run at the three different pressures illustrated how run time decreased and flow rate increased as the operating pressure increased. The insert in Figure 3.7 of a representative peak from all three chromatograms showed how peak width decreased at higher pressure while peak intensity remained constant.

A summary of the peak capacity data can be found in Table 3.5. The goal was to increase gradient volumes until a leveling off of peak capacity versus separations window was observed. As presented in Figure 3.8, the peak capacity from the separations at 45 kpsi plateaued at a lower value than for the separations at 30 kpsi. The separations at 15 kpsi reached a higher maximum peak capacity as compared to the higher pressure separations. At 15 kpsi, the linear velocity was 8 cm/min which is closer to the optimum velocity. At the higher pressures and flow rates, a higher C-term contributed more to the band broadening.

To determine how a proteomics sample would behave on this column, the same methods at various gradient volumes and pressures were used to separate the *E. coli* digestion standard. Though example separations at 15 kpsi in Figure 3.9 were very busy, an increase in resolution was observed as gradient volume increase which was indicated by the signal being closer to baseline between adjacent peaks. The benefit of reduced run time at higher pressures is shown in Figure 3.10 for a 56 µL gradient. In Figure 3.11**,** the number of *E. coli* peptide and protein identifications are plotted versus the separation window in parts a and b, respectively. The separations at 15 kpsi contained the most identifications followed by the separations at 30 kpsi and then by 45 kpsi. The peptide identifications begin to level off with respect to time faster than the protein identifications. For the shallowest gradients, peptide identifications actually start to decrease which was mostly likely due to the decrease in peak intensity for long separations. When the peptide identifications were plotted against peak capacity in part c, there was no strong

correlation. However, protein identifications were very linear when plotted against peak capacity as can be seen in part d. Because the peak capacity always increased as the separation window increased, the data points in parts c and d were still in order from smallest to largest gradient volume when reading the graph from left to right.

Beyond measuring the number of protein identifications, it was also important to consider productivity which can be described as protein identifications per minute. The highest productivity measured was for the most aggressive gradient (4% change in mobile phase B per column volume) at 45 kpsi, and the lowest productivity was observed for the shallowest gradient (0.5% change in mobile phase B per column volume) at 15 kpsi. The productivity for all separations was plotted in Figure 3.12. For high-throughput laboratories, the higher pressure separations would be most useful.

3.3.8 Separations with long columns

The greatest benefit from having the ability to run ultrahigh pressure separations was observed when running with a long column. In the red chromatogram in Figure 3.13, the standard protein digest was separated on a 44.1 cm x 75 µm ID column with 1.9 µm BEH C18 particles at 15 kpsi. The blue trace was from a 30 kpsi separation of the same sample on a 98.2 cm x 75 µm ID column with 1.9 µm BEH C18 particles. By increasing the pressure, the flow rates and run times were similar between the two separations. As evident from inset graph, the width of a representative peak decreased at higher pressure yet peak intensity remained the same. Several gradient volumes were run on the 98.2 cm column. The results are summarized in Table 3.5 and Figure 3.14 which also includes data from a shorter commercial column run on the standard nanoAcquity. By increasing the operating pressure, the peak capacity increased for separations on a longer column in the same amount of time as separations on a shorter column at

lower pressures. Also, the peak capacity plateaued at a higher value for the longer columns than the shorter columns.

The *E. coli* digestion standard was also run on the 98.2 cm column at varying gradient volumes as seen in Figure 3.15. An enlarged view of a portion of the longest chromatogram is shown in Figure 3.16. The return of the signal to baseline between several adjacent peaks demonstrated the gain in resolution from using long columns at elevated pressures and temperature for proteomics analysis. The number of peptide and protein identifications plotted in Figure 3.17 was higher for separations on the modified UHPLC than the commercial system with an increase of nearly 50%. However, there was little difference in the number of protein identifications between the 98.2 cm column run at 30 kpsi and the 44.1 cm column run at 15 kpsi even though the 98.2 cm column had a larger peak capacity.

The number of protein identifications is not the only metric by which to compare the results of two proteomics analyses. Improvement of protein coverage, or the percent amino acid sequence coverage, can also describe the merit of the experiment. For a large data set containing hundreds of proteins, comparing the coverage for each protein is not straight forward. For example, reducing protein coverage to an average can be misleading. The additional proteins identified in a separation with higher peak capacity were usually of lower abundance and had lower coverage, bringing down the average. Alternatively, comparing only proteins identified by both methods would limit the analysis to only easily detectible proteins which usually had higher coverage and, thus, mute the difference between the methods. Herein, an original method to compare protein coverage based on the mathematical concept of a normalized difference is described. We named this metric the normalized difference protein coverage (NDPC) and define it as the difference in coverage of a protein found in two methods divided by the sum of the

coverage. For example, consider the protein pyruvate kinase, which is involved in *E. coli* glycolysis.[38] For a 360 minute separation, pyruvate kinase had 47% coverage on the 98 cm column and 27% coverage on the 44.1 cm column. The NDPC is 0.27 as calculated in Equation 3-6.

$$\text{NDPC} = \frac{\text{Coverage}_1 - \text{Coverage}_2}{\text{Coverage}_1 + \text{Coverage}_2} = \frac{47\text{-}27}{47+27} = 0.27 \tag{3-6}$$

The Normalized Difference Protein Coverage (NDPC) is plotted in Figure 3.18 for each protein identified with the 360 minute gradient separation. If a protein was identified with higher sequence coverage from the separation on the 98.2 cm column run at 30 kpsi, its NDPC value was positive (blue bars). The red bars signified higher coverage with the separation on the 44.1 cm column at 15 kpsi. Proteins were plotted in order of decreasing coverage i.e. proteins wither higher coverage were plotted on the left and proteins with lower coverage on the right. Differences in coverage were minimal for highly covered proteins. As protein coverage decreased, more proteins had higher coverage with the 98.2 cm column. Similar comparisons were made for the 90 minute and 180 minute gradient separations and can be found in Appendix B.1. and Appendix B.2., respectively. To provide a better visual of the trend in coverage, the protein identifiers were removed from the graphs, and the NDPC were plotted in Figure 3.19. parts a, b, and c for the 90, 180, and 360 minute gradient separations, respectively. As evident by the larger portion of blue bars in part c, the greatest improvement in coverage between the long and shorter column was with shallowest gradient.

In an attempt to further simplify the comparison of coverage between multiple methods, while maintaining the meaning of the values, we propose the Grand NDPC which is calculated by the difference between the grand total protein coverage in method one and method two

normalized by the grand sum of protein coverage in both methods. A formula for the Grand NDPC is shown in Equation 3-7:

$$\text{Grand NDPC} = \frac{(\sum \text{Coverage}_{\text{method 1}})-(\sum \text{Coverage}_{\text{method 2}})}{\sum \text{Coverage}_{\text{method 1}}+\sum \text{Coverage}_{\text{method 2}}} \quad (3\text{-}7)$$

Perhaps a more relevant interpretation of the Grand NDPC would be to relate it to a fold-change improvement in coverage as follows:

$$\text{Fold-Change in Coverage} = \frac{\sum \text{Coverage}_{\text{method 1}}}{\sum \text{Coverage}_{\text{method 2}}} = \frac{1+\text{Grand NDPC}}{1-\text{Grand NDPC}} \quad (3\text{-}8)$$

If the Fold-Change was less than one, the negative reciprocal of the value was used as is conventional with fold-change calculations. The Grand NDPC and Fold-Change in Coverage is listed in Table 3.6 for the *E. coli* digest standard 90, 180, and 360 min gradient separations on the 98.2 cm column run at 30 kpsi and the 44.1 cm column at 15 kpsi. Positive values represented higher coverage on the long column, and negative values represented higher coverage on the shorter column. Grand NDPC and Fold-Change Coverage increased in favor of the long column as gradient length increased.

3.3.9 Separations with smaller particles

The last variable that was evaluated on the UHPLC was the use of columns with smaller particles. Flow rate, running pressure, and column diameter were kept constant for these experiments. Column length was shortened to compensate for the additional back pressure necessary for running with smaller particles. The standard protein digest was separated on a 39.2 cm x 75 µm ID column packed with 1.4 µm BEH C18 particles at increasing gradient volumes as shown in Figure 3.20. The inlaid graph depicted a representative peak. Similar to separations shown for columns previously discussed in the chapter, the peak width increased and peak height decreased as gradient volume increased. The smallest particles tested were 1.1 µm BEH C18

packed into a 28.5 cm x 75 µm ID column. These separations are shown in Figure 3.21. The inset graph of the representative peak had a width of 0.1 minute for the fastest gradient which was the narrowest width of any peak shown in this chapter. The peak width increased to 0.26 minutes for the slowest gradient on this column. A summary of the peak capacities are listed in Table 3.5 and plotted in Figure 3.22. The red line represents separations at 30 kpsi on a 39.2 cm x 75 µm ID column with 1.4 µm BEH C18 particles. The blue line represents separations on a 98.2 cm x 75 µm ID column with 1.9 µm BEH C18 particles. The green line represents separations on a 28.5 cm x 75 µm ID column with 1.1 µm BEH C18 particles. The black line represents separations on a commercial UPLC with a commercial column. The highest peak capacities were achieved with the longest column and the largest particles. Even for very short analysis times, peak capacities were higher with an aggressive gradient on a long column than a shallower gradient on a shorter column packed with smaller particles. Pressure requirements were proportional to length and inversely proportional to the particle diameter cubed. Therefore, length had to be sacrificed when running a column with smaller particles which resulted in the lower peak capacities.

The 39.2 cm x 75 µm ID column packed with 1.4 µm BEH C18 particles was also run at 15 and 45 kpsi as represented in Appendix B.3. The *E. coli* digestion standard was also analyzed at all these conditions with example chromatograms shown in the Appendix B.4. and Appendix B.5. The results are summarized in Table 3.5. Conclusions from this data were similar to that discussed in the "Separations at ultrahigh pressures" section. The 28.5 cm x 75 µm ID column with 1.1 µm BEH C18 particles broke before the *E. coli* digestion standard was analyzed. There were not enough particles to pack another column with similar performance.

3.3.10 Literature comparison

Several labs have employed longer columns and ultrahigh pressures to improve peak capacity and number of identifications for proteomic analyses. A representation of this work from the literature, data from the commercial system, and data from this chapter are plotted in Figure 3.23. The Marto group at Harvard[39] packed 5 µm particles into a long narrow capillary of 100 cm x 25 µm ID and ran on a commercial system at 8 kpsi nominal back pressure. The Smith group at PNNL[24] separated peptides on three different columns at 20 kpsi. The column length decreased to accommodate for the pressure required to use smaller particles. Data from this chapter collected at 30 kpsi with the 98.2 cm x 75 µm ID column packed with 1.9 µm BEH C18 particles outperformed the results found in the literature in less times.

3.4 Conclusions

A gradient elution system capable of 45 kpsi has been developed to improve the separation of proteomic samples. By implementing longer columns and smaller particles, the peak capacity and productivity were increased. The peak capacities achieved with this system for a standard peptide mixture ranged from 174 in 22 minutes for fast, steep gradients and 773 in 360 minutes for slower shallower gradients. The highest peak capacities were achieved with the longest column. Even for very short analyses, peak capacities were higher for an aggressive gradient on a long column than a shallower gradient on a shorter column with smaller particles. The peak capacities associated with this system led to increased protein identifications and sequence coverage.

This instrument would be well suited to perform the second dimension separations in a prefractionation-type multidimensional proteomics separation[7] or as the first dimension followed

by a fast separation on a microchip.[40] The improved separation efficiency available through this ultrahigh pressure system could prove useful in other –omics research such as metabolomics.

3.5 TABLES

Time (min)	Flow Rate (µL/min)	% Mobile Phase A	% Mobile Phase A	Curve	NanoAcquity Vent Valve	High Pressure Isolation Valve Freeze/Thaw Valve Vent Valve	Pneumatic Amplier Pump Initiation
Gradient Loading Method							
Initial	5	96.0	4.0	-	Off	On	Off
1.0	5	15.0	85	11	Off	On	Off
1.8	5	60.0	40	11	Off	On	Off
x + 1.8	5	96.0	4	6	Off	On	Off
x + 2.4	5	99.5	0.5	11	Off	On	Off
x + 4.0	4	99.5	0.5	11	Off	On	Off
x + 4.1	3	99.5	0.5	11	Off	On	Off
x + 4.2	2	99.5	0.5	11	Off	On	Off
x + 4.3	1	99.5	0.5	11	Off	On	Off
x + 4.4	0.01	99.5	0.5	11	Off	On	Off
x + 5.0 (end)	0.01	99.5	0.5	11	Off	On	Off
Sample Loading Method							
Initial	0.01	99.5	0.5	-	Off	On	Off
0.1	1	99.5	0.5	11	Off	On	Off
0.2	2	99.5	0.5	11	Off	On	Off
0.3	3	99.5	0.5	11	Off	On	Off
0.4	4	99.5	0.5	11	Off	On	Off
0.5	5	99.5	0.5	11	Off	On	Off
2.0	5	99.5	0.5	11	Off	On	Off
2.5	0.01	50	50	11	On	Off	Off
5.0	0.01	50	50	11	On	Off	On
Ultra High Pressure Separation Method							
Initial	0.01	50	50	11	On	Off	On
y	0.01	96	4	11	On	On	Off
y + 5.0 (end)	0.01	96	4	11	On	On	Off

Table 3.1. The methods as programmed into MassLynx were listed along with the valve timings. The gradient loading time was listed as x, where x equals the gradient volume divided by the flow rate when loading the gradient. The time to play back the gradient was listed as y.

		Column A	Column B	Column C	Column D
Column Length (cm)		44.1	98.2	39.2	28.5
Internal Diameter (µm)		75	75	75	75
Particle Diamter (µm)		1.9	1.9	1.4	1.1
		Flow Rate (nL/min)			
Pressure	15kpsi	350	-	190	-
	30kpsi	730	330	410	370
	45kpsi	1160	-	610	-
		Gradient Volume (µL)			
Percent Change MPB Per Column Volume	4.0%	14	31	12.5	8
	2.0%	28	62	25	16
	1.0%	56	124	50	31
	0.5%	113	249	100	62

Table 3.2. The dimensions for each of the analytical columns tested in this manuscript were listed along with their measured flow rates and programmed gradient volumes.

Gradient Volume, V, (µL)	**125**	**5.0**	**5.0**
Inner Diameter, d_c, (cm)	0.025	0.025	0.0050
Gradient Loading Flow Rate, F, (µL/min)	5.0	5.0	5.0
Linear Velocity, (cm/s) $u = \frac{4F}{\pi {d_c}^2}$	0.17	0.17	4.2
HETP (cm) $H_{CM} = \frac{{d_c}^2 u}{96 D_m}$	0.11	0.11	0.11
Gradient Length (cm) $L = \frac{4V}{\pi {d_c}^2}$	250	10	250
Number of Plates $N = \frac{L}{H_{CM}}$	2300	91	2300

Table 3.3. The number of theoretical plates was calculated for several gradient storage loop internal diameters and gradient volumes.

		Analysis Day														
Peptide Sequence	m/z	1	2	4	8	9	9	10	11	13	14	15	16	$\bar{x}$	s	%RSD
HLADLSK	392.2	41.8	38.6	38.9	40.1	40.4	40.0	37.8	38.2	43.2	41.0	43.5	40.5	40.3	1.8	4.5
IATAIEK	745.5	44.3	41.8	42.4	42.8	43.6	43.2	40.5	40.9	46.1	43.6	46.6	43.5	43.3	1.8	4.2
IGSEVYHNLK	580.3	45.4	43.3	44.0	44.2	45.1	44.8	42.0	42.4	47.6	44.9	48.2	45.0	44.8	1.8	4.1
LNQLLR	756.5	50.3	48.3	49.1	49.1	50.2	49.9	46.9	47.4	52.8	50.3	53.7	50.0	49.8	2.0	4.0
TFAEALR	807.4	50.8	48.9	49.7	49.7	50.8	50.4	47.5	48.0	53.4	50.9	54.3	50.6	50.4	2.0	3.9
SIVPSGASTGVHEALEMR	619.6	51.2	49.4	50.2	50.2	51.3	51.0	48.0	48.6	54.1	51.6	55.1	51.3	51.0	2.0	4.0
IEEELGDNAVFAGENFHHGDK	776.7	52.7	51.0	51.9	51.8	53.0	52.7	49.6	50.2	55.8	53.3	56.9	52.9	52.7	2.1	4.0
GNPTVEVELTTEK	708.9	52.9	51.2	52.1	52.0	53.1	52.8	49.8	50.3	56.0	53.4	57.1	53.1	52.8	2.1	4.0
VNQIGTLSESIK	644.9	53.4	51.7	52.5	52.4	53.7	53.3	50.2	50.8	56.5	53.9	57.6	53.6	53.3	2.1	3.9
YDLDFK	800.4	54.1	52.4	53.2	53.2	54.4	54.0	50.9	51.6	57.3	54.7	58.3	54.3	54.0	2.1	3.9
AADALLLK	814.5	55.5	53.9	54.6	54.5	55.8	55.4	52.3	52.9	58.6	56.1	59.9	55.6	55.4	2.1	3.9
NVNDVIAPAFVK	643.9	59.9	58.6	59.4	59.1	60.5	60.1	56.9	57.6	63.6	60.9	65.1	60.4	60.2	2.3	3.8
TAGIQIVADDLTVTNPK	878.5	60.9	59.6	60.7	60.3	61.8	61.4	58.2	58.9	65.0	62.2	66.6	61.8	61.5	2.4	3.9
LGANAILGVSLAASR	706.9	62.7	61.4	62.3	61.8	63.6	63.0	59.7	60.5	66.8	63.9	68.6	63.3	63.1	2.5	3.9
AVDDFLISLDGTANK	789.9	64.9	64.7	65.6	65.0	66.9	66.4	62.1	62.9	69.2	67.2	71.2	65.8	66.0	2.5	3.8
SGETEDTFIADLVVGLR	911.5	69.8	69.0	70.0	69.3	71.1	70.6	67.1	67.9	74.3	71.6	77.0	71.2	70.8	2.7	3.8
YGASAGNVGDEGGVAPNIQTAEEALDLIVDAIK	1086.6	72.3	72.0	72.9	72.1	74.1	73.5	69.9	70.7	77.3	74.6	80.3	74.3	73.7	2.9	3.9

Table 3.4. The retention times, in minutes, were listed for several peptides identified in an enolase digest standatd separated on a 110 cm x 75 µm column packed with 1.9 µm BEH C18 particles. The gradient volume was 12.5 µL and was repeated 12 times on 12 different days. The retentions times all had an %RSD of 4.5% or less.

Column Description	Pressure (kpsi)	Gradient Length (%B per Column Volume)	Separation Window (min)	Average Peak Width (min)	Peak Capacity	Protein IDs	Peptide ID
25 cm x 75 µm ID 1.9 µm d_p	8	4	15	0.17	88	111	1060
		2	30	0.29	103	169	1540
		1	60	0.37	161	201	1876
		0.5	120	0.92	191	196	1493
44.1 cm x 75 µm ID 1.9 µm d_p	15	4	35	0.13	264	207	2534
		2	69	0.18	385	255	2982
		1	132	0.29	455	302	3127
		0.5	275	0.46	596	362	2742
	30	4	18	0.10	174	156	1652
		2	34	0.14	254	199	2048
		1	67	0.18	379	232	2029
		0.5	137	0.32	433	260	2020
	45	4	11	0.09	125	127	1371
		2	24	0.14	174	166	1664
		1	47	0.18	269	212	1984
		0.5	93	0.27	344	238	1990
98.2 cm x 75 µm ID 1.9 µm d_p	30	4	90	0.20	457	265	2682
		2	180	0.29	622	290	2868
		1	360	0.47	773	395	2883
		0.5	720	0.82	877	343	2003
39.2 cm x 75 µm ID 1.4 µm d_p	15	4	67	0.21	316	222	3038
		2	113	0.29	385	263	3363
		1	198	0.41	482	291	3160
		0.5	400	0.55	724	232	1775
	30	4	34	0.14	246	184	2347
		2	60	0.17	352	273	3346
		1	123	0.34	366	321	3758
		0.5	240	0.42	566	359	2711
	45	4	21	0.10	215	147	1502
		2	42	0.15	293	178	1786
		1	83	0.23	376	223	2030
		0.5	162	0.34	481	193	1460
28.5 cm x 75 µm ID 1.1 µm d_p	30	4	22	0.13	174	n/a	n/a
		2	38	0.17	220		
		1	70	0.23	309		
		0.5	125	0.36	352		

Table 3.5. The average separation window, peak width (4σ), peak capacity, and number of protein and peptide identifications were listed for each column at each running condition.

Gradient Length (min)	Grand NDPC	Fold-Change Coverage
90	-0.0050	-1.01
180	0.057	1.12
360	0.10	1.22

Table 3.6. The Grand NDPC and Fold-Change Coverage were compared for *E. coli* digest separated on the 98.2 cm column run at 30 kpsi to the 44.1 cm column run at 15 kpsi for three gradient lengths. Positive values represented higher coverage on the long column, and negative values represented higher coverage on the shorter column. Grand NDPC and Fold-Change Coverage increased in favor of the long column as gradient length increased.

3.6 FIGURES

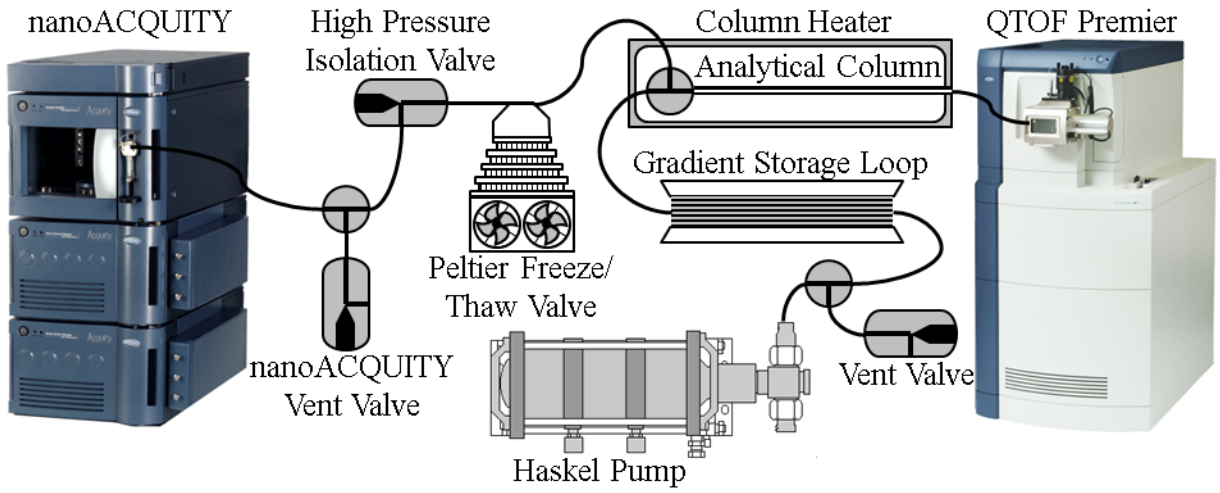

Figure 3.1. The nanoAcquity is shown with the additional tubing and valves necessary for separations at 45 kpsi driven by the Haskel pneumatic amplifier pump.

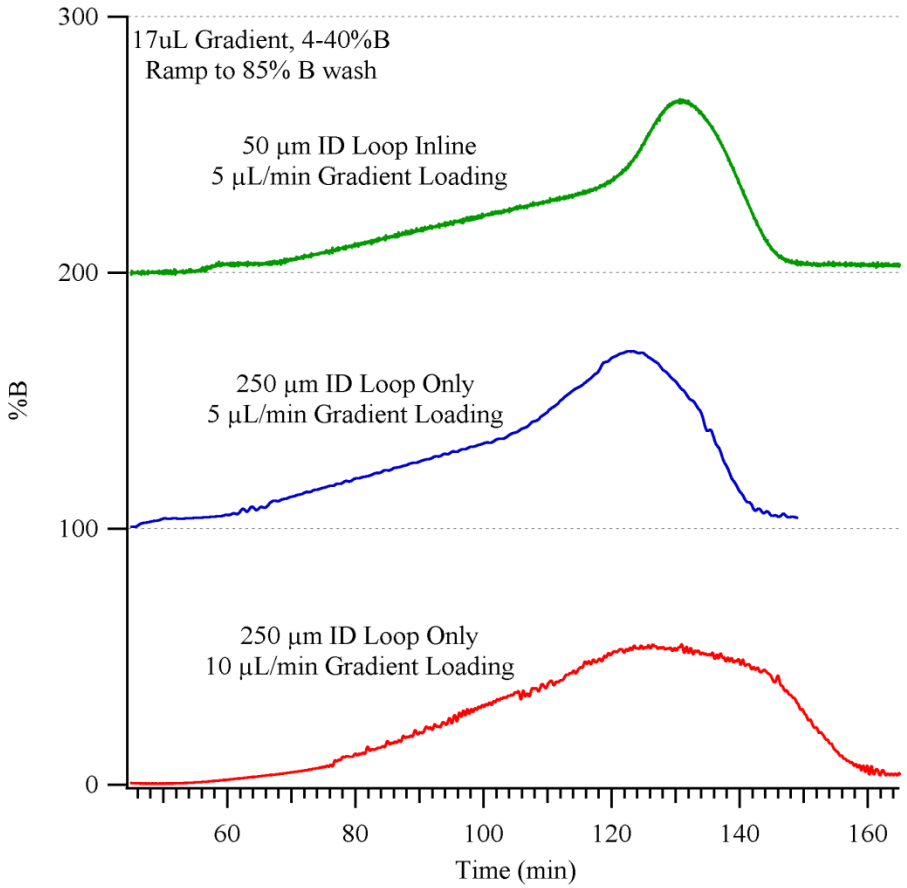

Figure 3.2. The gradient playback time of the UHPLC was monitored by the UV absorbance of acetone in mobile phase B. The gradient linearity was improved by using a lower flow rate for gradient loading and employing the 50 µL ID tubing at the head of the gradient storage loop.

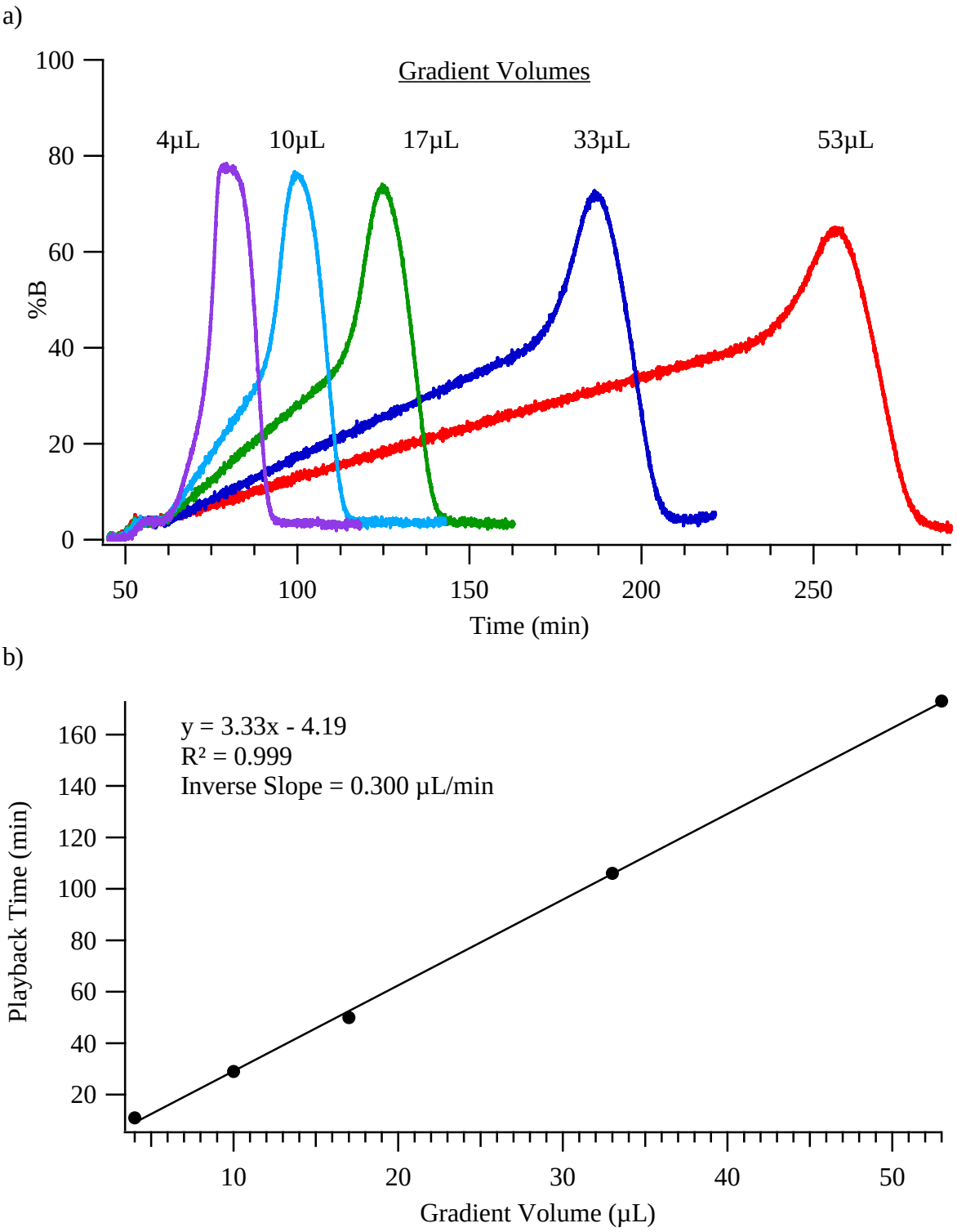

Figure 3.3. The gradient playback time of the UHPLC was monitored by the UV absorbance of acetone in mobile phase B and plotted in part (a) for several different gradient volumes which were noted on the graph. The playback time of the linear region was plotted versus gradient volume in part (b). A best fit line had the equation y = 3.33x – 4.19 and R^2 value of 0.999. The inverse slope was 0.300 µL/min which corresponded to flow rate.

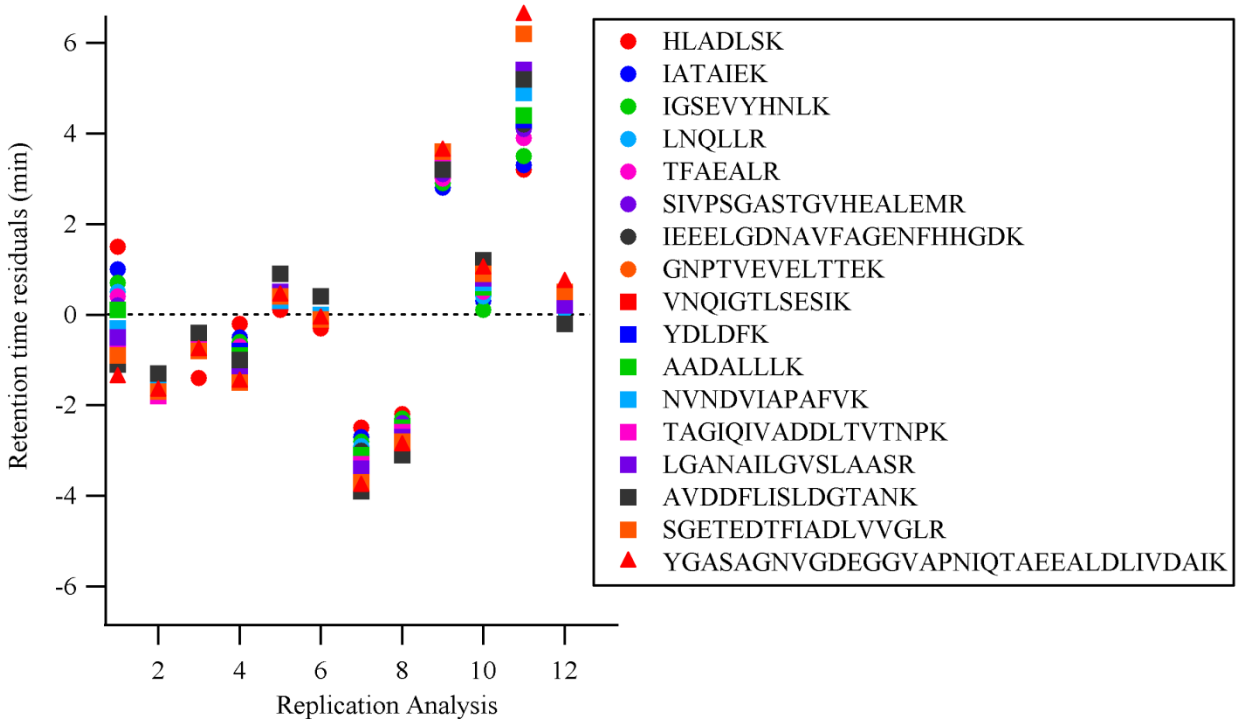

Figure 3.4. The retention time residuals were plotted versus run order for several peptides identified in an enolase digest standard separated on a 110 cm x 75 µm column packed with 1.9 µm BEH C18 particles. The gradient volume was 12.5 µL and was repeated 12 times on 12 different days. The variability of retention times was random with the R^2 values for a 5^{th} order polynomial fit of the residuals ranging between 0.57 and 0.69.

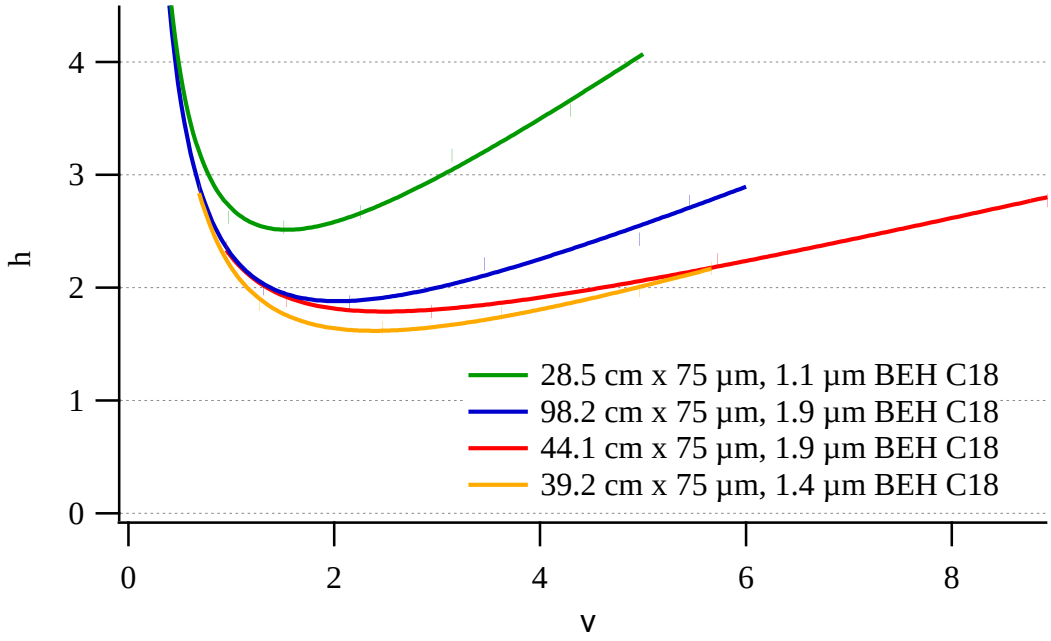

Figure 3.5. The Van Deemter plots with reduced terms of hydroquinone demonstrate the similarity in column performance for the columns tested in these experiments.

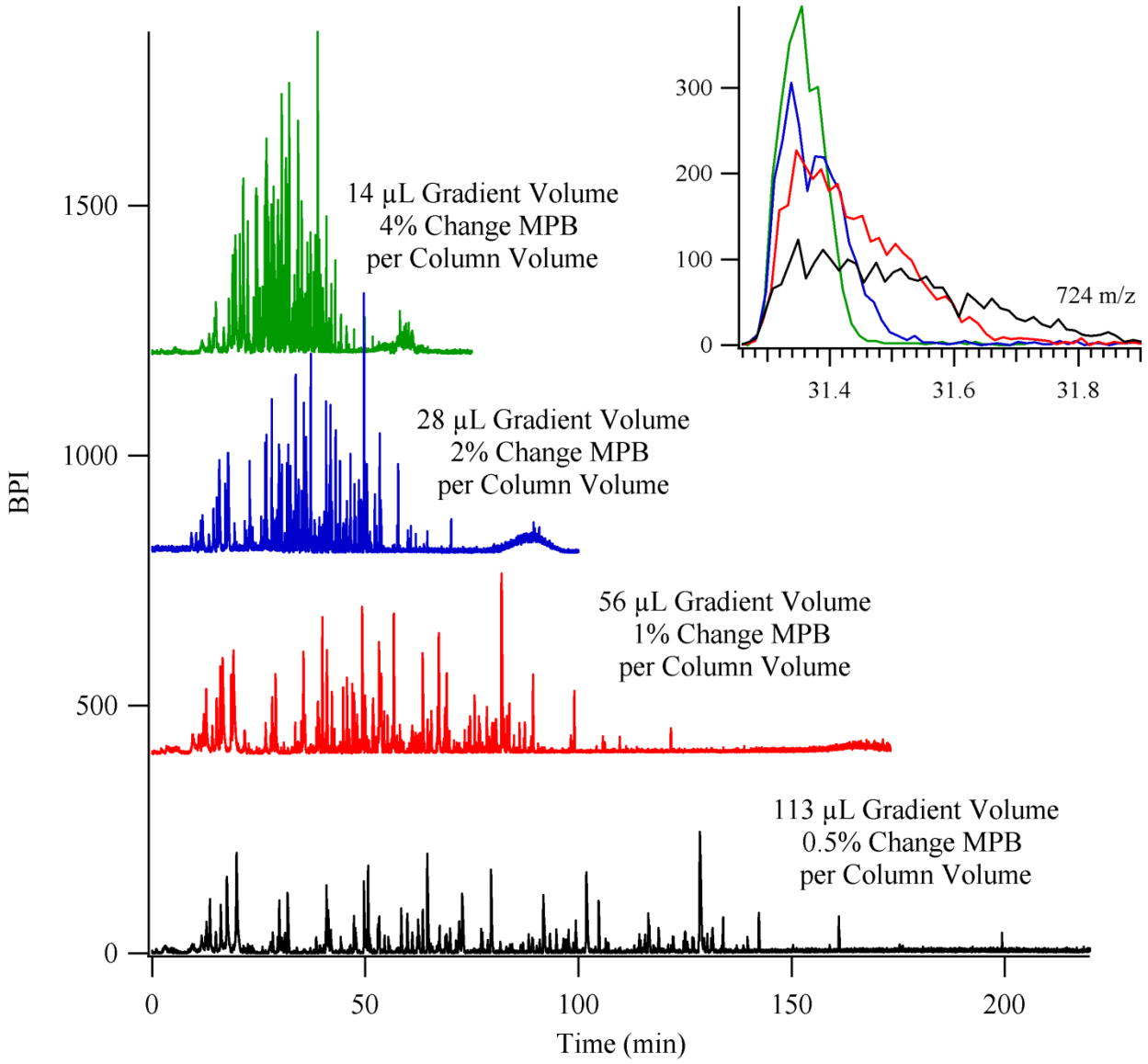

Figure 3.6. Chromatograms of MassPREP™ Digestion Standard Protein Expression Mixture 2 were collected for separations with increasing gradient volume on the 44.1 cm x 75 µm ID column packed with 1.9 µm BEH C18 particles. Separations were completed at 15 kpsi. The insert of a representative peptide peak with 724 m/z extracted from all four chromatograms demonstrated the increase in peak width and decrease in peak height as the as gradient volume increased.

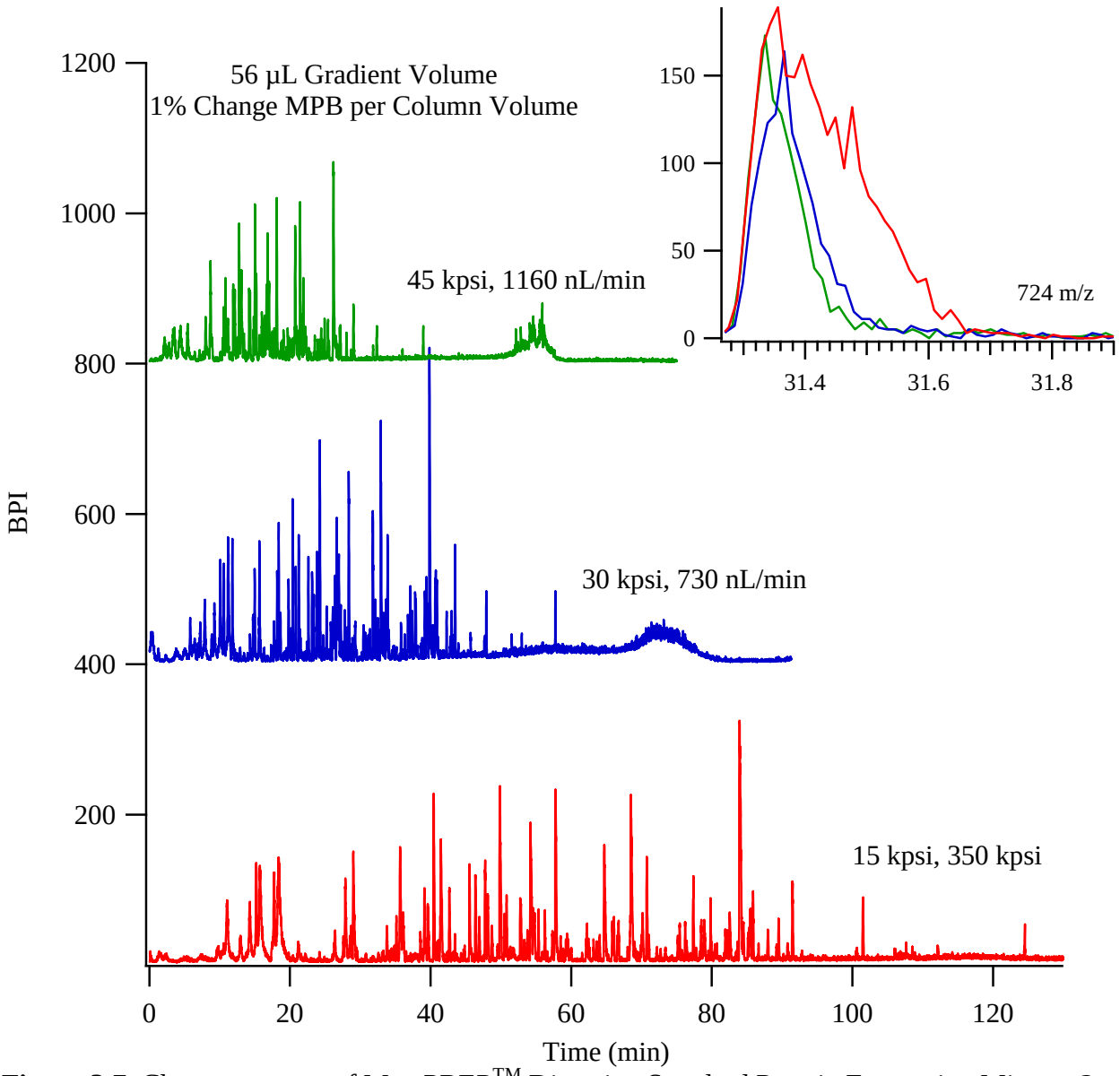

Figure 3.7. Chromatograms of MassPREP™ Digestion Standard Protein Expression Mixture 2 were collected for separations with increasing pressure and flow rate on the 44.1 cm x 75 µm ID column packed with 1.9 µm BEH C18 particles. Separations were completed with a 56 µL gradient volume. The insert of a representative peptide peak with 724 m/z extracted from all three chromatograms showed the decrease in peak width and constant signal intensity as pressure and flow rate increased.

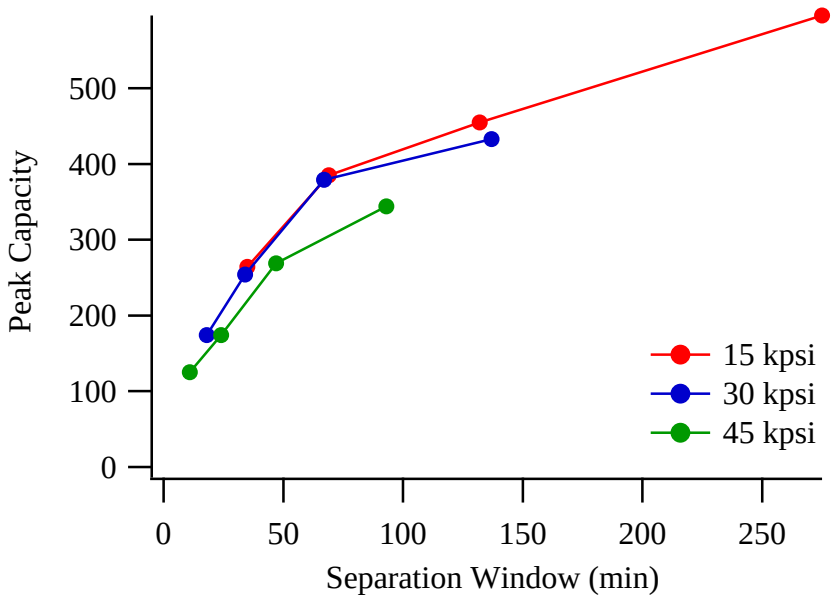

Figure 3.8. Peak capacity versus separation window was displayed for separations on a 44.1 cm x 75 µm ID column with 1.9 µm BEH C18 particles. Each line represented a different running pressure, and each point on a line (from left to right) represented the gradient profiles of 4, 2, 1, or 0.5 percent change in mobile phase composition per column volume.

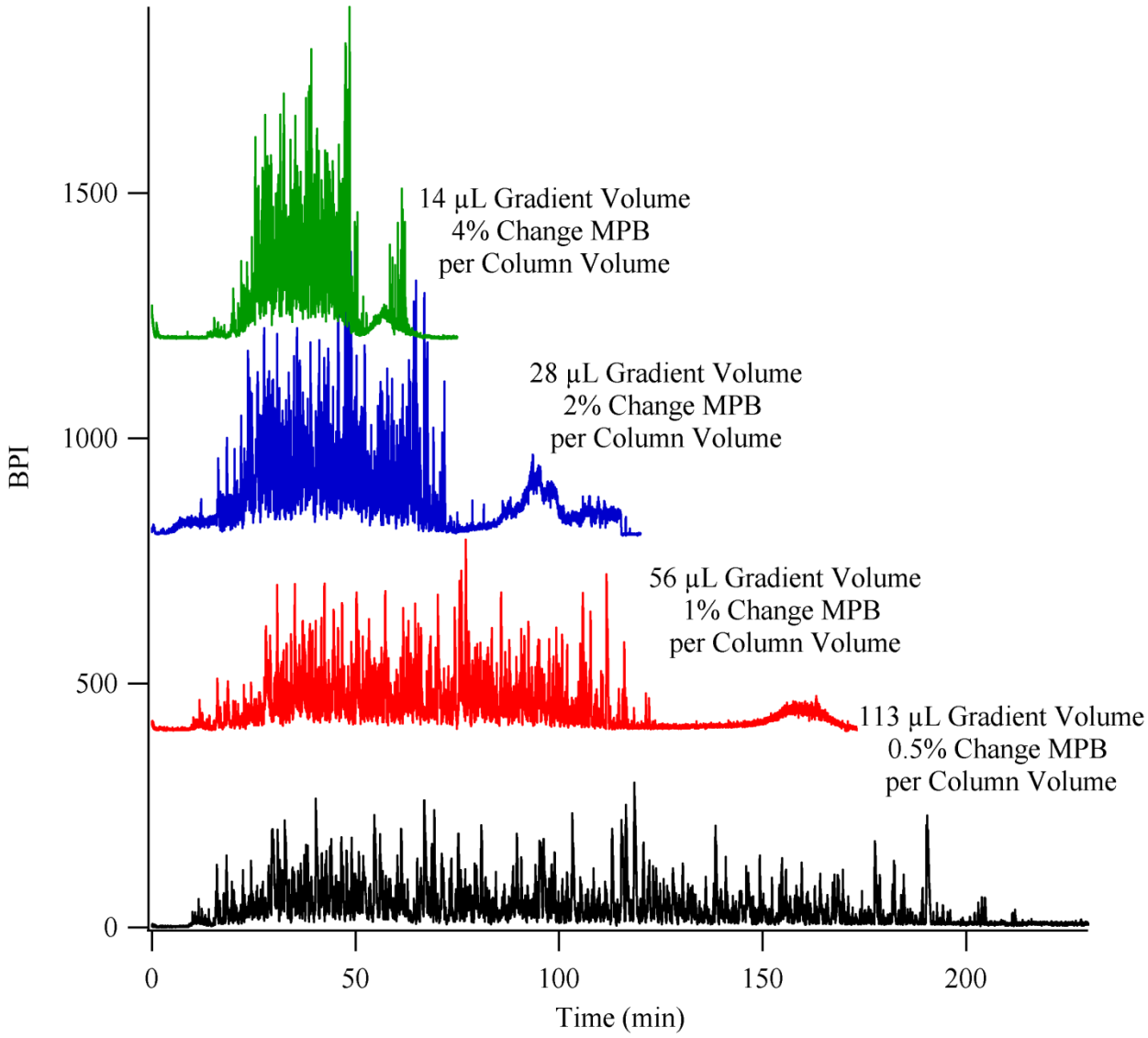

Figure 3.9. Chromatograms of MassPREP™ *E. coli* Digestion Standard were collected for separations with increasing gradient volume on the 44.1 cm x 75 µm ID column packed with 1.9 µm BEH C18 particles. Separations were completed at 15 kpsi. Though the chromatograms were very busy, an increase in resolution was observed as gradient volume increased which was indicated by the signal being closer to baseline between two adjacent peaks.

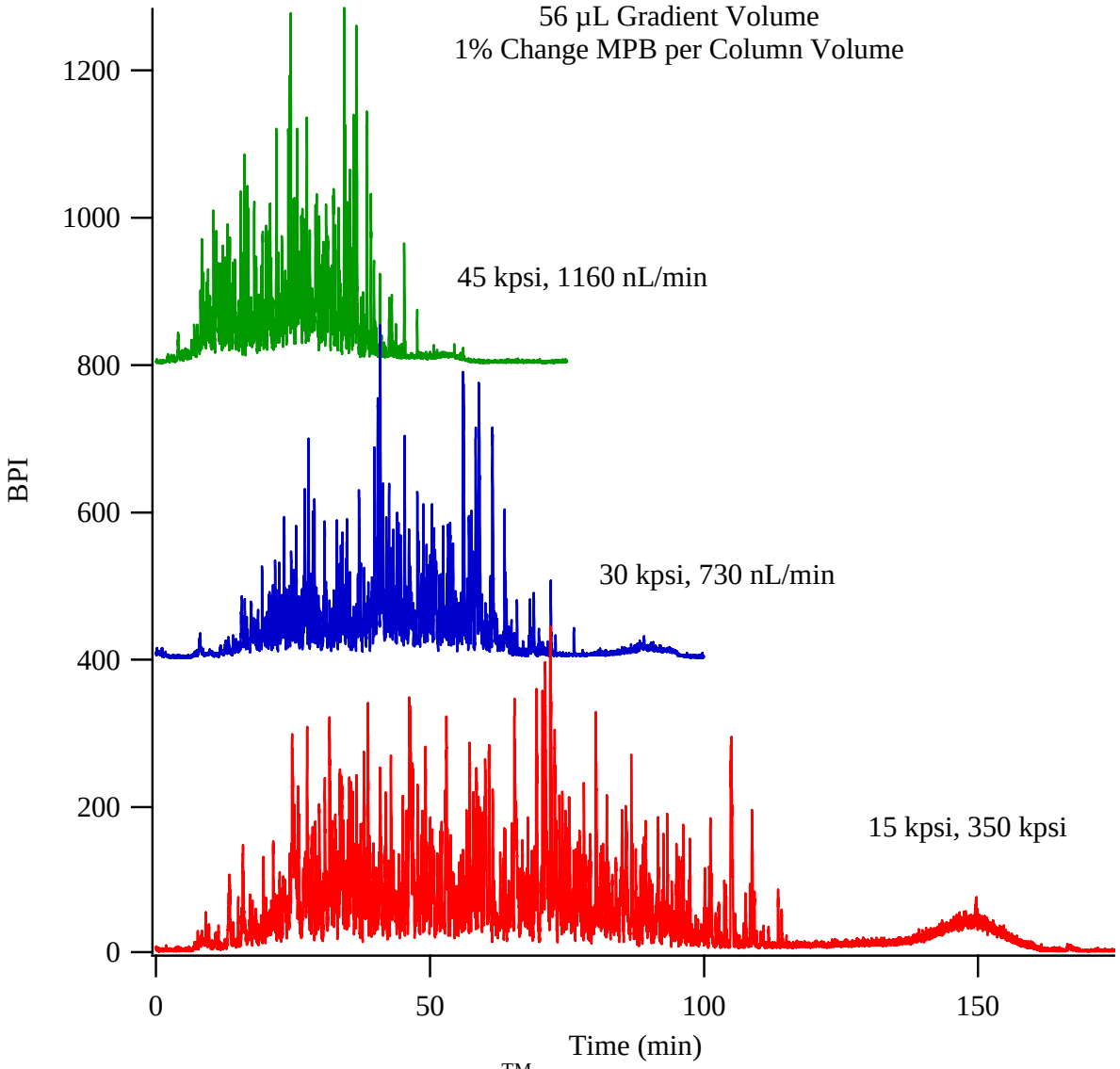

Figure 3.10. Chromatograms of MassPREP™ *E. coli* Digestion Standard were collected for separations with increasing pressure and flow rate on the 44.1 cm x 75 µm ID column packed with 1.9 µm BEH C18 particles. Separations were completed with a 56 µL gradient volume.

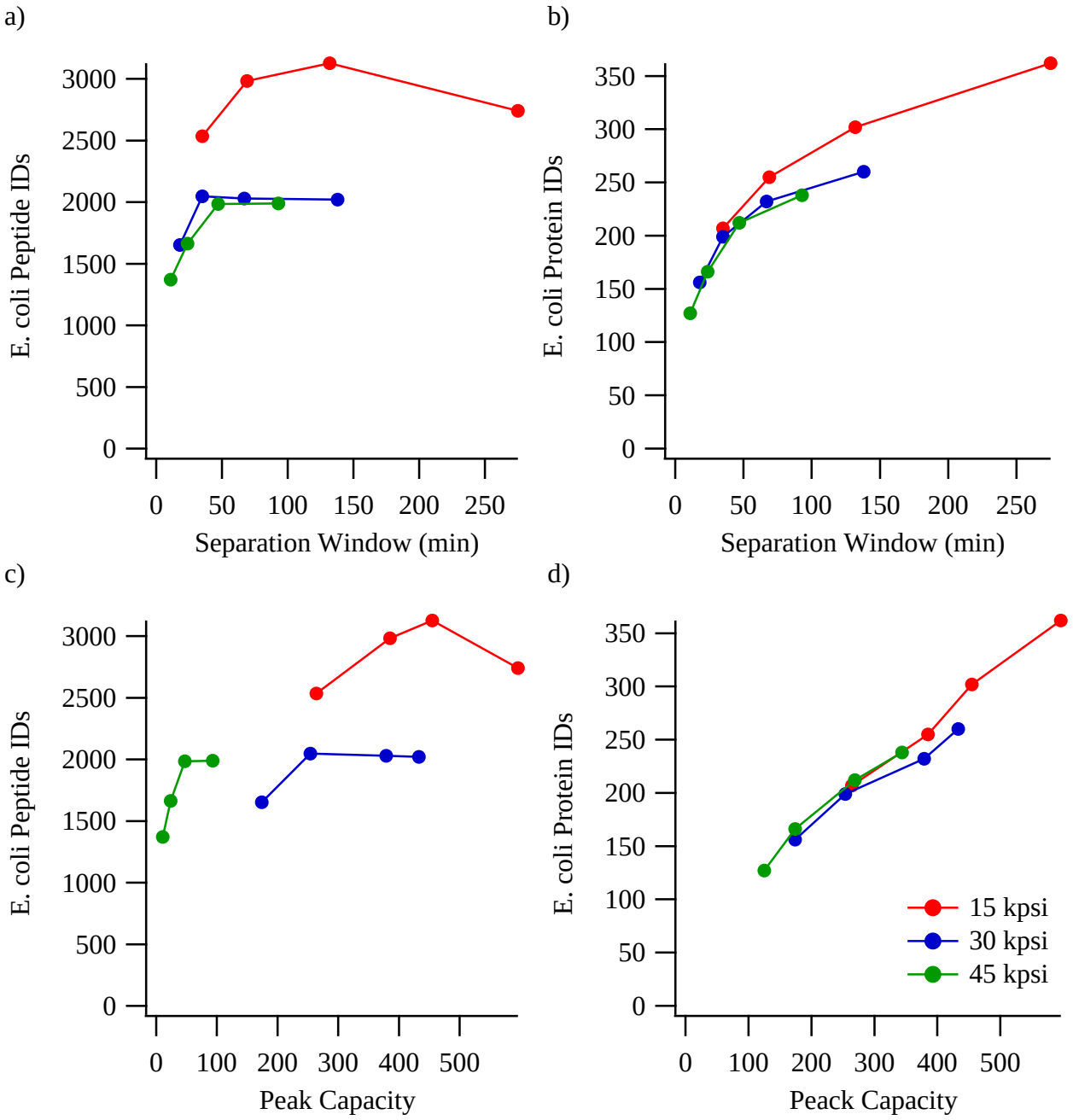

Figure 3.11. The peptide and protein identifications for *E. coli* were plotted versus the separation window and peak capacity for several separations on a 44.1 cm x 75 µm ID column with 1.9 µm BEH C18 particles. Each line represents a different running pressure, and each point on a line (from left to right) represented the gradient profiles of 4, 2, 1, or 0.5 percent change in mobile phase per column volume.

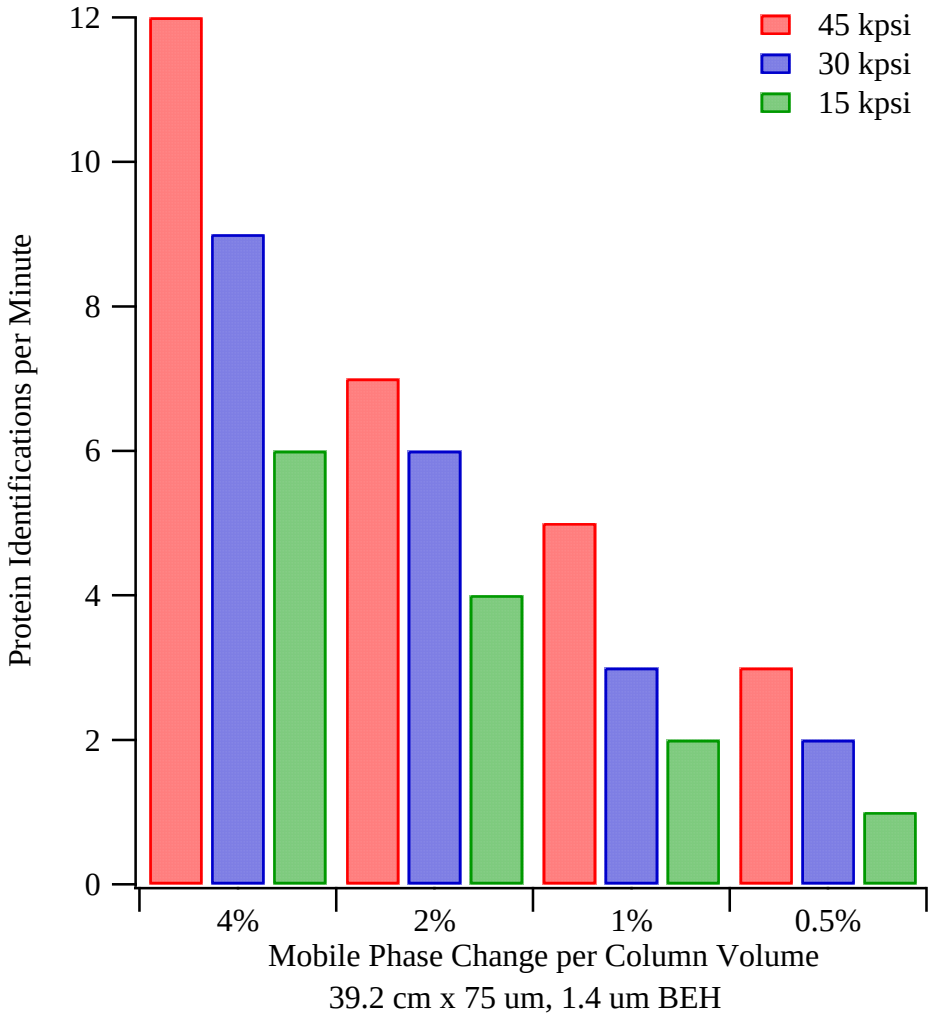

Figure 3.12. Protein identifications per minute or productivity was plotted for the *E. coli* protein identifications from analyses at varying gradient volumes and pressures on the 44.1 cm x 75 µm ID column with 1.9 µm BEH C18 particles. Productivity was highest for the steepest gradient run at the highest pressure.

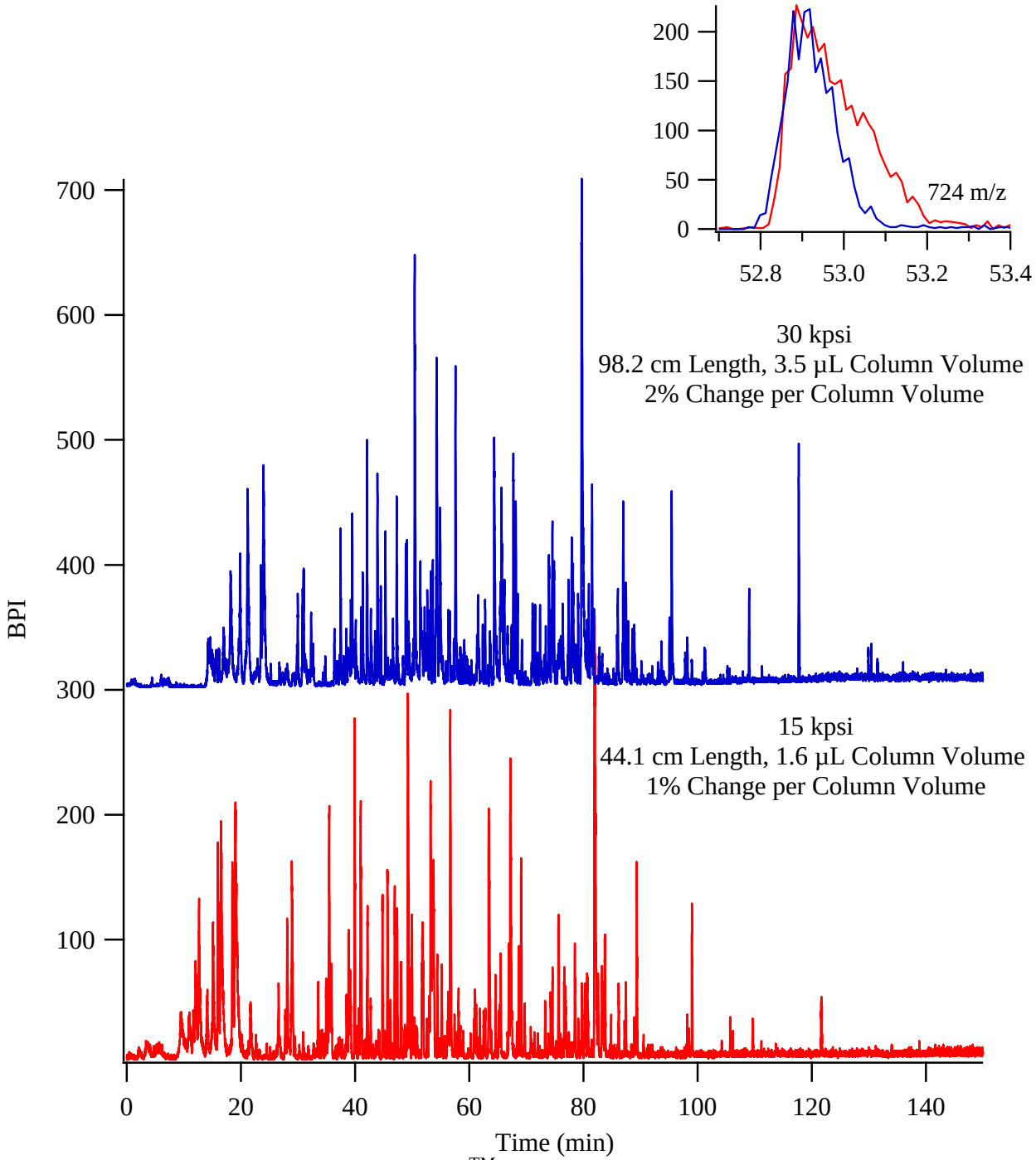

Figure 3.13. Chromatograms of MassPREP™ Digestion Standard Protein Expression Mixture 2 were collected for separations with increasing pressure on a short and long column. The separation time was similar for the 98.2 cm x 75 µm ID column and 44.1 cm x 75 µm ID column packed with 1.9 µm BEH C18 particles. The insert of a representative peptide peak with 724 m/z extracted from both chromatograms showed the decrease in peak width and constant signal intensity as pressure and column length increased.

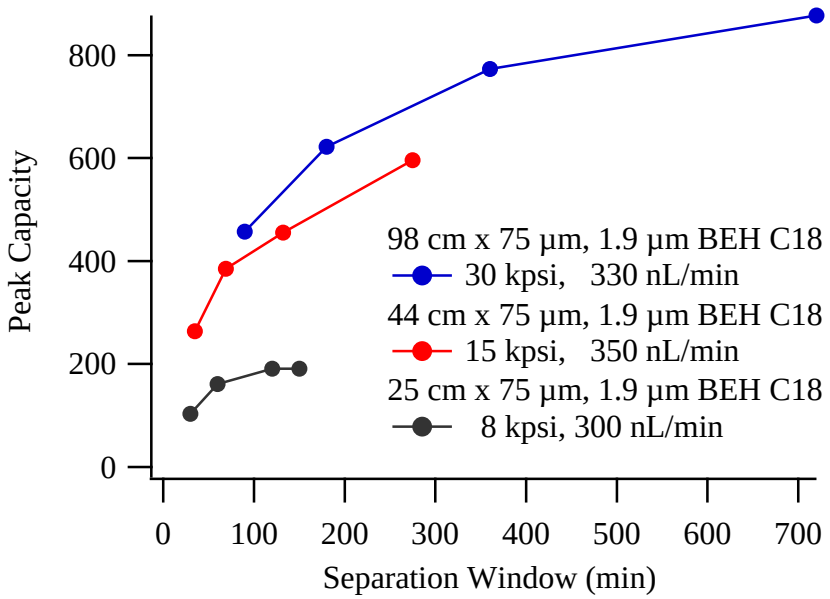

Figure 3.14. The increasing peak capacity versus separation window plot demonstrated the benefit of using higher pressures to run longer columns in the same amount of time as shorter columns. The red line represented separations at 15 kpsi on a 44.1 cm x 75 µm ID column with 1.9 µm BEH C18 particles. The blue line represented separations at 30 kpsi on a 98.2 cm x 75 µm ID column with 1.9 µm BEH C18 particles. The gray line represented separations on a commercial UPLC with a commercial column (25 cm x 75 µm ID column with 1.9 µm BEH C18 particles). Each point on a line (from left to right) represented the gradient profiles of 4, 2, 1, or 0.5 percent change in mobile phase per column volume.

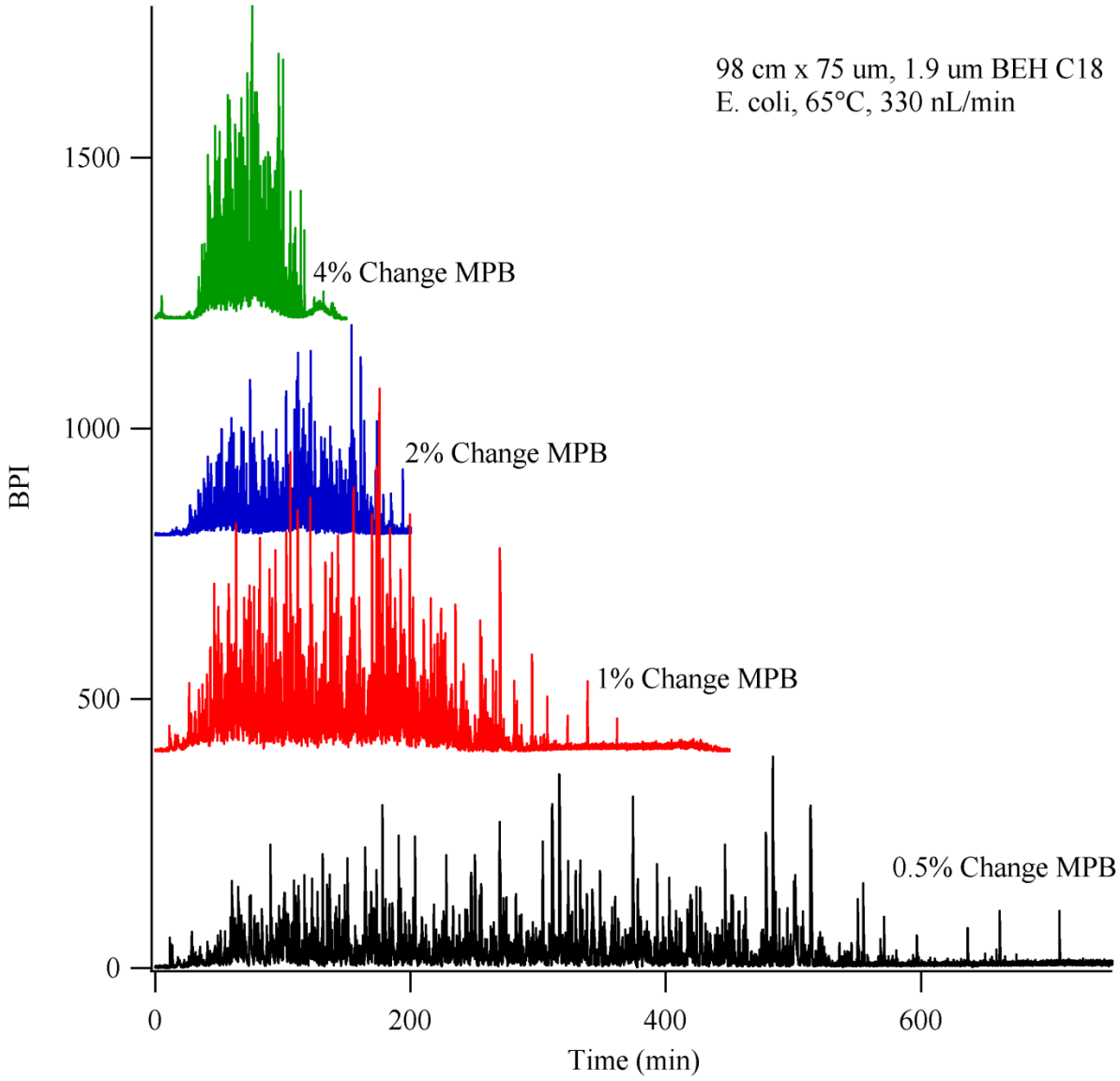

Figure 3.15. Chromatograms of MassPREP™ *E. coli* Digestion Standard were collected for separations with increasing gradient volume on the 98.2 cm x 75 µm ID column packed with 1.9 µm BEH C18 particles. Separations were completed at 30 kpsi. Though the chromatograms were very busy, an increase in resolution was observed as gradient volume increased which was indicated by the signal being closer to baseline between two adjacent peaks. These were the shotgun proteomic experiments with the highest peak capacities.

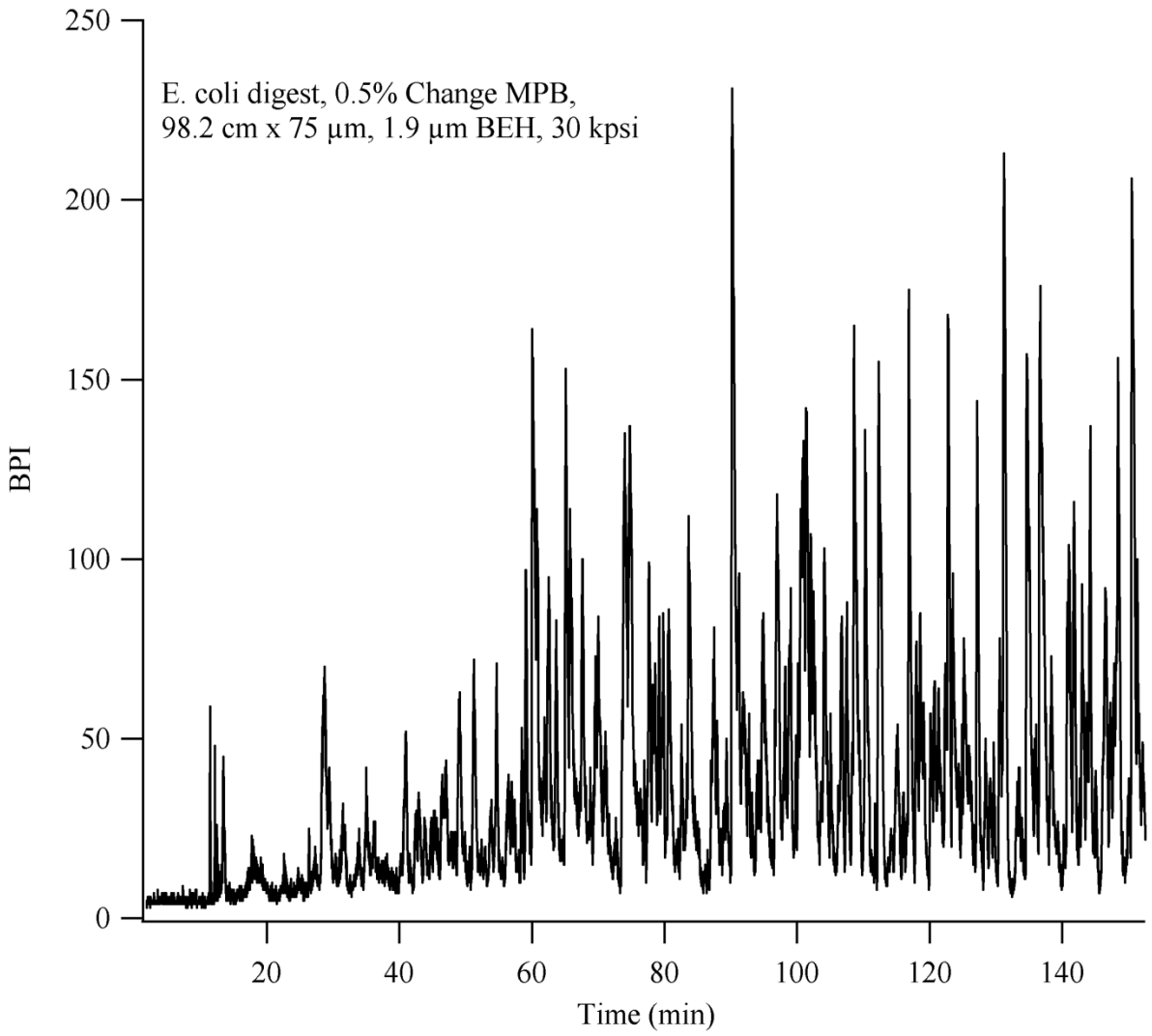

Figure 3.16. This chromatogram of MassPREP™ *E. coli* Digestion Standard from the 98.2 cm x 75 µm ID column packed with 1.9 µm BEH C18 particles is a zoomed in version of the purple chromatogram in Figure 3.15. The return of signal to baseline between several adjacent peaks demonstrated the gain in resolution from using long columns at elevated pressures and temperature for proteomics analysis.

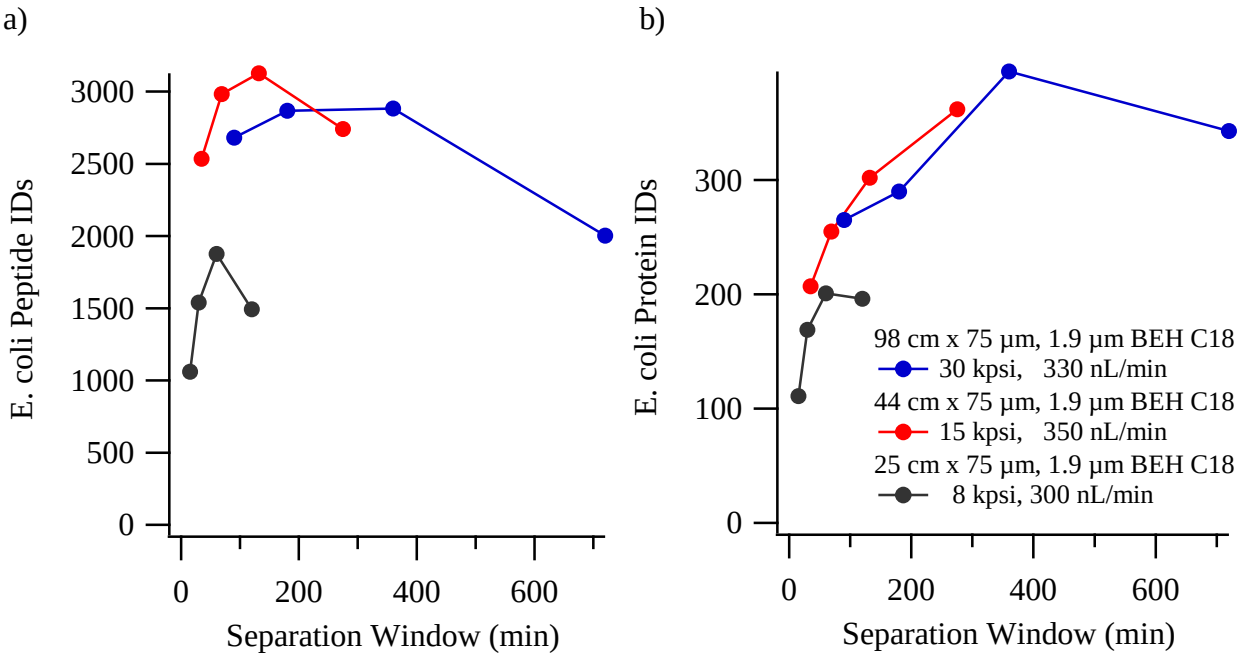

Figure 3.17. The peptide and protein identifications for *E. coli* were plotted versus the separation window in parts a and b, respectively. The red line represented separations at 15 kpsi on a 44.1 cm x 75 µm ID column with 1.9 µm BEH C18 particles. The blue line represented separations at 30 kpsi on a 98.2 cm x 75 µm ID column with 1.9 µm BEH C18 particles. The gray line represented separations on a commercial UPLC with a commercial column (25 cm x 75 µm ID column with 1.9 µm BEH 18 particles). Each point on a line (from left to right) represented the gradient profiles of 4, 2, 1, or 0.5 percent change in mobile phase per column volume.

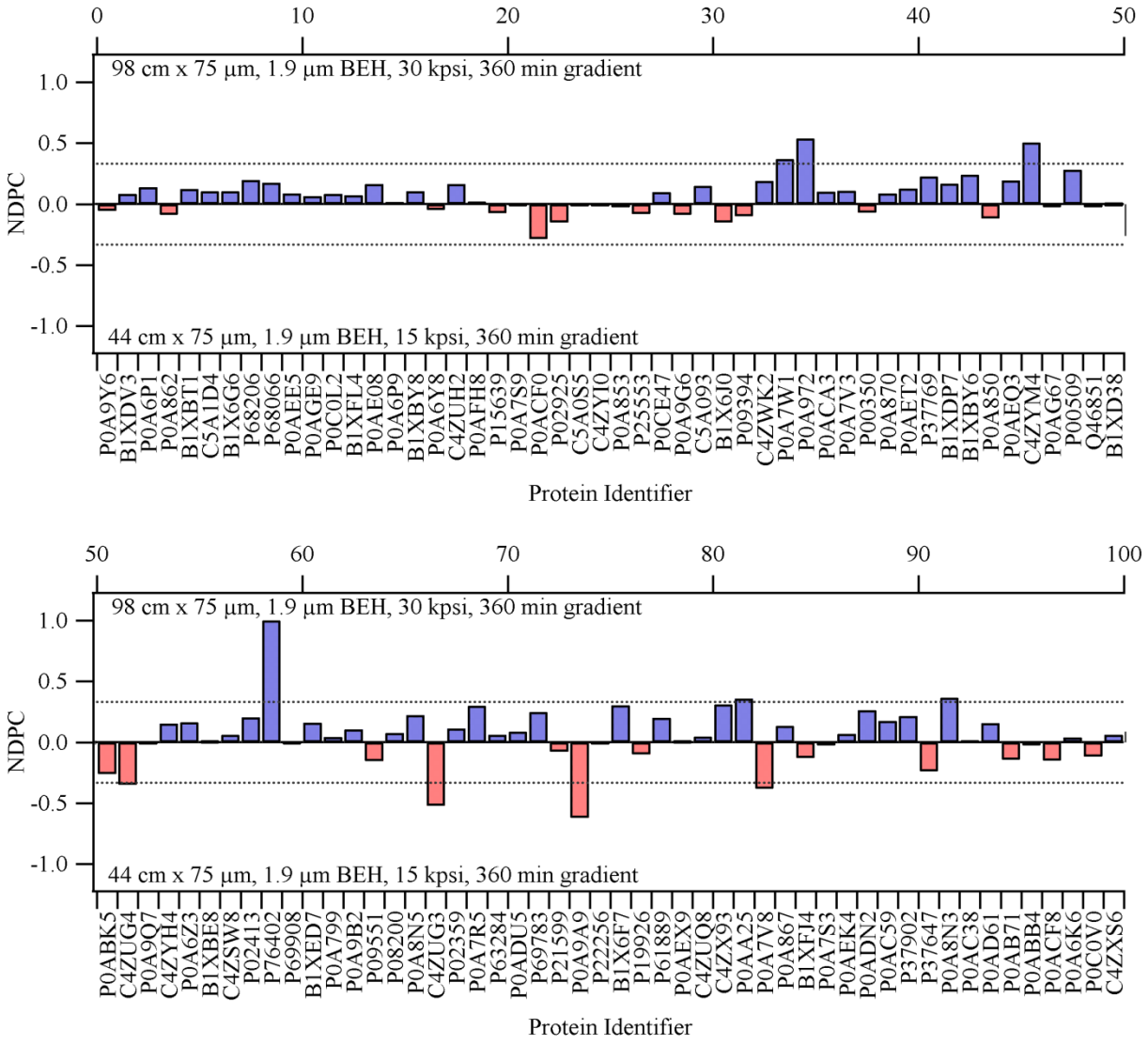

Figure 3.18. The NDPC comparing the analysis on the 98.2 cm column run at 30 kpsi to the 44.1 cm column run at 15 kpsi for a 360 min gradient was plotted for each protein identified in an E. coli digest standard. If a protein was identified with higher sequence coverage with the separation on the 98.2 cm column, its NDPC value was positive (blue bars). The red bars signified higher coverage with the separation on the 44.1 cm column. Proteins with higher coverage were plotted on the left, and proteins with lower coverage were on the right. Differences in coverage were minimal for highly covered proteins. As protein coverage decreased, more proteins were identified with higher coverage with the separation on the 98.2 cm column. The dashed line represented a two-fold difference in protein coverage.

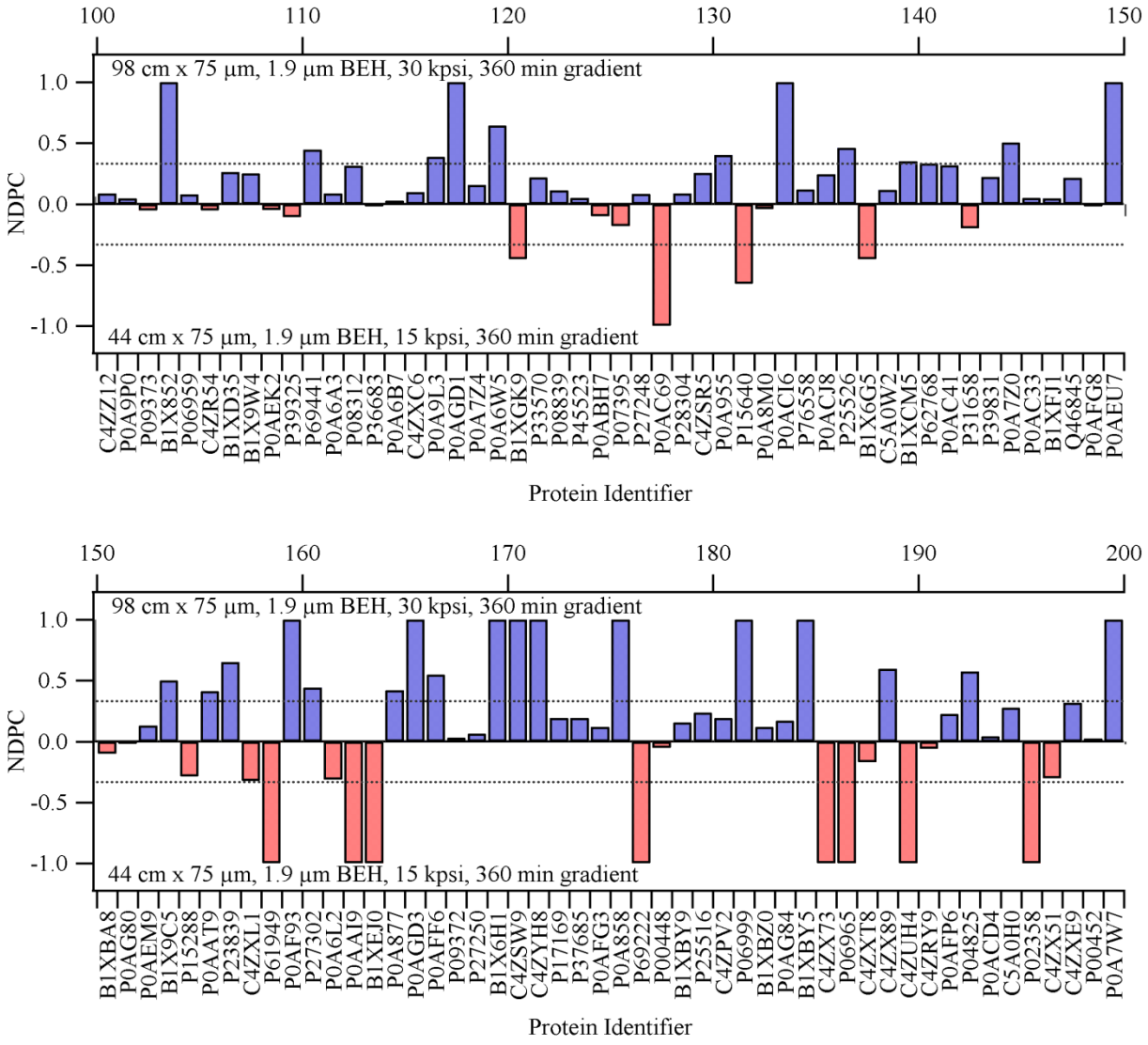

Figure 3.18. (continued)

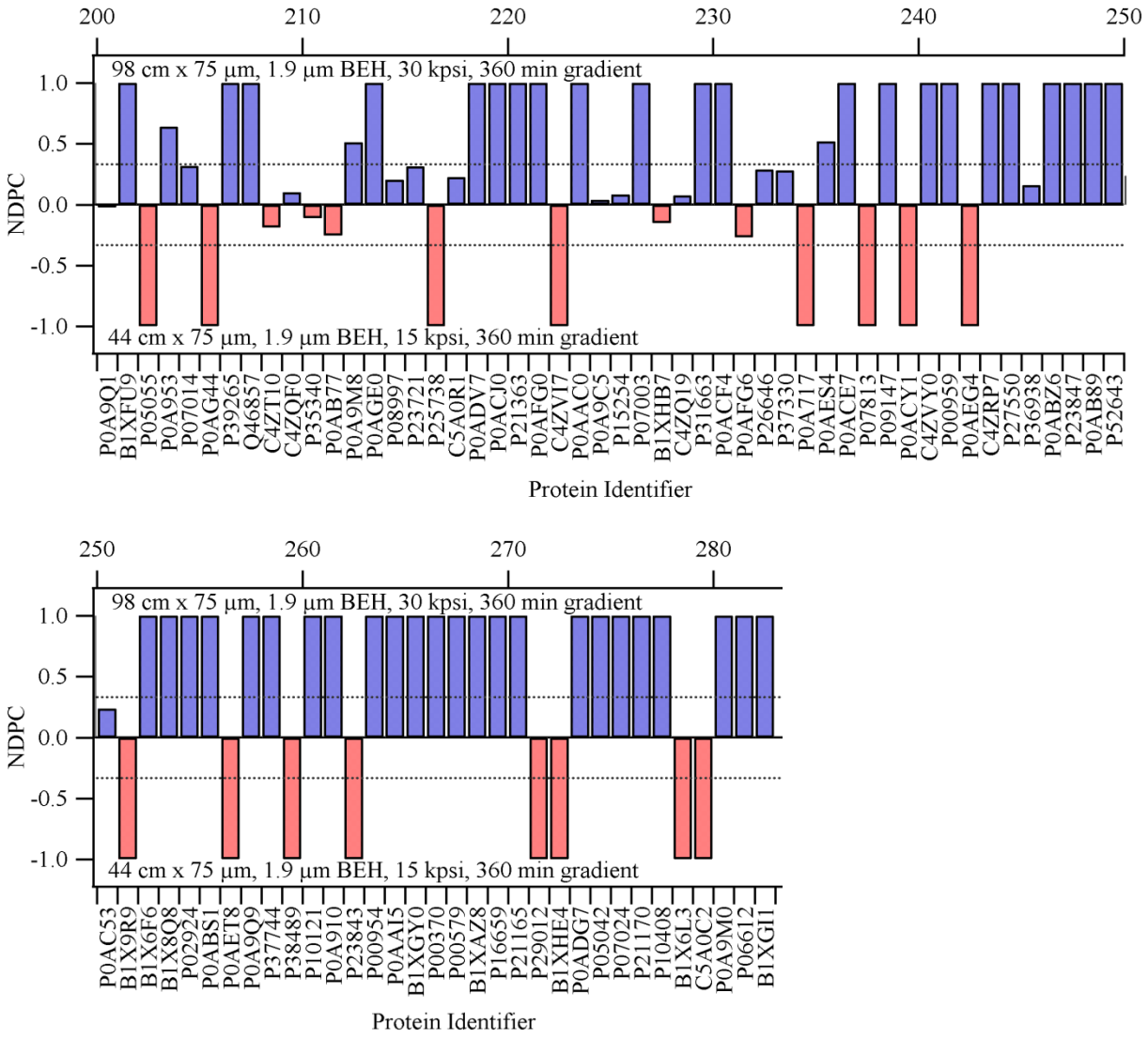

Figure 3.18. (continued)

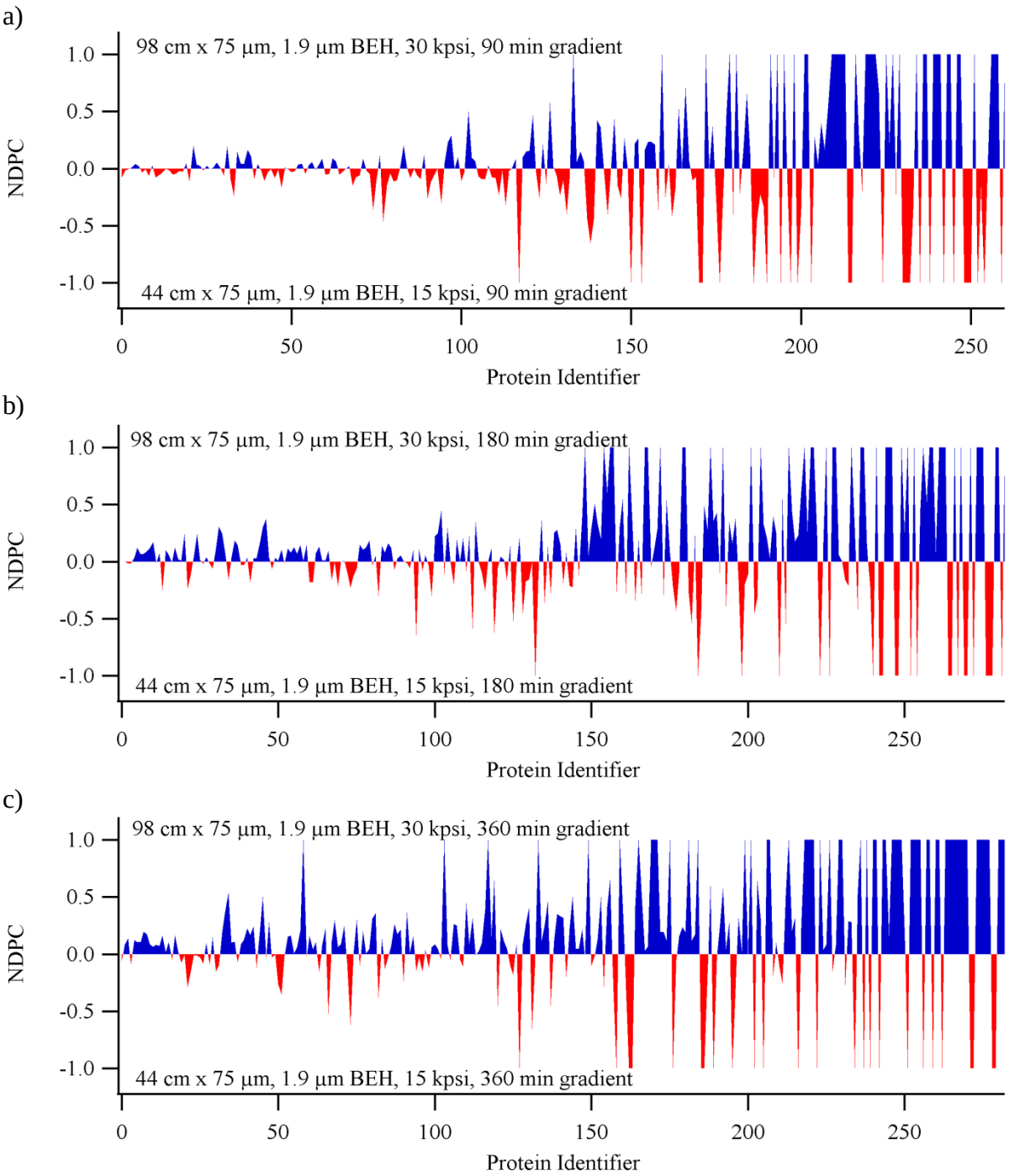

Figure 3.19. The NDPC comparing the analysis on the 98.2 cm column run at 30 kpsi to the 44.1 cm column run at 15 kpsi was plotted for each protein identified in an E. coli digest standard separated with a for a 90 min (part a), 180 min (part b), and 360 min (part c) gradient . If a protein was identified with higher sequence coverage with the separation on the 98.2 cm column, its NDPC value was positive (blue bars). The red bars signified higher coverage with the separation on the 44.1 cm column. Proteins with higher coverage were plotted on the left, and proteins with lower coverage were on the right. Differences in coverage were minimal for highly covered proteins. As protein coverage decreased, more proteins were identified with higher coverage with the separation on the 98.2 cm column.

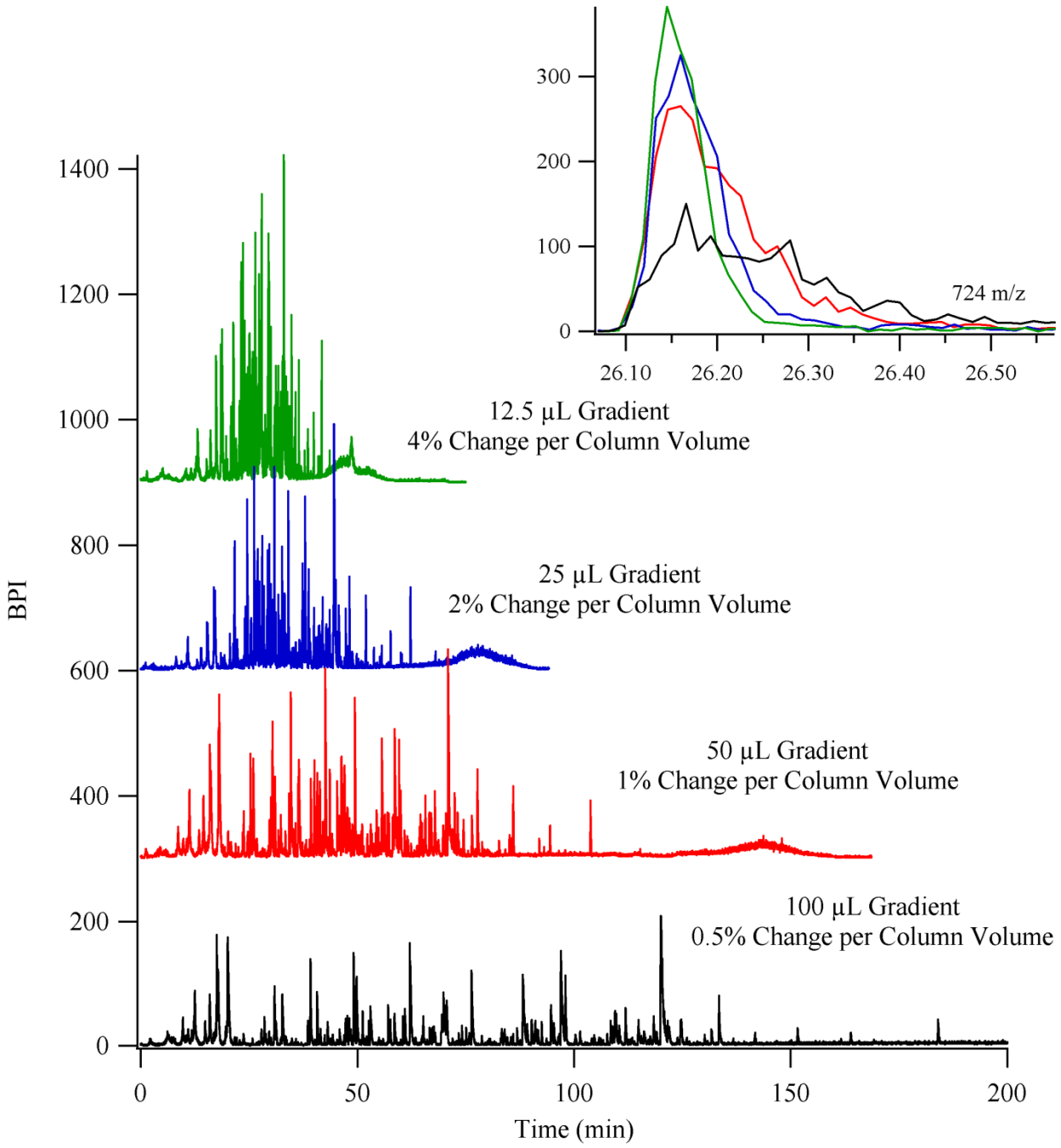

Figure 3.20. Chromatograms of MassPREP™ Digestion Standard Protein Expression Mixture 2 were collected for separations with increasing gradient volume on the 39.2 cm x 75 µm ID column packed with 1.4 µm BEH C18 particles. Separations were completed at 30 kpsi. The insert of a representative peptide peak with 724 m/z extracted from all four chromatograms showed the increase in peak width and decrease in peak height as the as gradient volume increased.

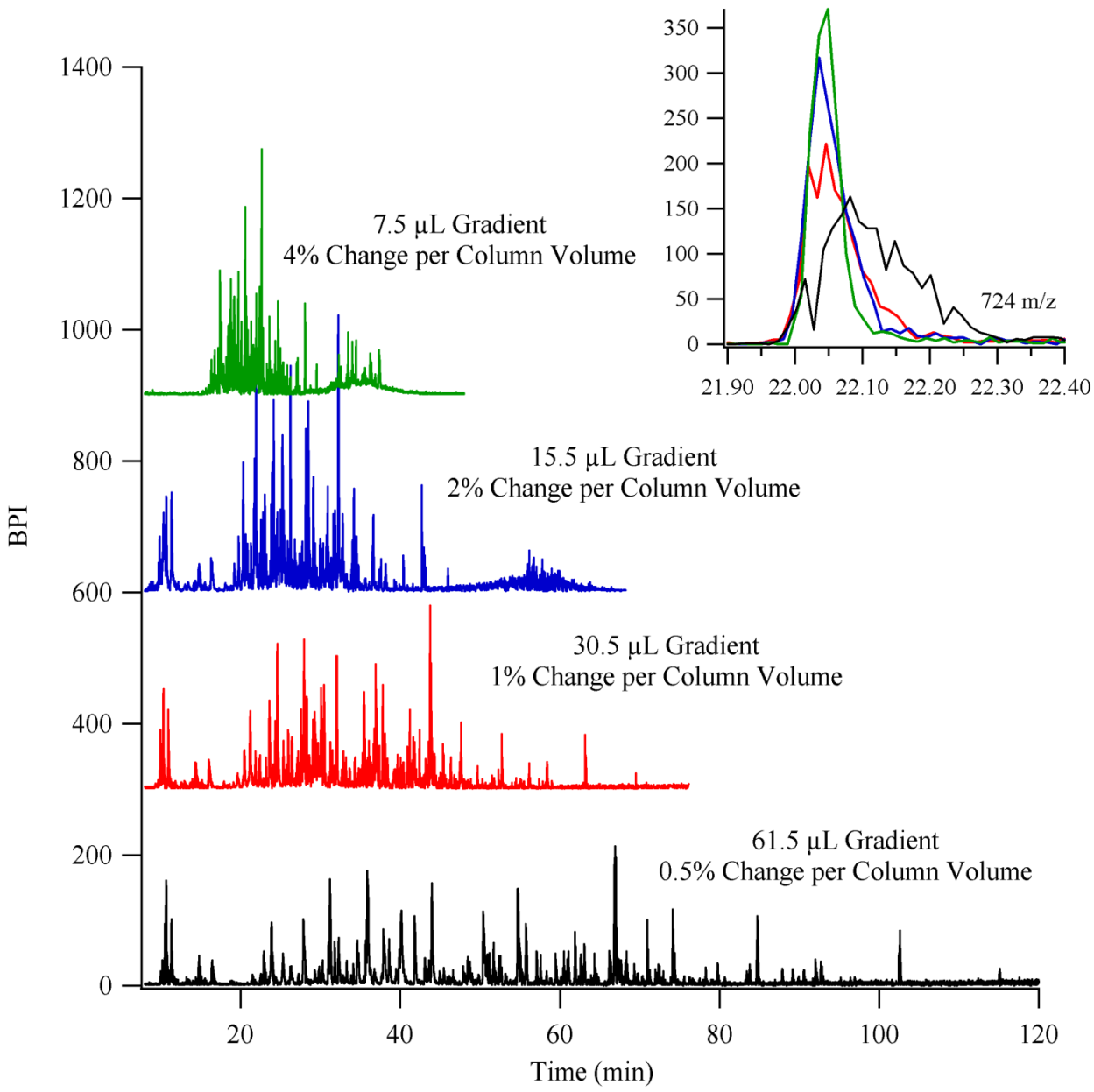

Figure 3.21. Chromatograms of MassPREP™ Digestion Standard Protein Expression Mixture 2 were collected for separations with increasing gradient volume on the 28.5 cm x 75 µm ID column packed with 1.1 µm BEH C18 particles. Separations were completed at 30 kpsi. The insert of a representative peptide peak with 724 m/z extracted from all four chromatograms showed the increase in peak width and decrease in peak height as the as gradient volume increased. These were the fasted separations demonstrated in this manuscript. The gain in speed was due to the implementation of small particles and ultrahigh pressures.

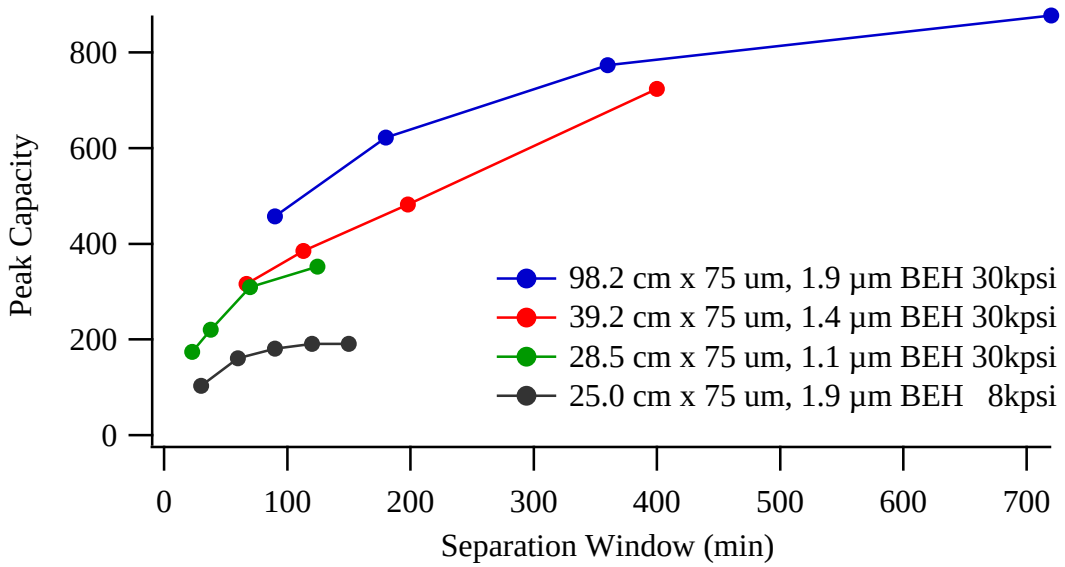

Figure 3.22. The increasing peak capacity versus separation window plot demonstrated the difference in performance for columns with different particle sizes. The red line represented separations at 30 kpsi on a 39.2 cm x 75 µm ID column with 1.4 µm BEH C18 particles. The blue line represented separations on a 98.2 cm x 75 µm ID column with 1.9 µm BEH C18 particles. The green line represented separations on a 28.5 cm x 75 µm ID column with 1.1 µm BEH C18 particles. The gray line represented separations on a commercial UPLC with a commercial column.

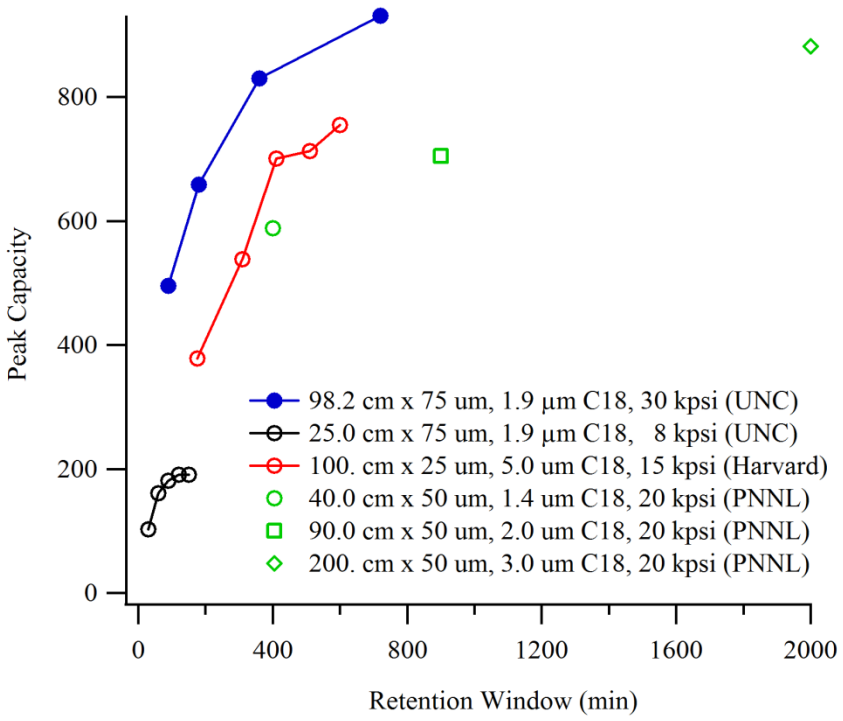

Figure 3.23. The peak capacity versus separation window plot compared the highest peak capacities demonstrated in this manuscript, as obtained with the 98.2 cm x 75 µm ID column with 1.9 µm BEH C18 particles, separations on the commercial nanoAcquity and several data sets found in the literature for separations with long columns and at high pressure (PNNL[24],Harvard[39]). The data presented in this manuscript achieved higher peak capacities in less time as compared to the literature data.

3.7 REFERENCES

1. Paik, Y.-K.; Jeong, S.-K.; Omenn, G. S.; Uhlen, M.; Hanash, S.; Cho, S. Y.; Lee, H.-J.; Na, K.; Choi, E.-Y.; Yan, F.; Zhang, F.; Zhang, Y.; Snyder, M.; Cheng, Y.; Chen, R.; Marko-Varga, G.; Deutsch, E. W.; Kim, H.; Kwon, J.-Y.; Aebersold, R.; Bairoch, A.; Taylor, A. D.; Kim, K. Y.; Lee, E.-Y.; Hochstrasser, D.; Legrain, P.; Hancock, W. S., The Chromosome-Centric Human Proteome Project for cataloging proteins encoded in the genome. *Nat Biotech* 2012, *30* (3), 221-223.

2. Anderson, N. L.; Anderson, N. G., The Human Plasma Proteome: History, Character, and Diagnostic Prospects. *Molecular & Cellular Proteomics* 2003, *2* (1), 50.

3. Xie, F.; Smith, R. D.; Shen, Y., Advanced proteomic liquid chromatography. *Journal of Chromatography A* 2012, *1261* (0), 78-90.

4. Yates, J. R.; Ruse, C. I.; Nakorchevsky, A., Proteomics by Mass Spectrometry: Approaches, Advances, and Applications. *Annual Review of Biomedical Engineering* 2009, *11* (1), 49-79.

5. Washburn, M. P.; Ulaszek, R.; Deciu, C.; Schieltz, D. M.; Yates, J. R., Analysis of Quantitative Proteomic Data Generated via Multidimensional Protein Identification Technology. *Analytical Chemistry* 2002, *74* (7), 1650-1657.

6. Wolters, D. A.; Washburn, M. P.; Yates, J. R., An Automated Multidimensional Protein Identification Technology for Shotgun Proteomics. *Analytical Chemistry* 2001, *73* (23), 5683-5690.

7. Stobaugh, J. T.; Fague, K. M.; Jorgenson, J. W., Prefractionation of Intact Proteins by Reversed-Phase and Anion-Exchange Chromatography for the Differential Proteomic Analysis of Saccharomyces cerevisiae. *Journal of Proteome Research* 2012, *12* (2), 626-636.

8. Gilar, M.; Olivova, P.; Daly, A. E.; Gebler, J. C., Two-dimensional separation of peptides using RP-RP-HPLC system with different pH in first and second separation dimensions. *Journal of Separation Science* 2005, *28* (14), 1694-1703.

9. Emmett, M. R.; Caprioli, R. M., Micro-electrospray mass spectrometry: ultra-high-sensitivity analysis of peptides and proteins. *Journal of the American Society for Mass Spectrometry* 1994, *5* (7), 605-613.

10. Gale, D. C.; Smith, R. D., Small volume and low flow-rate electrospray lonization mass spectrometry of aqueous samples. *Rapid Communications in Mass Spectrometry* 1993, *7* (11), 1017-1021.

11. Wilm, M. S.; Mann, M., Electrospray and Taylor-Cone theory, Dole's beam of macromolecules at last? *International Journal of Mass Spectrometry and Ion Processes* 1994, *136* (2–3), 167-180.

12. Wilm, M.; Mann, M., Analytical Properties of the Nanoelectrospray Ion Source. *Analytical Chemistry* 1996, *68* (1), 1-8.

13. Valentine, S. J.; Plasencia, M. D.; Liu, X.; Krishnan, M.; Naylor, S.; Udseth, H. R.; Smith, R. D.; Clemmer, D. E., Toward Plasma Proteome Profiling with Ion Mobility-Mass Spectrometry. *Journal of Proteome Research* 2006, *5* (11), 2977-2984.

14. FF, G.-G.; C, L.; SJ, H.; J, F.; C, B.; H, H.; AR, J., - A critical appraisal of techniques, software packages, and standards for. *D - 101131135* (- 1557-8100 (Electronic)), T - ppublish.

15. Hebert, A. S.; Richards, A. L.; Bailey, D. J.; Ulbrich, A.; Coughlin, E. E.; Westphall, M. S.; Coon, J. J., The One Hour Yeast Proteome. *Molecular & Cellular Proteomics* 2014, *13* (1), 339-347.

16. Annesley, T. M., Ion Suppression in Mass Spectrometry. *Clinical Chemistry* 2003, *49* (7), 1041-1044.

17. Giddings, J. C., Maximum number of components resolvable by gel filtration and other elution chromatographic methods. *Analytical Chemistry* 1967, *39* (8), 1027-1028.

18. Giddings, J. C., *Unified separation science*. Wiley: 1991.

19. Neue, U. D., Theory of peak capacity in gradient elution. *Journal of Chromatography A* 2005, *1079* (1–2), 153-161.

20. Patel, K. D.; Jerkovich, A. D.; Link, J. C.; Jorgenson, J. W., In-Depth Characterization of Slurry Packed Capillary Columns with 1.0-μm Nonporous Particles Using Reversed-Phase Isocratic Ultrahigh-Pressure Liquid Chromatography. *Analytical Chemistry* 2004, *76* (19), 5777-5786.

21. Liu, H.; Finch, J. W.; Lavallee, M. J.; Collamati, R. A.; Benevides, C. C.; Gebler, J. C., Effects of column length, particle size, gradient length and flow rate on peak capacity of nano-scale liquid chromatography for peptide separations. *Journal of Chromatography A* 2007, *1147* (1), 30-36.

22. de Villiers, A.; Lestremau, F.; Szucs, R.; Gélébart, S.; David, F.; Sandra, P., Evaluation of ultra performance liquid chromatography: Part I. Possibilities and limitations. *Journal of Chromatography A* 2006, *1127* (1–2), 60-69.

23. MacNair, J. E.; Lewis, K. C.; Jorgenson, J. W., Ultrahigh-Pressure Reversed-Phase Liquid Chromatography in Packed Capillary Columns. *Analytical Chemistry* 1997, *69* (6), 983-989.

24. Shen, Y.; Zhang, R.; Moore, R. J.; Kim, J.; Metz, T. O.; Hixson, K. K.; Zhao, R.; Livesay, E. A.; Udseth, H. R.; Smith, R. D., Automated 20 kpsi RPLC-MS and MS/MS with Chromatographic Peak Capacities of 1000−1500 and Capabilities in Proteomics and Metabolomics. *Analytical Chemistry* 2005, *77* (10), 3090-3100.

25. MacNair, J. E.; Patel, K. D.; Jorgenson, J. W., Ultrahigh-Pressure Reversed-Phase Capillary Liquid Chromatography: Isocratic and Gradient Elution Using Columns Packed with 1.0-μm Particles. *Analytical Chemistry* 1999, *71* (3), 700-708.

26. Link, J. C. Development and application of gradient ultrahigh pressure liquid chromatography for separations of complex biological mixtures. The University of North Carolina at Chapel Hill, 2004.

27. Eschelbach, J. W.; Jorgenson, J. W., Improved Protein Recovery in Reversed-Phase Liquid Chromatography by the Use of Ultrahigh Pressures. *Analytical Chemistry* 2006, *78* (5), 1697-1706.

28. Gritti, F.; Guiochon, G., Theoretical comparison of the performance of gradient elution chromatography at constant pressure and constant flow rate. *Journal of Chromatography A* 2012, *1253* (0), 71-82.

29. Gritti, F.; Stankovich, J. J.; Guiochon, G., Potential advantage of constant pressure versus constant flow gradient chromatography for the analysis of small molecules. *Journal of Chromatography A* 2012, *1263* (0), 51-60.

30. Dourdeville, T. A. Peltier based freeze-thaw valves and method of use. US Patent 7,128,081. Oct 31, 2006.

31. WatersCorp. nanoAcuity UPLC System *Instrument Specifications* [Online], 2010, p. 720001083en.

32. Aris, R., On the Dispersion of a Solute in a Fluid Flowing through a Tube. *Proceedings of the Royal Society of London. Series A. Mathematical and Physical Sciences* 1956, *235* (1200), 67-77.

33. Knox, J. H.; Gilbert, M. T., Kinetic optimization of straight open-tubular liquid chromatography. *Journal of Chromatography A* 1979, *186* (0), 405-418.

34. Neue, U. D., *HPLC Columns: Theory, Technology, and Practice*. Wiley: 1997.

35. Chen, H.; Horváth, C., High-speed high-performance liquid chromatography of peptides and proteins. *Journal of Chromatography A* 1995, *705* (1), 3-20.

36. Franklin, E. G. Utilization of Long Columns Packed with Sub-2 mum Particles Operated at High Pressures and Elevated Temperatures for High-Efficiency One-Dimensional Liquid Chromatographic Separations. The University of North Carolina at Chapel Hill, 2012.

37. Thompson, J. D.; Carr, P. W., High-Speed Liquid Chromatography by Simultaneous Optimization of Temperature and Eluent Composition. *Analytical Chemistry* 2002, *74* (16), 4150-4159.

38. Yoshida, K.-i.; Yamaguchi, M.; Ikeda, H.; Omae, K.; Tsurusaki, K.-i.; Fujita, Y., The fifth gene of the iol operon of Bacillus subtilis, iolE, encodes 2-keto-myo-inositol dehydratase. *Microbiology* 2004, *150* (3), 571-580.

39. Zhou, F.; Lu, Y.; Ficarro, S. B.; Webber, J. T.; Marto, J. A., Nanoflow Low Pressure High Peak Capacity Single Dimension LC-MS/MS Platform for High-Throughput, In-Depth Analysis of Mammalian Proteomes. *Analytical Chemistry* 2012, *84* (11), 5133-5139.

40. Batz, N. G.; Mellors, J. S.; Alarie, J. P.; Ramsey, J. M., Chemical Vapor Deposition of Aminopropyl Silanes in Microfluidic Channels for Highly Efficient Microchip Capillary Electrophoresis-Electrospray Ionization-Mass Spectrometry. *Analytical Chemistry* 2014, *86* (7), 3493-3500.

CHAPTER 4. Study of Peptide Stability in RPLC Mobile Phase at Elevated Temperatures and Pressures

4.1 Introduction

Proteomics samples are very diverse coming from a variety of organisms with different genomes and expressed phenotypes.[1] Biological samples contain many different proteins with different post-translational modifications.[2,3] Due to sample complexity, a separation with high peak capacity is required prior to analysis by mass spectrometry.[4,5]

As shown in Chapter 3, much higher peak capacities could be achieved through the use of long microcapillary columns packed with sub-2 micron particles. These separations took up to 10 hours and required elevated temperatures and pressures to achieve reasonable flow rates and dead times. The higher peak capacity, afforded by the modified UHPLC described in Chapter 3, yielded protein identifications and coverage much greater than that from a standard UPLC with a commercial column.

During development of a liquid chromatographic method, stability of the sample on the column is an important parameter to investigate. Several variables that can affect analyte stability are time on the column, temperature, pressure and mobile phase composition.[6,7] Peptide stability has not been previously investigated for the extreme liquid chromatography conditions described in Chapter 3.

Based on the reports of other biological assays, the following degradation pathways may occur: peptide bond hydrolysis,[8] formylation,[9] deamidation,[10] and oxidation.[11,12,13] Peptide bond hydrolysis is the only degradation pathway, from the previous list, that disrupts the peptide back

bone. The c-terminal side of serine, threonine, and asparagine are more susceptible to hydrolysis. Under acidic conditions, the rate of hydrolysis greatly increases. [8]

Many RPLC-MS methods have formic acid in the mobile phase which reduces the pH to less than 3. Formic acid is added because it neutralizes acidic analytes increasing their retention factor.[14] The presence of formic acid in the mobile phase may also formylate of the N-terminus of the peptide resulting in a mass shift of +28 Da.[15]

Deamidation is a common post-translational modification that may occur endogenously to asparagine and glutamine residues. The reaction begins with protonation of the amine group before it is hydrolyzed to form a free carboxylic acid.[16] The side group changes from $–NH_2$ (16 Da) to –OH (17 Da) which results in a mass shift of +1 Da.[17] Evidence of deamidation, as a result of sample processing, was observed after several days according to the literature. Exposure to elevated temperatures increases the reaction rate. However, the referenced study aged the peptide in a buffer similar to physiological conditions (0.1 M phosphate buffer, pH 7, 37°C),[10] and it is unknown how fast deamidation will occur in RPLC conditions.

Methionine and histidine are very susceptible to oxidation. Methionine can be converted to methionine sulfoxide or methionine sulfone through the addition of one or two oxygen atoms, respectively. Histidine residues can be oxidized to 2-oxo-histidine.[18] A mass shift of +16 Da is observed for the addition of each oxygen atom. To minimize the presence of oxygen and oxidation catalysts in the analytical method, mobile phases are degassed,[19] and ultra-pure (Optima LC-MS grade) solvents are used.[20] Due to the increased reaction rate at high temperatures and the likelihood of oxidation occurring endogenously, this modification is often included in the database search of proteomics data.[21,22]

On-column stability will differ from peptide to peptide making it impossible to predict and observe all possible degradation products.[6] To get a general idea of analyte stability, we exposed several standard protein digests to elevated temperatures and pressures mimicking the on-column conditions for the modified UHPLC described in Chapter 3. The stressed samples were analyzed by a fast LC-MS method and compared to a control. Exposure of the sample to high pressure (45 kpsi) resulted in no significant variability in the intensity of the identified peptides. Storage for more than two hours in an acidic, highly aqueous mobile phase at high temperature (>45°C) generated impurity peaks in the chromatogram. No significant difference was observed between the samples stored up to 45°C for 10 hours in mobile phase and the control. It should be noted that this is a limited study, and on-column sample stability should always be reassessed for samples and methods not investigated in this chapter.

4.2 Materials and method

4.2.1 Materials

Optima grade water + 0.1% formic acid and acetonitrile + 0.1% formic acid were purchased from Fisher Scientific (Fair Lawn, NJ). MassPREP™ Digestion Standard: Protein Expression Mixture 2 (Standard, Part #186002866) and enolase digest (Part #186002325) were obtained from Waters Corporation (Milford, MA). Argon gas was purchased from Airgas (Radnor, PA).

4.2.2 Sample stability at elevated pressures and temperatures

Standard 2 was reconstituted according to the product manual with 1 mL water + 0.1% formic acid. The modified UHPLC previously described in Chapter 3 was used to store and analyze the sample. The gradient was loaded in reverse onto the storage loop followed by 1 µL of the sample. The end of the storage loop, closest to the analytical column, was blocked by

placing it in the Freeze/Thaw peltier device and closing the high pressure isolation valve as portrayed in Figure 4.1.a. The sample was stored for 10 hours in the loop at ambient temperature and 45 kpsi. At 10 hours, the peltier valve was thawed, and the fluidic tubing was reconfigured for normal running conditions diagramed in Figure 4.1.b. The aged sample was then run at 15 kpsi and 30°C on a 30 cm x 75 µm column packed with 1.9 µm BEH C18 particles. The nominal flow rate was 300 nL/min. The gradient was 4-40%B in 27 µL followed by a high organic wash and equilibration to initial conditions. The column was coupled to a Waters qTOF Premier via nanoESI set for data-independent, MS^E, acquisition with 0.6 scans. The experiment was repeated at several different storage conditions as outlined in Table 4.1.

4.2.3 Sample stability at elevated temperatures

To test a larger number of storage conditions, enolase digest standard was reconstituted as per the manufacturer's guidelines with 1 mL of 80:20 water:acetonitrile + 0.1% formic acid. From the stock solution, 2 aliquots of 200 µL were transferred to separate microcentrifuge vials and diluted to a final volume of 1 mL. One aliquot was diluted to a final concentration of 96:4 water:acetonitrile + 0.1% formic acid to represent the initial conditions of the gradient separation. The other aliquot was diluted to a final concentration of 60:40 water:acetonitrile + 0.1% formic acid to represent the final gradient composition. From each solution, 80 µL portions were transferred to individual 1.7 mL polypropylene centrifuge tubes and bedded with argon. Samples were stored from ambient temperature to 65° for 2 to 10 hours. See Table 4.2. for a full list of sample storage conditions. Samples of diluent (4% and 40% acetonitrile in water + 0.1% formic acid) were also stored at 65° for 10 hours. The samples stored in 60:40 water:acetonitrile + 0.1% formic acid were lyophilized and reconstituted with 94:4 water:acetonitrile + 0.1% formic acid prior to analysis. All stability samples were transferred to glass Total Recovery

autosampler vials (Waters), bedded with Argon and closed with a pre-slit screw cap. Vials were stored on the autosampler at 10°C until analysis. The samples were analyzed in triplicate on a standard Waters nanoAcquity UPLC operated in trapping mode. Mobile phase A and B were water and acetonitrile, respectively, modified with 0.1% formic acid. One microliter of sample was injected and trapped on a 2 cm x 180 µm Symmetry C18 column at 0.5% mobile phase B. The samples were separated on a 25 cm x 75 µm analytical column packed with 1.9 µm BEH C18 particles run at 30°C. The gradient was 4-40% B over 30 minutes at 300 nL/min (7.5 kpsi nominal pressure). The column was coupled to a Waters qTOF Premier via nanoESI set for data-independent acquisition, MS^E mode, with 0.6 second scans.

4.2.4 Peptide data processing

The LC-MS/MS data were processed using ProteinLynx Global Server 2.5 (Waters). The MS^E spectra were searched against a database of alcohol dehydrogenase, bovine serum albumin, glycogen phosphorylase b, and/or enolase, as appropriate to the sample, and appended with a 1X reversed sequence. The amino acid sequences were found from the Uni-Prot protein knowledgebase (www.uniprot.org). The false discovery rate was set to 4%. Peptide intensities were extracted from the ProteinLynx ion accounting spreadsheet for the standard digest mixture. For the enolase standard, manual peak intensities were measured of each identified precursor ion. The peak intensities for each stability sample were compared to a freshly prepared sample by the 2-tailed student's T test. A significant difference was reported with 95% confidece if the p-value was less than 0.05.

4.3 Discussion

4.3.1 Stability testing considerations

The storage conditions discussed in this chapter aimed to age the samples in an environment similar to on-column conditions. To achieve this, the samples had to be stored in two different ways: (1) in the storage loop of the UHPLC and (2) in centrifuge tubes. The UHPLC storage loop enabled storage of a small sample volume at elevated temperatures and pressures. The sample was in a narrow (50 µm) internal diameter silica capillary similar to the on-column environment. However, the sample could only be stored in initial mobile phase conditions because it was to be subsequently loaded onto the column. Storage in highly organic mobile phase would inhibit trapping of the analytes into a narrow band at the head of the column and cause peak broadening. Another disadvantage to this storage method was the time investment. Only one sample could be stored at a time and other samples could not be run while a sample was being stored. Throughput was low allowing analysis of only two samples per day. After storage, there was only one chance for analysis. If there was bad electrospray or a clog, for example, the sample could not be recovered, and the storage procedure had to restart from time zero. For these reasons, it was difficult to test a large variety of stress conditions with replicate analyses. Therefore, the UHPLC storage loop method was only used to test sample stability at 45 kpsi. The offline method was used to evaluate sample stability at high temperatures and in solvents with a high organic composition.

The second method focused on storage at elevated temperatures in high and low percent organic solvents. This was an offline method allowing storage at many different conditions at once. There were 80 µL of sample stored at each condition which allowed for replicate analysis.

To provide conditions closest to on-column, the samples were bedded with argon to remove oxygen containing air that may have caused degradation.

An alternative storage method that was not explored would be to age the samples at high pressure in a column packing apparatus followed by off-line analysis. This method would consume a lot of sample (about 0.5 mL per condition), and it would be time consuming because only one condition can be tested at a time. Also, setting up the apparatus in an oven would be difficult. Another concern was that pushing fluid from the pump could contaminate or dilute the sample. Therefore, only the UHPLC storage loop and centrifuge tubes were used as vessels to age the sample.

4.3.2 Stability at high pressure

The chromatograms in Figure 4.2. compare the standard protein digest at initial conditions (black) to storage at elevated pressure (red), elevated temperature (blue), and elevated temperature and pressure (green) for 10 hours. The initial observation was that there were no catastrophic differences between the chromatograms. For both the samples stored at 45 kpsi (red and green traces), there were a few extra peaks eluting early in the chromatogram as compared to the chromatogram of the unstressed sample (black). For the samples stored at 65ºC (blue and green traces), less peaks appeared towards the end of the chromatogram as compared to the unstressed sample (black). However, this sort of qualitative and visual comparison of the chromatograms was very limited. There were many peaks in the middle of the chromatogram that were difficult to compare visually because the chromatogram was crowded in this region.

4.3.3 Database searching considerations

To more objectively compare the results, PLGS was used to identify the peaks as specific peptides from the Standard Protein Digest. The identifications were useful to track peptide

intensities at the different storage conditions. The typical PLGS workflow searches a database of tryptic peptides with the following variable post-translational modifications: acetylation of the N-terminus; deamidation of asparagine and glutamine; and oxidation of methionine. This peptide search would not include many degradation products formed during exposure to stress conditions. Therefore, additional digestion sights and peptide modifications were added to the workflow. These modifications were based on the predicted degradation pathways discussed in the introduction: formylation of the N-terminus due to formic acid in the mobile phase, asparagine and glutamine deamidation, and methionine and histidine oxidation. In addition to tryptic cleavage at arginine and lysine, cleavage at serine, threonine, and asparagine was also added to the search options because these residues are susceptible to hydrolysis under acidic conditions and high temperatures.

4.3.4 Venn diagram comparison

The similarities in peptide identifications were compared between the stressed and control samples in Figure 4.3. As a benchmark, the control sample was analyzed in duplicate. Run 1 and 2 identified 171 and 176 peptides, respectively, with 151 of those peptides identified in both replicates. The percent overlap of identifications was calculated as follows:

$$\%\ \text{overlap} = \frac{2\times\text{number of overlapping peptides identifications}}{\text{total number of peptide identifications}}\times 100 \tag{4-1}$$

$$\%\ \text{overlap} = \frac{2(151)}{(171+176)}\times 100 = 87\% \tag{4-2}$$

The overlap of 151 peptide identifications correlated to 87% of the results (Figure 4.3.a.). A similar number of identifications and percent overlap is seen in Figure 4.3.b. for the comparison of the control to the sample stored at 45 kpsi and ambient temperature for 10 hours. The overlap was 150 identifications (86%) with 176 peptides identified in the sample stored at high pressure. When comparing the control to the samples stored at elevated temperatures,

similarities in peptide identifications decreased. For the sample stored at 65ºC and ambient pressure for 10 hours, peptide identifications reduce to 125 with only 96 identifications (65%) overlapping with the control (Figure 4.3.c). When the sample was stored at 65ºC and 45 kpsi for 10 hours, only 118 peptides were identified with 101 peptides (70%) also identified in the control (Figure 4.3.d). From these comparisons, it was evident that exposure to high pressure did not change the number or identify of peptides in the sample but exposure to elevated temperature for 10 hours did change the sample.

4.3.5 Peptide intensity comparison

Changes in peptide intensities were also used as a metric for measuring sample stability. Results from the database search provided the precursor peak intensity for each identified peptide. To determine if a change in peptide precursor intensity was significant, the change had to be larger than that due to analytical variability. The analytical variability was assessed by plotting the log precursor intensities from the control sample to a replicate analysis in Figure 4.4. Dots close to the dashed y=x line represent peptide peaks with little variability between the two analyses. To describe variability from the y=x line, colored lines are drawn with the formula y=mx+b, where b was a constant level of uncertainty, and the m factor accounted for uncertainty relative to signal intensity (x). The mirror lines are also plotted across the y=x line. Several arbitrary values for m and b were selected for this equation as listed in the figure legend. Beside each equation in the legend is a percentage which corresponds to the number of points that are contained within these confidence curves. The greens lines, which plot $y=1.3x+10^{4.6}$, contained 94.4% of the points. When comparing two analyses, we expect a minimum of 94.4% of the data points to fall within these green lines. A smaller value would indicate changes in intensity due to factors other than analytical variability. Figure 4.5. compares the sample stored at high pressure

(45 kpsi) and ambient temperature to the control. Peptide intensities are relatively symmetrical around the y=x line with 95.2% of the data points falling between the confidence lines. This percentage is better than that measured for analytical variability which indicates no change in peptide intensity from storage at 45 kpsi for 10 hours. Figure 4.6. compares the high temperature (65ºC)/ambient pressure sample to the control. Slightly less of the data, 91.5%, was within the confidence curves. When a sample stored at elevated temperature (65ºC) and pressure (45 kpsi) was compared to the control, 88.8% of the points were contained within the confidence curves (Figure 4.7.). For Figure 4.6 and Figure 4.7., most of the variability occurs from data points falling below the y=x line which indicates a decrease of intensity for peptides in the elevated temperature sample.

Though this study had a small sample size, it indicated that temperature is a larger factor than pressure in sample stability. Therefore, a more thorough study was completed looking at stability of peptides stored in mobile phase at elevated temperatures.

4.3.6 Temperature degradation study

As stated earlier, storage in the sample loop was time consuming. To test more temperatures, exposure times, and mobile phase compositions, an offline approach was implemented. Also a simpler sample, enolase digest, was used to make it easier to track peaks. The samples were stored in 96:4 and 60:40 water:acetonitrile + 0.1% formic acid to match mobile phase compositions at the beginning and ending of the gradient. Blank solutions were also stored to determine if degradation products were being formed from the polypropylene microcentrifuge tubes used as storage containers. Every sample was run in triplicate and compared to the control. Stability was determined if the peak intensities were not calculated to be significantly different with a 95% confidence by a 2-tailed student's T test.

In the enolase control sample A, 19 peptide peaks were identified. The values in Table 4.3. list the number of significantly different peak intensities for the sample stored in 4% mobile phase B at 25, 35, 45, 55, and 65°C for 2, 4, 6, 8, and 10 hours. Most peptide peaks do not have significantly different intensities when stored at any temperature for 6 hours. After 8 and 10 hours, many more peptides have significantly different intensities. About 6-7 peaks, or 35% of all identifications, have differential intensities.

The samples stored in high organic mobile phase were compared to a different control sample, namely control sample B. This was necessary to account for any changes happening to the sample through sample preparation. There was interest in degradation occurring from exposure to high organic mobile phase at elevated temperatures. However, the high organic had to be removed by lyophilization before analysis which may modify the sample. Therefore, control sample B was prepared in 40% mobile phase B, lyophilized and reconstituted in 4% mobile phase B. In this control sample, 13 peptide peaks were identified. The number of significantly different peak intensities is listed in Table 4.4. for the enolase digest sampled stored in 40% mobile phase B at elevated temperatures for a period up to 10 hours. Most of the 13 identified peptide peaks do not have significantly different intensities when stored at any temperature for 6 hours. After 8 hours at 65°C, a couple more peptides have significantly different intensities. At this extreme condition, two to three peaks, or 19% of all identifications, had significantly different intensities.

The data was further mined for peptides with significantly different intensities. These were all identified to be tryptic peptides with no posttranslational modifications corresponding to possible degradation products.

A visual inspection was completed of all chromatograms to check for degradation peaks that were not identified by PLGS. In both the 4% and 40% organic samples, two additional peaks appeared in the chromatograms when stored at 55°C and 65°C. A third peak was observed in the 4% organic sample stored at 55°C and 65°C. The retention times and mass-to-charge ratios for these peaks are listed in Table 4.5. These peaks were not found in the control samples but two peaks (460.4 and 780.9 m/z) were observed in the chromatogram in Figure 4.8. of the blank sample stored at 55°C and 65°C. It is therefore concluded that these peaks are from the degradation of the polypropylene microcentrifuge tubes and not from enolase peptide degradation. The 199.1 m/z peak appeared when the enolase digest standard was stored in 4% mobile phase B for extended periods of time. The intensity of this peak (199.1 m/z) is plotted versus time exposed to 4% mobile phase B at elevated temperature in Figure 4.9. This peak appeared above baseline when the sample was stored above 45°C. This peak is not observed when the sample was stored in 40% mobile phase B.

4.3.7 Sources of analytical variability

Some sources of the previously mentioned analytical variability will be discussed. Electrospray instability may lead to random error in peak intensities. Over time the spray will begin to flutter reducing the ionization efficiency. A poor spray will lead to reduced peak intensities. After ionization, the analyte is fragmented in the mass spectrometer during MS^E, data-independent acquisition. In this type of experiment, the mass analyzer voltage is ramped causing more collision induced fragmentation. These are randomly timed events which lead to variability of ion intensity. The variability of intensity can lead to variability in the protein database search. A higher intensity leads to a higher probably of the peak being assigned to a peptide for identification. Reduced intensities may lead to the probability falling below the

threshold necessary to confidently assign the peak to a peptide. Efforts were taken to reduce the analytical variability but the results indicate that some is present.

4.4 Conclusion

Through the studies conducted in this Chapter, it is concluded that the exposure of peptides to ultrahigh pressures, up to 45 kpsi, did not cause measurable degradation. Exposure to elevated temperatures greater than 45°C in an acidic mobile phase environment for an excess of two hours may cause sample degradation. For separations greater than two hours, the column temperature should be no greater than 45°C. On-column degradation may occur at any temperature after 6 hours. These conclusions were made based on variability in peptide identifications and precursor peak intensities in excess of that observed from analytical variability.

The implementation of elevated pressures and temperatures increases peak capacity without increasing analysis time (Chapter 3). This research supports the use of elevated pressures and temperatures for proteomics analysis but recommends that on-column time does not exceed two hours for temperature greater than 45°C, or column temperature should not exceed 45°C for separations longer than two hours. For targeted analyses, on-column analyte stability should be reassessed.

4.5 TABLES

Pressure	Temperature
Ambient	Ambient (25°C)
Ambient	65°C
45 kpsi	Ambient (25°C)
45 kpsi	65°C

Table 4.1. To assess the stability of peptides at elevated pressures and temperatures, the MassPrep standard protein digest was storage for 10 hours at the conditions listed in this table.

Temperature	Time (h)				
(°C)	2	4	6	8	10
25	X	X	X	X	X
35	X	X	X	X	X
45	X	X	X	X	X
55	X	X	X	X	X
65	X	X	X	X	X

Table 4.2. To assess the stability of peptides at elevated temperatures for 2-10 hours, the enolase digest standard was storage at the conditions marked by an "X" on this table.

Temperature	Time (h)				
(°C)	2	4	6	8	10
25	0	3	1	4	7
35	1	1	0	4	6
45	2	1	0	3	6
55	2	0	0	0	7
65	1	1	2	0	2

Table 4.3. The number of significantly different peak intensities are listed for the enolase digest sample stored in 4% mobile phase B at 25, 35, 45, 55, and 65°C for 2, 4, 6, 8, and 10 hours. Intensities were compared to the unstressed, control sample A in which 19 peptide peaks were identified. Most of the identified peptide peaks do not have significantly different intensities when stored at any temperature for 6 hours. After 8 and 10 hours, many more peptides have significantly different intensities. At these extreme conditions, about 6-7 peaks, or 35% of all identifications, have significantly different intensities.

Temperature	Time (h)				
(°C)	2	4	6	8	10
25	0	1	1	1	2
35	0	4	1	1	0
45	1	0	1	0	0
55	1	1	1	1	0
65	1	1	1	3	2

Table 4.4. The number of significantly different peak intensities are listed for the enolase digest sample stored in 40% mobile phase B at 25, 35, 45, 55, and 65°C for 2, 4, 6, 8, and 10 hours. Intensities were compared to the unstressed, control sample B in which 13 peptide peaks were identified. Most of the identified peptide peaks do not have significantly different intensities when stored at any temperature for 6 hours. After 8 hours at 65°C, a couple more peptides have significantly different intensities. At this extreme condition, two to three peaks, or 19% of all identifications, had significantly different intensities.

Sample	Retention Time (min)	m/z
4% Mobile Phase B	28-31	199.1
4% and 40% Mobile Phase B	35.0	460.4
4% and 40% Mobile Phase B	36.2	780.9

Table 4.5. The retention times and mass-to-charge ratios (m/z) are listed for peaks that appeared after the enolase digest was stored in the indicated sample solution. The 199.1 m/z peak appeared when the enolase digest standard was stored in 4% mobile phase B for extended periods of time above 45°C. This peak is not observed when the sample was stored in 40% mobile phase B. The other two peaks were degradation products extracted from the polypropylene microcentrifuge tubes used for sample storage.

4.6 FIGURES

a)

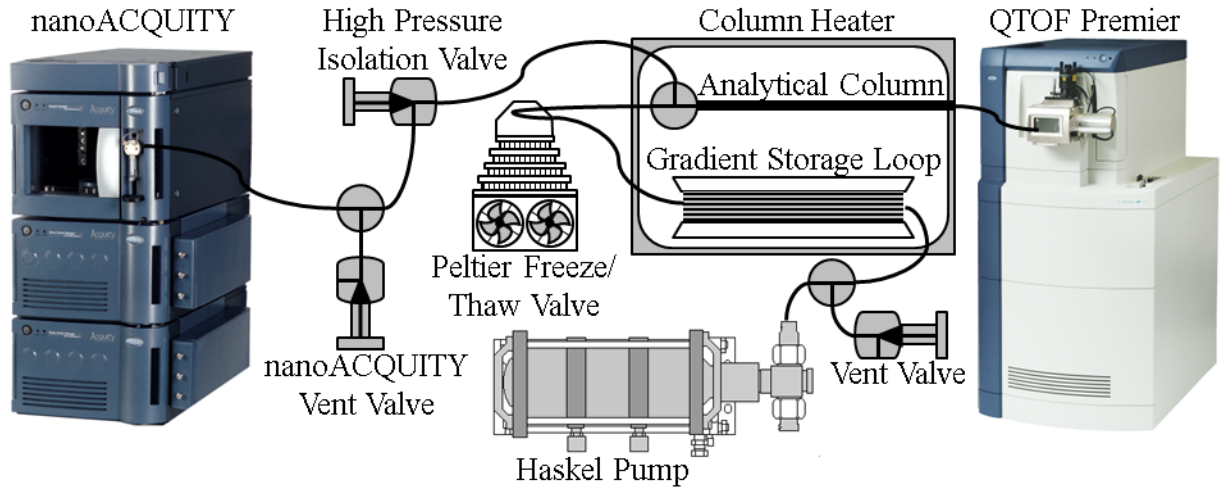

b)

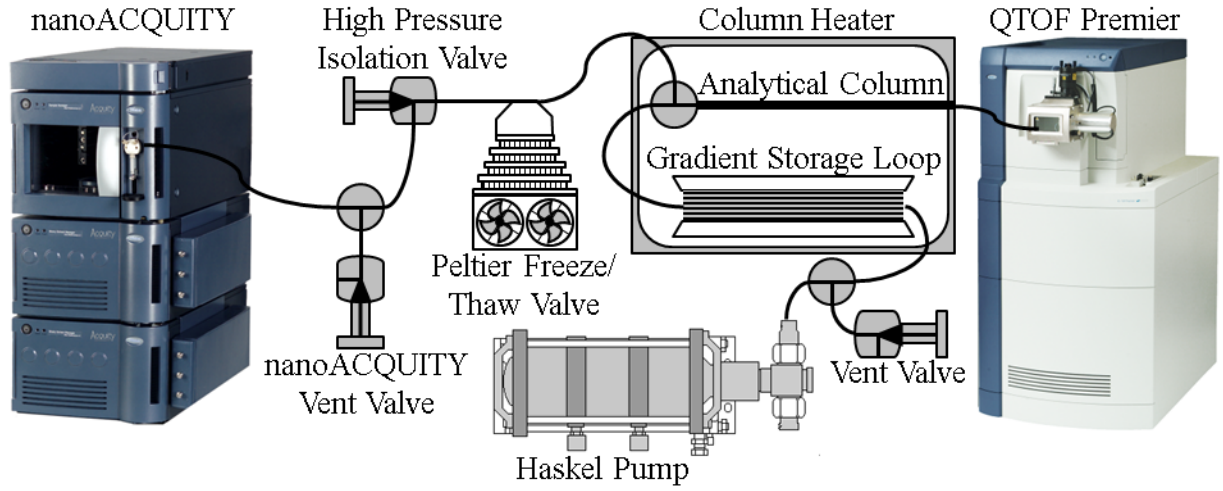

Figure 4.1. The instrument diagram (a) shows the fluidic configuration for sample storage at elevated pressures and temperatures. Part (b) shows the fluidic configuration for gradient/sample loading and sample analysis. For gradient/sample loading, all valves were opened except the nanoAcquity vent valve. For sample storage and analysis, all valves were closed except the nanoAcquity vent valve. The haskel pump and column heater were regulated to the desired pressure and temperature to stress the sample. During analysis, the haskel pump and column heater were regulated to 15 kpsi and 30°C.

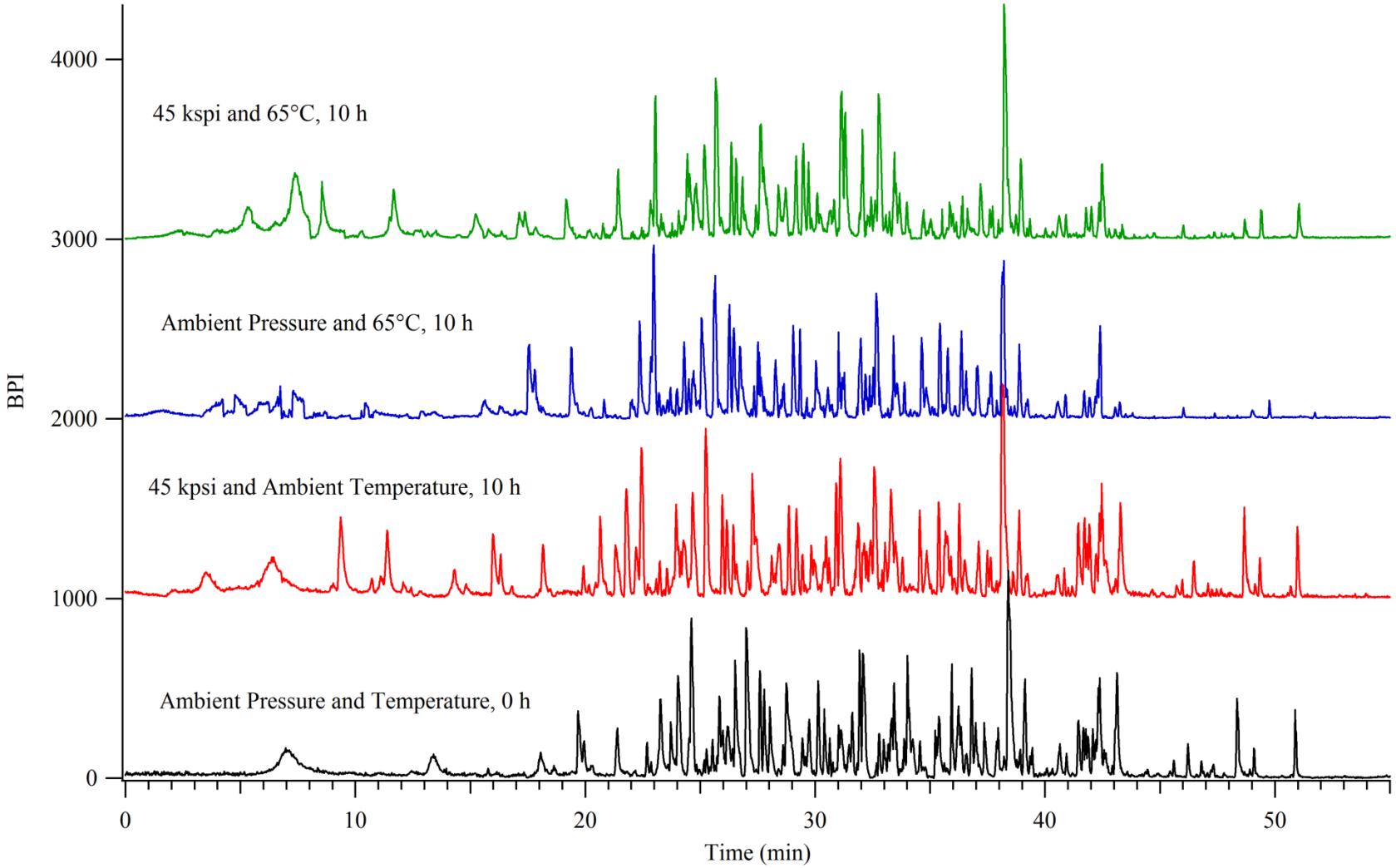

Figure 4.2. These chromatograms were from the analysis of the standard protein digest stored in the gradient storage loop. Storage conditions are listed above each chromatogram.

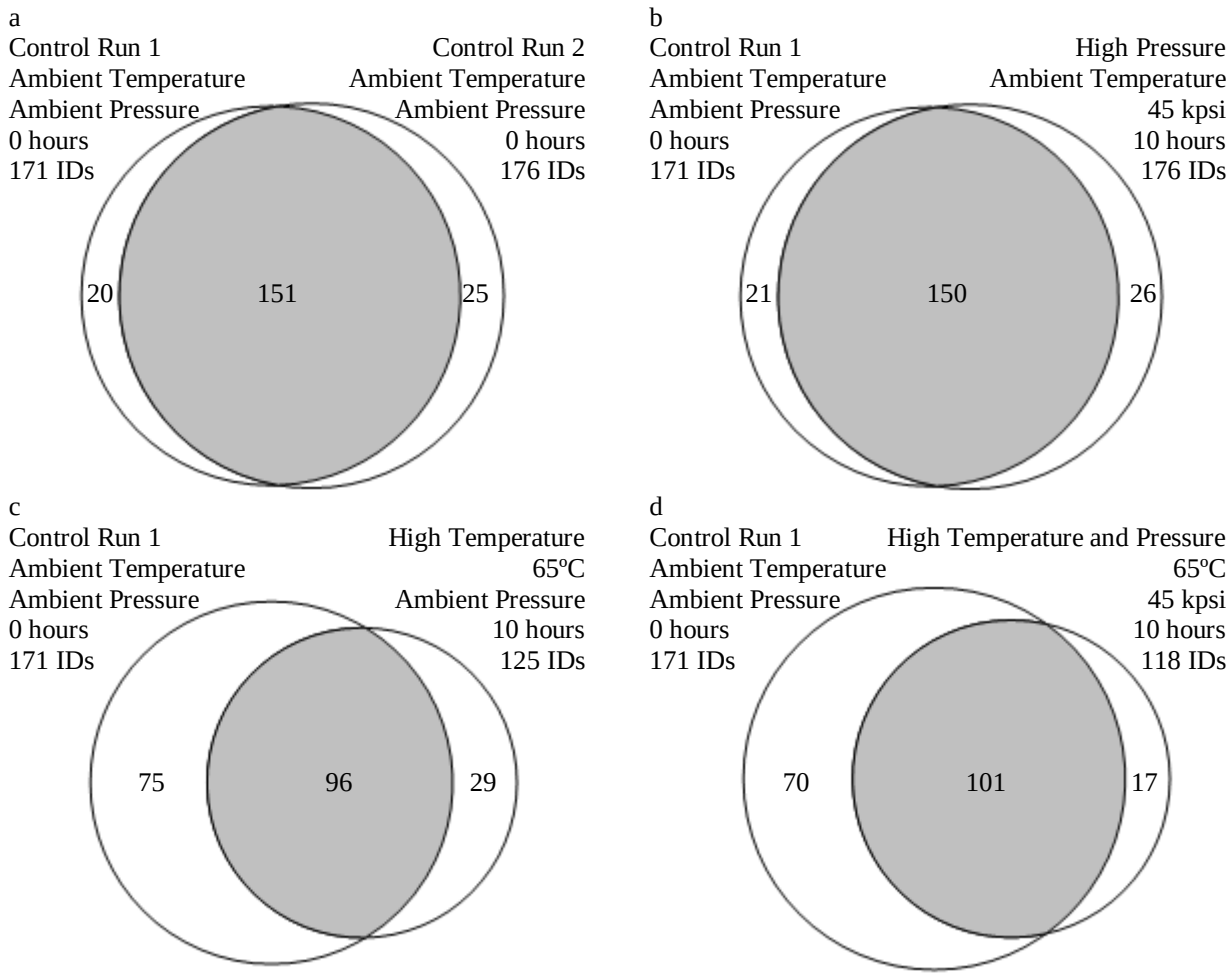

Figure 4.3. These Venn diagrams show the similarities in peptide identification for the standard protein digest control sample compared to a replicate analysis and to analysis of the sample stored at stress conditions.

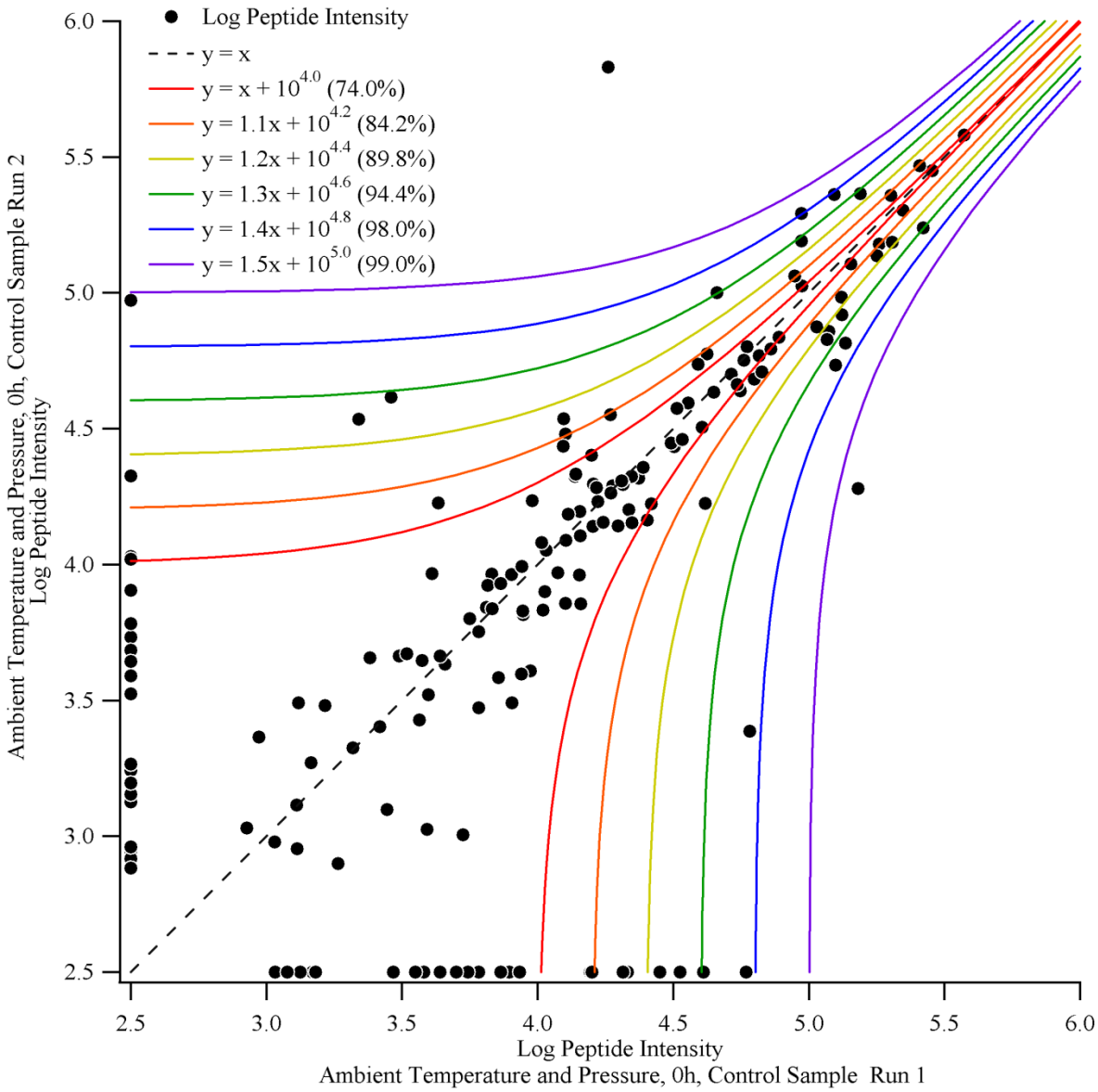

Figure 4.4. The log peptide intensities are plotted comparing two replicate analyses of the control standard protein digest. The confidence lines drawn on the graph are used to describe the scatter from the dashed y=x line due to analytical variability. The formulas for each line and the percent of data points contained within each set of lines are listed in the legend.

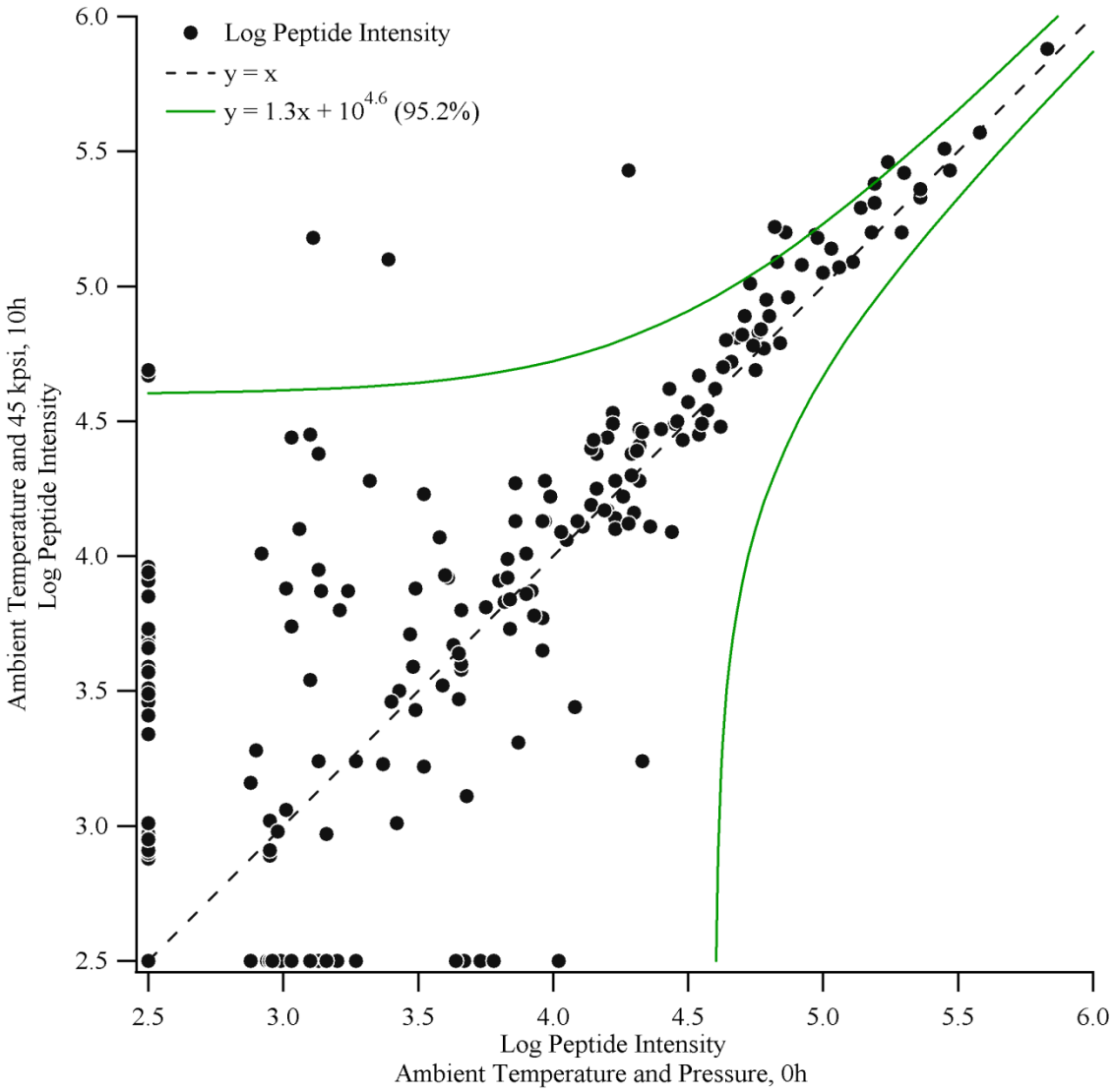

Figure 4.5. The log peptide intensities are plotted for the standard protein digest stored at 45 kpsi and ambient temperature for 10 hours compared to the control. As listed in the legend, 95.2% of the data points are contained within the green lines. This percentage is greater than that expected due to analytical variability which indicates no change in peptide intensity from storage at 45 kpsi for 10 hours.

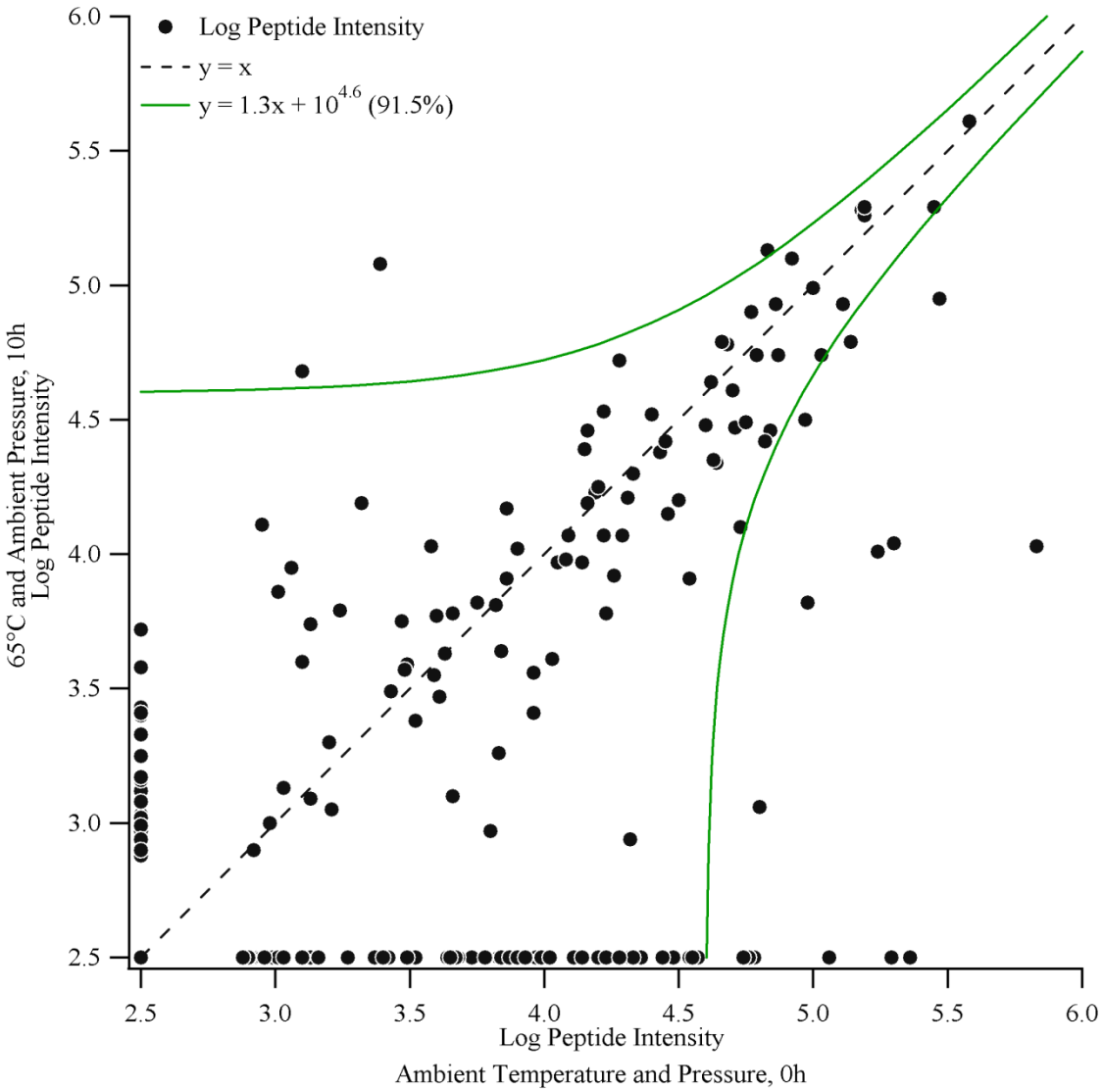

Figure 4.6. The log peptide intensities are plotted for the standard protein digest stored at 65°C and ambient pressure for 10 hours compared to the control. As listed in the legend, 91.5% of the data points are contained within the green lines. This percentage is less than that expected due to analytical variability. Most of the variability occurs from data points falling below the y=x dashed line which indicates a decrease of intensity for peptides in the elevated temperature sample.

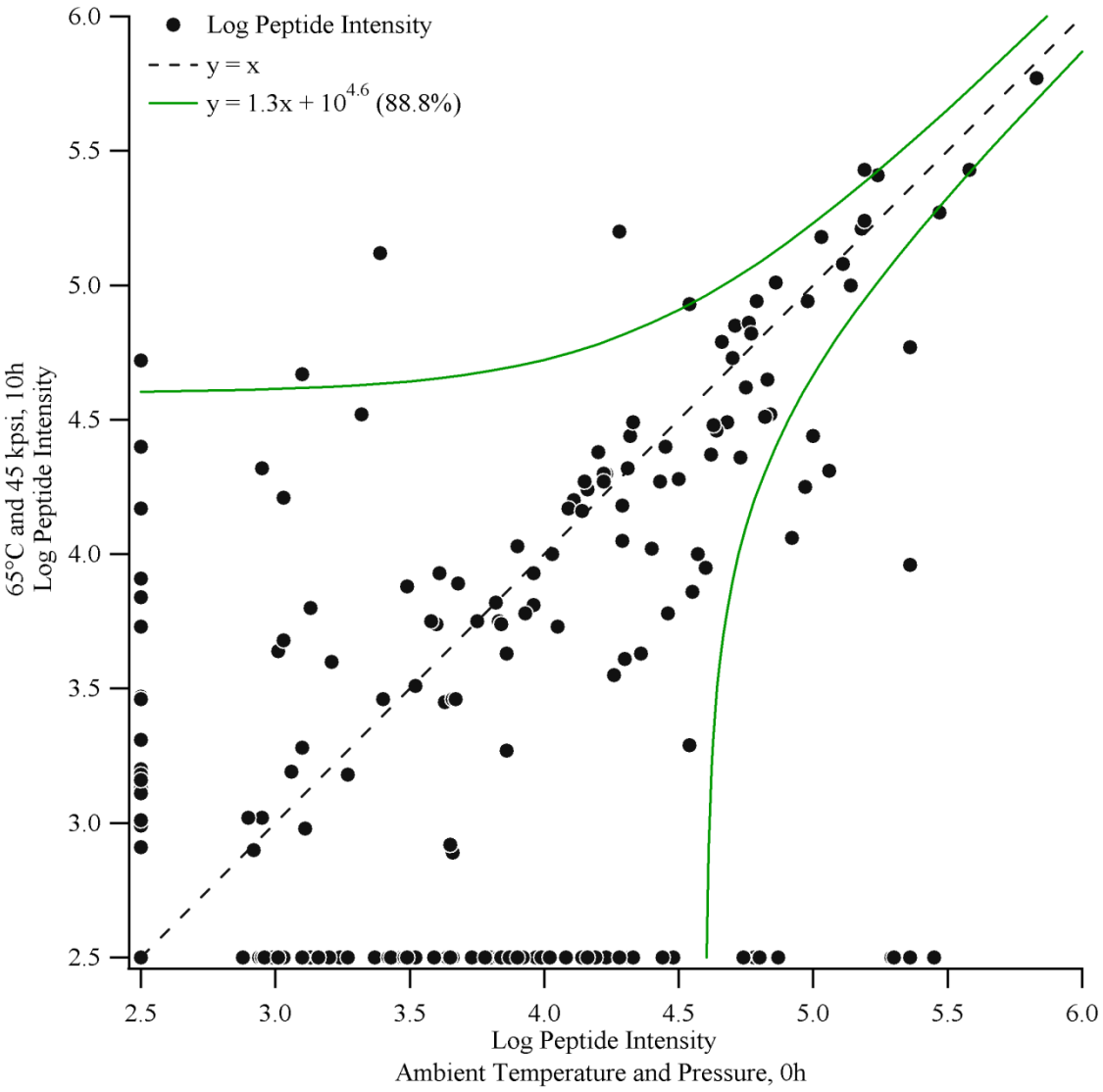

Figure 4.7. The log peptide intensities are plotted for the standard protein digest stored at 65°C and 45 kpsi for 10 hours compared to the control. As listed in the legend, 88.8% of the data points are contained within the green lines. This percentage is less than that expected due to analytical variability. Most of the variability occurs from data points falling below the y=x dashed line which indicates a decrease of intensity for peptides in the stressed sample.

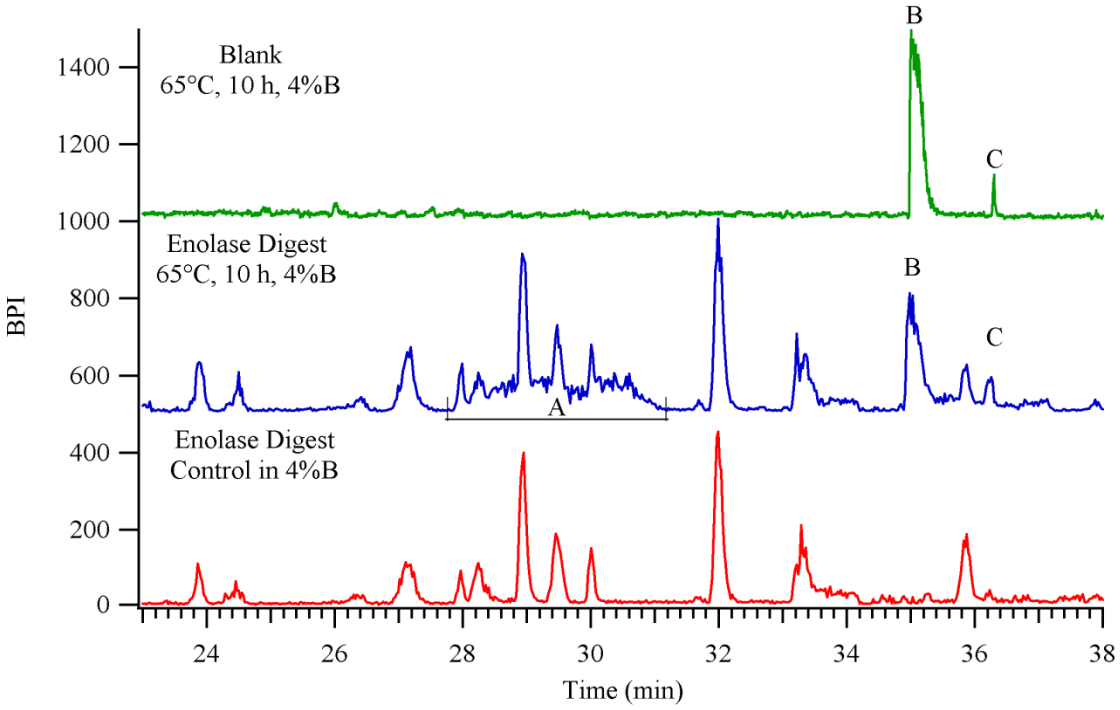

Figure 4.8. These red and blue chromatograms are from the analysis of the enolase digest control and stress sample stored at 65°C for 10 hours. Feature A (199.1 m/z) is a degradation peak that appeared when enolase was stored in 4% mobile phase B at elevated temperatures. The green chromatogram of mobile phase stored in the polypropylene microcentrifuge tubes at 65°C for 10 hours shows that peak B (460.4 m/z) and peak C (780.9 m/z) were extracted from the tube and are not peptide degradation products.

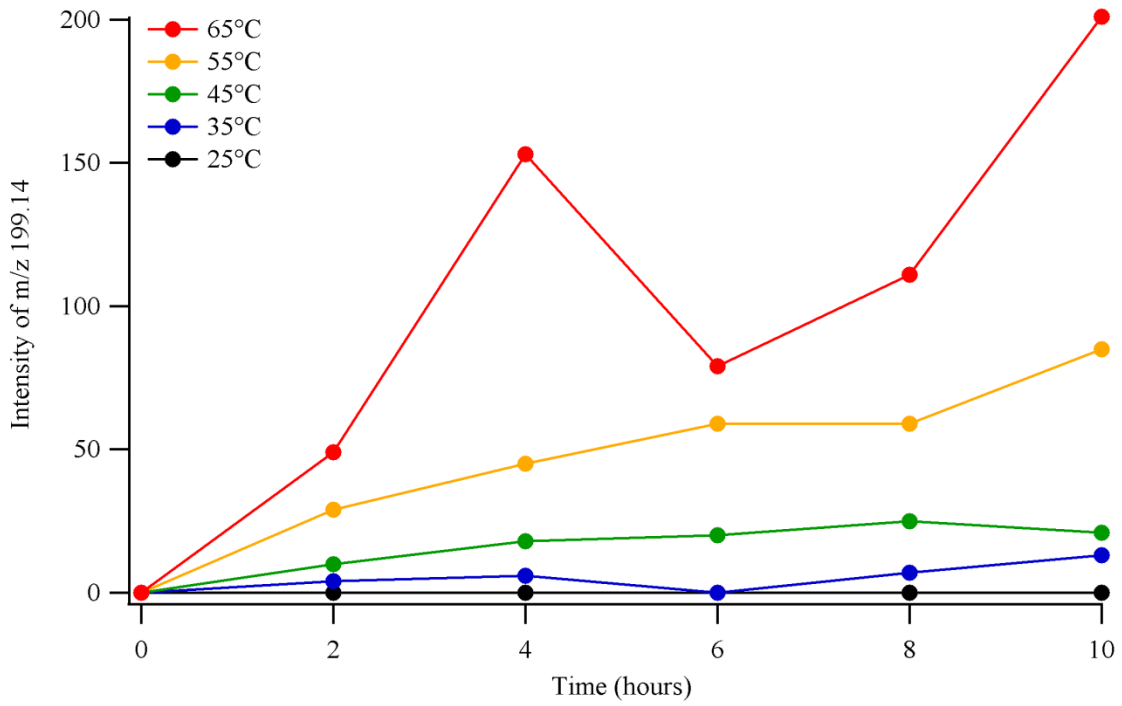

Figure 4.9. The intensity is plotted versus storage time for a degradation peak (199.1 m/z) that appeared when the enolase digest standard was stored in 4% mobile phase B for extended periods of time. This peak appeared when the sample was stored above 45°C. This peak is not observed when the sample was stored in 40% mobile phase B.

4.7 REFERENCES

1. Zhang, X.; Fang, A.; Riley, C. P.; Wang, M.; Regnier, F. E.; Buck, C., Multi-dimensional liquid chromatography in proteomics—A review. *Analytica Chimica Acta* 2010, *664* (2), 101-113.

2. Baker, E.; Liu, T.; Petyuk, V.; Burnum-Johnson, K.; Ibrahim, Y.; Anderson, G.; Smith, R., Mass spectrometry for translational proteomics: progress and clinical implications. *Genome Med* 2012, *4* (8), 1-11.

3. Meissner, F.; Mann, M., Quantitative shotgun proteomics: considerations for a high-quality workflow in immunology. *Nat. Immunol.* 2014, *15* (Copyright (C) 2014 American Chemical Society (ACS). All Rights Reserved.), 112-117.

4. Xie, F.; Smith, R. D.; Shen, Y., Advanced proteomic liquid chromatography. *Journal of Chromatography A* 2012, *1261* (0), 78-90.

5. Cox, J.; Mann, M., Quantitative, High-Resolution Proteomics for Data-Driven Systems Biology. *Annual Review of Biochemistry* 2011, *80* (1), 273-299.

6. Manning, M.; Patel, K.; Borchardt, R., Stability of Protein Pharmaceuticals. *Pharm Res* 1989, *6* (11), 903-918.

7. Kikwai, L.; Babu, R. J.; Kanikkannan, N.; Singh, M., Stability and degradation profiles of Spantide II in aqueous solutions. *European Journal of Pharmaceutical Sciences* 2006, *27* (2–3), 158-166.

8. Smith, R. M.; Hansen, D. E., The pH-Rate Profile for the Hydrolysis of a Peptide Bond. *Journal of the American Chemical Society* 1998, *120* (35), 8910-8913.

9. Wiśniewski, J. R.; Zougman, A.; Mann, M., Nε-Formylation of lysine is a widespread post-translational modification of nuclear proteins occurring at residues involved in regulation of chromatin function. *Nucleic Acids Research* 2008, *36* (2), 570-577.

10. Patel, K.; Borchardt, R., Chemical Pathways of Peptide Degradation. II. Kinetics of Deamidation of an Asparaginyl Residue in a Model Hexapeptide. *Pharm Res* 1990, *7* (7), 703-711.

11. Ji, J. A.; Zhang, B.; Cheng, W.; Wang, Y. J., Methionine, tryptophan, and histidine oxidation in a model protein, PTH: Mechanisms and stabilization. *Journal of Pharmaceutical Sciences* 2009, *98* (12), 4485-4500.

12. Patel, K.; Borchardt, R., Chemical Pathways of Peptide Degradation. III. Effect of Primary Sequence on the Pathways of Deamidation of Asparaginyl Residues in Hexapeptides. *Pharm Res* 1990, *7* (8), 787-793.

13. Bhatt, N.; Patel, K.; Borchardt, R., Chemical Pathways of Peptide Degradation. I. Deamidation of Adrenocorticotropic Hormone. *Pharm Res* 1990, *7* (6), 593-599.

14. Neue, U. D., *HPLC Columns: Theory, Technology, and Practice*. Wiley: 1997.

15. Alzate, O., *Neuroproteomics*. Taylor & Francis: 2010.

16. Geiger, T.; Clarke, S., Deamidation, isomerization, and racemization at asparaginyl and aspartyl residues in peptides. Succinimide-linked reactions that contribute to protein degradation. *Journal of Biological Chemistry* 1987, *262* (2), 785-794.

17. Yang, H.; Zubarev, R. A., Mass spectrometric analysis of asparagine deamidation and aspartate isomerization in polypeptides. *ELECTROPHORESIS* 2010, *31* (11), 1764-1772.

18. Srikanth, R.; Wilson, J.; Vachet, R. W., Correct identification of oxidized histidine residues using electron-transfer dissociation. *Journal of Mass Spectrometry* 2009, *44* (5), 755-762.

19. Dell'Ova, V. E.; Denton, M. B.; Burke, M. F., Ultrasonic degasser for use in liquid chromatography. *Analytical Chemistry* 1974, *46* (9), 1365-1366.

20. Ende, M.; Spiteller, G., Contaminants in mass spectrometry. *Mass Spectrometry Reviews* 1982, *1* (1), 29-62.

21. Chumsae, C.; Gaza-Bulseco, G.; Sun, J.; Liu, H., Comparison of methionine oxidation in thermal stability and chemically stressed samples of a fully human monoclonal antibody. *Journal of Chromatography B* 2007, *850* (1–2), 285-294.

22. Davies, M. J., The oxidative environment and protein damage. *Biochimica et Biophysica Acta (BBA) - Proteins and Proteomics* 2005, *1703* (2), 93-109.

CHAPTER 5. Prefractionation Frequency Study with a 32 kpsi UHPLC for the Multidimensional Separation of the *Saccharomyces cerevisiae* Proteome

5.1 Introduction

Studying the proteome gives understanding to the biological pathways that are occurring in the cell.[1,2,3] Due to the large number of protein encoding genes (6000 for *S. cerevisiae*),[4] separation of the components in a biological mixture is required before analysis.[5] There is no single dimension separation with the peak capacity necessary to completely resolve all the components of a cell lysate.[6] Multidimensional separations have commonly been used to provide more peak capacity.[7,8] According to Giddings, the peak capacity of a multidimensional separation is the multiplicative product of the peak capacities of the individual separations if the separations are orthogonal and resolution is not lost in coupling the separations.[9] For resolution to be preserved, the second dimension would have to be faster than practically possible in liquid chromatography (LC), or the first dimension would have to be extremely slowed down. Therefore, fractionation of the first dimension is often necessary when coupling two columns. The peak capacity of the first dimension then becomes the number of fractions. In order to reduce the loss of peak capacity caused by fractionation, the second dimension should have the greater peak capacity of the two separations.[10,11]

5.1.1 Prefractionation frequency

The peak capacity of the first dimension separation could be increased by taking more fractions. However, higher prefractionation frequencies increase the analysis time and increase the probability of splitting a peak across multiple fractions.[12] Peak splitting dilutes the analyte

and lowers the limit of detection.[13] From the study of prefractionation frequency in Chapter 2, we learned that protein identifications plateaued when 20 or more fractions were taken.

5.1.2 Separations at elevated pressures and temperatures

Therefore, it is necessary to pursue solutions for increasing the peak capacity of the second dimension. For liquid chromatography, ultrahigh performance LC (UPLC) has enabled the use of microcapillary columns with sub-2 micron particles which have greater peak capacity than standard bore columns.[14] However, the pressure capabilities of the pump on a standard UPLC limit the dimensions of commercial columns resulting in a maximum peak capacity of 200 in 90 minutes. In Chapter 3, new LC instrumentation with a constant pressure, high temperature approach for peptide separations was introduced. The system modified a standard UPLC with a pneumatic amplifier through a configuration of tubing and valves for separations up to 45000 psi. For a peptide analysis, the modified UHPLC, coupled to a qTOF Premier, produced a peak capacity of 500 in 90 minutes on a meter-long microcapillary column packed with sub-2 micron particles. Peak capacity plateaued above 800 in 12 hours. Several columns of varying lengths, packed with particles ranging from 1.1-1.9 μm, were characterized on the modified UHPLC. For faster analysis, higher peak capacities and protein identifications were realized when running an aggressive gradient on a long column with 1.9 μm particles than a shallower gradient on a shorter column with smaller particles. The peak capacities produced with the modified UHPLC were greater than that previously reported in the literature.[15,16]

Separations at higher temperatures reduce the viscosity of the mobile phase. Therefore, longer columns can be used without reducing flow rate and increasing analysis time at a given pressure. The higher temperatures also reduce the change in mobile phase viscosity throughout the gradient on a constant pressure system.[17,18,19] The resistance to mass transfer is reduced at

high temperatures which flattens the C-term portion of a Van Deemter plot and consequently shifts optimal velocity to a higher value.[20] The stability of the analyte, exposed to elevated pressure and temperatures, was assessed in Chapter 4. Exposure of peptides to ultrahigh pressures, up to 45 kpsi, did not show evidence of degradation. Peptide stability in acidic reversed-phase LC solvents was confirmed for up to 2 hours at 65°C and for up to six hours at 45°C.

5.1.3 Orthogonality through prefractionation

For proteomics separations, benefits of the top-down (protein) and bottom-up (peptide) strategies are often debated.[21] Commonly, proteins are digested into peptides prior to analysis to increase the solubility of the analyte.[22] However, the sample is now more complex because there are numerous peptides for each protein.[23] Also, an inference problem occurs with the rebuilding of a protein from the spectral data.[24] The same peptide sequence may exist in two different proteins, and it is difficult to determine to which protein the peptide should be assigned. Even with these challenges, the bottom-up approach is more commonly practiced due to the greater solubility of protein digests.[25]

More recently, a prefractionation approach has been implemented in which the intact proteins are fractionated by the first dimension separation, and fractions are enzymatically digested prior to analysis by LC-MS.[26,27] Experimentally, prefractionation methods are more orthogonal than other multidimensional separations because the sample is completely changed via digestion between separations.[28] Digestion, most commonly by trypsin, between the separations enables the use of reversed-phase columns in both dimensions which tend to have higher peak capacity than other LC separation modes such as ion exchange and size exclusion chromatography.[29] As opposed to bottom-up 2DLC experiments where peptides from a single

protein may be spread over the entire chromatogram, peptides from a single protein are confined to a single fraction easing computational requirements. This may reduce the protein inference problem in which a single peptide may be mistakenly assigned to multiple proteins.[24]

5.1.4 Equal-mass prefractionation

The practical 2D peak capacity increases if each fraction contains the same amount of protein. The summed absorbance from the first dimension chromatogram is an appropriate guide for determining equal-mass prefractionation (Chapter 2). The efficiency of the digestion can also be increased with equal-mass fractionation as shown in this chapter. For most prefractionation experiments, the enzyme to protein ratio is determined by assuming that the total protein loaded onto the first dimension column was evenly distributed amongst the fractions.[28] If there is excess enzyme, autolysis of trypsin will occur.[30] Peaks from trypsin peptides dominate the second dimension chromatograms for these fractions (Chapter 2). A low enzyme to protein ratio increases the probability that proteins are not fully digested.[31] A poor digestion leads to poor amino acid sequence coverage of the protein and the inability to detect the protein.[23]

The scope of this chapter was to couple prefractionation by equal-mass with the modified UHPLC for the analysis of a model proteome, *S. cerevisiae* (Baker's yeast). The effect of prefractionation frequency on proteome coverage was assessed. The results were compared to separations, of equal-mass fractions, on a standard UPLC as studied in Chapter 2. By incorporating the modified UHPLC into the 2D experiment, the number of protein identifications and percent sequence coverage increased as compared to the results in Chapter 2. The improvement was realized with a lower prefractionation frequency and 2D separation time.

5.2 Materials and method

5.2.1 Materials

Water, acetonitrile, isopropyl alcohol and ammonium hydroxide were purchased from Fisher Scientific (Fair Lawn, NJ). Ammonium acetate, ammonium bicarbonate, formic acid, trifluoroacetic acid and iodoacetamide were purchased from Sigma-Aldrich Co. (St. Louis, MO). Rapigest^{TM} SF acid-labile surfactant and bovine serum album (BSA) digest standard were obtained from Waters Corporation (Milford, MA). Dithiothreitol was purchased from Research Products International. Water and acetonitrile were Optima LC-MS grade, and all other chemicals were ACS reagent grade or higher. The harvest and lysis of the *S. cerevisiae* on glycerol was previously described in Chapter 2.

5.2.2 Intact protein prefractionation

The prefractionation of intact proteins, as outlined in Figure 5.1., was performed on a 4.6 x 250 mm PLRP-S column with 5 µm particles, 300 Å (Agilent, Santa Clara, CA) heated to 80 °C. Four milligrams of total protein were injected onto the column. The mobile phase composition and gradient profile is shown in Table 5.1. The separation was followed by UV spectrophotometry to give a qualitative chromatogram. The wavelength was set to 214 nm, which is the lambda max of the peptide bond.[32] One-minute wide fractions were collected in microcentrifuge tubes, lyophilized and stored at -80°C until further analysis.

5.2.3 Equal-mass fractionation

Each absorbance value for the UV chromatogram was summed with all previous absorbance values from 10 to 48 minutes which corresponded to the time after the injection plug and before the wash as follows

$$\text{Summed Absorbance } (\Sigma A) = \sum_{t_d}^{t_d+t_g} A_t \qquad (5\text{-}1)$$

where A = absorbance, t = time, t_d = dead time, and t_g = gradient time.

The ΣA was normalized and plotted versus the first dimension separation time in Figure 5.2.a. The y-axis was annotated with hash marks in increments 0.05 which split the axis into 20 even parts. Lines were drawn from the hash marks on the y-axis to the corresponding x-coordinate on the normalized ΣA curve. These x-coordinates were used to determine size of the first dimension fractions. Each lyophilized one-minute-wide fraction (described in section 5.2.2.) was reconstituted in 25 µL of 50 mM ammonium bicarbonate, pH 8. Three microliters of 6.67% (w/v) RapiGest™ SF in buffer were added. Solutions were vortexed, sonicated for 15 minutes, and incubated at 80 ºC for 15 minutes to denature the proteins. The solutions were distributed into 20 equal-mass fractions, as outlined in Table 5.2.

5.2.4 Protein digestion

The digestion is more efficient when carried out in a minimal amount of solvent. Therefore, the 20 equal-mass fractions were lyophilized and reconstituted in 25 µL of 50 mM ammonium bicarbonate. Three microliters of 6.67% (w/v) RapiGest™ SF in buffer were added. Solutions were vortexed, sonicated for 15 minutes, and incubated at 80 ºC for 15 minutes to denature the proteins. The proteins were reduced by adding 1 µL of 100 mM dithiothreitol, vortexed, sonicated for 5 minutes, and incubated for 30 min at 60ºC. Proteins were then alkylated with 1 µL of 200 mM iodoacetamide, vortexed, sonicated for 5 minutes, and stored protected from light for 30 min at room temperature. The proteins were then digested by adding 10 µL of 667 ng/µL TPCK-modified trypsin in 50 mM ammonium bicarbonate (overnight, 37ºC). The trypsin concentration was approximated to be a 50:1 (w/w) protein to enzyme ratio if the initial protein amount was equally distributed across the 20 fractions. The digestion was quenched and the RapiGest™ SF was degraded using 44 µL 98:1:1 (v:v:v) water:acetonitrile:trifluoroacetic

acid (45 min, 37ºC). The fractions were centrifuged for 10 minutes at 14,000 Xg to pellet the hydrolyzed surfactant, after which they were ready for analysis. The samples were transferred to LC vials and spiked with 1.3 µL of a 1 pmol/L internal standard BSA digest (Waters).

To form the set of 10 fractions, 20 µL of neighboring pairs of fractions from the set of 20 was combined, lyophilized, and reconstituted with 10 µL 50 mM ammonium bicarbonate and 10 µL 98:1:1 (v:v:v) water:acetonitrile:trifluoroacetic acid. Likewise, the set of 5 fractions was formed by combining 20 µL of every 4 consecutive fractions from the set of 20, lyophilizing, and reconstituting with 10 µL 50 mM ammonium bicarbonate and 10 µL 98:1:1 (v:v:v) water:acetonitrile:trifluoroacetic acid. All fractionation schemes are outlined in Table 5.2 and depicted in Figure 5.2.

5.2.5 Peptide analysis by UHPLC-MS/MS

Each fraction was analyzed in duplicate by capillary RPLC-MS/MS using the UHPLC system described in Chapter 3 coupled to a QTOF Premier MS. Mobile phase A was Optima Grade water with 0.1% formic acid (Fisher), and mobile phase B was Optima-grade acetonitrile with 0.1% formic acid (Fisher). Two microliters of the sample were pre-concentrated at the head of a 110 cm x 75 µm, 1.9 µm BEH C18 column with 0.5% mobile phase B, and then separated with a 25 µL gradient from 4-40%B followed by a wash at 85%B and equilibration at initial conditions (Table 5.3). The column was run at 32 kpsi and 65°C to produce a 300 nL/min flow rate. The outlet of the RPLC column was connected via a 30 cm x 20 µm ID piece of fused silica capillary to an uncoated fused silica nanospray emitter with a 20 µm ID and pulled to a 10 µm tip (New Objective, Woburn, MA) operated at 2.6 kV. Data-independent acquisition, or MS^E scans, was performed with the instrument set to acquire parent ion scans from m/z 50-1990 over

0.6 sec at 5.0 V. The collision energy was then ramped from 15-40 V over 0.6 sec with 0.1 sec interscan delay.

5.2.6 Peptide data processing

The peptide LC-MS/MS data were processed using ProteinLynx Global Server 2.5 (Waters). The MS^E spectra were searched against a database of known yeast proteins from the Uni-Prot protein knowledgebase (www.uniprot.org) with a reversed sequence appended to the end. The false discovery rate was set to 100% to yield data compatible for further processing.

After the database search was complete, the results were imported into Scaffold 4.2.0 (Proteome Software, Portland, OR). The minimum protein probability and peptide probability filters were set to a 5% false discovery rate, and the minimum number of peptides required for protein identification was set to 3. Peptides matching multiple proteins were exclusively assigned to the protein with the most evidence. The spectral counts for each peptide assigned to a protein were summed to give the quantitative value of that protein. The value was normalized by multiplying the average total number of spectra, for all yeast samples grown on the same media, divided by the individual sample's total number of spectra.[33,34]

5.3 Discussion

5.3.1 Protein identifications

By combining the prefractionation techniques studied in Chapter 2 with the new UHPLC developed in Chapter 3, the return on protein identifications per unit time was greatly increased. In Figure 5.3**,** the number of protein identifications versus number of fractions is plotted for each prefractionation experiment. The number of fractions is proportional to the separation time as each fraction had a 1.5 hour retention window. The red line shows the improvement for equal-mass fractionation versus equal-time fractionation (blue line) as was discussed in Chapter 2. The

green line demonstrates the improvement in protein identifications when UHPLC with a 110 cm long column was employed for the second dimension separation. The set of 5 fractions analyzed on the long column identified 472 proteins which exceeded the number of proteins identified by the analysis on the standard system even with increased first dimension fractionation. When first dimension sampling was increased to 10 fractions, 701 proteins were identified. The number of identifications leveled off at 20 fractions with 776 protein identifications. With the ability to operate at higher pressures, the peak capacity gained through the use of a longer column resulted in the identification of more proteins with less first dimension fractions and less total separation time.

5.3.2 Analysis time

To make a fair comparison between the standard UPLC and modified UHPLC system, the second dimension separation times had to be similar. This was somewhat difficult as the standard system is programmed with a gradient time and constant flow rate whereas the modified system is programmed with a gradient volume and constant pressure. The gradient volume was 25 μL, and modified UHPLC was pressured to 32 kpsi. The measured flow rate was 300 nL/min at 65°C and 4% mobile phase B. Because mobile phase composition was changing throughout the run, the flow rate was also changing slightly but theoretically by less than 5% as previously explained.[17,18,19] Peaks eluted for 100 minutes as evident by the chromatograms in Figure 5.4.

Though the separation window was similar for the separation on the modified UHPLC and standard UPLC, the total run time for the separations on the modified system was longer. The standard system had a trap column to preconcentrate the sample and ultimately reduce the injection time. Addition of a trap column to the modified system resulted in band broadening which was suspected to occur from mixing in the nano-tee between the trap and analytical

column. In the future, the modified system should be engineered to have a total run time more comparable to the standard system.

5.3.3 Increased peptide peak intensity

Another observation from the 2D chromatograms in Figure 5.4. is that peak intensities are much greater with the modified UHPLC. Chapter 3 demonstrated that through the use of long columns and elevated pressures, narrower peak widths could be achieved as compared to a separation with the standard system. The peptides were focused into narrow peaks which contributed to the higher intensity. With increased intensity, more peptide peaks were above the limit of detection which contributed to the increase in protein identifications with the modified UHPLC system.

5.3.4 Protein identifications per fractions

To further discuss the number of protein identifications achieved with the modified UHPLC, the number of proteins identified per fraction is plotted in Figure 5.5. for each prefractionation frequency. The light gray bars show the total protein identifications in each fraction, and the dark gray bars signify the unique protein identifications in each fraction. The total protein count was defined as any protein found within a given fraction; thus, if a protein were to be found in multiple fractions it would be counted in each fraction. The unique protein values count each protein entry only once. Proteins identified in multiple fractions were assigned to the fraction in which it was most intense. Though there were few peaks during the beginning and end of the first dimension chromatogram, as evident from the overlaid red trace, proteins were still identified in the analysis of the peptide digests of these fractions. On average, more unique proteins were identified per fraction as prefractionation frequency decreased but total proteins identifications per fraction remained constant.

To compare the number of proteins identified per fraction with the modified UHPLC to that run on the standard system, Figure 5.6, Figure 5.7 and Figure 5.8 should be considered for 20, 10 and 5 fractions, respectively. In each figure, part (a) shows the protein identifications per fraction using the long column at elevated pressures while part (b) shows data collected with the standard system. At every fractionation frequency, more proteins were identified per fraction especially for the first fraction with the modified UHPLC. The increased peak capacity from using the long column at elevated pressure contributed to the increase in protein identifications.

5.3.5 Protein digestion

As observed in Figures 5.5 – 5.7, there was a large increase in protein identifications in fraction one when the second dimension analysis occurred at 32 kpsi. The increase in identifications was greater for this particular fraction due to when the digestion occurred in the experimental protocol and due to the incorporation of sonication after each step of the protocol. For the samples run on the standard system, digestion occurred before the equal-time fractions were combined into equal-mass fractions. For the samples run on the modified system, digestion occurred after recombination into equal-mass fractions, and sonication was incorporated throughout the digestion protocol. Combining the fractions based on first dimension separation data, more evenly distributed the proteins amongst the fractions. Therefore, the enzyme to protein ratio was more consistent for each fraction. With a better estimation of this ratio, autolysis of the enzyme was less likely in fractions corresponding to less intense first dimension peaks. Also, less protein remained undigested in the fractions containing large amounts of protein. Sonication aided in the denaturing of proteins which facilitated the delivery of enzyme to the digestion sights. Digestion of equal-mass fractions is recommended for future prefractionation experiments.

5.3.6 Protein molecular weight distribution

The molecular weight distributions of identified proteins are displayed in in Figure 5.9a for the separations at 32 kpsi and Figure 5.9b for the separations at 8 kpsi. The molecular weight distribution corresponding to the 5, 10 and 20 fractions are portrayed by the black, gray and white bars, respectively. Proteins were identified with molecular weight s up to 250 kDa. For all methods, the median molecular weight was 39-40 kDa which was similar to the literature value of approximately 42.2 kDa for the *S. cerevisiae* proteome.[35] For the fractions run at 32 kpsi, the increase in identifications occurred mostly for lower molecular weight proteins, 20-70 kDa.

The molecular weight chromatograms in Figure 5.10 for 20 (parts a,b), 10 (parts c,d), and 5 (parts e,f) first dimension fractions plot protein mass on the y-axis and first dimension fraction on the x-axis. The log quantitative value for each protein is plotted as a gray-scale intensity in the z-direction. The molecular weight chromatograms on the left (Figure 5.10 a,c,e) were from the modified UHPLC at 32 kpsi with a 110 cm column, and the chromatograms on the right (Figure 5.10 b,d,f) were from the standard UPLC at 8 kpsi with a 25 cm commercial column. The correlation between protein molecular weight and first dimension fraction was stronger for the separations at 32 kpsi. In other words, the later fractions contained proteins with larger molecular weights. Larger proteins would have more sites to interact with the stationary phase causing them to elute later in the first dimension fractions. Though the first dimension separation method was the same for all experiments, the separations at 8 kpsi and 32 kpsi were completed with two different first dimension prefractionation sets due to limited sample volume. The differences in the mass chromatograms may also be due to the changes the digestion protocol as explained in the previous section.

5.3.7 Venn diagram comparisons

Analysis on the long column at elevated pressures resulted in a greater than two fold-change in protein identifications as compared to the standard system for the analysis of 5 and 10 fractions as seen in Figure 5.11. (a and b). About 90% of the proteins identified with the standard system were also identified by analysis on the modified UHPLC. When first dimension sampling increased to 20 fractions, the improvement between analysis on the modified and standard UHPLC systems decreased to 79% more identifications. An 84% overlap in identifications was observed for the 20 fractions run on both systems. The increased fractionation frequency may cause proteins to be split amongst multiple fractions resulting in the slightly lower improvement for this data set.

In Figure 5.12, the overlap in protein identifications was compared for 5, 10 and 20 first dimension fractions analyzed by the modified UHPLC-MS. When fractionation was doubled from 5 to 10, 198 additional proteins were identified, and 46 protein identifications were lost for a net increase of 27%. Another doubling of fractionation from 10 to 20, resulted in 212 additional protein identifications at a cost of 51 protein identifications for a net gain of 22%. The total number of protein identifications in the Venn diagrams in Figure 5.11 and Figure 5.12 included every unique protein entry in the replicate analyses. The numbers were slightly larger than the protein identifications in Figure 5.3 which corresponded to the average number (arithmetic mean) of identifications between two replicate analyses. The Venn comparisons further demonstrate that excessive prefractionation should be avoided to reduce peak splitting. With the modified UHPLC and long microcapillary column, the peak capacity in the second dimension is increased reducing the need for a high prefractionation frequency.

5.3.8 Fractions per protein

The first dimension chromatogram was crowded with many overlapping peaks making it impractical to determine peak widths for individual proteins. As an alternative merit, fractions per protein was defined as the number of fractions in which a single protein was identified. The graph in Figure 5.13 shows the percentage of proteins identified in one, two and three-or-more fractions for each prefractionation frequency. The majority of proteins were identified in only one fraction. As fractionation frequency increased, more proteins were identified in multiple fractions. These fractions may or may not be adjacent. When a protein was split between multiple fractions, it was diluted which may cause it to fall below the limit of detection. When comparing the fractions per protein for data collected with the modified and standard UHPLC, a larger percentage of proteins were identified in multiple fractions with the modified system. Since the first dimension separations were identical, there could not be increased protein peak splitting or broadening. Also, blank runs after the second dimension separations did not show evidence of carryover. The increased identification of proteins across multiple fractions was most likely related to the increased peak intensities in the second dimension separation as explained earlier and shown in Figure 5.4. Hypothetically, a protein peak split across two fractions has the majority of the peak contained in fraction 1 and the tail of the peak contained in fraction 2. When both fractions are digested and analyzed by LC-MS, the corresponding peptide peaks would be more intense in fraction 1 than fraction 2 because most of the protein molecules are contained in fraction 1. For fraction 2, the intensity of the peptide peaks run on the standard system may fall below the limit of detection. With the peak intensity gained from the long column run at elevated pressures, the protein could be identified in fraction 2 from its assigned peptides.

5.3.9 Protein coverage

Besides increasing the number of protein identifications, the separations at 32 kpsi also increased the protein coverage. To compare the methods, coverage was reported in Table 5.4. for several proteins involved in the metabolic processes of yeast. However, looking at coverage protein by protein for a complete proteome can be overwhelming. Averaging the coverage for all identified proteins would be misleading as the additional proteins identified in a separation with higher peak capacity are usually of lower abundance and have a lower coverage, bringing down the average. Alternatively, only proteins found by both methods could be considered. However, this would limit the comparison to easily detectible proteins which usually have higher coverage and, thus, mute the difference between the methods. Thus, we proposed the normalized difference protein coverage (NDPC), as described in Chapter 2, and will use NDPC to compare coverage between the separations on the modified and standard UHPLC.

The NDPC is defined as the difference in coverage for a particular protein between two methods normalized by the sum of its coverage in the two methods as shown in the following equation:

$$\text{NDPC} = \frac{\text{Coverage}_{a,i} - \text{Coverage}_{a,j}}{\text{Coverage}_{a,i} + \text{Coverage}_{a,j}}, \tag{5-2}$$

where $Coverage_{a,i}$ was the percent coverage of protein a in method i, and $Coverage_{a,j}$ was the percent coverage of protein a in method j. For example, the NDPC for fumarate hydratase (FUMH), a protein involved in the citric acid cycle of *S. cerevisiae*, is calculated to compare 5 fractions run on at 32 kpsi on the modified UHPLC and 8 kpsi on the standard UPLC:

$$\text{NDPC} = \frac{\text{Coverage}_{\text{FUMH,5 Fractions, 32 kpsi}} - \text{Coverage}_{\text{FUMH, 5 Fractions, 8 kpsi}}}{\text{Coverage}_{\text{FUMH,5 Fractions, 32 kpsi}} + \text{Coverage}_{\text{FUMH, 5 Fractions, 8 kpsi}}} \tag{5-3}$$

$$= \frac{54-30}{54+30} = 0.29 \tag{5-4}$$

With this example, a protein found with higher coverage in the fractions run on a longer column at 32 kpsi would have a positive NDPC. A negative NDPC signifies the protein was found with higher coverage in the fractions run on the standard UPLC. A value of +1 means the protein was only identified in the fractions run on the longer column at 32 kpsi, and a value of -1 means the protein was only identified in the fractions run on the standard system. Equal coverage in both methods results in a NDPC value of zero. The data collected with the modified and standard UHPLC are compared for 5 fractions in Figure 5.14, for 10 fractions in Appendix C.1. and for 20 fractions in Appendix C.2. The NDPC values are plotted with the proteins ordered from largest to smallest denominator, putting the proteins with highest coverage on the left, and the lowest coverage on the right. The NDPC increases as the denominator (summed protein coverage) decreased. This highlights the fact that comparing proteins identified by both methods would mute the improvement to protein coverage. These figures are large and split amongst several pages. To better comprehend the trend, the protein identifier information was removed so the graphs could fit onto a single page in Figure 5.15. The abundance of positive values signifies higher coverage with the 110cm long column at 32 kpsi for every fractionation frequency.

In an attempt to further simplify the comparison of coverage between multiple methods, while maintaining the meaning of the values, we propose the Grand NDPC which is defined by the difference between the grand total protein coverage in method one and method two normalized by the grand sum of protein coverage in both methods as shown in Equation 5-3:

$$\text{Grand NDPC} = \frac{(\sum \text{Coverage}_{\text{method 1}})-(\sum \text{Coverage}_{\text{method 2}})}{\sum \text{Coverage}_{\text{method 1}}+\sum \text{Coverage}_{\text{method 2}}} \quad (5\text{-}5)$$

Perhaps a more relevant interpretation of the Grand NDPC would be to relate it to a fold-change improvement in coverage as follows:

$$\text{Fold-Change in Coverage} = \frac{\sum \text{Coverage}_{\text{method 1}}}{\sum \text{Coverage}_{\text{method 2}}} = \frac{1+ \text{Grand NDPC}}{1- \text{Grand NDPC}} \quad (5\text{-}6)$$

If the fold-change is less than one, the negative reciprocal of the value is used as is conventional with fold-change calculations. The Grand NDPC and Fold-Change in Coverage is listed in Table 5.5. Positive values represent higher coverage with the 110 cm long column at 32 kpsi. For each prefractionation frequency, a greater than two-fold change in protein coverage was observed when the second dimension separation occurred on the 110cm long column at 32 kpsi as opposed to the 25 cm commercial column at 8 kpsi.

5.4 Conclusions

A challenge in proteomics has always been to obtain more information from the sample without increasing the analysis time. By using *S. cerevisiae* lysate as a model proteome for a prefractionation type multidimensional separation, the effects of prefractionation frequency and second dimension peak capacity on protein identifications were investigated. The gained peak capacity from performing the second dimension separation on a long column at 32 kpsi yielded an increase in protein identifications and approximately doubled the amino acid sequence coverage compared to separations on a standard system. With five first dimension fractions, the modified UHPLC identified 472 proteins while only 171 proteins were identified with the standard UPLC. It took 20 fractions, which quadrupled the separation time, to yield a maximum of 456 fractions with the standard UPLC. Identifications reached 776 proteins with 20 fractions run on the modified UHPLC. The instrumentation and methods described in this chapter will enable completion of differential proteomics studies in a shorter amount of time and produce more information about the samples.

5.5 TABLES

Time (min)	Flow Rate (mL/min)	90:5:5 H_2O:ACN:IPA + 0.2% TFA (%A)	50:50 ACN:IPA + 0.2% TFA (%B)
0	1.0	100	0
2	1.0	100	0
5	1.0	75	25
40	1.0	50	50
45	1.0	35	65
45.1	1.0	0	100
50	1.0	0	100
50.1	1.0	100	0

Table 5.1. Chromatographic conditions for the reversed-phase prefractionation of intact proteins.

a)

Fraction	First Dimension Time (min)	Normalized ΣAbsorbance
1	10-13	0.05
2	14-16	0.1
3	17	0.15
4	18	0.2
5	19	0.25
6	20	0.3
7	21	0.35
8	22	0.4
9	23	0.45
10	24	0.5
11	25	0.55
12	26	0.6
13	27	0.65
14	28	0.7
15	29	0.75
16	30	0.8
17	31	0.85
18	32	0.9
19	33-35	0.95
20	35-48	1

b)

Fraction	First Dimension Time (min)	Normalized ΣAbsorbance
1	10-16	0.1
2	17-18	0.2
3	19-20	0.3
4	21-22	0.4
5	23-24	0.5
6	25-26	0.6
7	27-28	0.7
8	29-30	0.8
9	31-32	0.9
10	33-48	1

c)

Fraction	First Dimension Time (min)	Normalized ΣAbsorbance
1	10-18	0.2
2	19-22	0.4
3	23-26	0.6
4	27-30	0.8
5	31-48	1

Table 5.2. The fractionation schemes for a set of 20 (a), 10 (b), and 5 (c) first dimension fractions are listed with the associated first dimension separation times and the normalized Σ absorbance.

Time (min)	Flow Rate (µL/min)	% Mobile Phase A	% Mobile Phase A	Curve	NanoAcquity Vent Valve	High Pressure Isolation Valve Freeze/Thaw Valve &Vent Valve	Pneumatic Amplier Pump Initiation
Gradient Loading Method							
Initial	5	96.0	4.0	-	Off	On	Off
1.0	5	15.0	85	11	Off	On	Off
1.8	5	60.0	40	11	Off	On	Off
6.8	5	96.0	4	6	Off	On	Off
7.4	5	99.5	0.5	11	Off	On	Off
8.0	4	99.5	0.5	11	Off	On	Off
8.1	3	99.5	0.5	11	Off	On	Off
8.2	2	99.5	0.5	11	Off	On	Off
8.3	1	99.5	0.5	11	Off	On	Off
8.4	0.01	99.5	0.5	11	Off	On	Off
9.0 (end)	0.01	99.5	0.5	11	Off	On	Off
Sample Loading Method							
Initial	0.01	99.5	0.5	-	Off	On	Off
0.1	1	99.5	0.5	11	Off	On	Off
0.2	2	99.5	0.5	11	Off	On	Off
0.3	3	99.5	0.5	11	Off	On	Off
0.4	4	99.5	0.5	11	Off	On	Off
0.5	5	99.5	0.5	11	Off	On	Off
2.0	5	99.5	0.5	11	Off	On	Off
2.5	0.01	50	50	11	On	Off	Off
5.0	0.01	50	50	11	On	Off	On
35.0 (end)	0.01	50	50	11	On	Off	On
Ultra High Pressure Separation Method							
Initial	0.01	50	50	11	On	Off	On
150.0	0.01	96	4	11	On	On	Off
155.0 (end)	0.01	96	4	11	On	On	Off

Table 5.3. The method for the second dimension separation at ultrahigh pressure as programmed into MassLynx is listed along with the valve timings.

Name	Entry	Protein Coverage (%)				Assigned Peptides			
		Shotgun	5	10	20	Shotgun	5	10	20
Isocitrate lyase	ACEA	-	43	71	69	-	19	35	36
Aconitate hydratase	ACON	20	65	53	69	13	53	54	72
Acetyl-coenzyme A synthetase 1	ACS1	33	63	46	64	18	53	63	69
Acetyl-coenzyme A synthetase 2	ACS2	-	10	10	20	-	2	4	8
Alcohol dehydrogenase 1	ADH1	56	74	73	74	11	26	29	29
Alcohol dehydrogenase 2	ADH2	68	76	79	77	26	42	45	47
Alcohol dehydrogenase 3	ADH3	-	35	55	65	-	10	16	20
Alcohol dehydrogenase 6	ADH6	-	-	13	38	-	-	3	11
Aldehyde dehydrogenase 2	ALDH2	-	39	50	61	-	15	19	26
Aldehyde dehydrogenase 3	ALDH3	-	9	19	20	-	2	3	3
K-activated aldehyde dehydrogenase	ALDH4	75	88	83	85	37	53	63	66
Fructose-bisphosphate aldolase	ALF	54	73	80	91	17	29	34	38
Citrate synthase	CISY1	35	61	59	65	15	35	35	46
Succinate dehydrogenase	DHSA	-	26	31	53	-	10	15	25
Dihydrolipoyl dehydrogenase	DLDH	23	65	70	76	6	32	36	42
Enolase 1	ENO1	75	86	86	88	31	21	25	26
Enolase 2	ENO2	72	88	83	92	12	51	57	62
Fumarate reductase	FRDS	-	42	55	60	-	18	22	30
Fumarate hydratase	FUMH	-	54	61	57	-	24	28	31
Glyceraldehyde-3-P dehydrogenase 1	G3P1	83	92	85	92	14	45	28	32
Glyceraldehyde-3-P dehydrogenase 2	G3P2	88	91	85	91	6	10	10	13
Glyceraldehyde-3-P dehydrogenase 3	G3P3	92	92	96	94	35	24	49	52
Glucose-6-phosphate isomerase	G6PI	44	62	69	68	21	37	45	50
Glycerol-3-phosphate dehydrogenase	GPD1	-	65	63	59	-	24	27	27
Glycerol-3-phosphate dehydrogenase	GPD2	-	11	32	26	-	2	8	9
Glycerol-3-phosphatase 2	GPP2	-	-	-	19	-	-	-	4
Hexokinase-1	HXKA	42	68	75	83	16	30	37	51
Hexokinase-2	HXKB	40	73	71	82	11	31	42	42
Glucokinase-1	HXKG	57	74	71	87	23	41	51	57
Isocitrate dehydrogenase 1	IDH1	11	59	59	65	3	23	22	24
Isocitrate dehydrogenase 2	IDH2	12	71	64	81	2	17	16	24
6-phosphofructokinase subunit α	K6PF1	23	57	57	68	15	62	76	86
Pyruvate kinase 1	KPYK1	77	86	82	88	33	54	61	64
Malate synthase 1	MASY	-	48	48	57	-	26	22	38
Malate dehydrogenase, cyto	MDHC	10	52	53	56	3	16	16	22
Malate dehydrogenase, mito	MDHM	60	77	75	84	15	24	24	31
2-oxoglutarate dehydrogenase E1	ODO1	9	34	54	51	6	29	47	56
γ-glutamyl phosphate reductase	ODO2	-	38	47	48	-	14	19	25
Pyruvate dehydrogenase E1 comp β	ODPB	-	49	37	66	-	11	10	18
Phosphoenolpyruvate carboxykinase	PCKA	44	72	83	74	19	48	54	59
Pyruvate decarboxylase isozyme 1	PDC1	62	69	65	71	30	40	45	53
Pyruvate decarboxylase isozyme 5	PDC5	-	-	17	27	-	-	5	13
Pyruvate decarboxylase isozyme 6	PDC6	-	19	28	37	-	5	11	19
Phosphoglycerate kinase	PGK	87	90	83	93	38	54	57	61
Phosphoglycerate mutase 1	PMG1	84	83	90	80	22	26	29	31
Pyruvate carboxylase 1	PYC1	-	43	40	48	-	40	42	23
Pyruvate carboxylase 2	PYC2	-	34	34	44	-	10	9	52
Succinyl-CoA ligase subunit α	SUCA	52	75	69	72	12	22	26	27
Succinyl-CoA ligase subunit β	SUCB	19	49	59	72	7	31	37	40
Transaldolase 1	TAL1	24	62	62	81	6	17	35	41
Transaldolase 2	TAL2	-	65	41	61	-	21	15	25
Transketolase 1	TKT1	-	54	73	68	-	35	48	50
Transketolase 2	TKT2	-	32	42	48	-	16	24	29
Triosephosphate isomerase	TPIS	71	90	93	88	15	28	28	31
Average		50	59	60	66	17	27	31	36

Table 5.4. For the separations on the modified UHPLC, the protein coverage (%) and number of peptides used to identify each protein is reported for the some of the proteins involved in *S. cerevisiae* metabolism

Fractions	Grand NDPC	Fold Change In Coverage
5	0.48	2.9
10	0.39	2.3
20	0.37	2.2

Table 5.5. The Grand NDPC and Fold-Change in Coverage are listed for each fractionation frequency. Positive values represent higher coverage when the 110cm long column at 32 kpsi was used for the second dimension separation as compared to the shorter column run on the standard system. The Fold-Change in Coverage increased as fractionation frequency decreased.

5.6 FIGURES

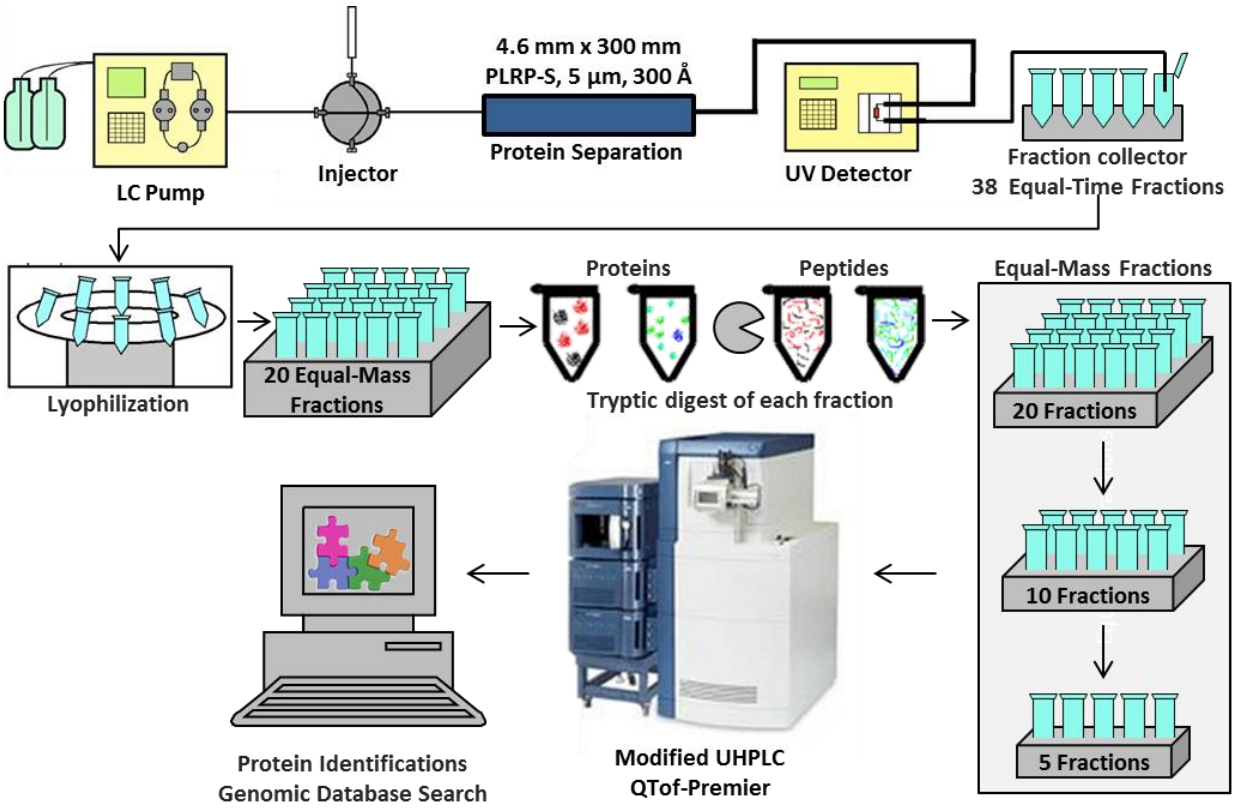

Figure 5.1. The workflow for the prefractionation method started with HPLC-UV of the intact proteins. Thirty-eight one-minute-wide fractions were collected, lyophilized, and pooled into 20 equal-mass fractions. The 20 equal-mass fractions were digested and also pooled into 10 and 5 equal-mass fractions. The set of 20, 10, and 5 equal-mass fractions were analyzed with a second dimension separation by the modified UHPLC-MS at 32 kpsi. The spectral data were searched against a genomic database to identify the proteins.

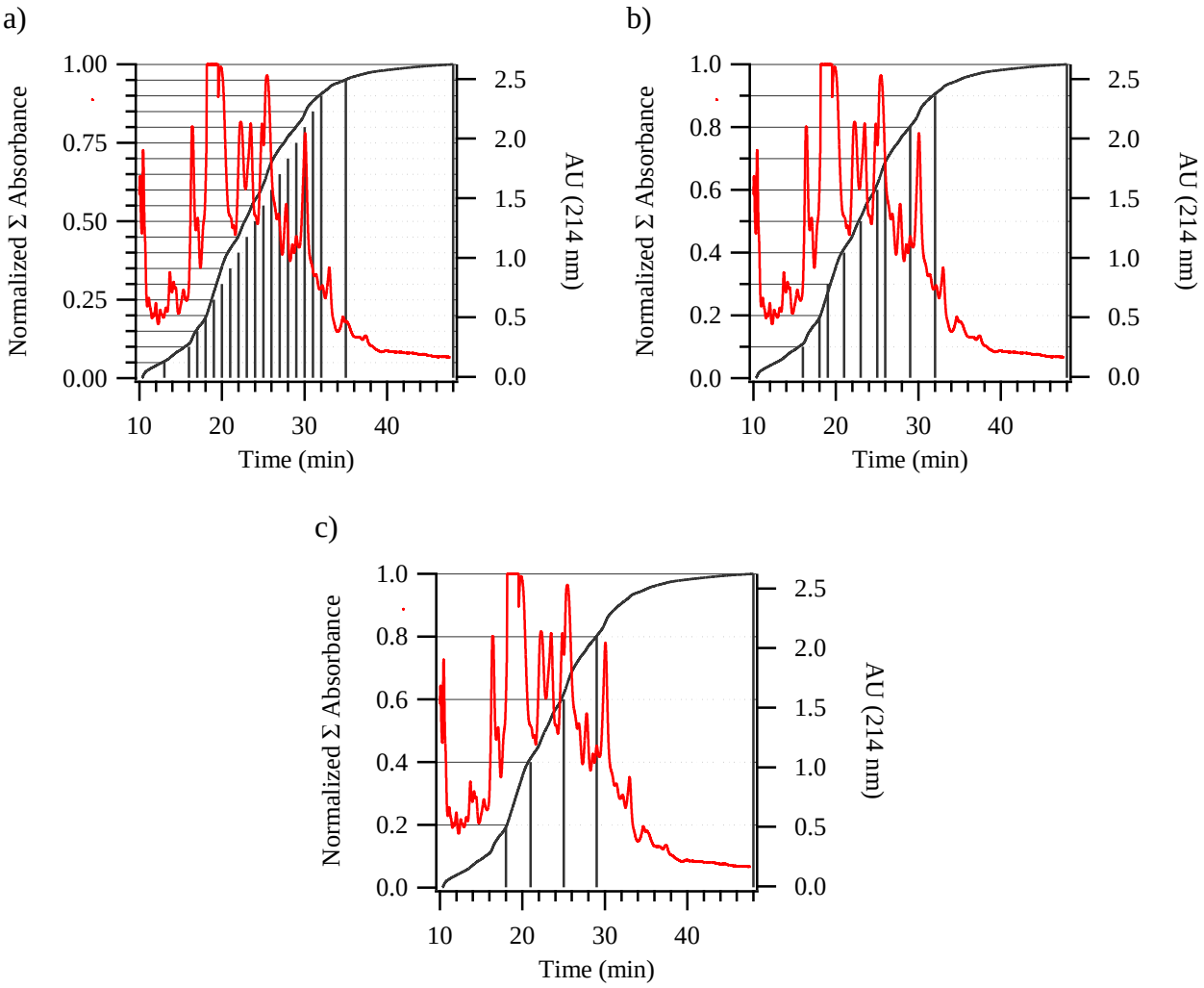

Figure 5.2. The normalized ΣAbsorbance trace is plotted versus the first dimension separation time to determine the equal-mass prefractionation timings. The y-axis is equally divided into 20 (a), 10 (b), and 5 (c) fractions. A line is drawn from the Σ Absorbance trace to the x-axis to determine when to take fractions from the first dimension. The UV chromatogram is overlaid on these plots to show how the area under the peaks is relatively equal in every fraction.

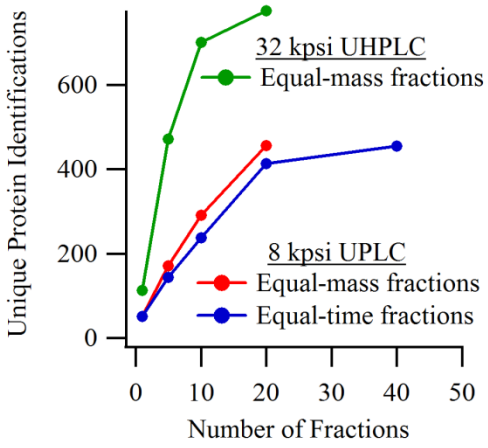

Figure 5.3. The number of protein identifications is plotted versus number of first dimension fractions. The green line is for the prefractionation experiment, described in this chapter, run on the modified UHPLC at 32 kpsi. As a comparison, the results from this chapter where superimposed on Figure 2.5 (red and blue traces) for a prefractionation study with a standard UPLC. The number of protein identifications greatly increased through use of long columns on the UHPLC.

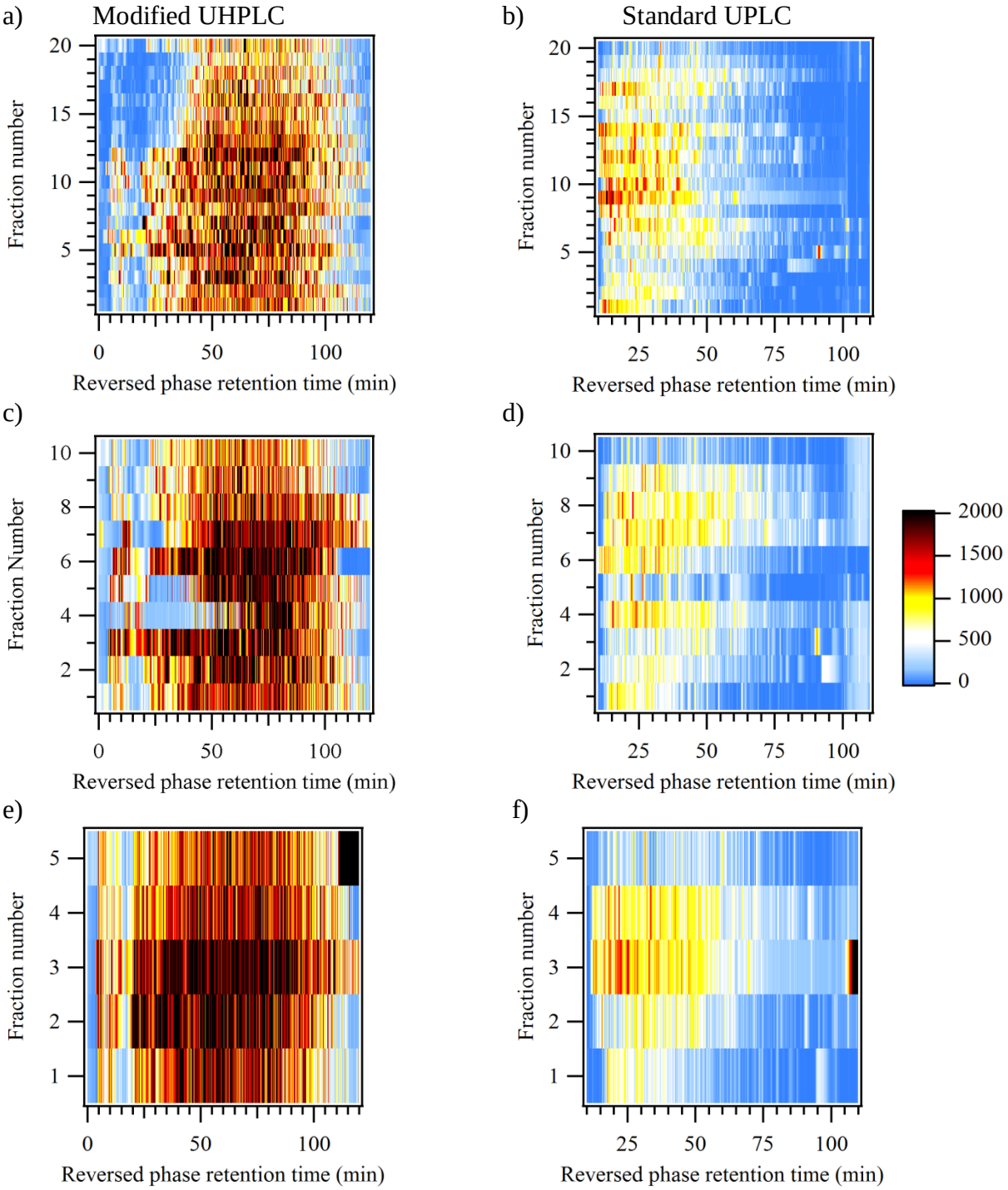

Figure 5.4. Two-dimensional chromatograms for 20 (a,b), 10 (c,d), and 5 (e,f) first dimension fractions are plotted with the first dimension (protein) fraction number versus the second dimension (peptide) separation. Base peak intensity BPI is plotted in the z-direction. Chromatograms on the left (a,c,e) are from the modified UHPLCat 32 kpsi with a 110 cm column, and chromatograms on the right (b,d,f) are run on a standard UPLC at 8 kpsi with a 25 cm commercial column. The same amount of protein was loaded onto the column in both analyses. The gain in intensity was due to the decreased peak widths on the longer column.

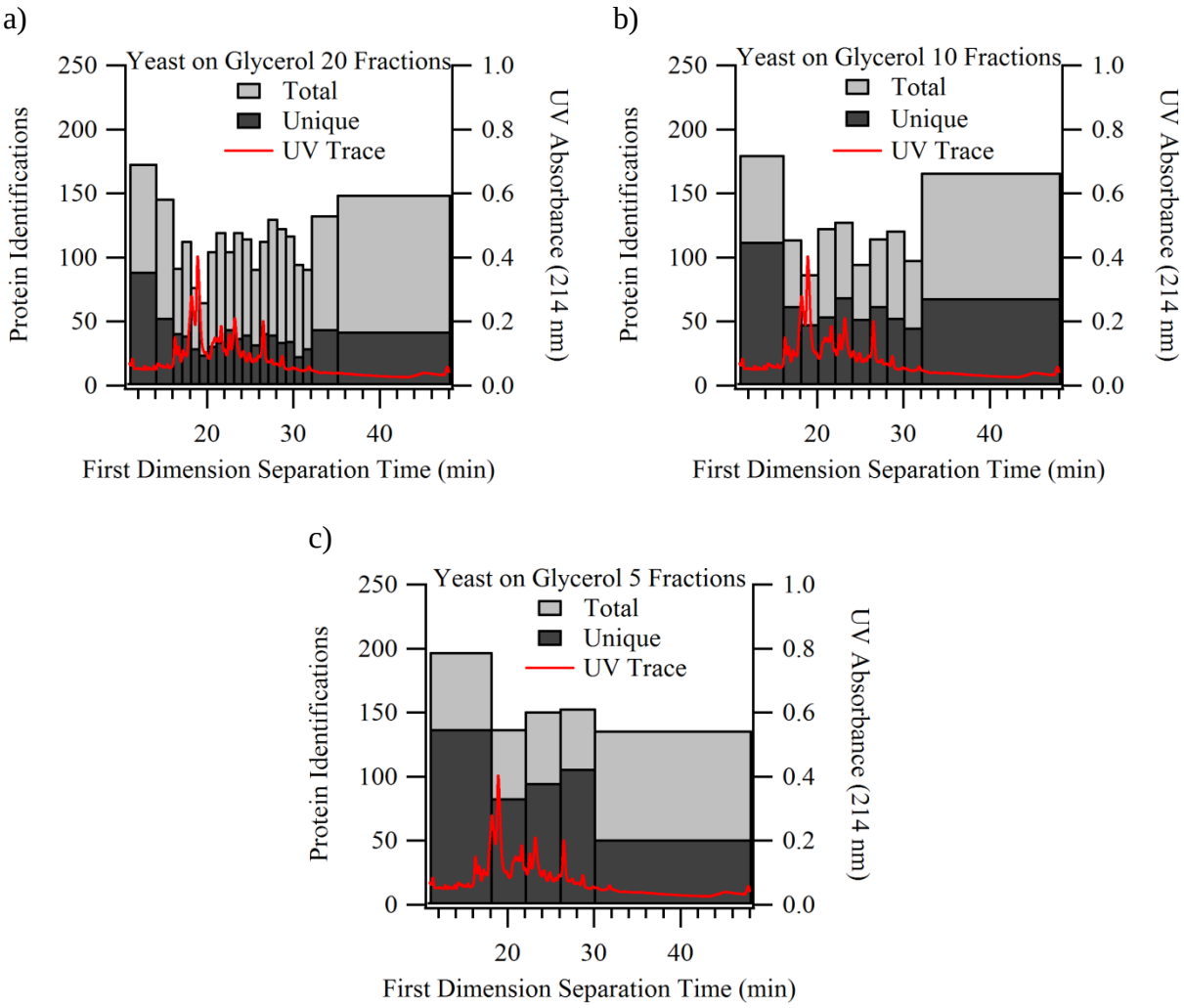

Figure 5.5. On average, more unique proteins were identified per fraction as prefractionation frequency decreased but total proteins identifications per fraction remained constant. The light gray bars show the total protein identifications in each fraction, and the dark gray bars signify the unique protein identifications in each fraction for 20 (a), 10 (b), and 5 (c) first dimensional fractions analyzed on the modified UHPLC at 32 kpsi. The x-axis is the first dimension separation time with the UV absorbance overlaid in red.

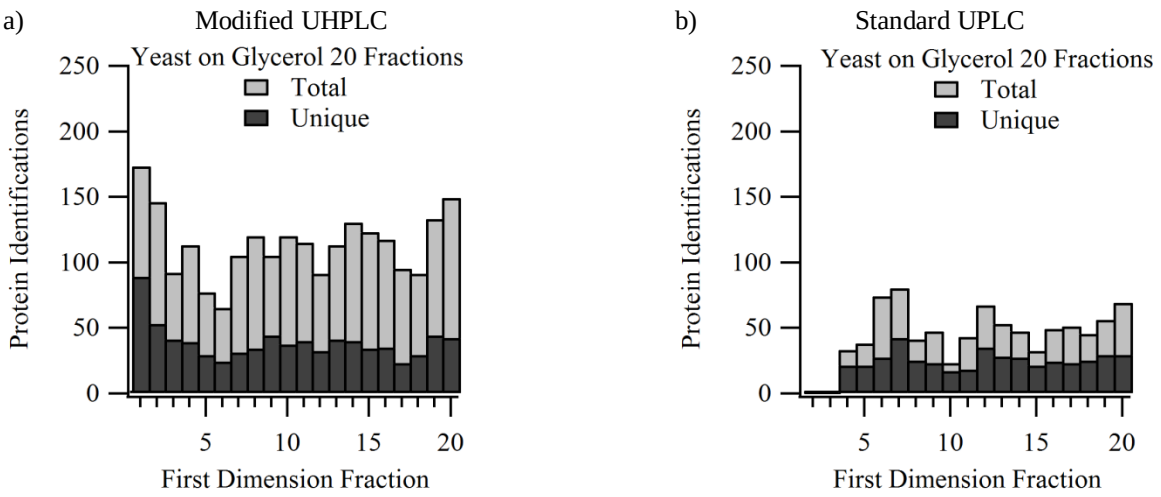

Figure 5.6. More proteins were identified per fraction when the fractions were run on the 110 cm column at 32 kpsi (a) as compared to the standard UPLC (b). The light gray bars show the total protein identifications in each fraction, and the dark gray bars signify the unique protein identifications in each fraction for 20 first dimension fractions.

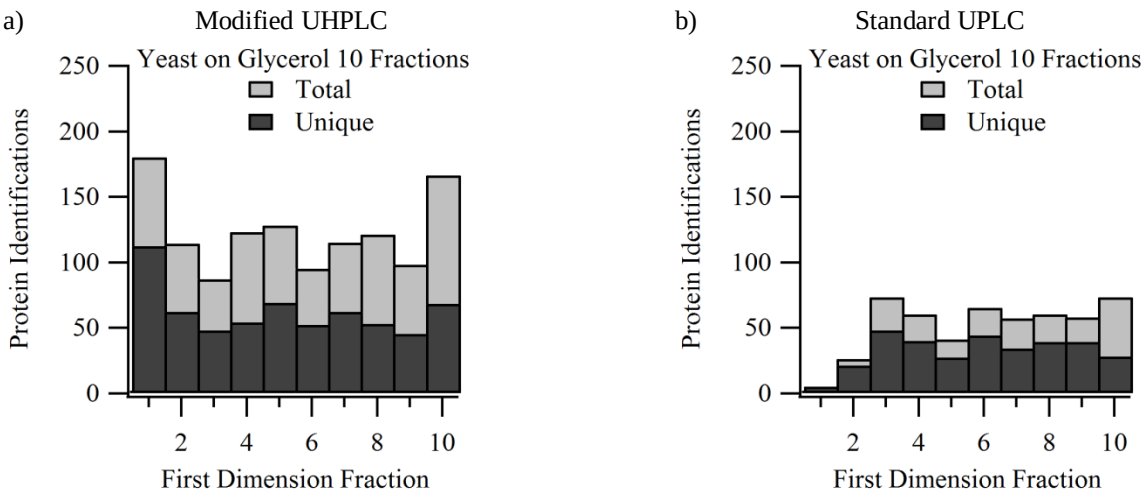

Figure 5.7. More proteins were identified per fraction when the fractions were run on the 110 cm column at 32 kpsi (a) as compared to the standard UPLC (b).The light gray bars show the total protein identifications in each fraction, and the dark gray bars signify the unique protein identifications in each fraction for 10 first dimension fractions.

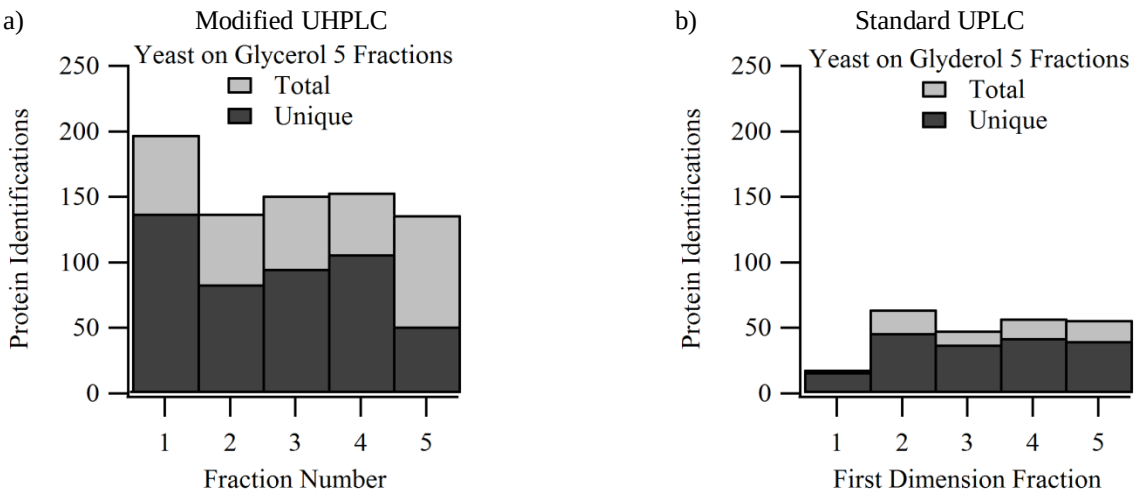

Figure 5.8. More proteins were identified per fraction when the fractions were run on the 110 cm column at 32 kpsi (a) as compared to the standard UPLC (b).The light gray bars show the total protein identifications in each fraction, and the dark gray bars signify the unique protein identifications in each fraction for 5 first dimension fractions.

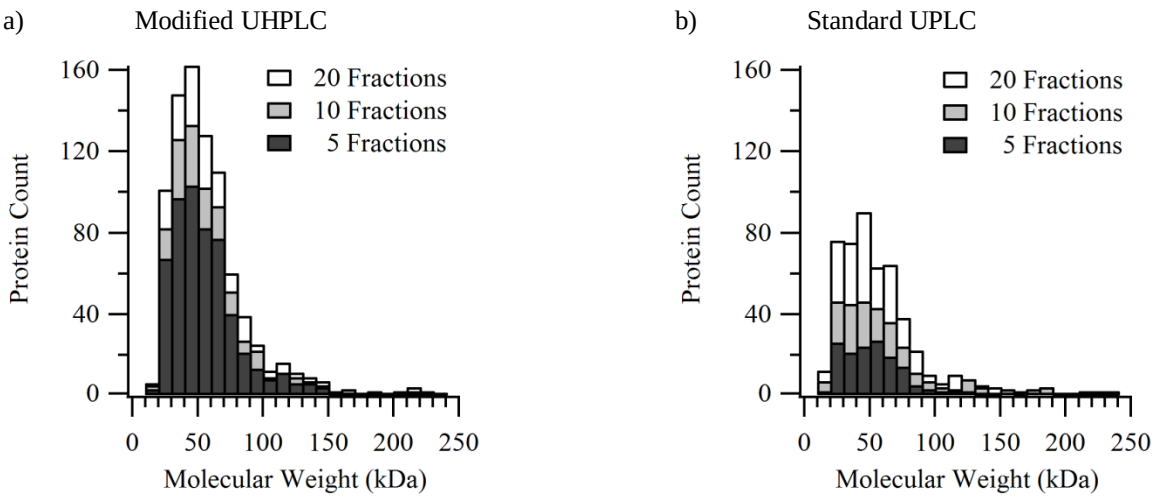

Figure 5.9. These histograms display the protein molecular weight distributions for the separations at 32 kpsi (a) and for the separations at 8 kpsi (b). The mass distribution corresponding to the 5, 10 and 20 fractions are portrayed by the black, gray and white bars, respectively. Proteins were identified with masses up to 250 kDa. For all methods, the median molecular weight was 39-40 kDa. For the fractions run at 32 kpsi, the increase in identifications occurred mostly for lower mass proteins 20-70 kDa.

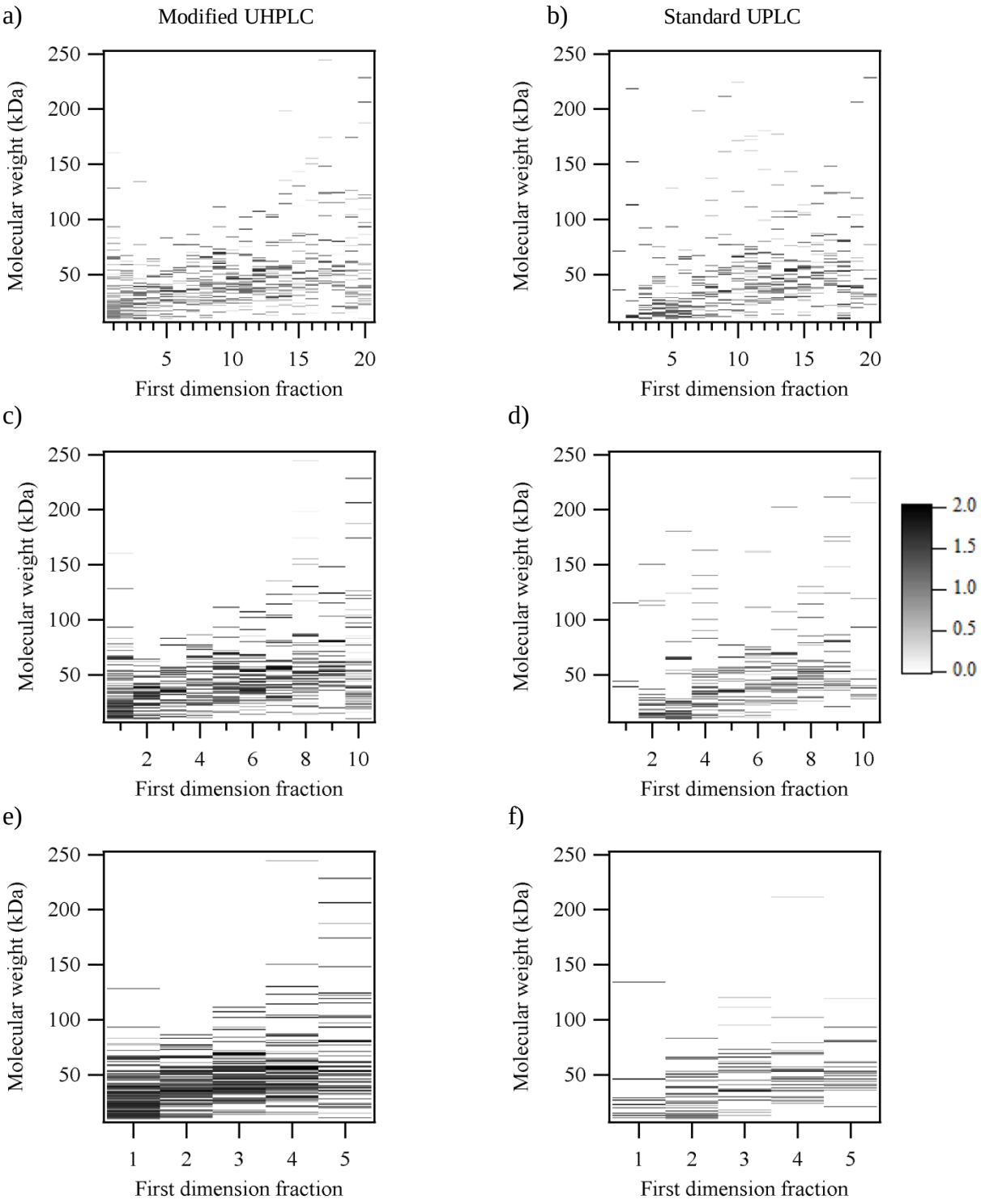

Figure 5.10. The mass chromatograms for 20 (a,b), 10 (c,d), and 5 (e,f) first dimension fractions are plotted as protein mass versus first dimension fraction. The log quantitative value for each protein is plotted in the z-direction. Chromatograms on the left (a,c,e) are from the modified UHPLC at 32 kpsi on a 110 cm column, and chromatograms on the right (b,d,f) are from the standard UPLC at 8 kpsi on a 25 cm commercial column.

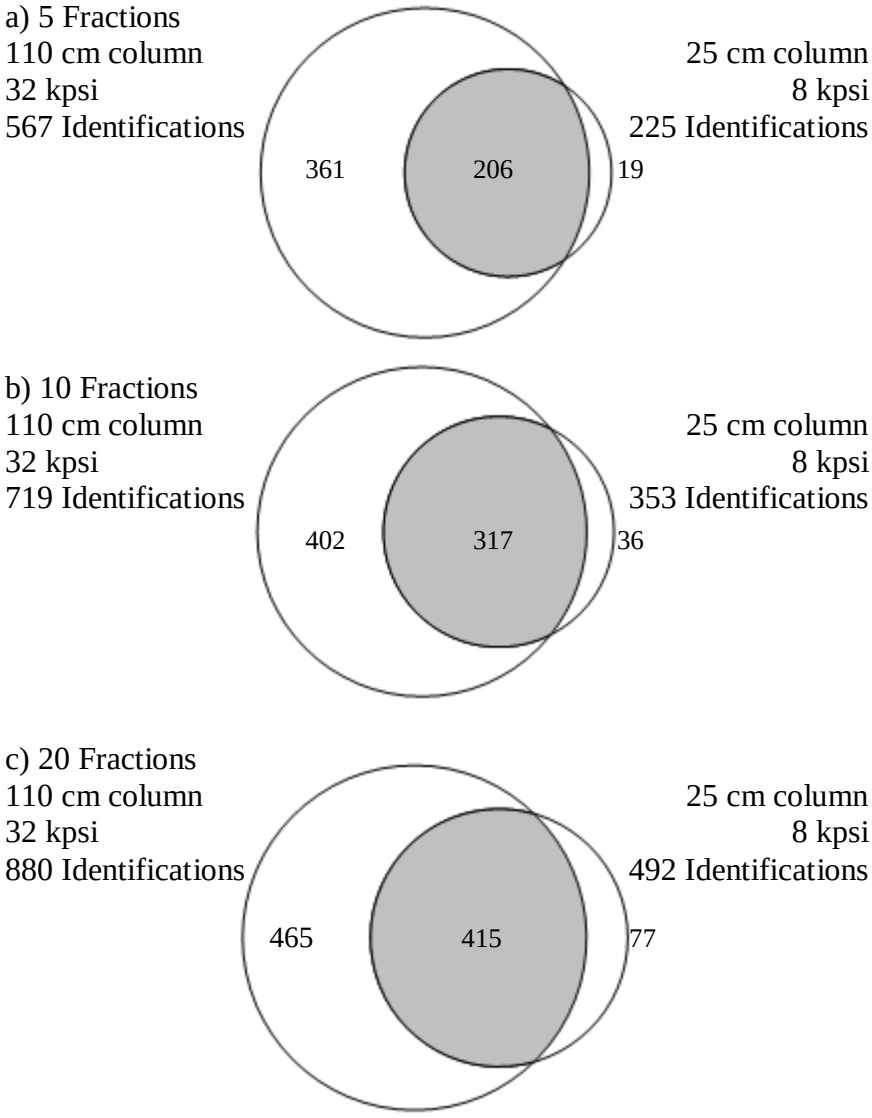

Figure 5.11. Similarities in protein identifications are compared for 5 (a), 10 (b), and 20 (c) first dimension fractions run on the 110 cm column at 32 kpsi to fractions run on a standard UPLC.

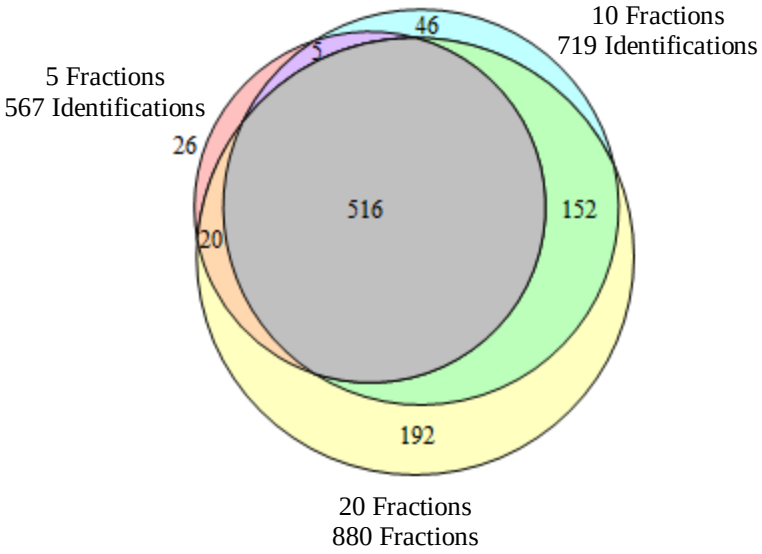

Figure 5.12. The Venn diagram demonstrates the overlap in protein identifications for 5, 10, and 20 equal-mass fractions run on the 110 cm column at 32 kpsi.

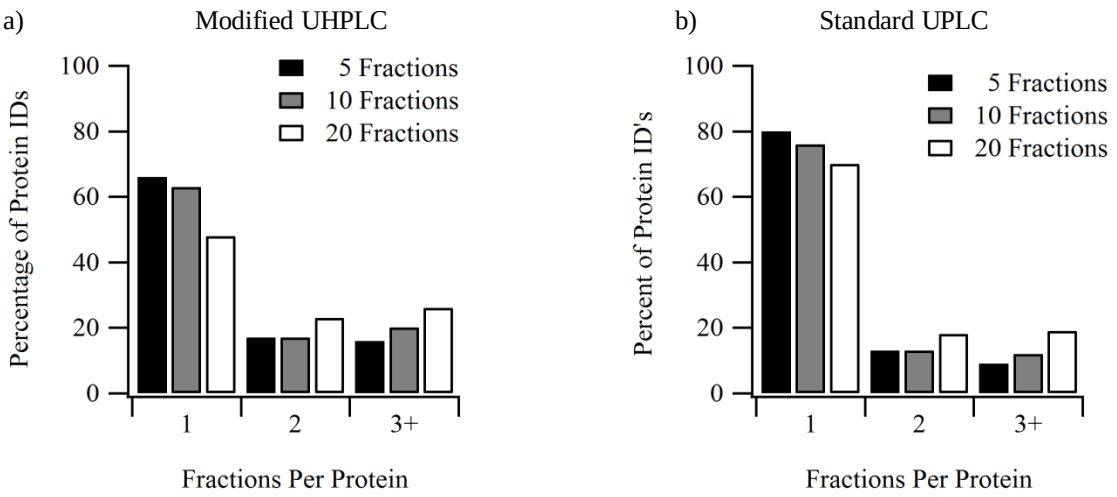

Figure 5.13. Fractions per protein describe the percentage of proteins that were identified in one, two or more (3+) fractions run on the 110 cm column at 32 kpsi (a) and the standard UPLC (b). As prefractionation frequency increased, more proteins were identified in multiple fractions. A larger percentage of the proteins were identified in multiple fractions with the modified system. The increased identification of proteins across multiple fractions was mostly likely related to the increased peak intensities in the second dimension separation.

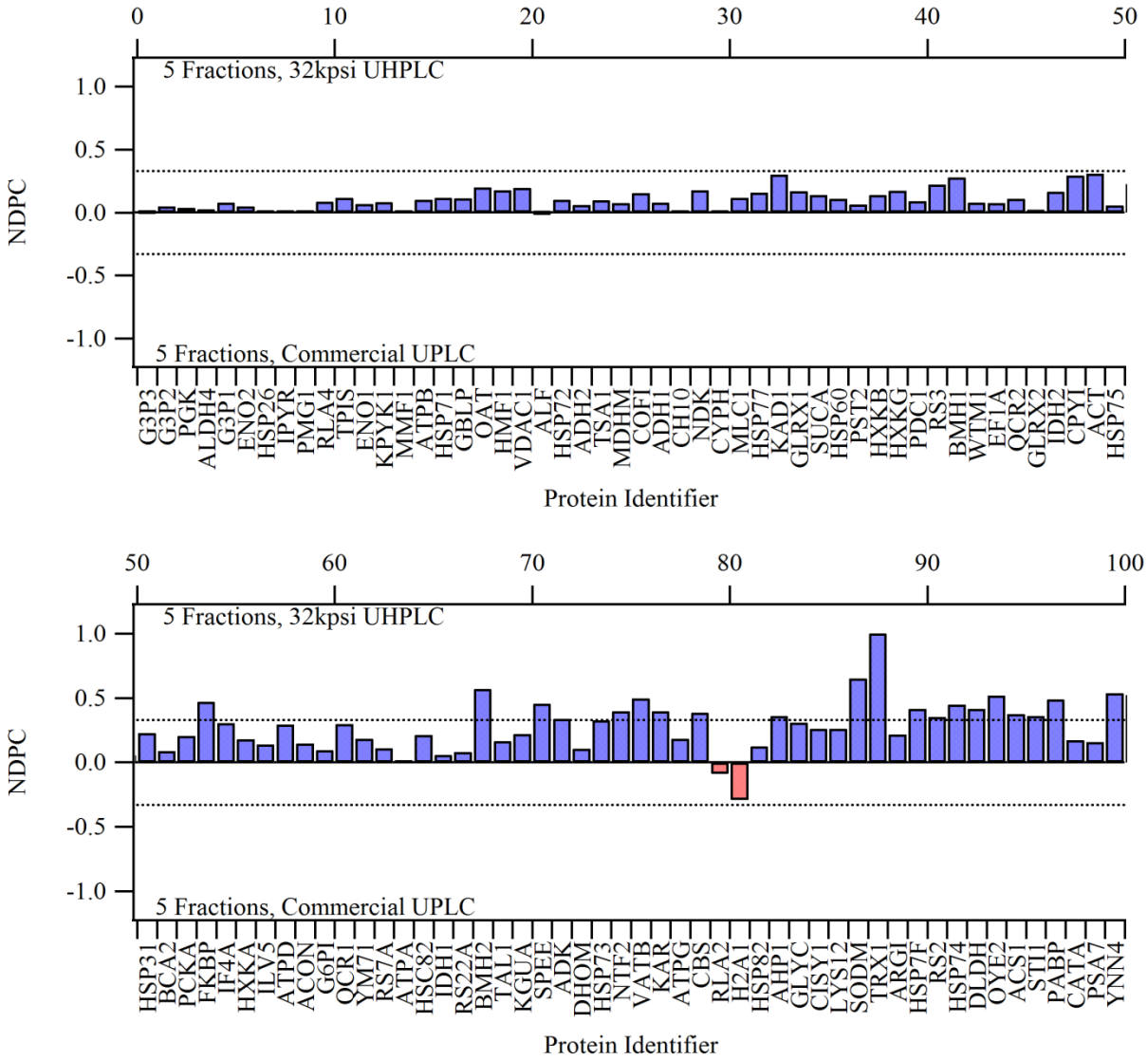

Figure 5.14. To compare the 5 fractions run on the modified system to the 5 fractions run on the standard UPLC, the NDPC is plotted with proteins with higher coverage on the left, and proteins with lower coverage on the right. If a protein was identified with higher sequence coverage when analyzed on the modified UHPLC, its NDPC value is positive (blue bars). The red bars signify higher coverage in the analysis on the standard UPLC. Differences in coverage were minimal for highly covered proteins. As protein coverage decreased, more proteins were identified with higher coverage from the analysis on the modified UHPLC. The dashed lines indicate a level of two-fold greater protein coverage. (This was a large graph and split into multiple parts.)

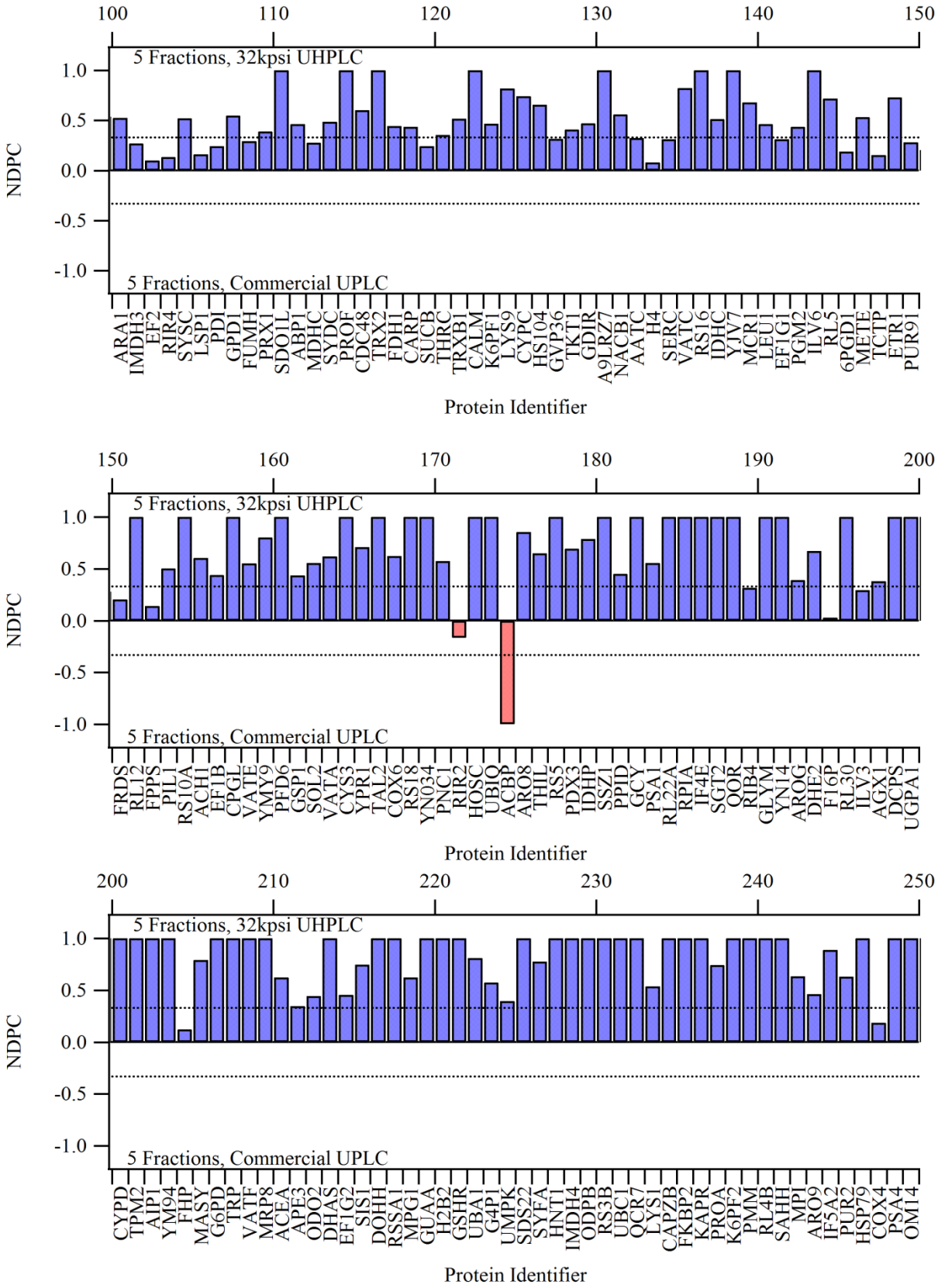

Figure 5.14. (continued)

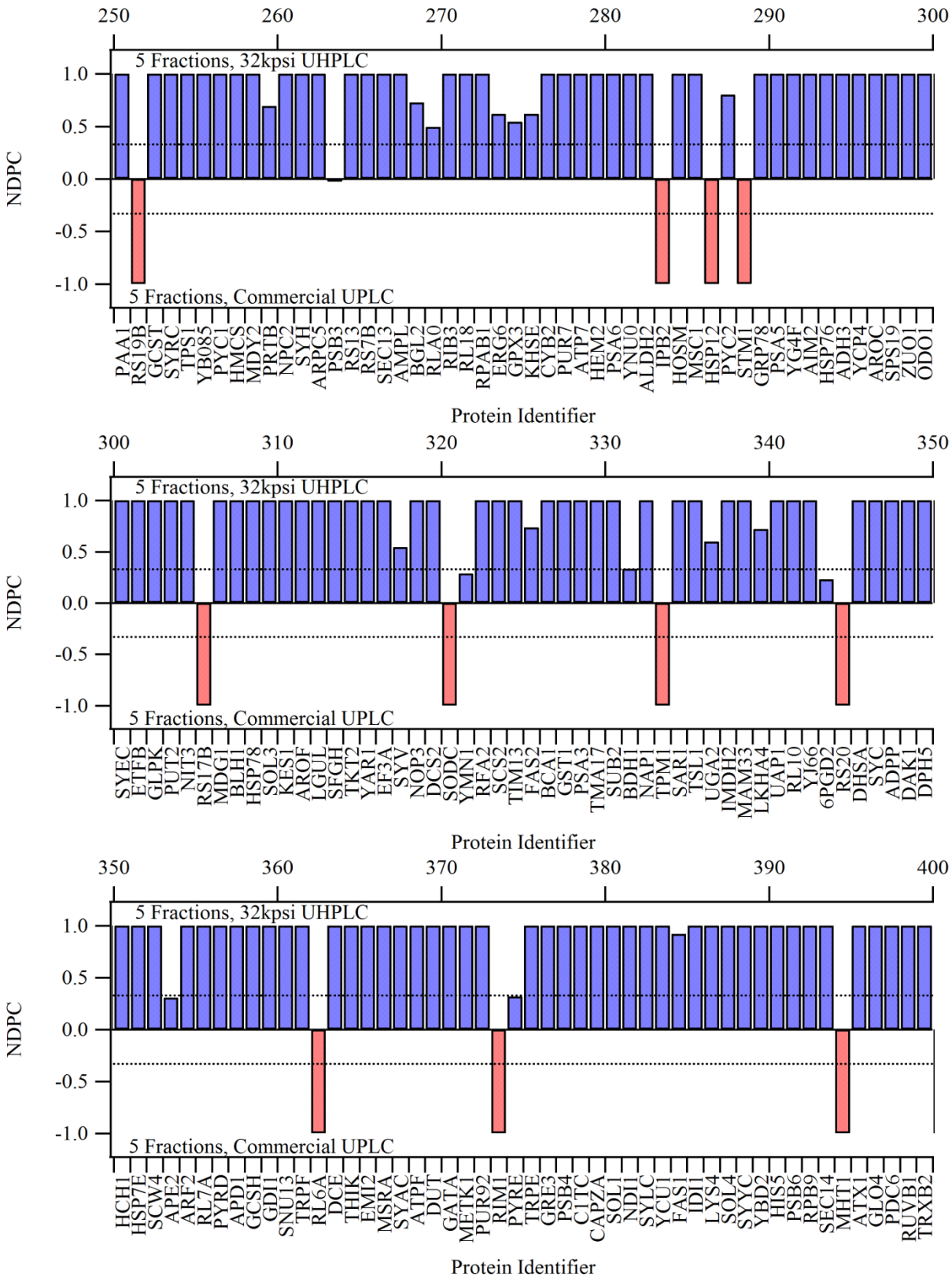

Figure 5.14. (continued)

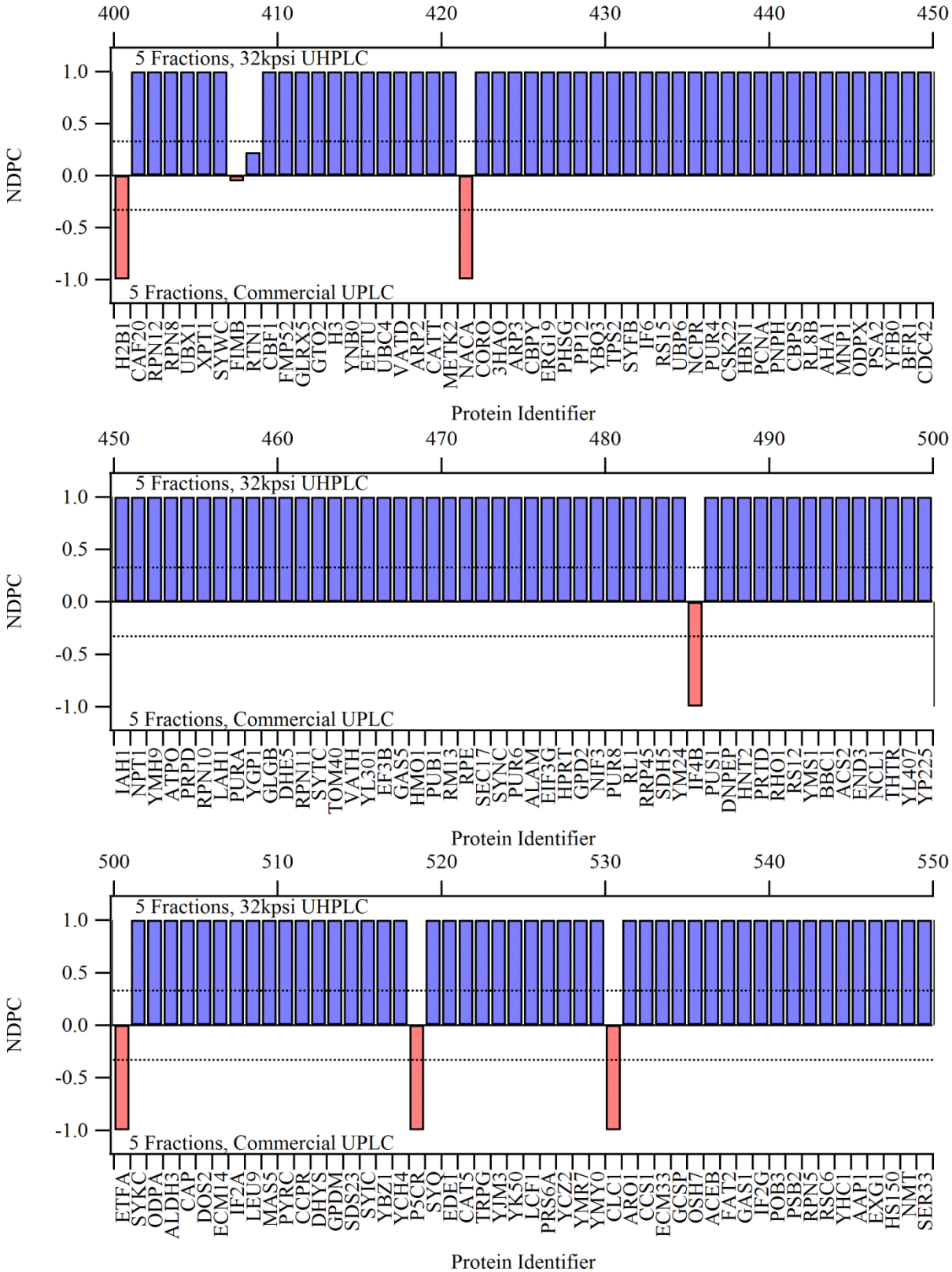

Figure 5.14. (continued)

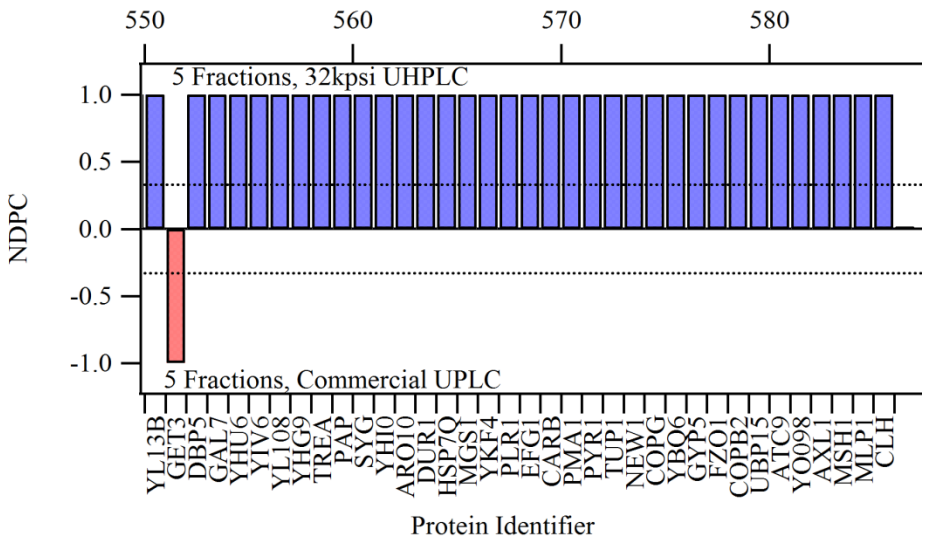

Figure 5.14. (continued)

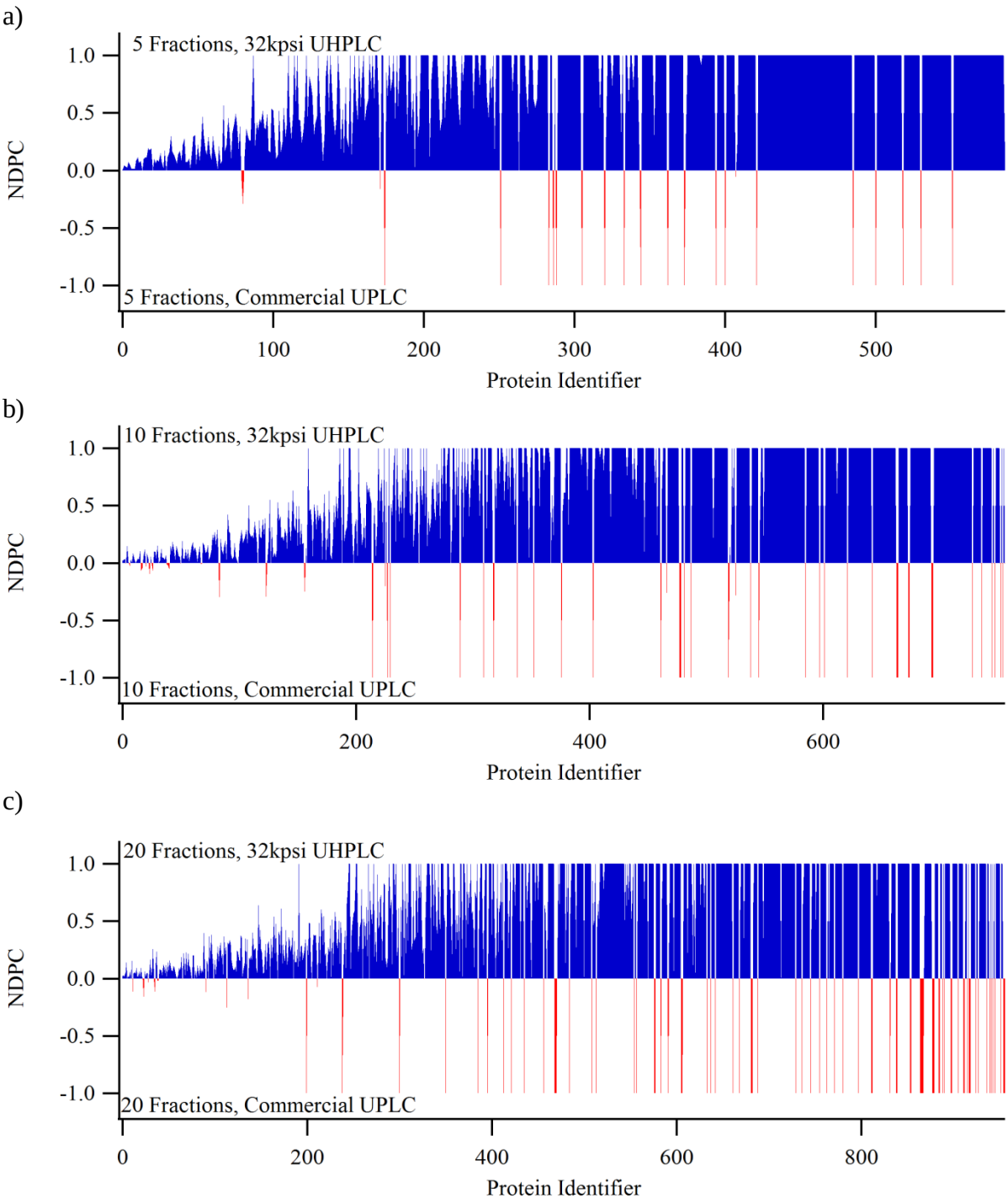

Figure 5.15. The NDPC plotted here compare proteins identified with the modified and standard UHPLCs for 5 (a), 10 (b), and 20 (c) first dimension fractions. If a protein was identified with higher sequence coverage with the modified UHPLC, the NDPC value is positive (blue lines). The red lines signify higher coverage with the standard UPLC. Proteins with higher coverage are plotted on the left, and proteins with lower coverage are on the right. More proteins were identified with higher coverage by with the modified UHPLC.

5.7 REFERENCES

1. Kenyon, G. L.; DeMarini, D. M.; Fuchs, E.; Galas, D. J.; Kirsch, J. F.; Leyh, T. S.; Moos, W. H.; Petsko, G. A.; Ringe, D.; Rubin, G. M.; Sheahan, L. C., Defining the Mandate of Proteomics in the Post-Genomics Era: Workshop Report: ©2002 National Academy of Sciences, Washington, D.C., USA. Reprinted with permission from the National Academies Press for the National Academy of Sciences. *Molecular & Cellular Proteomics* 2002, *1* (10), 763-780.

2. Omenn, G. S., The Human Proteome Organization Plasma Proteome Project pilot phase: reference specimens, technology platform comparisons, and standardized data submissions and analyses. *PROTEOMICS* 2004, *4* (5), 1235-1240.

3. Paik, Y.-K.; Jeong, S.-K.; Omenn, G. S.; Uhlen, M.; Hanash, S.; Cho, S. Y.; Lee, H.-J.; Na, K.; Choi, E.-Y.; Yan, F.; Zhang, F.; Zhang, Y.; Snyder, M.; Cheng, Y.; Chen, R.; Marko-Varga, G.; Deutsch, E. W.; Kim, H.; Kwon, J.-Y.; Aebersold, R.; Bairoch, A.; Taylor, A. D.; Kim, K. Y.; Lee, E.-Y.; Hochstrasser, D.; Legrain, P.; Hancock, W. S., The Chromosome-Centric Human Proteome Project for cataloging proteins encoded in the genome. *Nat Biotech* 2012, *30* (3), 221-223.

4. Pray, L., Eukaryotic genome complexity. *Nature Education* 2008, *1* (1).

5. Righetti, P. G.; Campostrini, N.; Pascali, J.; Hamdan, M.; Astner, H., Quantitative proteomics: a review of different methodologies. *Eur J Mass Spectrom (Chichester, Eng)* 2004, *10* (3), 335-48.

6. Gilar, M.; Olivova, P.; Daly, A. E.; Gebler, J. C., Two-dimensional separation of peptides using RP-RP-HPLC system with different pH in first and second separation dimensions. *Journal of Separation Science* 2005, *28* (14), 1694-1703.

7. Klose, J., Protein mapping by combined isoelectric focusing and electrophoresis of mouse tissues. *Humangenetik* 1975, *26* (3), 231-243.

8. O'Farrell, P. H., High resolution two-dimensional electrophoresis of proteins. *Journal of Biological Chemistry* 1975, *250* (10), 4007-4021.

9. Giddings, J. C., *Unified separation science*. Wiley: 1991.

10. Bushey, M. M.; Jorgenson, J. W., Automated instrumentation for comprehensive two-dimensional high-performance liquid chromatography of proteins. *Analytical Chemistry* 1990, *62* (2), 161-167.

11. Sandra, K.; Moshir, M.; D'hondt, F.; Tuytten, R.; Verleysen, K.; Kas, K.; François, I.; Sandra, P., Highly efficient peptide separations in proteomics: Part 2: Bi- and multidimensional liquid-based separation techniques. *Journal of Chromatography B* 2009, *877* (11–12), 1019-1039.

12. Gilar, M.; Daly, A. E.; Kele, M.; Neue, U. D.; Gebler, J. C., Implications of column peak capacity on the separation of complex peptide mixtures in single- and two-dimensional high-performance liquid chromatography. *Journal of Chromatography A* 2004, *1061* (2), 183-192.

13. Schure, M. R., Limit of Detection, Dilution Factors, and Technique Compatibility in Multidimensional Separations Utilizing Chromatography, Capillary Electrophoresis, and Field-Flow Fractionation. *Analytical Chemistry* 1999, *71* (8), 1645-1657.

14. MacNair, J. E.; Patel, K. D.; Jorgenson, J. W., Ultrahigh-Pressure Reversed-Phase Capillary Liquid Chromatography: Isocratic and Gradient Elution Using Columns Packed with 1.0-μm Particles. *Analytical Chemistry* 1999, *71* (3), 700-708.

15. Shen, Y.; Zhang, R.; Moore, R. J.; Kim, J.; Metz, T. O.; Hixson, K. K.; Zhao, R.; Livesay, E. A.; Udseth, H. R.; Smith, R. D., Automated 20 kpsi RPLC-MS and MS/MS with Chromatographic Peak Capacities of 1000−1500 and Capabilities in Proteomics and Metabolomics. *Analytical Chemistry* 2005, *77* (10), 3090-3100.

16. Zhou, F.; Lu, Y.; Ficarro, S. B.; Webber, J. T.; Marto, J. A., Nanoflow Low Pressure High Peak Capacity Single Dimension LC-MS/MS Platform for High-Throughput, In-Depth Analysis of Mammalian Proteomes. *Analytical Chemistry* 2012, *84* (11), 5133-5139.

17. Chen, H.; Horváth, C., High-speed high-performance liquid chromatography of peptides and proteins. *Journal of Chromatography A* 1995, *705* (1), 3-20.

18. Franklin, E. G. Utilization of Long Columns Packed with Sub-2 mum Particles Operated at High Pressures and Elevated Temperatures for High-Efficiency One-Dimensional Liquid Chromatographic Separations. The University of North Carolina at Chapel Hill, 2012.

19. Thompson, J. D.; Carr, P. W., High-Speed Liquid Chromatography by Simultaneous Optimization of Temperature and Eluent Composition. *Analytical Chemistry* 2002, *74* (16), 4150-4159.

20. Neue, U. D., *HPLC Columns: Theory, Technology, and Practice*. Wiley: 1997.

21. Kelleher, N. L.; Lin, H. Y.; Valaskovic, G. A.; Aaserud, D. J.; Fridriksson, E. K.; McLafferty, F. W., Top Down versus Bottom Up Protein Characterization by Tandem High-Resolution Mass Spectrometry. *Journal of the American Chemical Society* 1999, *121* (4), 806-812.

22. Wolters, D. A.; Washburn, M. P.; Yates, J. R., An Automated Multidimensional Protein Identification Technology for Shotgun Proteomics. *Analytical Chemistry* 2001, *73* (23), 5683-5690.

23. Steen, H.; Mann, M., The ABC's (and XYZ's) of peptide sequencing. *Nature reviews Molecular cell biology* 2004, *5* (9), 699-711.

24. Nesvizhskii, A. I.; Aebersold, R., Interpretation of Shotgun Proteomic Data: The Protein Inference Problem. *Molecular & Cellular Proteomics* 2005, *4* (10), 1419-1440.

25. Di Palma, S.; Hennrich, M. L.; Heck, A. J. R.; Mohammed, S., Recent advances in peptide separation by multidimensional liquid chromatography for proteome analysis. *Journal of Proteomics* 2012, *75* (13), 3791-3813.

26. Martosella, J.; Zolotarjova, N.; Liu, H.; Nicol, G.; Boyes, B. E., Reversed-Phase High-Performance Liquid Chromatographic Prefractionation of Immunodepleted Human Serum Proteins to Enhance Mass Spectrometry Identification of Lower-Abundant Proteins. *Journal of Proteome Research* 2005, *4* (5), 1522-1537.

27. Dowell, J. A.; Frost, D. C.; Zhang, J.; Li, L., Comparison of Two-Dimensional Fractionation Techniques for Shotgun Proteomics. *Analytical Chemistry* 2008, *80* (17), 6715-6723.

28. Stobaugh, J. T.; Fague, K. M.; Jorgenson, J. W., Prefractionation of Intact Proteins by Reversed-Phase and Anion-Exchange Chromatography for the Differential Proteomic Analysis of Saccharomyces cerevisiae. *Journal of Proteome Research* 2012, *12* (2), 626-636.

29. Issaq, H. J.; Chan, K. C.; Janini, G. M.; Conrads, T. P.; Veenstra, T. D., Multidimensional separation of peptides for effective proteomic analysis. *Journal of Chromatography B* 2005, *817* (1), 35-47.

30. Vestling, M. M.; Murphy, C. M.; Fenselau, C., Recognition of trypsin autolysis products by high-performance liquid chromatography and mass spectrometry. *Analytical Chemistry* 1990, *62* (21), 2391-2394.

31. Fersht, A., *Structure and Mechanism in Protein Science: A Guide to Enzyme Catalysis and Protein Folding*. W. H. Freeman: 1999.

32. Aguilar, M. I., *HPLC of Peptides and Proteins: Methods and Protocols*. Humana Press: 2004.

33. Searle, B. C., Scaffold: A bioinformatic tool for validating MS/MS-based proteomic studies. *PROTEOMICS* 2010, *10* (6), 1265-1269.

34. Eng, J. K.; Searle, B. C.; Clauser, K. R.; Tabb, D. L., A Face in the Crowd: Recognizing Peptides Through Database Search. *Molecular & Cellular Proteomics* 2011, *10* (11).

35. Wagner, A., Energy Constraints on the Evolution of Gene Expression. *Molecular Biology and Evolution* 2005, *22* (6), 1365-1374.

CHAPTER 6. Multidimensional Separations at 32 kpsi using Long Microcapillary Columns for the Differential Proteomics Analysis of *Saccharomyces cerevisiae*

6.1 Introduction

The study of protein expression has been important in understanding biological pathways. Studying the differential protein expression of an organism with two different phenotypes has brought light to the role proteins play in these pathways.[1,2] *Saccharomyces cerevisiae*, commonly known as baker's yeast, is a model organism for testing new analysis methods because its proteome is relatively well understood.[3] The validity of several common proteomics methods was first demonstrated by analyzing baker's yeast.[4,5] Since the yeast proteome is a complex biological mixture, many of these methods begin with a separation by liquid chromatography (LC) before analysis by mass spectrometry (MS).[6]

Though great improvements have been made in the field of liquid chromatography,[7,8] no single separation exists with the peak capacity necessary to effectively separate an entire proteome.[9] Multidimensional separations were developed as a means to improve peak capacity.[10] Early multidimensional separations coupled a long size exclusion or cation-exchange column to a reversed phase column.[11,12,13] Other scientists packed biphasic columns with reversed phase sorbent at the outlet and strong cation-exchange sorbent at the inlet to separate proteome digests.[14,15] More recent work focused on the separation of intact proteins by three modes before analysis by ESI-FTICR-MS. The three separation modes included two electrophoretic separations by isoelectric focusing and size followed by reversed-phase LC.[16,17]

To aid in sample solubility, proteomics experiments commonly start with digestion prior to separation. This shotgun approach increases the complexity of the biological mixture prior to analysis.[18] More recently, a prefractionation approach has been implemented in which the intact proteins are fractionated by the first dimension separation, and fractions are enzymatically digested prior to analysis by LC-MS.[19,20] Experimentally, prefractionation methods are more orthogonal than other multidimensional separations because the sample is completely changed via digestion between separations.[21] Digestion between the separations enables the use of reversed phase columns in both dimensions which tend to have higher peak capacity than other LC separation modes such as ion exchange and size exclusion chromatography.[22] The number of fractions collected will determine the peak capacity of the first dimension separation. However, high prefractionation frequencies will increase analysis time and increase the probability of splitting a protein between two fractions, and thus dilute the analyte. A study of prefractionation frequency was completed in Chapter 5. The results indicated that five fractions yielded adequate information about the yeast proteome if a long microcapillary column is used in the second dimension.

In concert with improvements to separation techniques, scientists have improved mass spectrometric detection of large biomolecules. The development of ion mobility added a post ionization separation.[23] High resolution mass spectrometers such as FTICR and especially orbitraps have become more common laboratory instruments.[24] Time-of-flight (TOF) instruments are also widely used for proteomics experiments.[25] However, ionization suppression and matrix effects still plague mass spectrometric techniques, necessitating separation prior to analysis.[26,27]

To help with the quantitative analysis of mass spectral data, many sample labeling techniques such as iTRAQ and SILAC have been developed. However, the label-free technique remains popular for relative quantification.[28] The major advantage to label-free relative quantification is that no further manipulation of the sample is required. Also, the spectra are not busy with isobaric and isotopic data. The validity of quantification based on spectral counts with the label-free method has been demonstrated in the literature.[14,15,24]

The differential study in this manuscript investigated yeast grown on dextrose and glycerol. Dextrose is the preferred growth medium. Growth on an alternative carbon source yields protein expressions characteristic of an environmental stress response.[29] A previous study of this differential expression from the Jorgenson Lab separated the soluble portion of the yeast proteome by RPLC into 20 equal-time fractions. The fractions were digested before analysis by a standard UPLC-qTOF-MS.[21] Herein, a method is described which samples the first dimension by equal-mass prefractionation into just five fractions. A UHPLC capable of separations above 30 kpsi increased the peak capacity of the second dimension separation. This prefractionation experiment reduced the previously reported separation time by four fold. With the improved separation, 527 proteins were identified in the dextrose sample and 539 in the glycerol sample which is more than the previously reported analysis.

6.2 Materials and method

6.2.1 Materials

Water, acetonitrile, isopropyl alcohol and ammonium hydroxide were purchased from Fisher Scientific (Fair Lawn, NJ). Ammonium acetate, ammonium bicarbonate, formic acid, trifluoroacetic acid and iodoacetamide were purchased from Sigma-Aldrich Co. (St. Louis, MO). Rapigest^{TM} SF acid-labile surfactant and bovine serum album digest standard (BSA) were

obtained from Waters Corporation (Milford, MA). Dithiothreitol was purchased from Research Products International (Mt. Prospect, IL), and TPCK-modified trypsin was purchased from Pierce (Rockford, IL). Water and acetonitrile were Optima LC-MS grade, and all other chemicals were ACS reagent grade or higher. Growth, harvesting, and lysis of *S. cerevisiae* from glycerol and dextrose media were previously described.[21]

6.2.2 Intact protein prefractionation

The prefractionation of intact proteins, outlined in Figure 6.1., was performed on a 4.6 x 250 mm PLRP-S column with 5 µm particles (Agilent, Santa Clara, CA) heated to 80 °C. Four milligrams of total protein were injected onto the column. The gradient profile is shown in Table 6.1. The separation was followed by UV spectrophotometry to give a qualitative chromatogram of the separation. The wavelength was set to 214 nm, which is the lambda max of the peptide bond. One-minute wide fractions, containing 1 mL of effluent each, were collected in microcentrifuge tubes. To concentrate the fractions, they were lyophilized and then reconstituted in 25 µL of 50 mM ammonium bicarbonate. Three microliters of 6.67% (w/v) RapiGest™ SF in buffer were added. Solutions were vortexed, sonicated for 15 minutes, and incubated at 80 ºC for 15 minutes to denature the proteins..

6.2.3 Equal-mass prefractionation

To determine fractionation by equal-mass, each absorbance value for the UV chromatogram was summed with all previous absorbance values from 10 to 48 minutes which corresponded to the time after the injection plug until just before the wash. Summed absorbance was calculated as follows

$$\text{Summed Absorbance } (\Sigma A) = \sum_{t_d}^{t_d+t_g} A_t \qquad (6\text{-}1)$$

where A = absorbance, t = time, t_d = dead time, and t_g = gradient time. The Σ absorbance was normalized and plotted versus first dimension separation time in Figure 6.2. The Σ absorbance was divided into increments of 0.05 which split the axis into 20 even parts. The times associated with the 20 Σ absorbance values were rounded to the nearest minute. These times were used to redistribute the 38 one-minute-wide fractions into 20 equal-mass fractions. Each of the 20 fractions has an equal-mass of total protein but a varying amount of solvent.

6.2.4 Protein digestion

The digestion is more efficient when carried out in a minimal amount of solvent. Therefore, the 20 equal-mass fractions were also lyophilized and reconstituted in 25 µL of 50 mM ammonium bicarbonate. Three microliters of 6.67% (w/v) RapiGest™ SF in buffer were added. Solutions were vortexed, sonicated for 15 minutes, and incubated at 80 ºC for 15 minutes to denature the proteins. The proteins were reduced by adding 1 µL of 100 mM dithiothreitol, vortexed, sonicated for 5 minutes, and incubated for 30 min at 60ºC. Proteins were then alkylated with 1 µL of 200 mM iodoacetamide, vortexed, sonicated for 5 minutes, and stored protected from light for 30 min at room temperature. The proteins were then digested by adding 10 µL of 667 ng/µL TPCK-modified trypsin in 50 mM ammonium bicarbonate, pH 8 (overnight, 37ºC). The trypsin amount was approximated to be a 50:1 (w/w) protein to enzyme ratio if the initial protein amount was equally distributed across the 20 fractions. The digestion was quenched, and the RapiGest™ SF was degraded using 44 µL 98:1:1 (v:v:v) water:acetonitrile:trifluoroacetic acid (45 min, 37ºC). The fractions were centrifuged for 10 minutes at 14,000 Xg to pellet the hydrolyzed surfactant, after which they were ready for analysis. The samples were transferred to LC vials and spiked with 1.3 µL of a 1 pmol/L internal standard BSA digest (Waters).

To form the sets of 5 fractions, 20 µL of every four consecutive fractions from the set of 20 were combined, lyophilized, and reconstituted with 10 µL 50 mM ammonium bicarbonate and 10 µL 98:1:1 (v:v:v) water:acetonitrile:trifluoroacetic acid. The fractionation schemes are outlined in Table 6.2.

6.2.5 Peptide analysis by UHPLC-MS^E

Each fraction was analyzed in triplicate by capillary RPLC-MS using the UHPLC system described in Chapter 3 coupled to a QTOF Premier MS. Mobile phase A was Optima Grade water with 0.1% formic acid (Fisher), and mobile phase B was Optima-grade acetonitrile with 0.1% formic acid (Fisher). The samples were pre-concentrated on a 110 cm x 75 µm ID, 1.9 µm BEH C18 column with 0.5% mobile phase B, and then separated with a 25 µL gradient from 4-40%B followed by a wash at 85% and equilibration at initial conditions. The gradient program is listed in Table 6.3. The column was run at 32 kpsi at 65°C to produce a 300 nL/min flow rate. The outlet of the RPLC column was connected via a 30 cm x 20 µm ID piece of silica capillary to an uncoated fused silica nanospray emitter with a 20 µm ID and pulled to a 10 µm tip (New Objective, Woburn, MA) operated at 2.6 kV. Data-independent acquisition (MS^E) was performed with the instrument set to acquire parent ion scans from m/z 50-1990 over 0.6 sec at 5.0 V. The collision energy was then ramped from 15-40 V over 0.6 sec with 0.1 sec interscan delay.

6.2.6 Peptide data processing

The peptide LC-MS/MS data were processed using ProteinLynx Global Server 2.5 (Waters). The MS^E spectra were searched against a database of known yeast proteins from the Uni-Prot protein knowledgebase (www.uniprot.org) with a reversed sequence appended to the end. The false discovery rate was set to 100% to yield data compatible for further processing.

After the database search was complete, the results were imported into Scaffold 4.2.0 (Proteome Software, Portland, OR). The minimum protein probability and peptide probability filters were set to a 5% false discovery rate, and a minimum of three peptides were required to identify a protein. Peptides matching multiple proteins were exclusively assigned to the protein with the most evidence. The proteins were quantified by the normalized total precursor intensity. The precursor intensities assigned to a protein were totaled to give the quantitative value of that protein. The values were normalized by subtracting each sample's median log intensity then adding back the median log intensity for all samples.[30,31,32,33] A student's 2-sided t-test was performed on the triplicate samples. Proteins with a p-value less than 0.050 between the two yeast samples and a fold change greater than 2.0 were considered to be differentially expressed with 95% confidence or greater.

6.3 Discussion

Reversed-phase prefractionation of the lysate from yeast grown on dextrose and glycerol produced 38 one-minute-wide fractions. Measures were taken during method development to evenly distribute the proteins across the first dimension separation. However, most observed peaks from the first dimension chromatogram occurred in the middle of the retention window. Analysis of all 38 fractions would be unproductive as many proteins were undoubtedly split between multiple fractions diluting the analyte. Fractions with less intense first dimensional peaks would yield little information in the second dimension analysis. The offline nature of this multidimensional separation gave us flexibility to further process the fractions before second dimension analysis. For these reasons, the fractions were recombined into equal-mass fractions before digestion, as outlined in Table 6.2.

According to the prefractionation frequency study in Chapter 5, it was determined that 5 fractions were adequate to yield sufficient information from the yeast proteome when fractions were run on a long, 110 cm microcapillary column at 32 kpsi. The multidimensional chromatograms are shown in Figure 6.3. From these plots, it is observed that the separation space was well utilized, peaks fill most of the 2D space, and the peaks are orthogonal.

6.3.1 Protein prefractionation

To more deeply analyze the first dimension separation, the resulting chromatograms are overlaid onto bar graphs in Figure 6.4. The number of proteins identified in each fraction is displayed for yeast grown on dextrose (a) and glycerol (b). Between 96 and 176 total proteins were identified per fraction as drawn with light gray bars. Unique identifications are drawn with dark gray bars. The total protein count was defined as any protein found within a given fraction; thus, if a protein were to be found in multiple fractions it would be counted in each fraction. The unique protein values count each protein entry only once. A protein identified in multiple fractions is assigned to the fraction in which it had the highest quantitative value. Between 55 and 122 unique proteins were identified per fraction. The area under the first dimension chromatogram should be equal for each fraction. There were few peaks towards the end of the chromatogram so a large portion of the first dimension separation was pooled into one fraction. A large number of proteins were identified from peptide analysis of the last fraction. By pooling this area into one fraction, information can be gained about the yeast proteome without a large commitment of analysis time.

The crowded and over lapping peaks in the first dimension separation prohibited the measurement of peak widths. As an alternative, the number of fractions per protein, as shown in Figure 6.5., was used to describe in how many first dimension fractions a protein was identified.

Most proteins were identified in only one fraction. For yeast on dextrose, 68% of the proteins were identified in only one fraction, 16% were identified in two fractions, and the remaining 16% were identified in three or more fractions. Similarly for yeast grown on glycerol, 66% of the proteins were identified in one fraction, 19% were identified in two fractions, and 14% were identified in three or more fractions. This was a slight improvement over our lab's previous results in which 60% of the proteins were identified in one fraction, 20% were identified in two fractions, and 20% were identified in three or more fractions.[21] Our previous method had twenty first dimension fractions which increased the odds of splitting first dimension protein peaks between multiple fractions. The improvement was only slight because the intensities of the second dimension peptide peaks were much greater for the experiment described in this manuscript. With a longer column run at higher pressure, peaks were narrower and more intense increasing the likelihood of identifying proteins with lower abundance in multiple factions (See Chapter 5).

6.3.2 Benefits of increasing second dimension peak capacity

The total number of proteins identified in the dextrose and glycerol sample was 527 and 539, respectively, with 350 or 65% of the proteins being identified in both samples as portrayed by the Venn diagram in Figure 6.6. These results were similar to our previously reported differential proteomics study using the prefractionation method.[21] However, the peak capacity of the second dimension separation described in this chapter was approximately 450, about 2.5 times the peak capacity of our earlier work, even though second dimension separation times were similar. The gain in second dimension peak capacity took burden off the prefractionation step. Therefore, more information could be elucidated out of only five fractions as opposed to the 20 fractions described previously.

The theoretical two-dimensional peak capacity was 2,250 with this experiment and 4,000 for our earlier experiment.[21] The experiment described here better distributed the sample throughout the multidimensional separation space which would increase fractional coverage. Stoll and coworkers suggested multiplying the theoretical peak capacity by the fractional coverage factor to give a better estimate of the practical peak capacity for 2D separations.[34] The results from Chapter 2 suggested that improving peak capacity in the first dimension alone had a limit as to how many proteins may be identified. Proteomics experiments involve many steps and techniques. Improvements to not one but all techniques will be necessary to more deeply mine information from the proteome. Ultrahigh pressure separation on long, microcapillary columns increased to the number of proteins identified and decreased total separation time.

6.3.3 Increasing protein coverage

The improvements to the multidimensional separation did not only improve the number of protein identifications but also the protein coverage. The coverage and number of peptides identified for several proteins involved in yeast metabolism are listed in Table 6.4. Chapter 2 proposed the Normalized Difference Protein Coverage (NDPC) to compare protein coverage between multiple methods. The same metric was used to compare the difference in coverage for proteins identified in this chapter and our earlier work[21] normalized by the total coverage between both experiments. The Grand NDPC combines the NDPC for all proteins into a single value by calculating the difference between the grand total protein coverage normalized by the grand sum of protein coverage in both methods as follows:

$$\text{Grand NDPC} = \frac{(\sum \text{Coverage}_{\text{Chapter 6}})-(\sum \text{Coverage}_{\text{Literature}})}{\sum \text{Coverage}_{\text{Chapter 6}}+\sum \text{Coverage}_{\text{Literature}}} \quad (6\text{-}2)$$

The Grand NDPC can be related to a Fold-Change in Coverage as follows:

$$\text{Fold-Change in Coverage} = \frac{\sum \text{Coverage}_{\text{method 1}}}{\sum \text{Coverage}_{\text{method 2}}} = \frac{1+ \text{Grand NDPC}}{1- \text{Grand NDPC}} \quad (6\text{-}3)$$

If the fold-change is less than one, the negative reciprocal of the value is used as is conventional with fold-change calculations. The Grand NDPC and Fold-Change in Coverage are listed in Table 6.5. The positive values represent higher coverage with the 5 equal-mass fractions run on the 110 cm long column at 32 kpsi as described in this chapter. A negative value would have indicated higher coverage by our previous results from the 20 equal-time fraction run on the 25 cm commercial column at 8 kpsi on the standard UPLC.[21] The improvement is small but impressive when one considers that separation time was reduced four fold.

6.3.4 Differential proteins

The differential proteins were qualified with a fold change of greater than two and a p-value of less than 0.05 which corresponds to a negative $\log_{10}$ p-value of 1.3 and 95% confidence. The volcano plot in Figure 6.7.a. graphs the negative $\log_{10}$ p-value versus $\log_2$ fold change. A negative or positive fold change is a convention for up-regulation of the protein in yeast grown on dextrose or glycerol, respectively. The points in the upper left and right of the plot represent proteins with the largest difference in abundance between the two samples and with the most confidence. Protein quantity is not captured in the volcano plot so the log quantitative values of all significantly different proteins are plotted in Figure 6.7.b. Proteins up-regulated in the dextrose or glycerol sample are closer to the y-axis or x-axis, respectively. Points falling along the axes were only identified in the sample corresponding to that axis. There were 274 proteins that were determined to be significantly different. The most interesting of these proteins would have a large abundance in only one sample and are represented by points in the top-left and bottom-right of Figure 6.7.b.

Of the significantly different proteins, several were identified to be part of the metabolic pathways of yeast which, according to the literature, would have differences in expression when exposed to different carbon sources.[35] Proteins involved in the metabolic pathways of interest are listed in Table 6.6. with their associated p-value, intensity, and fold change. Several metabolic pathways of *S. cervisiae* including glycerol catabolism/glycerolneogenesis, glycolysis/ gluconeogenesis, fermentation, the TCA cycle, and the glyoxylate cycle are depicted in Figure 6.8. Proteins identified in blue or red represent up-regulation of the protein in yeast which was grown on the dextrose or glycerol media, respectively. The differential protein fold-changes measured by the methods described here follow the trends in protein expression predicted by the literature for growth in dextrose deficient media which will invoke an environmental stress response.[35]

Glycolysis is the digestion of glucose to pyruvate, which can then be converted into energy through the TCA cycle, glyoxylate cycle, or fermentation. The first step in glycolysis is to phosphorylate glucose with the hexokinase family of enzymes (HXKA, HXKB). Glucokinase (HXKG) has a slightly different role because it acts as a regulator for glucose consumption. Previous studies reported increased transcription of glucokinase when yeast was grown on glycerol[36,37] which was confirmed in the results from this study.

In the pathway from glucose to pyruvate are the transketolase (TKT1, TKT2) and transaldolase (TAL1, TAL2) protein families. These proteins are also involved in metabolizing carbon energy sources through the pentose phosphate pathway (PPP). In normal cell function, TKT1 and TAL1 are the predominant proteins involved in the conversion of fructose-6-P to glyceraldehyde-3-P.[38,39] TKT1 and TAL1 were identified by this method but not differentially. In the absence of glucose, it has been previously concluded that TKT2 will dominate the conversion

of fructose-6-P to glyceraldehyde-3-P. The literature is inconclusive on the role of TAL2.[40] The results from this manuscript found both TKT2 and TAL2 proteins to be up-regulated in yeast grown on glycerol.

Through the pentose phosphate pathway (PPP), glucose is transformed into ribulose-5-phosphate which is a step in the formation of ribonucleic acids and ribosomal proteins. Cells grown under stress conditions, such as a dextrose deficient environment, will exhibit a lack of ribosomal protein.[29] Therefore, an abundance of ribosomal proteins should exist in the yeast grown on dextrose. A total of 67 ribosomal proteins were identified with 19 up-regulated and only one down-regulated in the dextrose sample.

Analogous to glycolysis is glycerol metabolism, which converts glycerol into pyruvate. For the yeast grown on glycerol, it is predicted that the proteins used in glycerol catabolism such as GLPK and GPD1 would be up-regulated[41,42] while the proteins used in glycerolneogenesis, such as GPP1 and GPP2, would be down-regulated.[43] This phenomenon was observed for GLPK, GPD1 and GPP1. No significant difference was observed for GPP2 and GPD2 expression.

After its biogenesis, pyruvate is fermented into ethanol if there is an excess amount of glucose present. A protein complex is formed by PDC1, PDC5 and PDC6. This complex is involved in the conversion of pyruvate to acetaldehyde during fermentation.[44] These three subunits were identified with PDC5 and PDC6 being up-regulated in the dextrose sample. Acetaldehyde is then converted into ethanol. The alcohol dehydrogenases (ADH1, ADH3, ADH6) involved in the conversion were all identified with ADH6 being more abundant in yeast grown on dextrose.

In the absence of dextrose, pyruvate enters the TCA and glyoxylate cycles[45] which can occur directly by conversion to oxaloacetate with pyruvate carboxylases (PYC1, PYC2) or through the acetyl-CoA bypass mechanism involving pyruvate dehydrogenase (ODPB) and dihydrolipoyl dehydrogenase (DLDH). Additionally, any ethanol that may be present is metabolized by alcohol dehydrogenase (ADH2), aldehyde dehydrogenases (ALDH2, ALDH4) and acetyl-coenzyme A synthetase (ACS1) for entrance into the TCA or glyoxylate cycle.[42,46,47,48,49] Of the 24 proteins involved in processing pyruvate through the TCA and glyosylate cycles, 18 were significantly more abundant in the yeast grown on glycerol. The other six proteins showed no significant fold change in abundance between the two samples.

The roles of ALDH5 and ACS2 are not completely defined in the literature but some studies indicate that their function differs from that of other aldehyde dehydrogenases and acetyl-coenzyme A synthetases.[50] One theory is that ALDH5 and ACS2 regulate ethanol to keep it below toxicity levels, maintaining a healthy environment for the biosynthesis other metabolites important to cell growth.[51,52] In this experiment, ALDH5 and ACS2 were found to be up-regulated in dextrose.

A final difference between yeast grown on alternative carbon sources is the location of metabolism in the cell. Fermentation with dextrose occurs in the cytoplasm, while the TCA and glyoxylate cycles, metabolizing glycerol, occur in the mitochondria.[53] To support increased activity in the mitochondria, more mitochondrial proteins would have to be transcribed. The results from this study identified 65 mitochondrial proteins with 26 up-regulated and only one down-regulated in the yeast sample grown on glycerol.

6.4 Conclusions

The multidimensional UHPLC-MS analysis identified 527 proteins in yeast grown on dextrose and 539 proteins in yeast grown on glycerol. The differential abundances were determined for many proteins involved in yeast metabolism of the two different carbon sources. By utilizing the first dimension chromatographic intensity to prefractionate the sample by equal-mass, the digestion was improved by better estimating the protein to enzyme ratio. This prefractionation technique better estimated column loading for the second dimension and improved the practical peak capacity of the multidimensional separation. Increased peak capacity of the second dimension separation, with a long microcapillary column run at elevated pressure, reduced the need for a high prefractionation frequency without reducing the number of protein identifications. With fewer first dimension fractions, analysis time was decreased by 75% as compared to a previously reported study by the Jorgenson Lab.[21] Proteomic experiments involve many steps and techniques. Improvements to not one but all techniques will be necessary to more deeply mine information from the proteome. Ultrahigh pressure separations on long, microcapillary columns provided improvement to the number and coverage of proteins identifications in a differential proteomics analysis of *S. cerevisiae*.

6.5 TABLES

Time (min)	Flow Rate (mL/min)	90:5:5 H_2O:ACN:IPA + 0.2% TFA (%A)	50:50 ACN:IPA + 0.2% TFA (%B)
0	1.0	100	0
2	1.0	100	0
5	1.0	75	25
40	1.0	50	50
45	1.0	35	65
45.1	1.0	0	100
50	1.0	0	100
50.1	1.0	100	0

Table 6.1. Chromatographic conditions for the reversed-phase prefractionation of intact proteins.

Fraction	Normalized ΣAbsorbance	First Dimension Time (min) Dextrose	First Dimension Time (min) Glycerol
1	0.2	10-18	10-18
2	0.4	19-22	19-22
3	0.6	23-26	23-26
4	0.8	27-31	27-30
5	1	32-48	31-48

Table 6.2. The first dimension prefractionation times of yeast grown on dextrose and glycerol are listed with the associated normalized Σ absorbance.

Time (min)	Flow Rate (µL/min)	% Mobile Phase A	% Mobile Phase A	Curve	NanoAcquity Vent Valve	High Pressure Isolation Valve Freeze/Thaw Valve &Vent Valve	Pneumatic Amplier Pump Initiation
Gradient Loading Method							
Initial	5	96.0	4.0	-	Off	On	Off
1.0	5	15.0	85	11	Off	On	Off
1.8	5	60.0	40	11	Off	On	Off
6.8	5	96.0	4	6	Off	On	Off
7.4	5	99.5	0.5	11	Off	On	Off
8.0	4	99.5	0.5	11	Off	On	Off
8.1	3	99.5	0.5	11	Off	On	Off
8.2	2	99.5	0.5	11	Off	On	Off
8.3	1	99.5	0.5	11	Off	On	Off
8.4	0.01	99.5	0.5	11	Off	On	Off
9.0 (end)	0.01	99.5	0.5	11	Off	On	Off
Sample Loading Method							
Initial	0.01	99.5	0.5	-	Off	On	Off
0.1	1	99.5	0.5	11	Off	On	Off
0.2	2	99.5	0.5	11	Off	On	Off
0.3	3	99.5	0.5	11	Off	On	Off
0.4	4	99.5	0.5	11	Off	On	Off
0.5	5	99.5	0.5	11	Off	On	Off
2.0	5	99.5	0.5	11	Off	On	Off
2.5	0.01	50	50	11	On	Off	Off
5.0	0.01	50	50	11	On	Off	On
35.0 (end)	0.01	50	50	11	On	Off	On
Ultra High Pressure Separation Method							
Initial	0.01	50	50	11	On	Off	On
150.0	0.01	96	4	11	On	On	Off
155.0 (end)	0.01	96	4	11	On	On	Off

Table 6.3. The method for the second dimension separation at ultrahigh pressure, as programmed into MassLynx, is listed along with the valve timings.

Name	Accession	Coverage (%)		Assigned Peptides	
		Dextrose	Glycerol	Dextrose	Glycerol
Isocitrate lyase	ACEA	-	32	-	15
Aconitate hydratase	ACON	35	58	23	48
Acetyl-coenzyme A synthetase 1	ACS1	-	57	-	51
Acetyl-coenzyme A synthetase 2	ACS2	28	6	10	1
Alcohol dehydrogenase 1	ADH1	71	73	24	23
Alcohol dehydrogenase 2	ADH2	55	75	27	41
Alcohol dehydrogenase 3	ADH3	28	29	5	9
Alcohol dehydrogenase 6	ADH6	20	-	4	-
Aldehyde dehydrogenase 2	ALDH2	5	24	1	10
K-activated aldehyde dehydrogenase	ALDH4	38	87	21	53
Aldehyde dehydrogenase 5	ALDH5	21	-	8	-
Fructose-bisphosphate aldolase	ALF	81	69	30	28
Citrate synthase	CISY1	18	61	7	34
Succinate dehydrogenase	DHSA	-	20	-	8
Dihydrolipoyl dehydrogenase	DLDH	-	63	-	31
Enolase 1	ENO1	84	85	18	22
Enolase 2	ENO2	92	87	54	47
Fumarate reductase	FRDS	44	45	15	17
Fumarate hydratase	FUMH	6	50	2	22
Glyceraldehyde-3-P dehydrogenase 1	G3P1	66	92	33	45
Glyceraldehyde-3-P dehydrogenase 2	G3P2	91	88	11	9
Glyceraldehyde-3-P dehydrogenase 3	G3P3	94	92	27	25
Glucose-6-phosphate isomerase	G6PI	70	56	45	32
Glycerol-3-phosphate dehydrogenase	GPD1	8	60	2	23
Glycerol-3-phosphate dehydrogenase	GPD2	-	7	-	1
Glycerol-3-phosphatase 1	GPP1	86	-	22	-
Glycerol-3-phosphatase 2	GPP2	15	-	2	-
Hexokinase-1	HXKA	34	65	12	24
Hexokinase-2	HXKB	66	70	30	31
Glucokinase-1	HXKG	12	72	3	39
Isocitrate dehydrogenase 1	IDH1	45	60	15	23
Isocitrate dehydrogenase 2	IDH2	6	71	1	17
6-phosphofructokinase subunit α	K6PF1	60	52	61	54
Pyruvate kinase 1	KPYK1	86	85	58	53
Malate synthase 1	MASY	-	42	-	22
NAD-dependent malic enzyme	MAOM	8	-	4	-
Malate dehydrogenase, cyto	MDHC	-	45	-	13
Malate dehydrogenase, mito	MDHM	56	75	14	22
2-oxoglutarate dehydrogenase E1	ODO1	-	31	-	25
γ-glutamyl phosphate reductase	ODO2	-	40	-	12
Pyruvate dehydrogenase E1 comp β	ODPB	48	43	13	10
Phosphoenolpyruvate carboxykinase	PCKA	2	74	1	47
Pyruvate decarboxylase isozyme 1	PDC1	75	66	46	39
Pyruvate decarboxylase isozyme 5	PDC5	36	-	12	-
Pyruvate decarboxylase isozyme 6	PDC6	43	23	13	6
Phosphoglycerate kinase	PGK	92	89	58	54
Phosphoglycerate mutase 1	PMG1	84	82	29	26
Pyruvate carboxylase 1	PYC1	9	32	8	31
Pyruvate carboxylase 2	PYC2	11	21	3	4
Succinyl-CoA ligase subunit α	SUCA	40	71	10	20
Succinyl-CoA ligase subunit β	SUCB	-	38	-	25
Transaldolase 1	TAL1	68	66	28	20
Transaldolase 2	TAL2	-	59	-	16
Transketolase 1	TKT1	65	52	36	34
Transketolase 2	TKT2	-	21	-	10
Triosephosphate isomerase	TPIS	89	90	28	27

Table 6.4. The protein coverage (%) and number of peptides used to identify each protein are reported for the some of the proteins involved in *S. cerevisiae* metabolism.

Sample	Grand NDPC	Fold Change In Coverage
Dextrose	0.074	1.1
Glycerol	0.033	1.1

Table 6.5. The Grand NDPC and Fold-Change in Coverage are listed for each fractionation frequency. The positive values represent higher coverage with the 5 equal-mass fractions run on the 110 cm long column at 32 kpsi as described in this chapter. A negative value would have indicated higher coverage by our previous results from the 20 equal-time fraction run on the 25 cm commercial column at 8 kpsi on the standard UPLC.[21] The improvement is small but impressive when one considers that the total separation time was reduced four fold.

Name	Accession	T-Test	P-Value	Fold Change	Quantitative Value	
					Dextrose	Glycerol
Isocitrate lyase	ACEA	0%	0.082000	-	n.d.	857
Aconitate hydratase	ACON	95%	< 0.00010	4.8	2204	10493
Acetyl-coenzyme A synthetase 1	ACS1	95%	< 0.00010	G Only	n.d.	20339
Acetyl-coenzyme A synthetase 2	ACS2	95%	0.020000	-9.0	663	73
Alcohol dehydrogenase 1	ADH1	0%	0.530000	-	53597	50028
Alcohol dehydrogenase 2	ADH2	95%	0.000300	4.2	22123	93634
Alcohol dehydrogenase 3	ADH3	0%	0.080000	-	848	1825
Alcohol dehydrogenase 6	ADH6	95%	0.001800	D Only	612	n.d.
Aldehyde dehydrogenase 2	ALDH2	95%	0.000150	20.4	32	658
K-activated aldehyde dehydrogenase	ALDH4	95%	< 0.00010	46.1	2099	96753
Aldehyde dehydrogenase 5	ALDH5	95%	0.0048	D Only	183	n.d.
Fructose-bisphosphate aldolase	ALF	0%	0.420000	-	34954	30292
Citrate synthase	CISY1	95%	< 0.00010	41.3	301	12399
Succinate dehydrogenase	DHSA	95%	0.005100	G Only	n.d.	419
Dihydrolipoyl dehydrogenase	DLDH	95%	0.000130	G Only	n.d.	8330
Enolase 1	ENO1	0%	0.310000	-	54308	65808
Enolase 2	ENO2	0%	0.130000	-	74304	56488
Fumarate reductase	FRDS	0%	0.830000	-	908	884
Fumarate hydratase	FUMH	95%	0.000540	40.3	117	4725
Glyceraldehyde-3-P dehydrogenase 1	G3P1	0%	0.068000	-	47511	62124
Glyceraldehyde-3-P dehydrogenase 2	G3P2	0%	0.680000	-	61006	57022
Glyceraldehyde-3-P dehydrogenase 3	G3P3	0%	0.081000	-	92025	100055
Glucose-6-phosphate isomerase	G6PI	95%	0.009400	-2.8	37367	13228
Glycerol-3-phosphate dehydrogenase	GPD1	95%	0.002200	80.0	52	4163
Glycerol-3-phosphate dehydrogenase	GPD2	0%	0.370000	-	n.d.	118
Glycerol-3-phosphatase 1	GPP1	95%	< 0.00010	D Only	6633	n.d.
Glycerol-3-phosphatase 2	GPP2	0%	0.370000	-	778	n.d.
Hexokinase-1	HXKA	0%	0.095000	-	2652	14030
Hexokinase-2	HXKB	0%	0.740000	-	11961	11304
Glucokinase-1	HXKG	95%	0.000320	67.7	294	19918
Isocitrate dehydrogenase 1	IDH1	95%	0.002300	4.1	1579	6403
Isocitrate dehydrogenase 2	IDH2	95%	0.002700	63.6	49	3130
6-phosphofructokinase subunit α	K6PF1	95%	0.015000	-1.7	8623	4993
Pyruvate kinase 1	KPYK1	95%	0.001100	-1.7	77980	45254
Malate synthase 1	MASY	95%	0.006700	G Only	n.d.	2237
NAD-dependent malic enzyme	MAOM	0%	0.200000	-	80	n.d.
Malate dehydrogenase, cyto	MDHC	95%	0.018000	G Only	n.d.	2842
Malate dehydrogenase, mito	MDHM	95%	0.003100	12.3	1360	16737
2-oxoglutarate dehydrogenase E1	ODO1	95%	0.000840	G Only	n.d.	2355
γ-glutamyl phosphate reductase	ODO2	95%	< 0.00010	G Only	n.d.	1464
Pyruvate dehydrogenase E1 comp β	ODPB	95%	0.005700	-1.4	2054	1478
Phosphoenolpyruvate carboxykinase	PCKA	95%	0.000530	615.2	31	19101
Pyruvate decarboxylase isozyme 1	PDC1	0%	0.440000	-	62000	52551
Pyruvate decarboxylase isozyme 5	PDC5	95%	< 0.00010	D Only	12020	n.d.
Pyruvate decarboxylase isozyme 6	PDC6	95%	0.000430	-2.9	15540	5325
Phosphoglycerate kinase	PGK	0%	0.450000	-	76423	69924
Phosphoglycerate mutase 1	PMG1	95%	0.048000	-1.6	30171	19396
Pyruvate carboxylase 1	PYC1	95%	0.011000	9.0	377	3413
Pyruvate carboxylase 2	PYC2	0%	0.250000	-	491	1826
Succinyl-CoA ligase subunit α	SUCA	95%	< 0.00010	14.1	547	7687
Succinyl-CoA ligase subunit β	SUCB	95%	0.036000	G Only	n.d.	2594
Transaldolase 1	TAL1	0%	0.680000	-	4930	6025
Transaldolase 2	TAL2	95%	0.002500	G Only	n.d.	1763
Transketolase 1	TKT1	0%	0.083000	-	7813	5823
Transketolase 2	TKT2	95%	0.017000	G Only	n.d.	994
Triosephosphate isomerase	TPIS	95%	0.028000	-1.4	22844	16042

Table 6.6. The T-test confidence value, p-value, fold change, and average quantitative value was reported for the some of the proteins involved in *S. cerevisiae* metabolism. The quantative value was determined as the Normalized Total Precursor Intensity ($x10^{-3}$). (*n.d.: Not detected.)

6.6 FIGURES

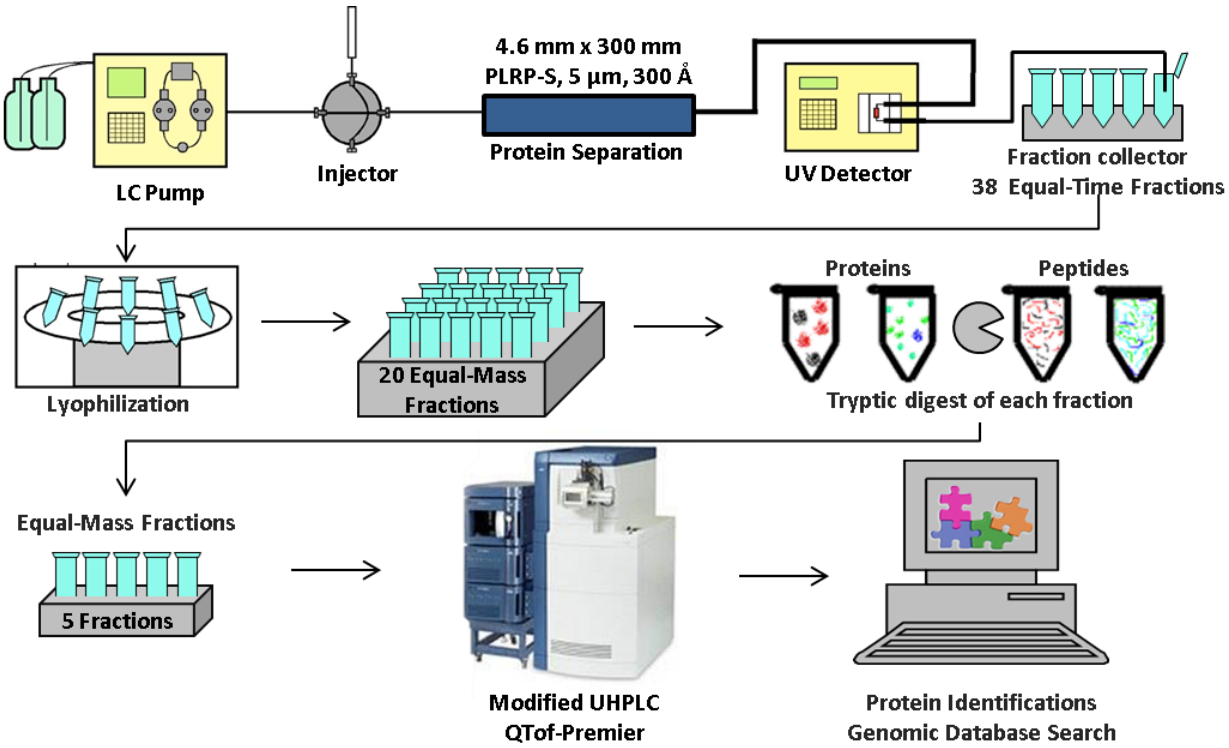

Figure 6.1. The workflow for the prefractionation method started with HPLC-UV of the intact proteins. Thirty-eight one-minute-wide fractions were collected, lyophilized, and pooled into 20 equal-mass fractions. The equal-mass fractions were digested and pooled into 5 equal-mass fractions before the second dimension analysis by the modified UHPLC-MS at 32 kpsi. The spectral data was searched against a genomic database to identify the proteins.

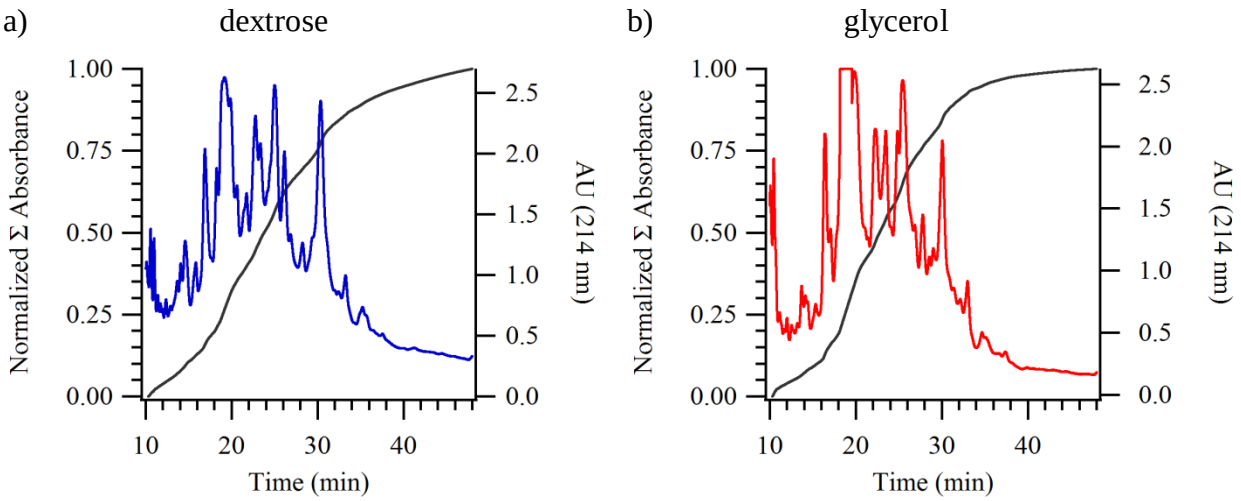

Figure 6.2. The normalized Σ absorbance, plotted here with the UV chromatograms, was used to distribute the first dimension separation for yeast grown on dextrose (a) and glycerol (b) into equal-mass fractions.

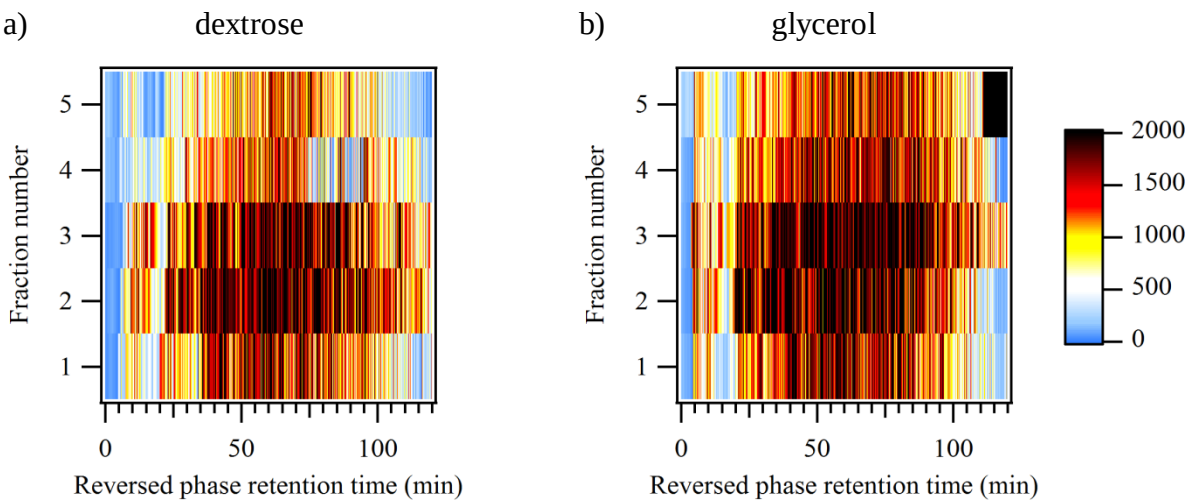

Figure 6.3. Two-dimensional chromatograms for yeast grown on dextrose (a) and glycerol (b) are plotted with the first dimension (protein) fraction number on the vertical axes and the second dimension (peptide) separation on the bottom axes. Peak intensity (BPI) is plotted in the z-direction.

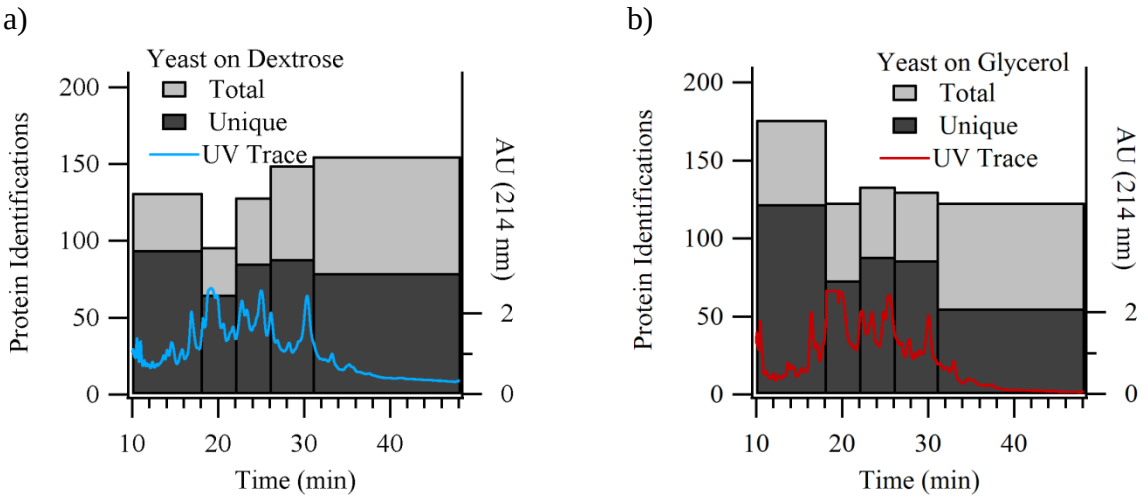

Figure 6.4. The light gray bars show the total protein identifications in each fraction, and the dark gray bars signify the unique protein identifications in each fraction for yeast grown on dextrose (a) and glycerol (b) with the UV chromatogram of the first dimension separation overlaid.

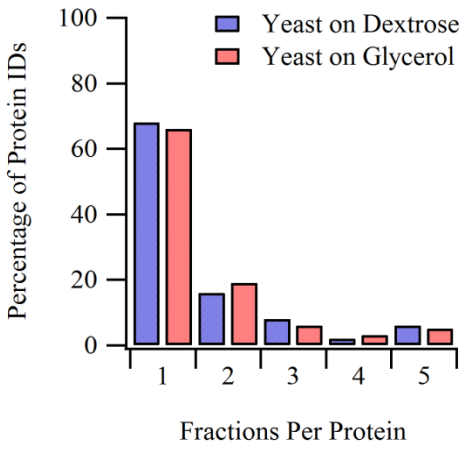

Figure 6.5. Fractions per protein describe the percentage of protein identifications that were detected in one, two, three, four, or all five fractions.

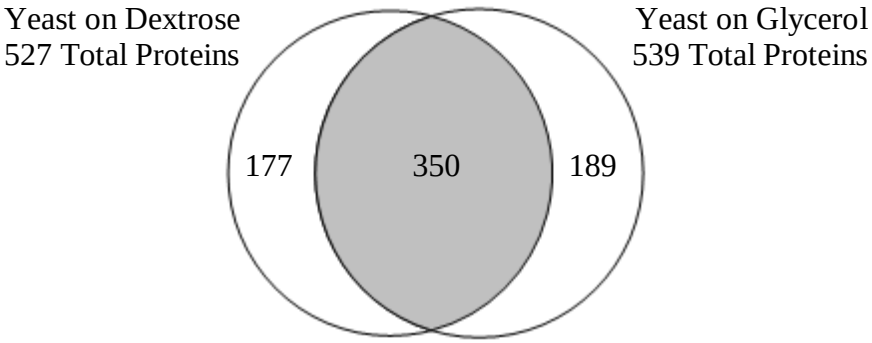

Figure 6.6. The overlap in identifications is shown for yeast grown on dextrose and glycerol.

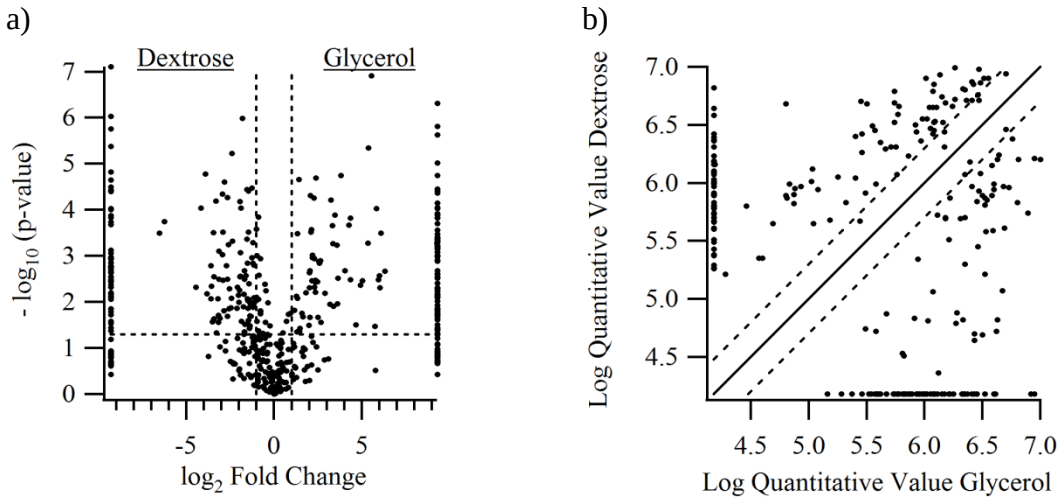

Figure 6.7. The $-\log_{10}$ (p-value) is plotted versus the $\log_2$ fold change (a). All points above the horizontal dashed line represent significantly different protein quantities with 95% minimum confidence. A negative or positive fold change is a convention for up-regulation of the protein in yeast grown on dextrose or glycerol, respectively. All points outside the vertical dashed lines represent a fold change greater that two. Protein quantity is not captured in the volcano plot so the log of the quantitative value for all significantly different proteins is plotted (b). Proteins up-regulated in the dextrose or glycerol sample are closer to the y-axis or x-axis, respectively. Points falling along the axis were only identified in the sample corresponding to that axis. The solid line represents y=x, and the dashed line represents a fold change of two.

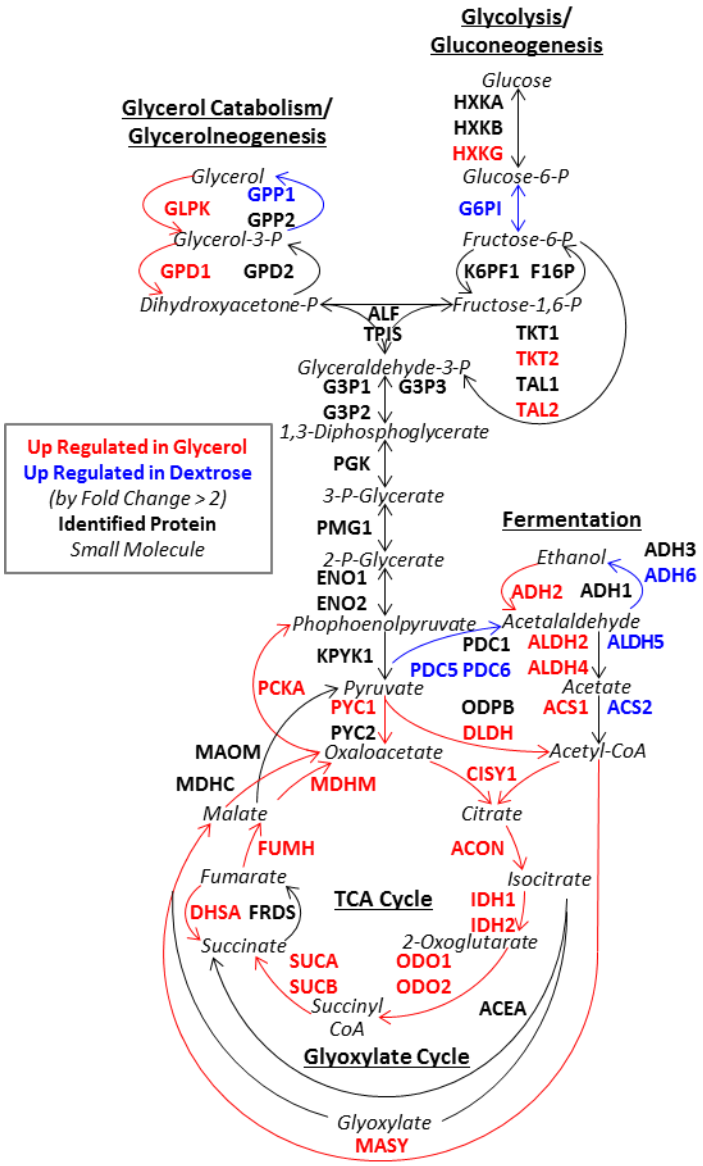

Figure 6.8. Several metabolic pathways of *S. cervisiae* including glycerol catabolism, glycerolneogenesis, glycolysis, gluconeogenesis, fermentation, TCA cycle, and glyoxylate cycle are depicted with protein identifiers in blue or red if the protein was up-regulated when yeast was grown on the dextrose or glycerol media, respectively. Identifiers in black represent proteins that were identified without a significant difference in abundance. They gray text shows what metabolite are involved in the pathways.

6.7 REFERENCES

1. Baker, E.; Liu, T.; Petyuk, V.; Burnum-Johnson, K.; Ibrahim, Y.; Anderson, G.; Smith, R., Mass spectrometry for translational proteomics: progress and clinical implications. *Genome Med* 2012, *4* (8), 1-11.

2. Meissner, F.; Mann, M., Quantitative shotgun proteomics: considerations for a high-quality workflow in immunology. *Nat. Immunol.* 2014, *15* (Copyright (C) 2014 American Chemical Society (ACS). All Rights Reserved.), 112-117.

3. Cherry, J. M.; Hong, E. L.; Amundsen, C.; Balakrishnan, R.; Binkley, G.; Chan, E. T.; Christie, K. R.; Costanzo, M. C.; Dwight, S. S.; Engel, S. R.; Fisk, D. G.; Hirschman, J. E.; Hitz, B. C.; Karra, K.; Krieger, C. J.; Miyasato, S. R.; Nash, R. S.; Park, J.; Skrzypek, M. S.; Simison, M.; Weng, S.; Wong, E. D., Saccharomyces Genome Database: the genomics resource of budding yeast. *Nucleic Acids Research* 2012, *40* (D1), D700-D705.

4. de Godoy, L. M. F.; Olsen, J. V.; Cox, J.; Nielsen, M. L.; Hubner, N. C.; Frohlich, F.; Walther, T. C.; Mann, M., Comprehensive mass-spectrometry-based proteome quantification of haploid versus diploid yeast. *Nature* 2008, *455* (7217), 1251-1254.

5. Ghaemmaghami, S.; Huh, W.-K.; Bower, K.; Howson, R. W.; Belle, A.; Dephoure, N.; O'Shea, E. K.; Weissman, J. S., Global analysis of protein expression in yeast. *Nature* 2003, *425* (6959), 737-741.

6. Xie, F.; Smith, R. D.; Shen, Y., Advanced proteomic liquid chromatography. *Journal of Chromatography A* 2012, *1261* (0), 78-90.

7. Shen, Y.; Zhang, R.; Moore, R. J.; Kim, J.; Metz, T. O.; Hixson, K. K.; Zhao, R.; Livesay, E. A.; Udseth, H. R.; Smith, R. D., Automated 20 kpsi RPLC-MS and MS/MS with Chromatographic Peak Capacities of 1000−1500 and Capabilities in Proteomics and Metabolomics. *Analytical Chemistry* 2005, *77* (10), 3090-3100.

8. Zhou, F.; Lu, Y.; Ficarro, S. B.; Webber, J. T.; Marto, J. A., Nanoflow Low Pressure High Peak Capacity Single Dimension LC-MS/MS Platform for High-Throughput, In-Depth Analysis of Mammalian Proteomes. *Analytical Chemistry* 2012, *84* (11), 5133-5139.

9. Gilar, M.; Olivova, P.; Daly, A. E.; Gebler, J. C., Two-dimensional separation of peptides using RP-RP-HPLC system with different pH in first and second separation dimensions. *Journal of Separation Science* 2005, *28* (14), 1694-1703.

10. Giddings, J. C., *Unified separation science*. Wiley: 1991.

11. Opiteck, G. J.; Lewis, K. C.; Jorgenson, J. W.; Anderegg, R. J., Comprehensive On-Line LC/LC/MS of Proteins. *Analytical Chemistry* 1997, *69* (8), 1518-1524.

12. Opiteck, G. J.; Jorgenson, J. W.; Anderegg, R. J., Two-Dimensional SEC/RPLC Coupled to Mass Spectrometry for the Analysis of Peptides. *Analytical Chemistry* 1997, *69* (13), 2283-2291.

13. Bushey, M. M.; Jorgenson, J. W., Automated instrumentation for comprehensive two-dimensional high-performance liquid chromatography of proteins. *Analytical Chemistry* 1990, *62* (2), 161-167.

14. Wolters, D. A.; Washburn, M. P.; Yates, J. R., An Automated Multidimensional Protein Identification Technology for Shotgun Proteomics. *Analytical Chemistry* 2001, *73* (23), 5683-5690.

15. Washburn, M. P.; Ulaszek, R.; Deciu, C.; Schieltz, D. M.; Yates, J. R., Analysis of Quantitative Proteomic Data Generated via Multidimensional Protein Identification Technology. *Analytical Chemistry* 2002, *74* (7), 1650-1657.

16. Vellaichamy, A.; Tran, J. C.; Catherman, A. D.; Lee, J. E.; Kellie, J. F.; Sweet, S. M. M.; Zamdborg, L.; Thomas, P. M.; Ahlf, D. R.; Durbin, K. R.; Valaskovic, G. A.; Kelleher, N. L., Size-Sorting Combined with Improved Nanocapillary Liquid Chromatography−Mass Spectrometry for Identification of Intact Proteins up to 80 kDa. *Analytical Chemistry* 2010, *82* (4), 1234-1244.

17. Tran, J. C.; Zamdborg, L.; Ahlf, D. R.; Lee, J. E.; Catherman, A. D.; Durbin, K. R.; Tipton, J. D.; Vellaichamy, A.; Kellie, J. F.; Li, M.; Wu, C.; Sweet, S. M. M.; Early, B. P.; Siuti, N.; LeDuc, R. D.; Compton, P. D.; Thomas, P. M.; Kelleher, N. L., Mapping intact protein isoforms in discovery mode using top-down proteomics. *Nature* 2011, *480* (7376), 254-258.

18. Nesvizhskii, A. I.; Aebersold, R., Interpretation of Shotgun Proteomic Data: The Protein Inference Problem. *Molecular & Cellular Proteomics* 2005, *4* (10), 1419-1440.

19. Martosella, J.; Zolotarjova, N.; Liu, H.; Nicol, G.; Boyes, B. E., Reversed-Phase High-Performance Liquid Chromatographic Prefractionation of Immunodepleted Human Serum Proteins to Enhance Mass Spectrometry Identification of Lower-Abundant Proteins. *Journal of Proteome Research* 2005, *4* (5), 1522-1537.

20. Dowell, J. A.; Frost, D. C.; Zhang, J.; Li, L., Comparison of Two-Dimensional Fractionation Techniques for Shotgun Proteomics. *Analytical Chemistry* 2008, *80* (17), 6715-6723.

21. Stobaugh, J. T.; Fague, K. M.; Jorgenson, J. W., Prefractionation of Intact Proteins by Reversed-Phase and Anion-Exchange Chromatography for the Differential Proteomic Analysis of Saccharomyces cerevisiae. *Journal of Proteome Research* 2012, *12* (2), 626-636.

22. Issaq, H. J.; Chan, K. C.; Janini, G. M.; Conrads, T. P.; Veenstra, T. D., Multidimensional separation of peptides for effective proteomic analysis. *Journal of Chromatography B* 2005, *817* (1), 35-47.

23. Fenn, L.; Kliman, M.; Mahsut, A.; Zhao, S.; McLean, J., Characterizing ion mobility-mass spectrometry conformation space for the analysis of complex biological samples. *Anal Bioanal Chem* 2009, *394* (1), 235-244.

24. Hebert, A. S.; Richards, A. L.; Bailey, D. J.; Ulbrich, A.; Coughlin, E. E.; Westphall, M. S.; Coon, J. J., The One Hour Yeast Proteome. *Molecular & Cellular Proteomics* 2014, *13* (1), 339-347.

25. Yates, J. R.; Ruse, C. I.; Nakorchevsky, A., Proteomics by Mass Spectrometry: Approaches, Advances, and Applications. *Annual Review of Biomedical Engineering* 2009, *11* (1), 49-79.

26. Wilm, M. S.; Mann, M., Electrospray and Taylor-Cone theory, Dole's beam of macromolecules at last? *International Journal of Mass Spectrometry and Ion Processes* 1994, *136* (2–3), 167-180.

27. Wilm, M.; Mann, M., Analytical Properties of the Nanoelectrospray Ion Source. *Analytical Chemistry* 1996, *68* (1), 1-8.

28. Matzke, M. M.; Brown, J. N.; Gritsenko, M. A.; Metz, T. O.; Pounds, J. G.; Rodland, K. D.; Shukla, A. K.; Smith, R. D.; Waters, K. M.; McDermott, J. E.; Webb-Robertson, B.-J., A comparative analysis of computational approaches to relative protein quantification using peptide peak intensities in label-free LC-MS proteomics experiments. *PROTEOMICS* 2013, *13* (3-4), 493-503.

29. Gasch, A. P.; Spellman, P. T.; Kao, C. M.; Carmel-Harel, O.; Eisen, M. B.; Storz, G.; Botstein, D.; Brown, P. O., Genomic Expression Programs in the Response of Yeast Cells to Environmental Changes. *Molecular Biology of the Cell* 2000, *11* (12), 4241-4257.

30. Searle, B. C., Scaffold: A bioinformatic tool for validating MS/MS-based proteomic studies. *PROTEOMICS* 2010, *10* (6), 1265-1269.

31. Eng, J. K.; Searle, B. C.; Clauser, K. R.; Tabb, D. L., A Face in the Crowd: Recognizing Peptides Through Database Search. *Molecular & Cellular Proteomics* 2011, *10* (11).

32. Bantscheff, M.; Lemeer, S.; Savitski, M.; Kuster, B., Quantitative mass spectrometry in proteomics: critical review update from 2007 to the present. *Anal Bioanal Chem* 2012, *404* (4), 939-965.

33. Raubenheimer, D.; Simpson, S. L., Analysis of covariance: an alternative to nutritional indices. *Entomologia Experimentalis et Applicata* 1992, *62* (3), 221-231.

34. Davis, J. M.; Stoll, D. R.; Carr, P. W., Dependence of Effective Peak Capacity in Comprehensive Two-Dimensional Separations on the Distribution of Peak Capacity between the Two Dimensions. *Analytical Chemistry* 2008, *80* (21), 8122-8134.

35. Fraenkel, D. G., Carbohydrate metabolism [in yeast]. *Cold Spring Harbor Monogr. Ser.* 1982, *11B*, 1-37.

36. Fernandez, R.; Herrero, P.; Moreno, R., Inhibition and Inactivation of Glucose-phosphorylating Enzymes from Sacchavomyces cevevisiae by D-Xylose. *Microbiology* 1895, *131*, 2705-2709.

37. Herrero, P.; Galíndez, J.; Ruiz, N.; Martínez-Campa, C.; Moreno, F., Transcriptional regulation of the Saccharomyces cerevisiae HXK1, HXK2 and GLK1 genes. *Yeast* 1995, *11* (2), 137-144.

38. Yang, J.; Bae, J. Y.; Lee, Y. M.; Kwon, H.; Moon, H.-Y.; Kang, H. A.; Yee, S.-b.; Kim, W.; Choi, W., Construction of Saccharomyces cerevisiae strains with enhanced ethanol tolerance by mutagenesis of the TATA-binding protein gene and identification of novel genes associated with ethanol tolerance. *Biotechnology and Bioengineering* 2011, *108* (8), 1776-1787.

39. Castelli, L. M.; Lui, J.; Campbell, S. G.; Rowe, W.; Zeef, L. A. H.; Holmes, L. E. A.; Hoyle, N. P.; Bone, J.; Selley, J. N.; Sims, P. F. G.; Ashe, M. P., Glucose depletion inhibits translation initiation via eIF4A loss and subsequent 48S preinitiation complex accumulation, while the pentose phosphate pathway is coordinately up-regulated. *Molecular Biology of the Cell* 2011, *22* (18), 3379-3393.

40. Zampar, G. G.; Kümmel, A.; Ewald, J.; Jol, S.; Niebel, B.; Picotti, P.; Aebersold, R.; Sauer, U.; Zamboni, N.; Heinemann, M., Temporal system-level organization of the switch from glycolytic to gluconeogenic operation in yeast. *Molecular Systems Biology* 2013, *9* (1).

41. Sprague, G. F.; Cronan, J. E., Isolation and characterization of Saccharomyces cerevisiae mutants defective in glycerol catabolism. *Journal of Bacteriology* 1977, *129* (3), 1335-1342.

42. Grauslund, M.; Lopes, J. M.; Rønnow, B., Expression of GUT1, which encodes glycerol kinase in Saccharomyces cerevisiae, is controlled by the positive regulators Adr1p, Ino2p and Ino4p and the negative regulator Opi1p in a carbon source-dependent fashion. *Nucleic Acids Research* 1999, *27* (22), 4391-4398.

43. Cronwright, G. R.; Rohwer, J. M.; Prior, B. A., Metabolic Control Analysis of Glycerol Synthesis in Saccharomyces cerevisiae. *Applied and Environmental Microbiology* 2002, *68* (9), 4448-4456.

44. ter Schure, E. G.; Flikweert, M. T.; van Dijken, J. P.; Pronk, J. T.; Verrips, C. T., Pyruvate Decarboxylase Catalyzes Decarboxylation of Branched-Chain 2-Oxo Acids but Is Not Essential for Fusel Alcohol Production by Saccharomyces cerevisiae. *Applied and Environmental Microbiology* 1998, *64* (4), 1303-1307.

45. Brewster, N. K.; Val, D. L.; Walker, M. E.; Wallace, J. C., Regulation of Pyruvate Carboxylase Isozyme (PYC1, PYC2) Gene Expression in Saccharomyces cerevisiae

during Fermentative and Nonfermentative Growth. *Archives of Biochemistry and Biophysics* 1994, *311* (1), 62-71.

46. Pavlik, P.; Simon, M.; Schuster, T.; Ruis, H., The glycerol kinase (GUT1) gene of Saccharomyces cerevisiae cloning and characterization. *Current Genetics* 1993, *24* (1), 21-25.

47. Blumberg, H.; Hartshorne, T. A.; Young, E. T., Regulation of expression and activity of the yeast transcription factor ADR1. *Molecular and Cellular Biology* 1988, *8* (5), 1868-1876.

48. Kratzer, S.; Schüller, H.-J., Transcriptional control of the yeast acetyl-CoA synthetase gene, ACS1, by the positive regulators CAT8 and ADR1 and the pleiotropic repressor UME6. *Molecular Microbiology* 1997, *26* (4), 631-641.

49. Simon, M.; Binder, M.; Adam, G.; Hartig, A.; Ruis, H., Control of peroxisome proliferation in Saccharomyces cerevisiae by ADR1, SNF1 (CAT1, CCR1) and SNF4 (CAT3). *Yeast* 1992, *8* (4), 303-309.

50. Wang, X.; Mann, C. J.; Bai, Y.; Ni, L.; Weiner, H., Molecular Cloning, Characterization, and Potential Roles of Cytosolic and Mitochondrial Aldehyde Dehydrogenases in Ethanol Metabolism in Saccharomyces cerevisiae. *Journal of Bacteriology* 1998, *180* (4), 822-830.

51. Van Den Berg, M. A.; Steensma, H. Y., ACS2, a Saccharomyces Cerevisiae Gene Encoding Acetyl-Coenzyme A Synthetase, Essential for Growth on Glucose. *European Journal of Biochemistry* 1995, *231* (3), 704-713.

52. Takahashi, H.; McCaffery, J. M.; Irizarry, R. A.; Boeke, J. D., Nucleocytosolic Acetyl-Coenzyme A Synthetase Is Required for Histone Acetylation and Global Transcription. *Molecular Cell* 2006, *23* (2), 207-217.

53. Moldave, K., *Progress in Nucleic Acid Research and Molecular Biology*. Elsevier Science: 1997.

APPENDIX A. SUPPLEMENTAL DATA FOR CHAPTER 2

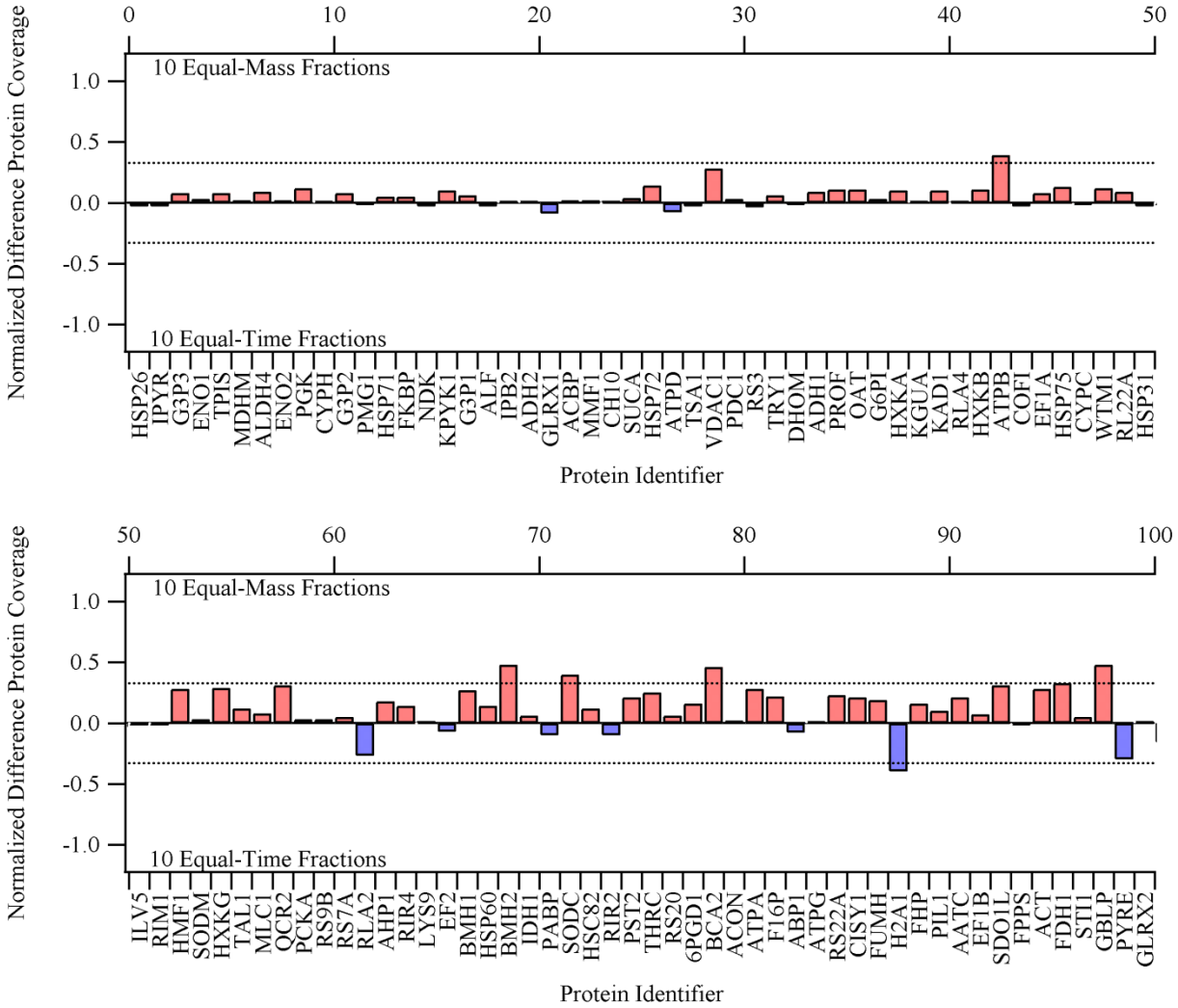

Appendix A.1. To compare the 10 equal-mass and 10 equal-time fractions, the Normalized Difference Protein Coverage (NDPC) was plotted with proteins with higher coverage on the left, and proteins with lower coverage on the right. If a protein was identified with higher sequence coverage in the 10 equal-mass fractions, its NDPC value was positive (red bars). The blue bars signified higher coverage in the 10 equal-time fractions. Differences in coverage were minimal for highly covered proteins. As protein coverage decreased, more proteins were identified with higher coverage in the equal-mass fractions. The dashed lines indicate a level of two-fold greater protein coverage.

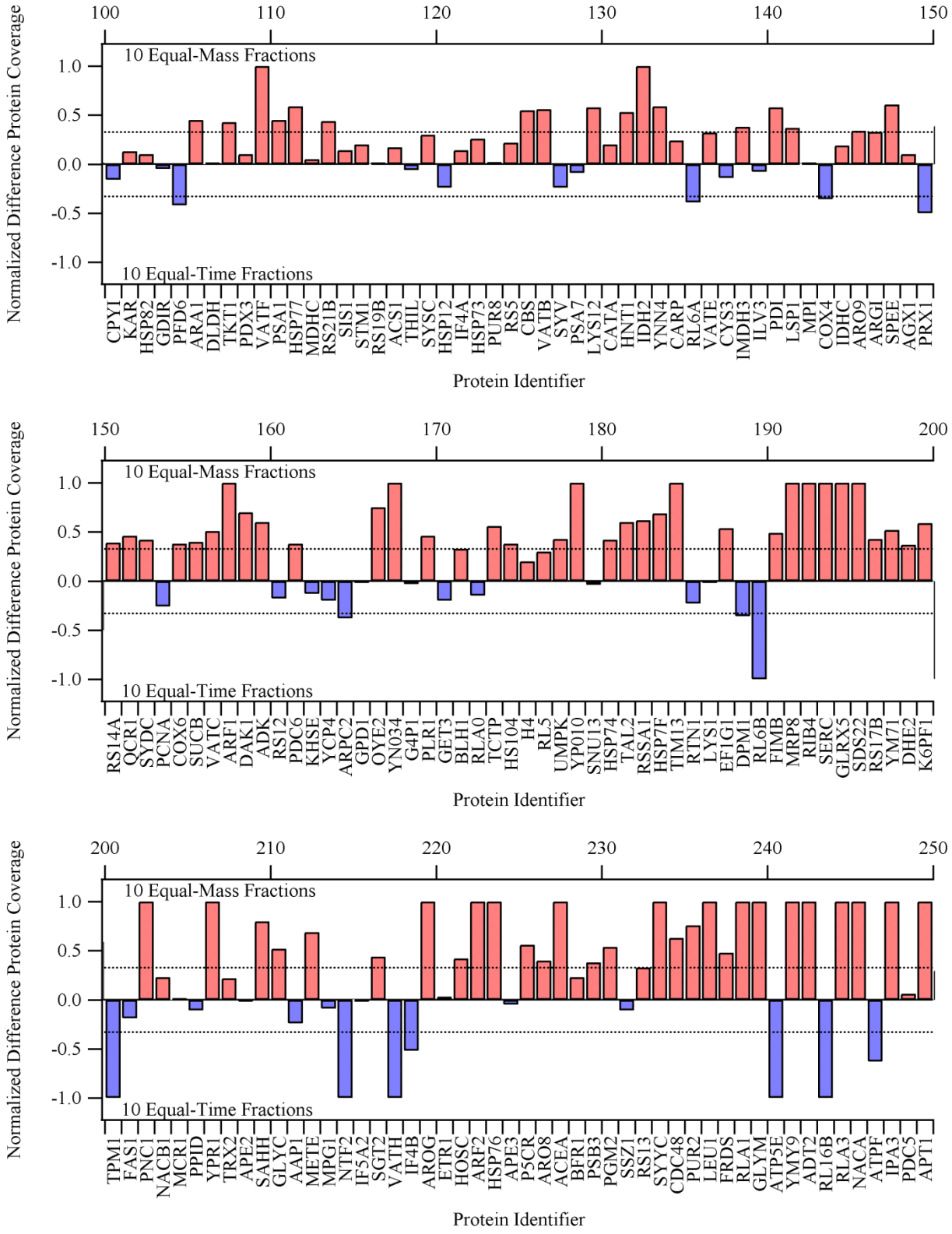

Appendix A.1. (continued)

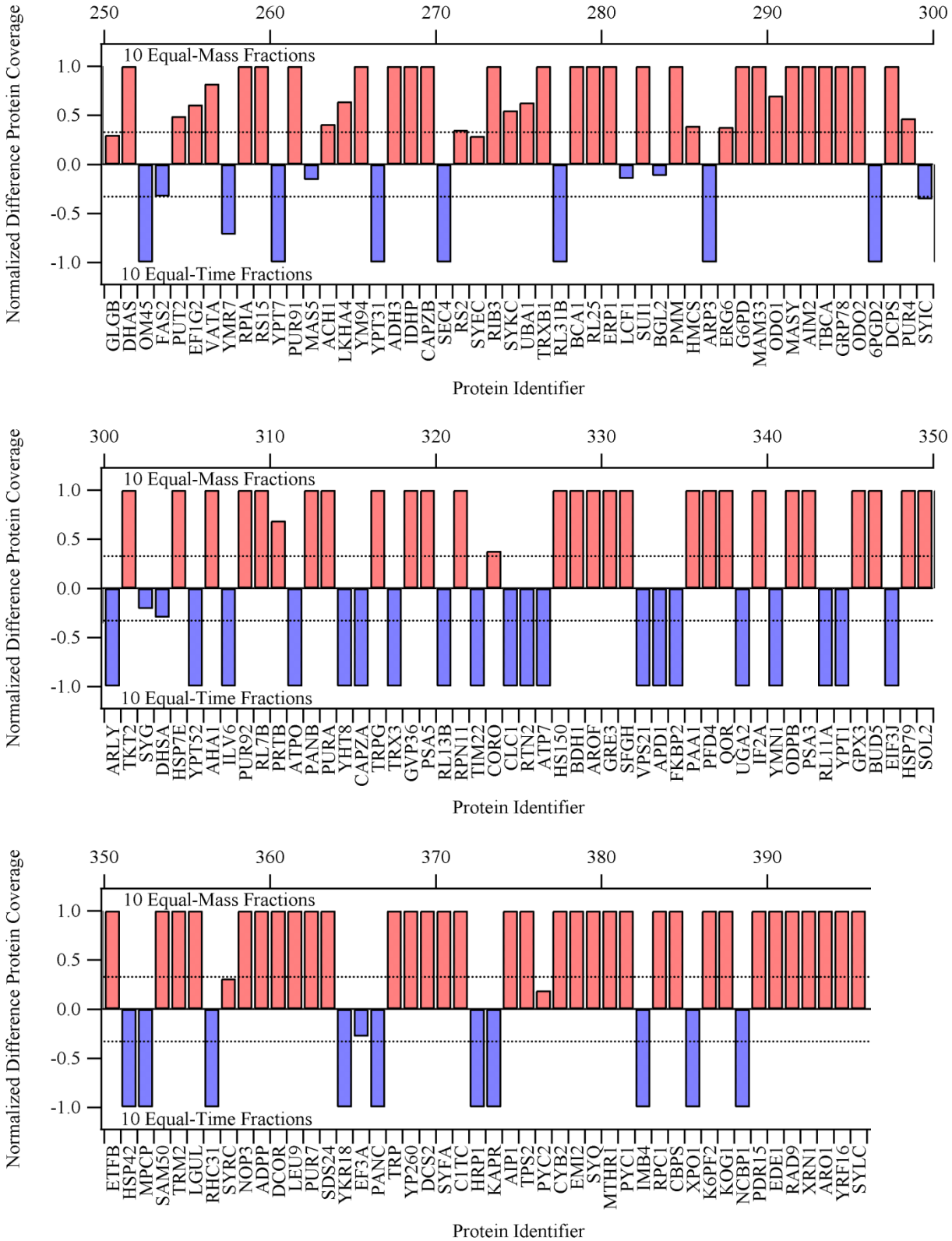

Appendix A.1. (continued)

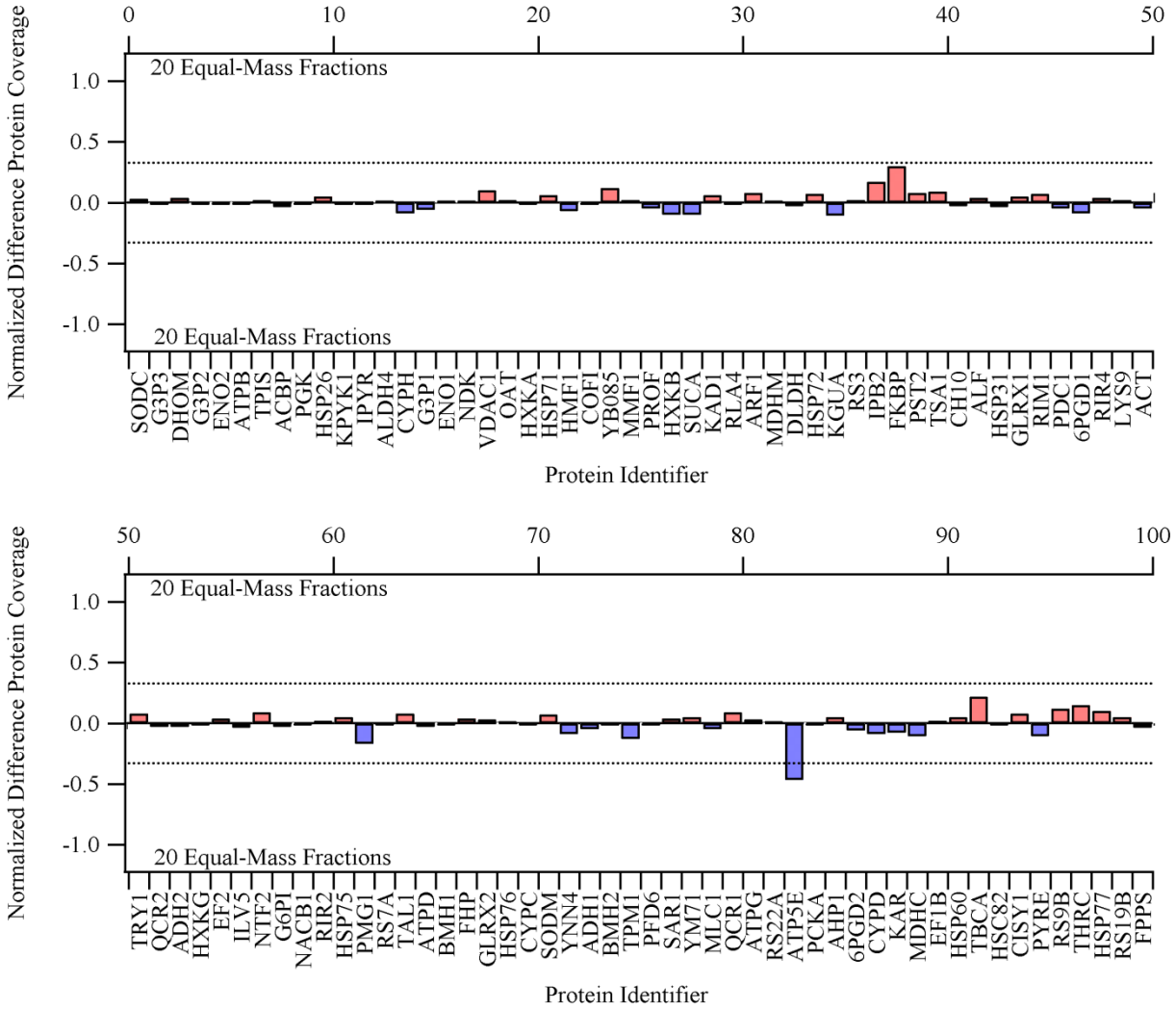

Appendix A.2. To compare the 20 equal-mass and 20 equal-time fractions, the Normalized Difference Protein Coverage (NDPC) was plotted with proteins with higher coverage on the left, and proteins with lower coverage on the right. If a protein was identified with higher sequence coverage in the 20 equal-mass fractions, its NDPC value was positive (red bars). The blue bars signified higher coverage in the 20 equal-time fractions. Differences in coverage were minimal for highly covered proteins. For 20 fractions, the NDPC did not favor the equal-mass or the equal-time fractionation methods. The dashed lines indicate a level of two-fold greater protein coverage.

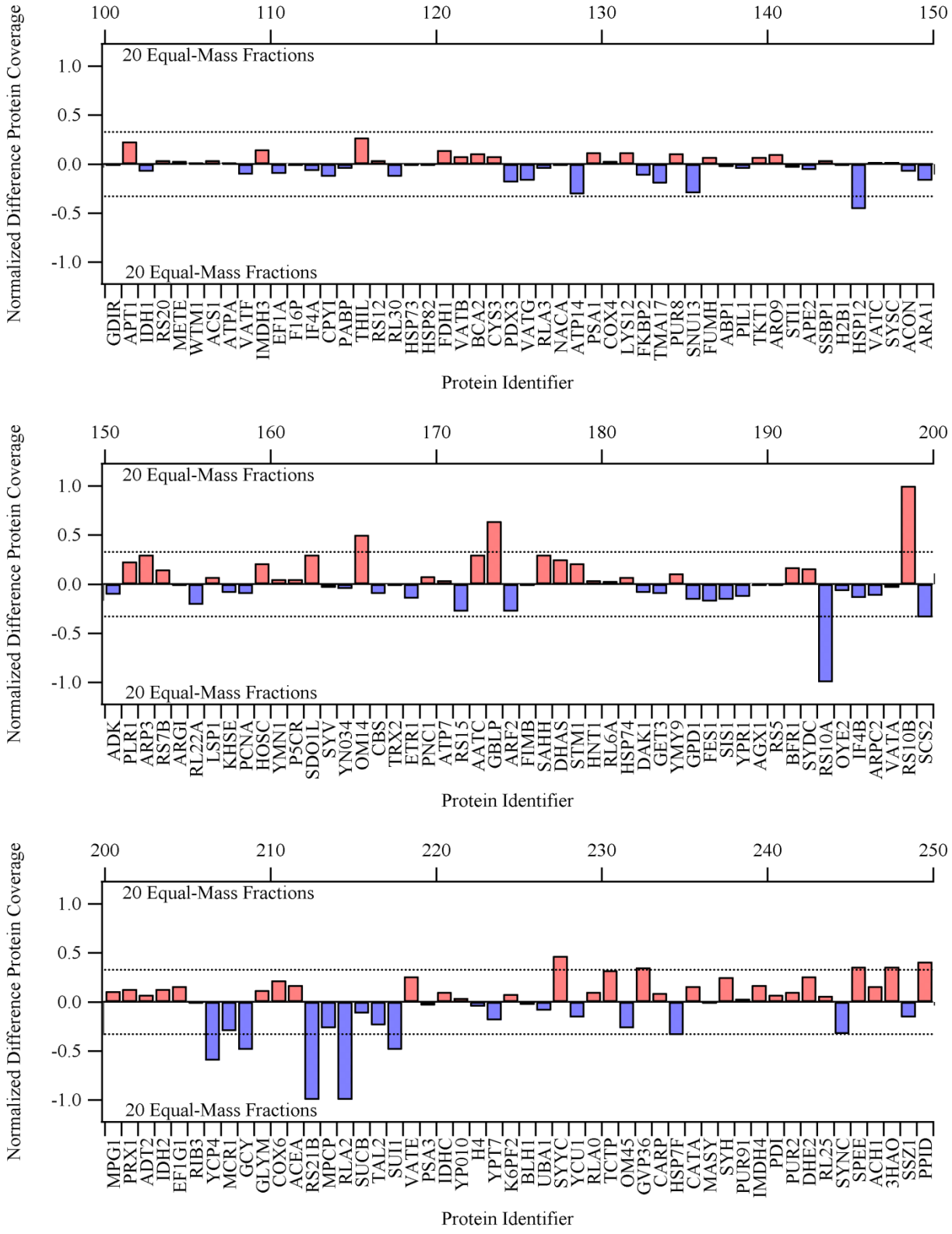

Appendix A.2. (continued)

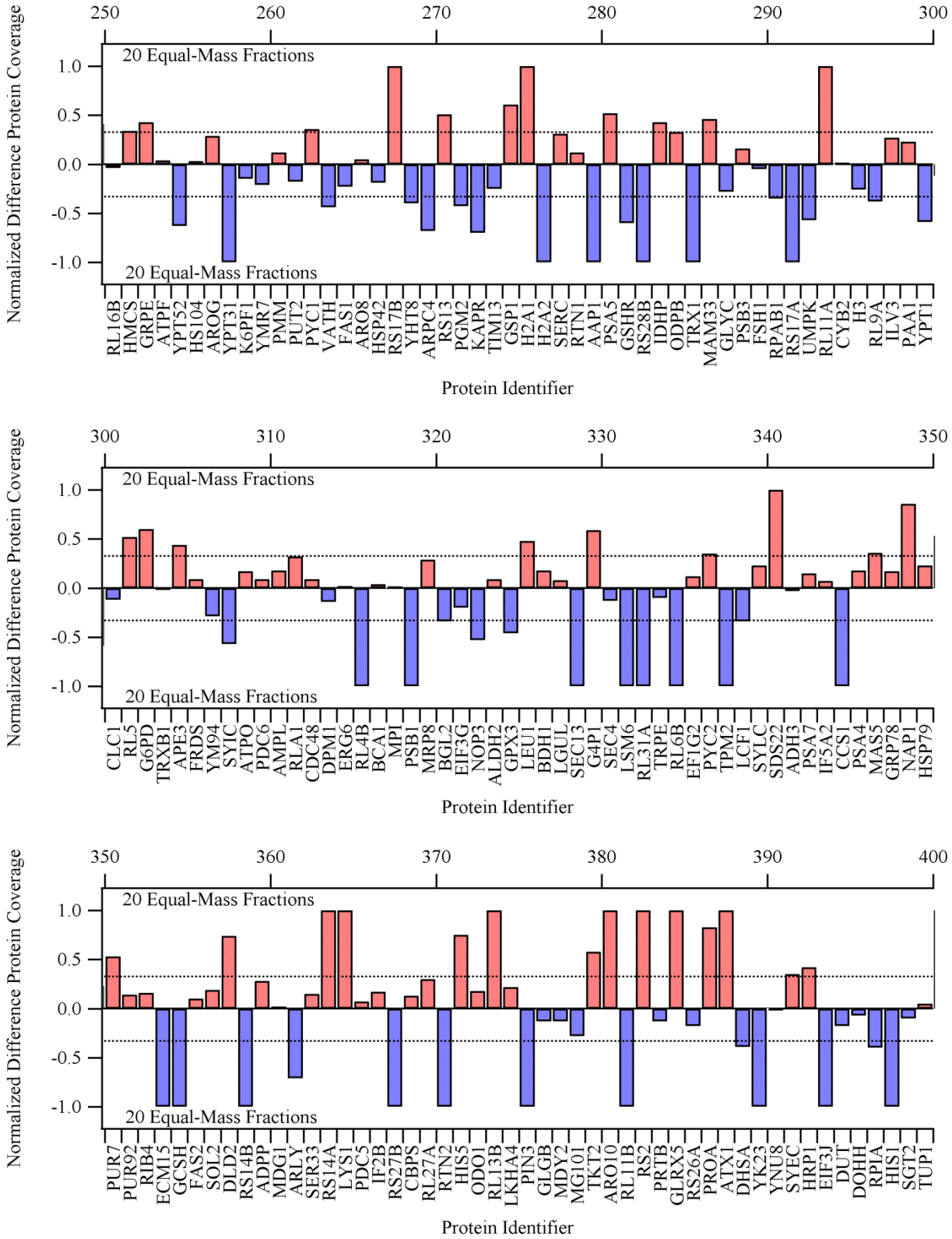

Appendix A.2. (continued)

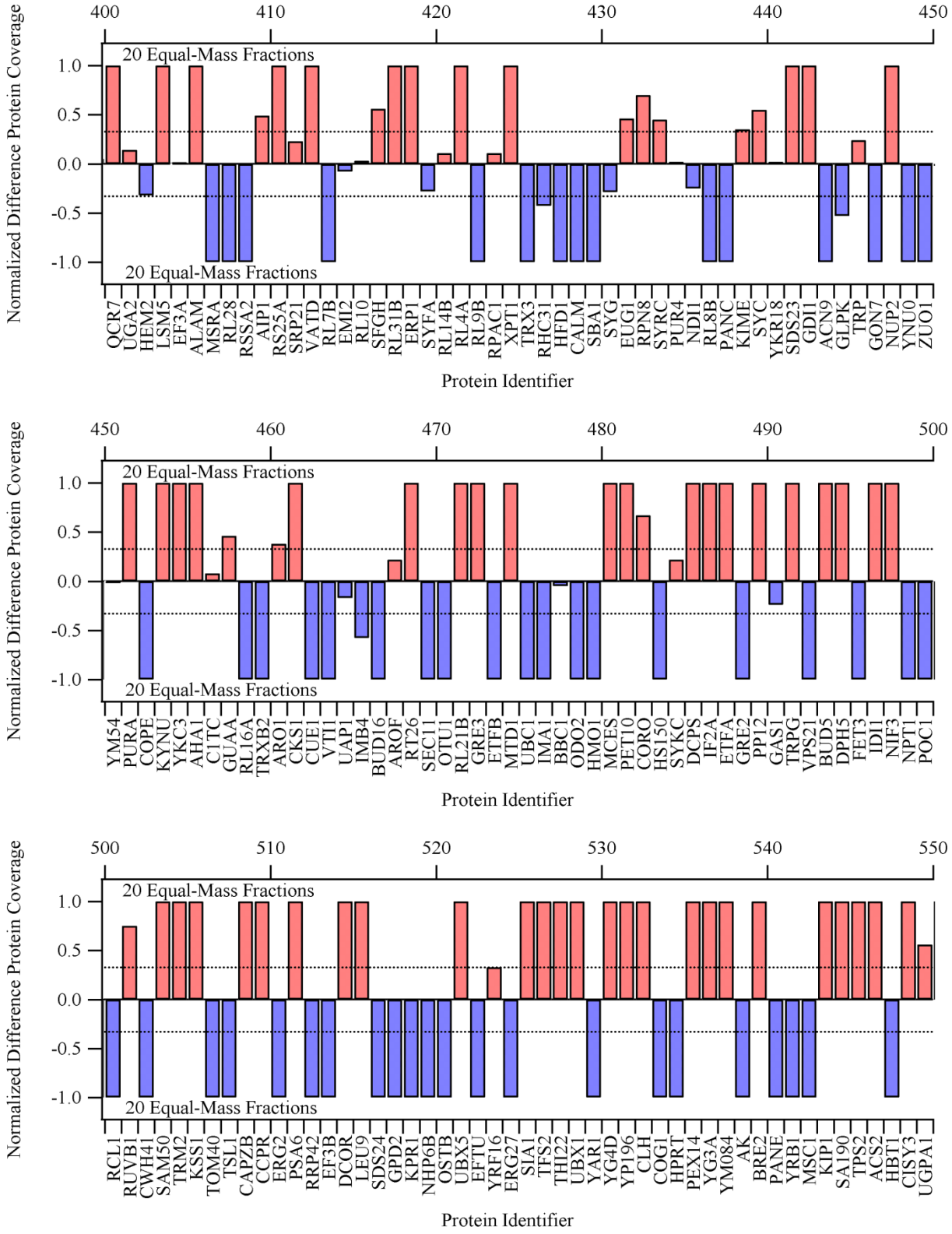

Appendix A.2. (continued)

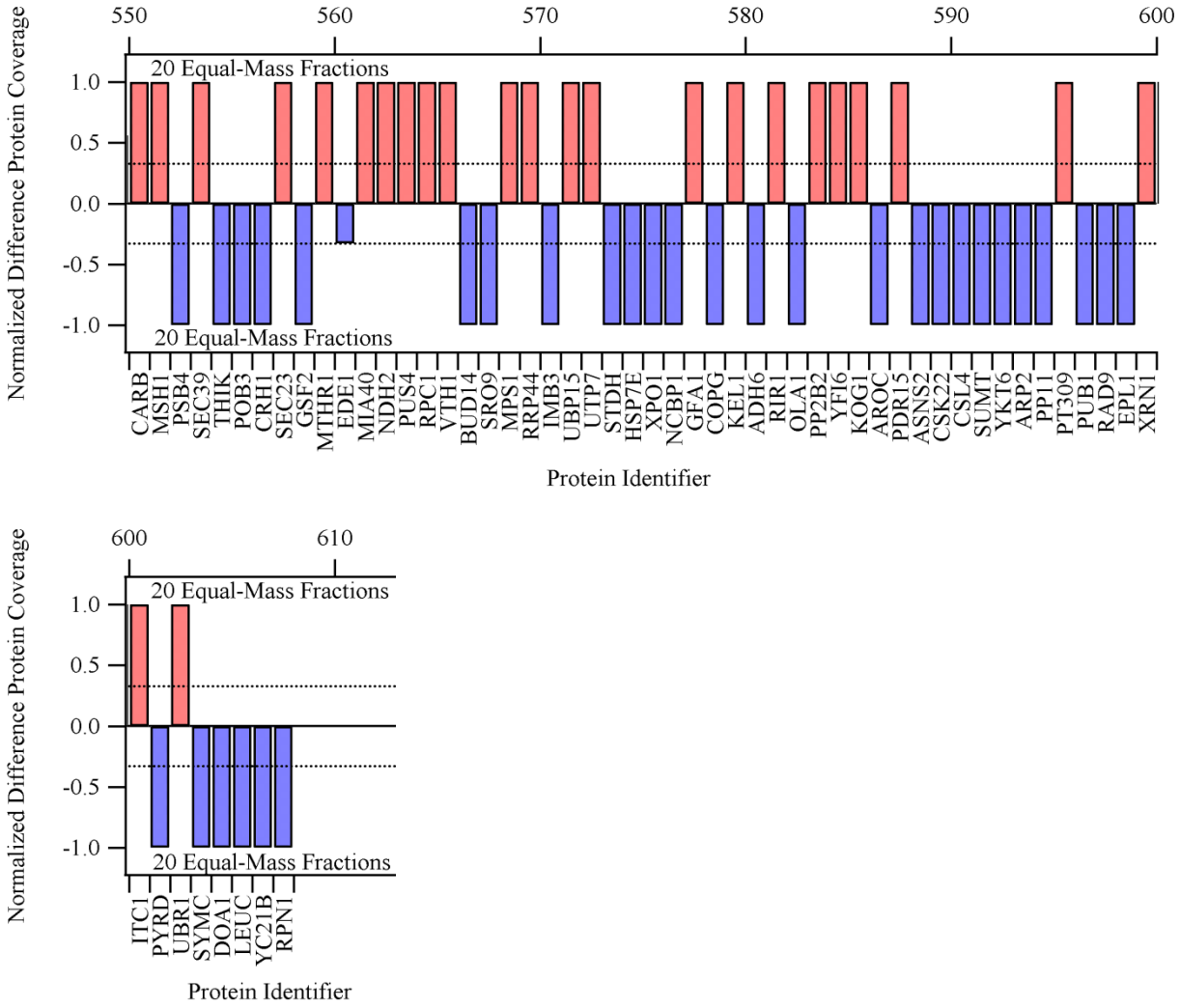

Appendix A.2. (continued)

APPENDIX B. SUPPLEMENTAL DATA FOR CHAPTER 3

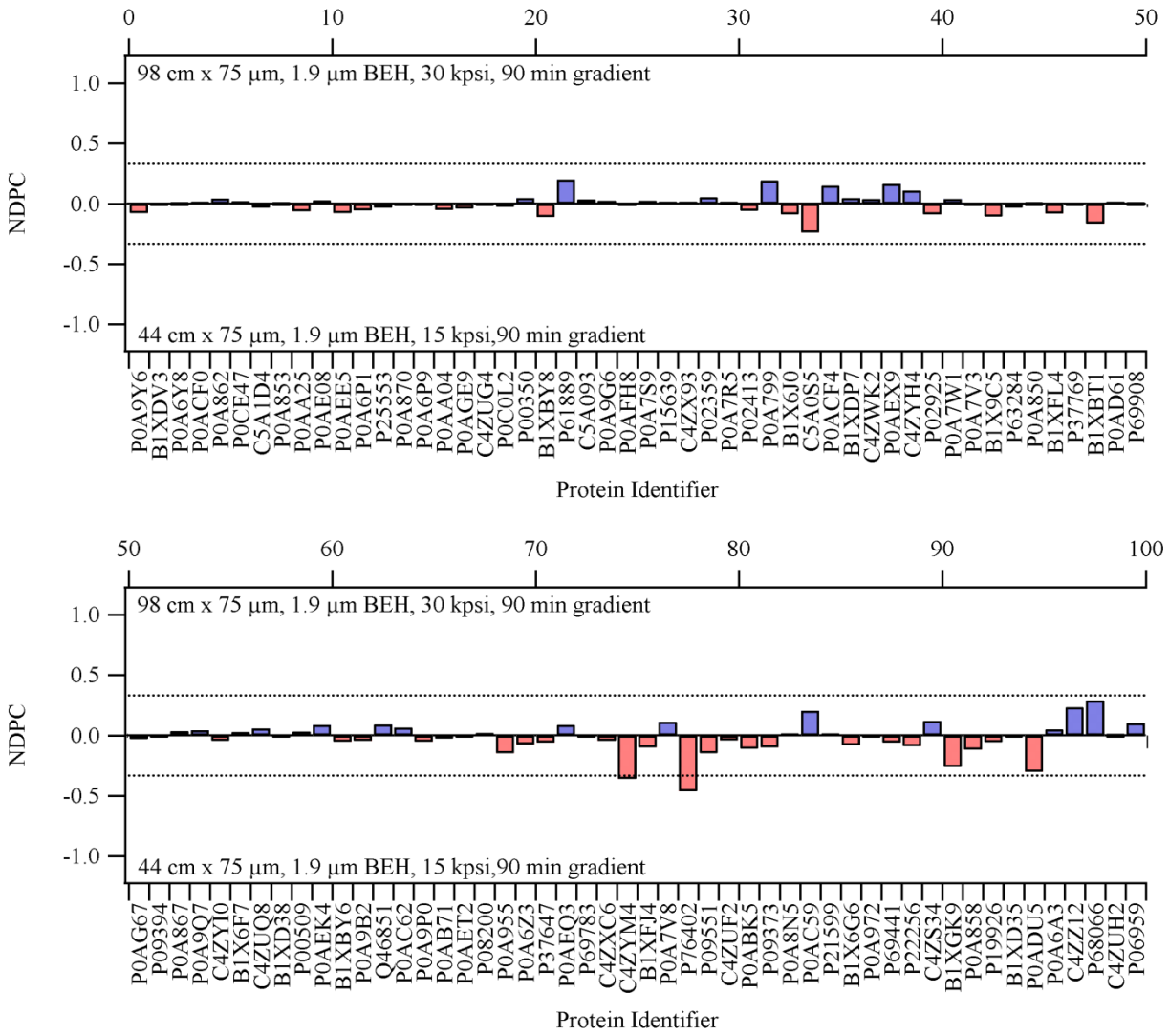

Appendix B.1. The NDPC comparing the analysis on the 98.2 cm column run at 30 kpsi to the 44.1 cm column run at 15 kpsi for a 90 min gradient was plotted for each protein identified in an *E. coli* digest standard. If a protein was identified with higher sequence coverage with the separation on the 98.2 cm column, its NDPC value was positive (blue bars). The red bars signified higher coverage with the separation on the 44.1 cm column. Proteins with higher coverage were plotted on the left, and proteins with lower coverage were on the right. Differences in coverage were minimal for highly covered proteins. As protein coverage decreased, more proteins were identified with higher coverage with the separation on the 98.2 cm column. The dashed line represented a two-fold difference in protein coverage.

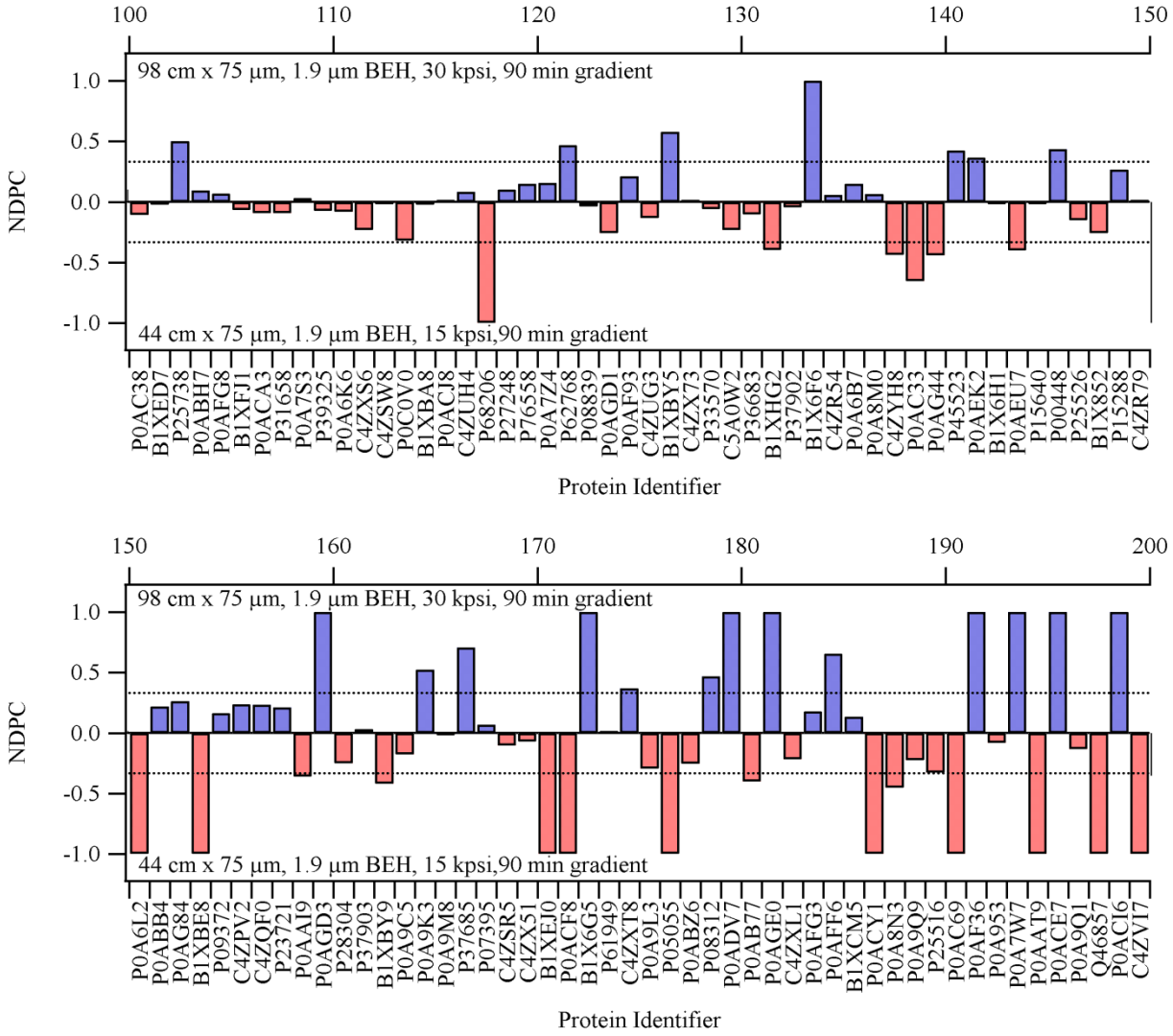

Appendix B.1. (continued)

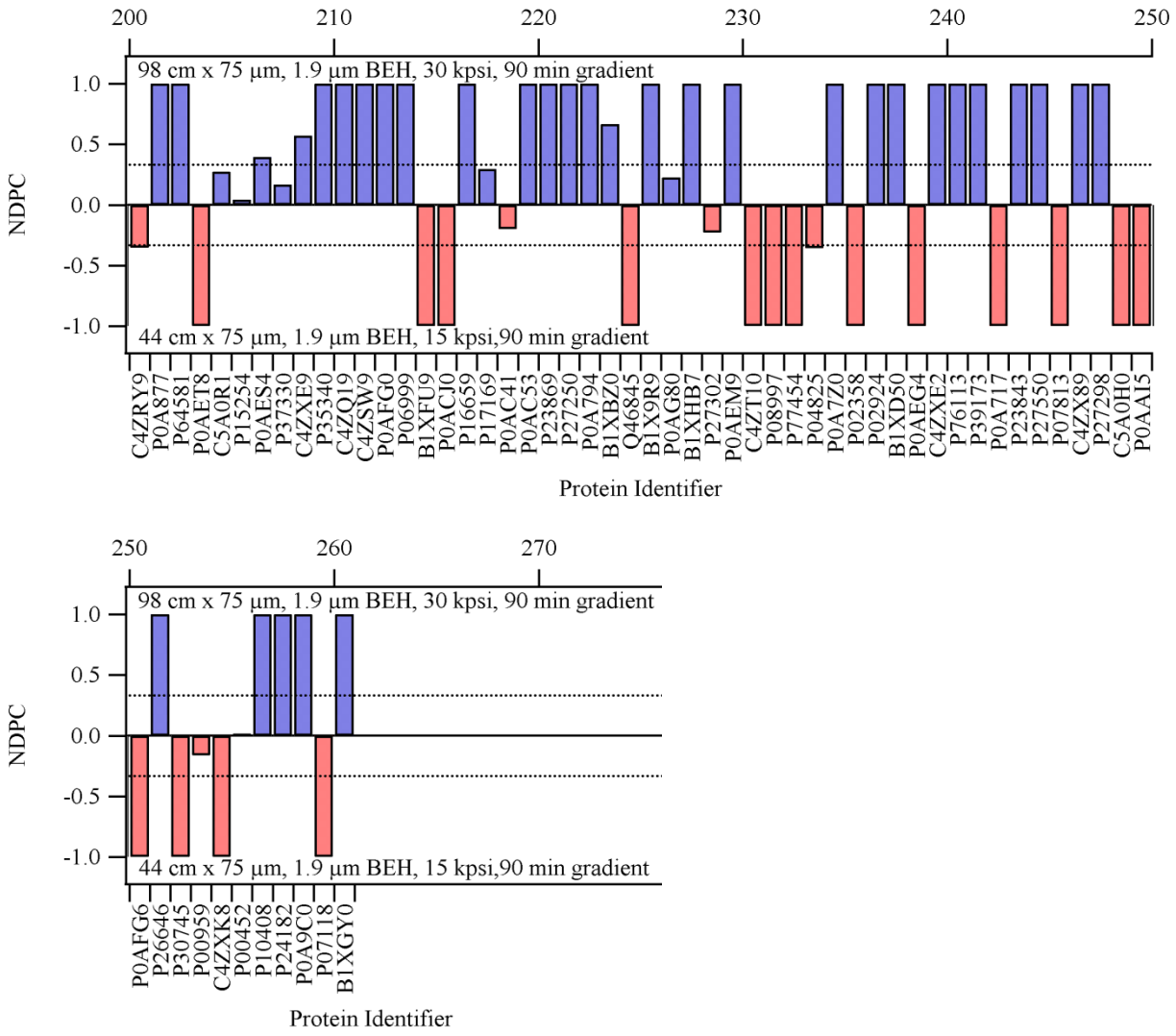

Appendix B.1. (continued)

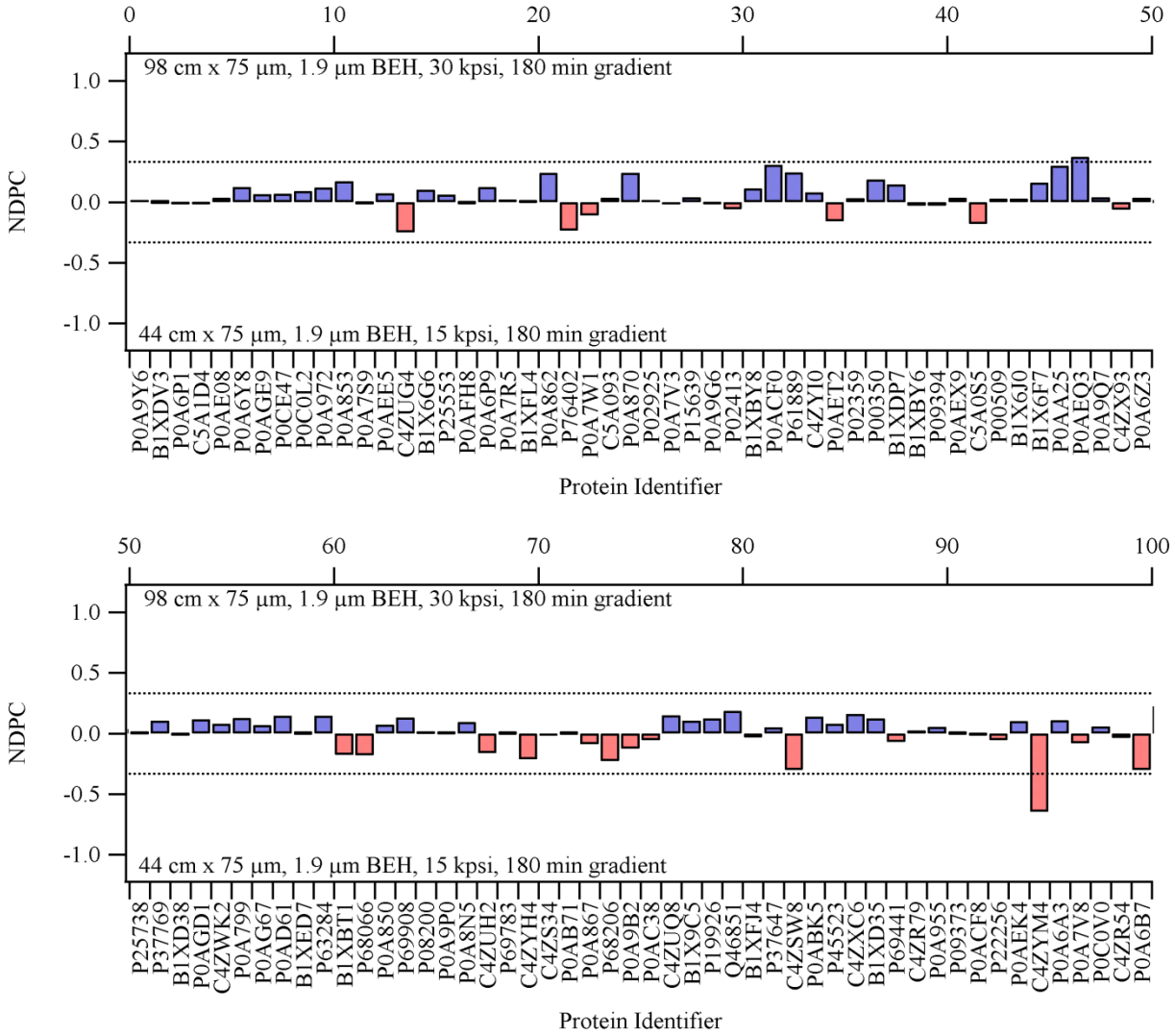

Appendix B.2. The NDPC comparing the analysis on the 98.2 cm column run at 30 kpsi to the 44.1 cm column run at 15 kpsi for a 180 min gradient was plotted for each protein identified in an E. coli digest standard. If a protein was identified with higher sequence coverage with the separation on the 98.2 cm column, its NDPC value was positive (blue bars). The red bars signified higher coverage with the separation on the 44.1 cm column. Proteins with higher coverage were plotted on the left, and proteins with lower coverage were on the right. Differences in coverage were minimal for highly covered proteins. As protein coverage decreased, more proteins were identified with higher coverage with the separation on the 98.2 cm column. The dashed line represented a two-fold difference in protein coverage.

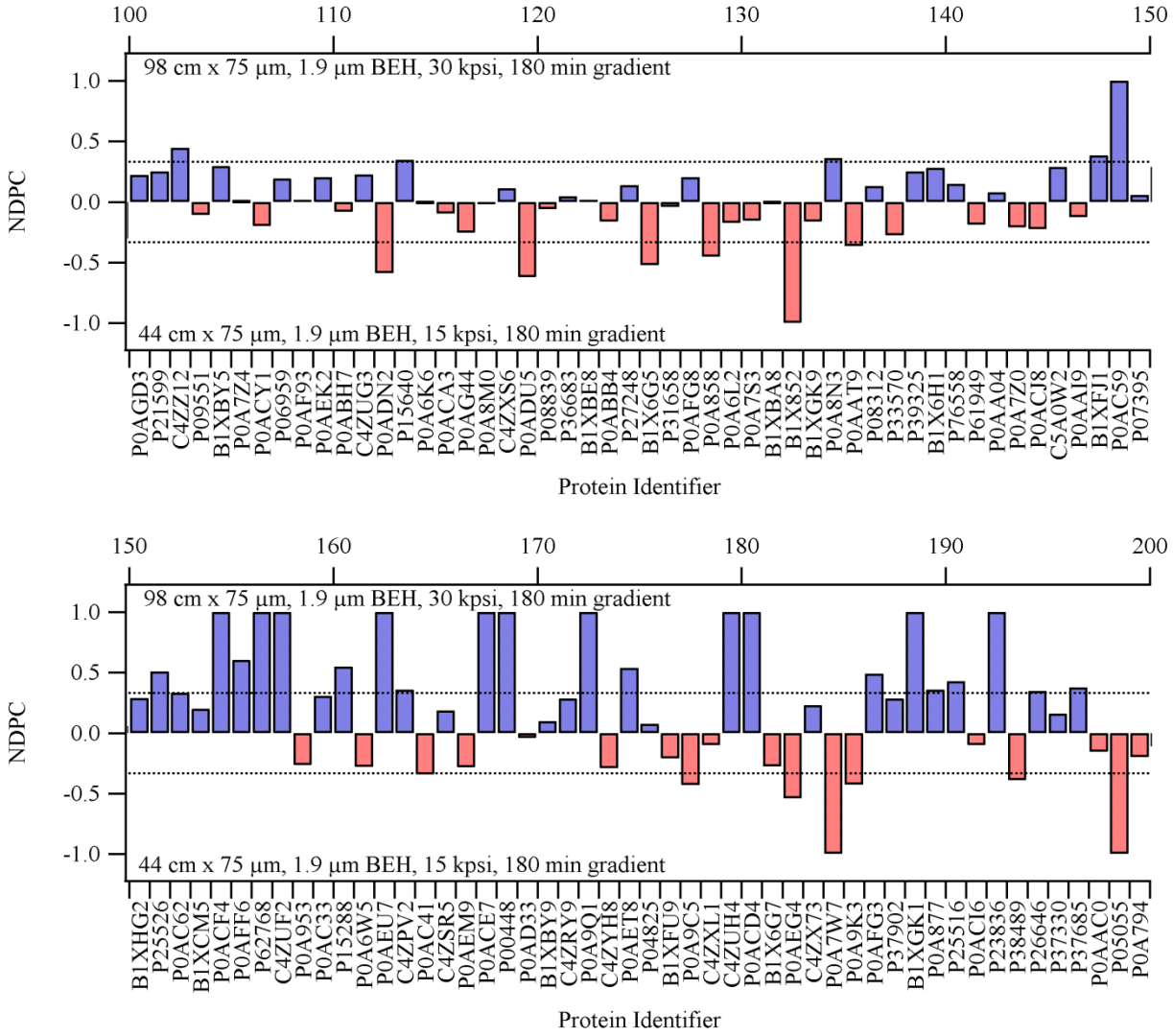

Appendix B.2. (continued)

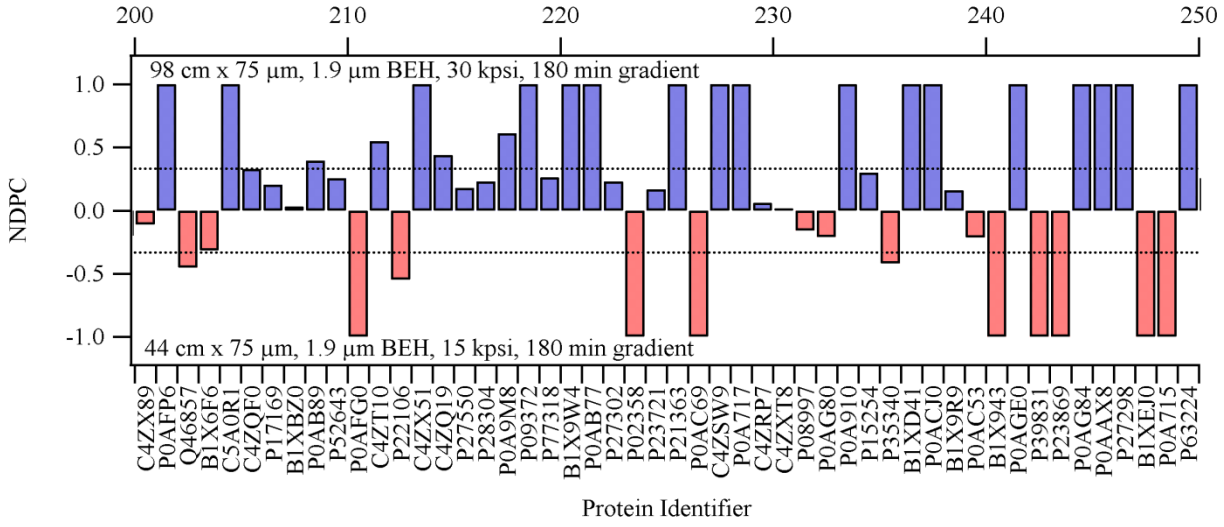

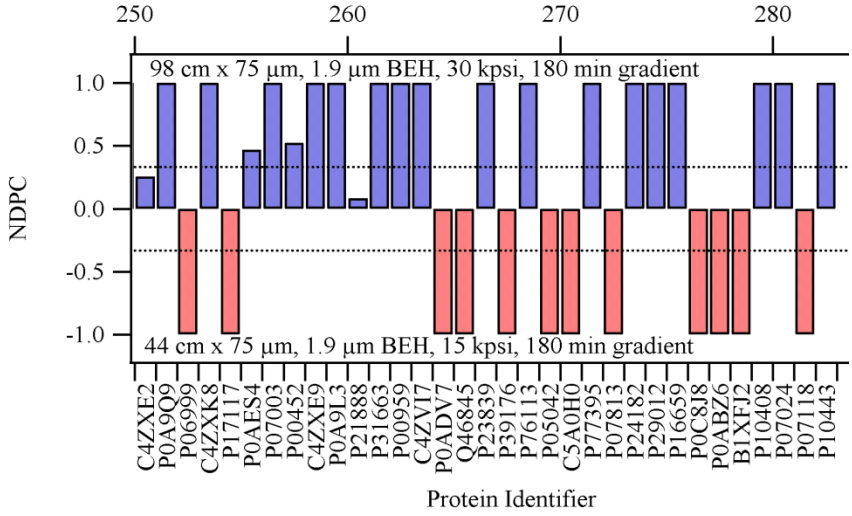

Appendix B.2. (continued)

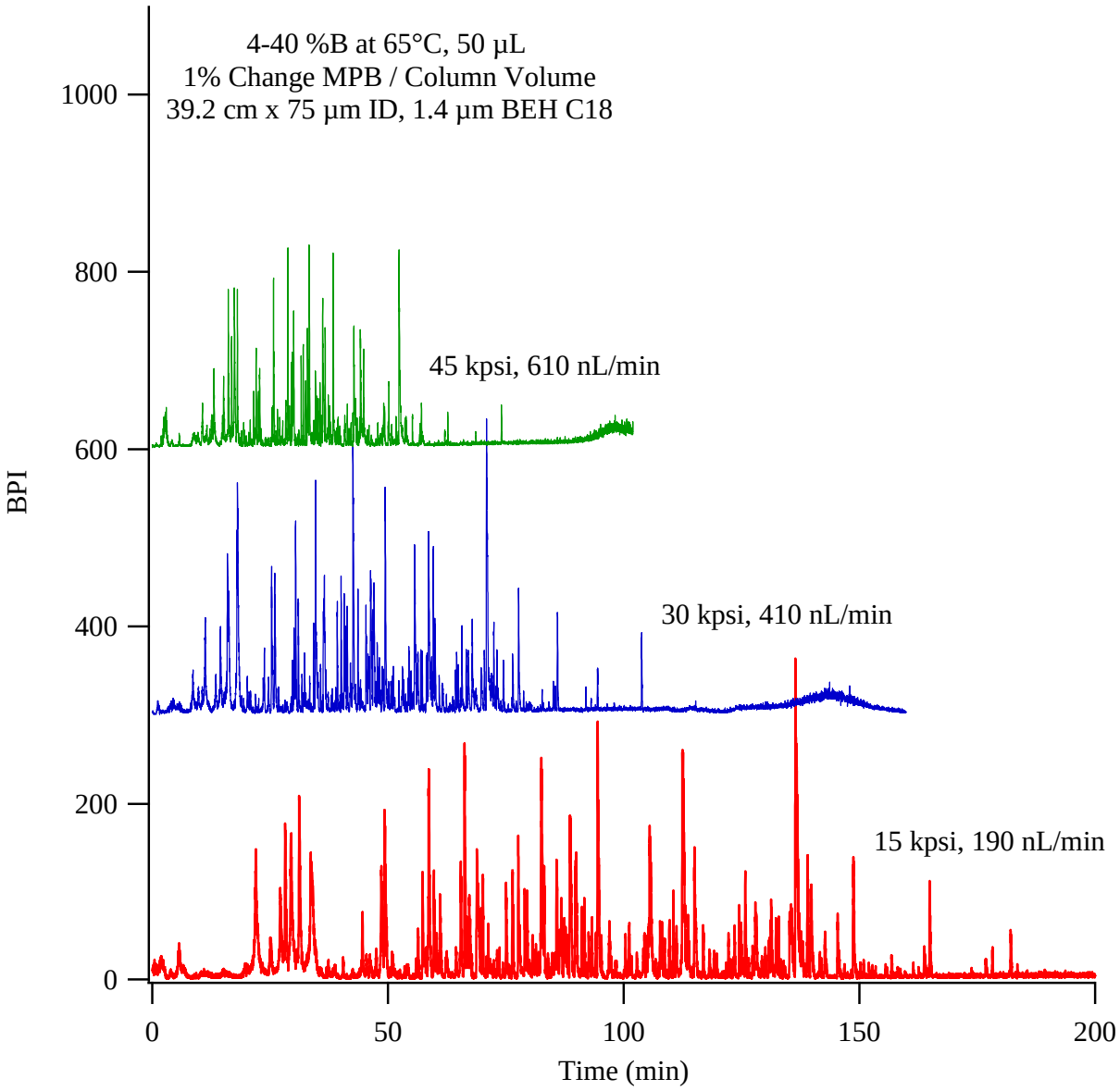

Appendix B.3. Chromatograms of MassPREP™ Digestion Standard Protein Expression Mixture 2 were collected for separations with increasing pressure and flow rate on the 39.2 cm x 75 µm ID column packed with 1.4 µm BEH C18 particles. Separations were completed with a 50µL gradient volume. The insert of a representative peptide peak with 724 m/z extracted from all three chromatograms showed the decrease in peak width and constant signal intensity as pressure and flow rate increased.

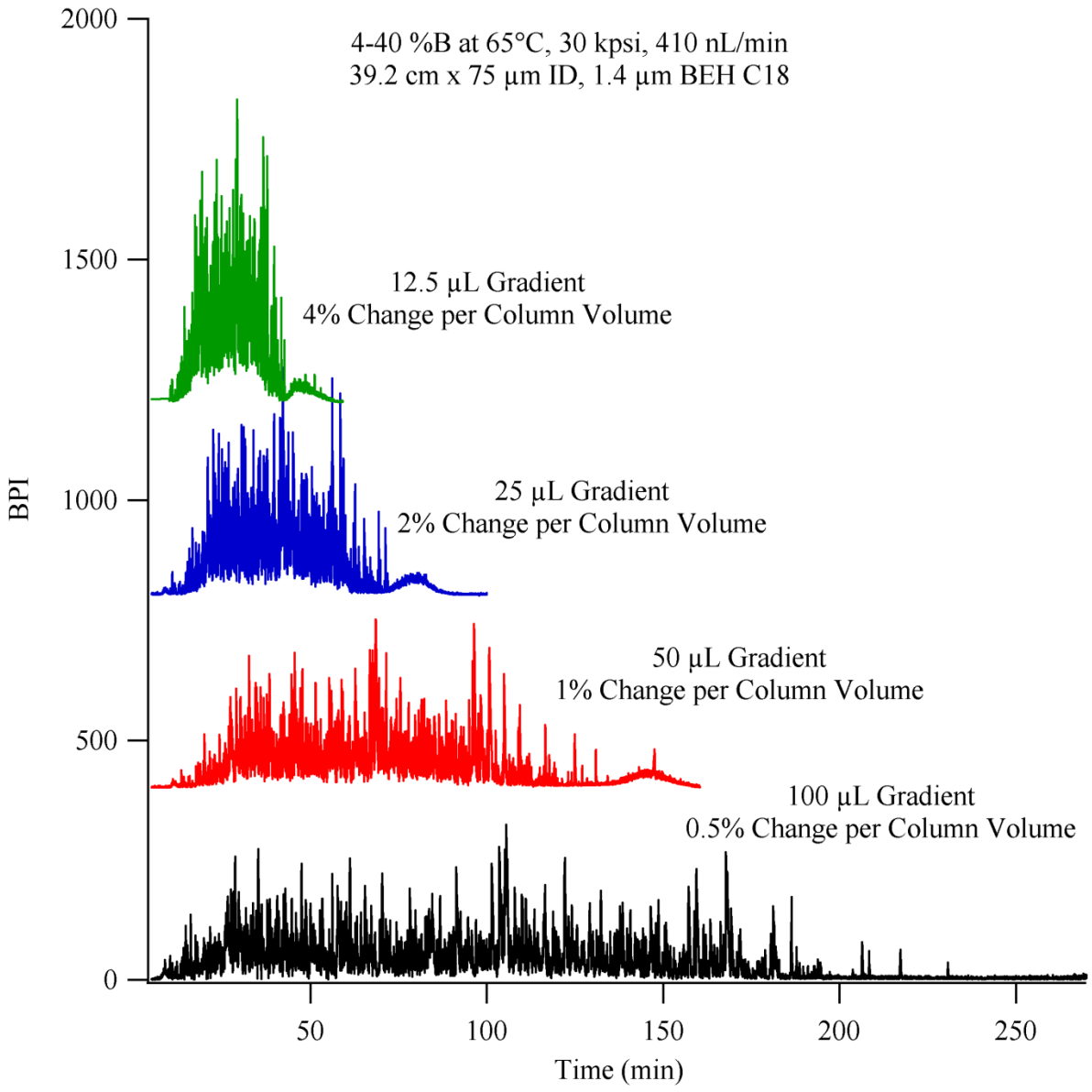

Appendix B.4. Chromatograms of MassPREP™ *E. coli* Digestion Standard were collected for separations with increasing gradient volume on the 39.2 cm x 75 µm ID column packed with 1.4 µm BEH C18 particles. Separations were completed at 30 kpsi. Though the chromatograms were very busy, an increase in resolution was observed as gradient volume increased which was indicated by the signal being closer to baseline between two adjacent peaks.

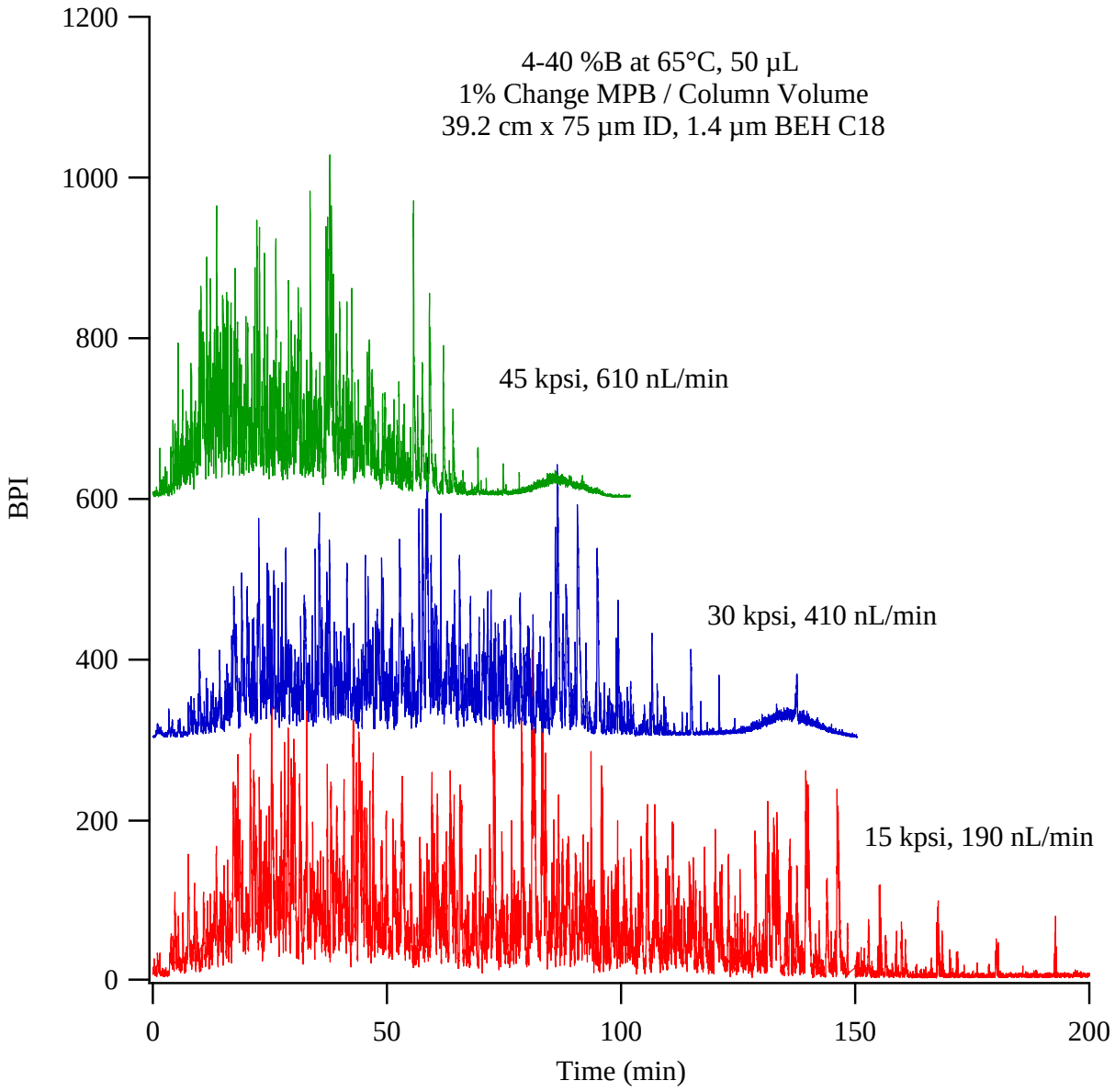

Appendix B.5. Chromatograms of MassPREP™ *E. coli* Digestion Standard were collected for separations with increasing pressure and flow rate on the 39.2 cm x 75 µm ID column packed with 1.4 µm BEH C18 particles. Separations were completed with a 50µL gradient volume.

APPENDIX C. SUPPLEMENTAL DATA FOR CHAPTER 5

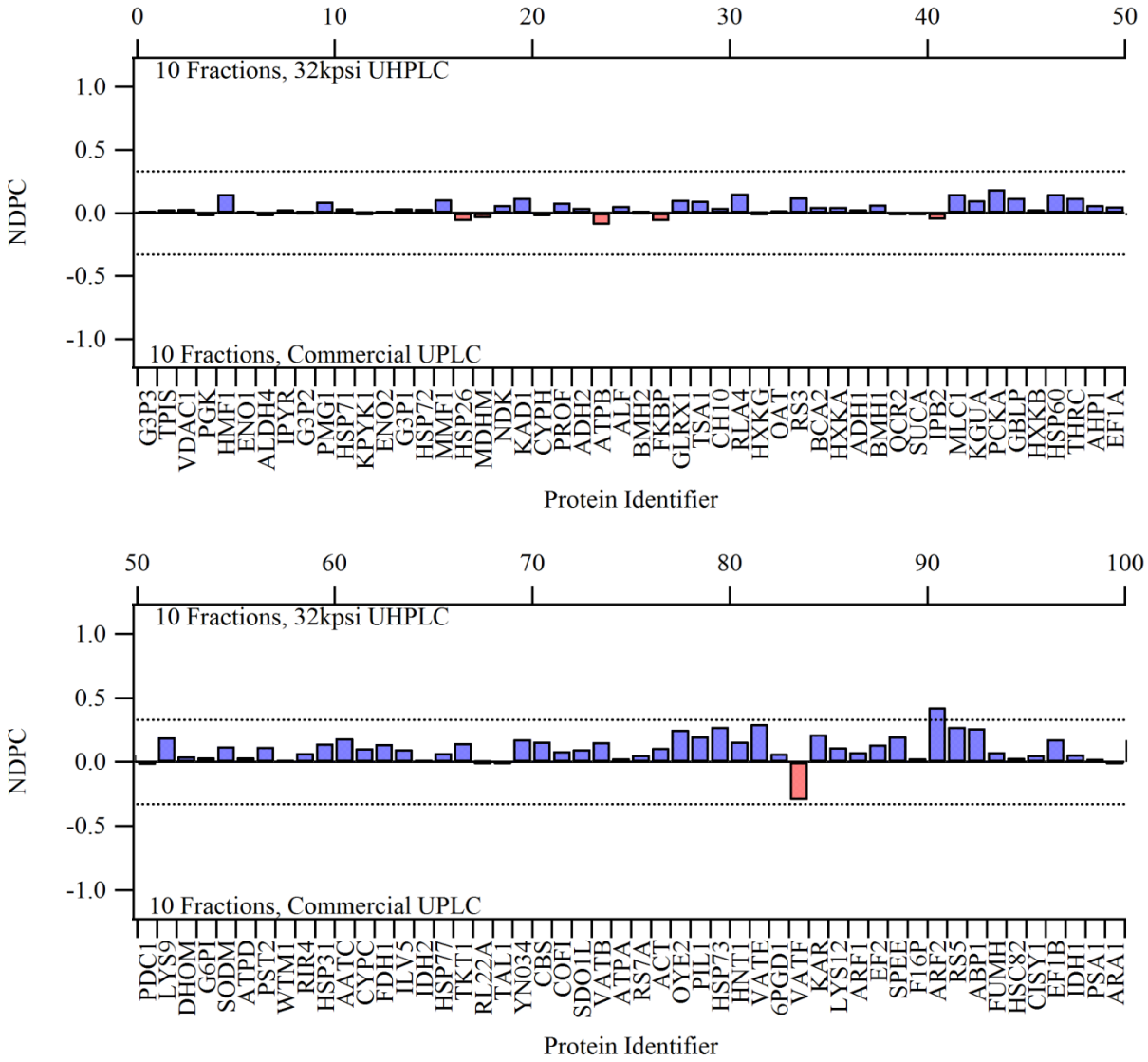

Appendix C.1. To compare the 10 fractions run on the modified system to the 10 fractions run on the standard UPLC, the NDPC is plotted with proteins with higher coverage on the left, and proteins with lower coverage on the right. If a protein was identified with higher sequence coverage when analyzed on the modified UHPLC, its NDPC value is positive (blue bars). The red bars signify higher coverage in the analysis on the standard UPLC. Differences in coverage were minimal for highly covered proteins. As protein coverage decreased, more proteins were identified with higher coverage from the analysis on the modified UHPLC. The dashed lines indicate a level of two-fold greater protein coverage. (This was a large graph and split into multiple parts.)

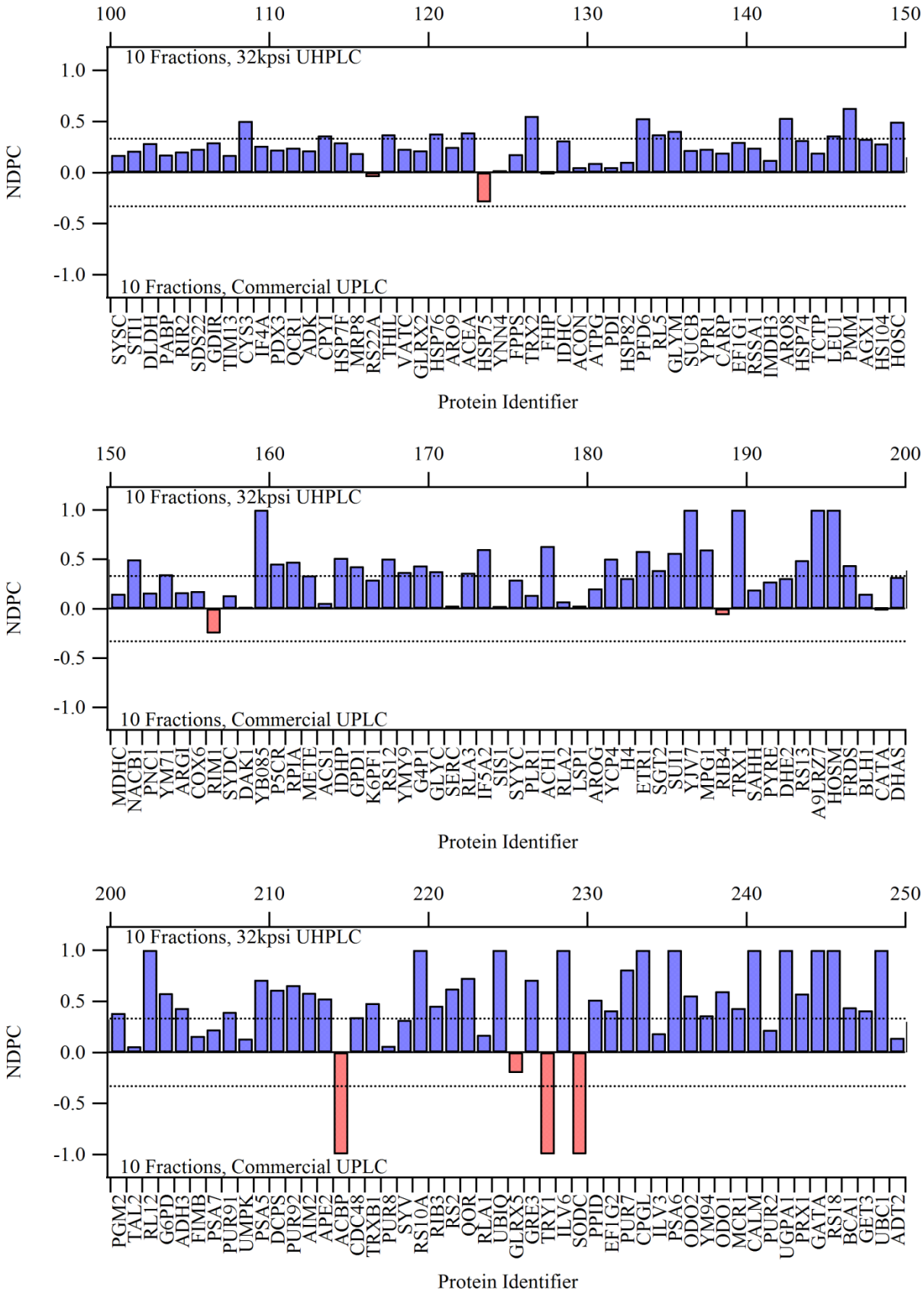

Appendix C.1. (continued)

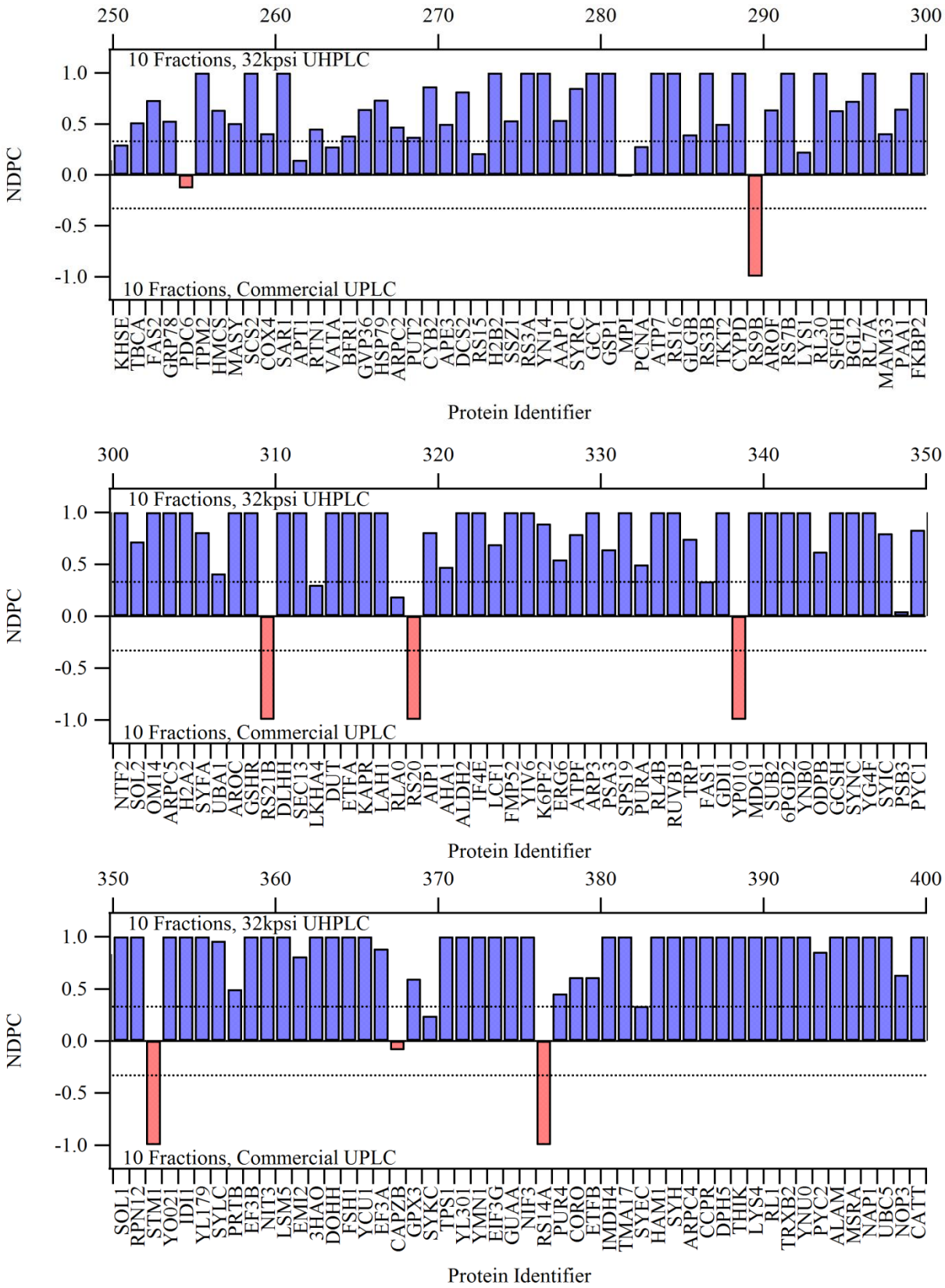

Appendix C.1. (continued)

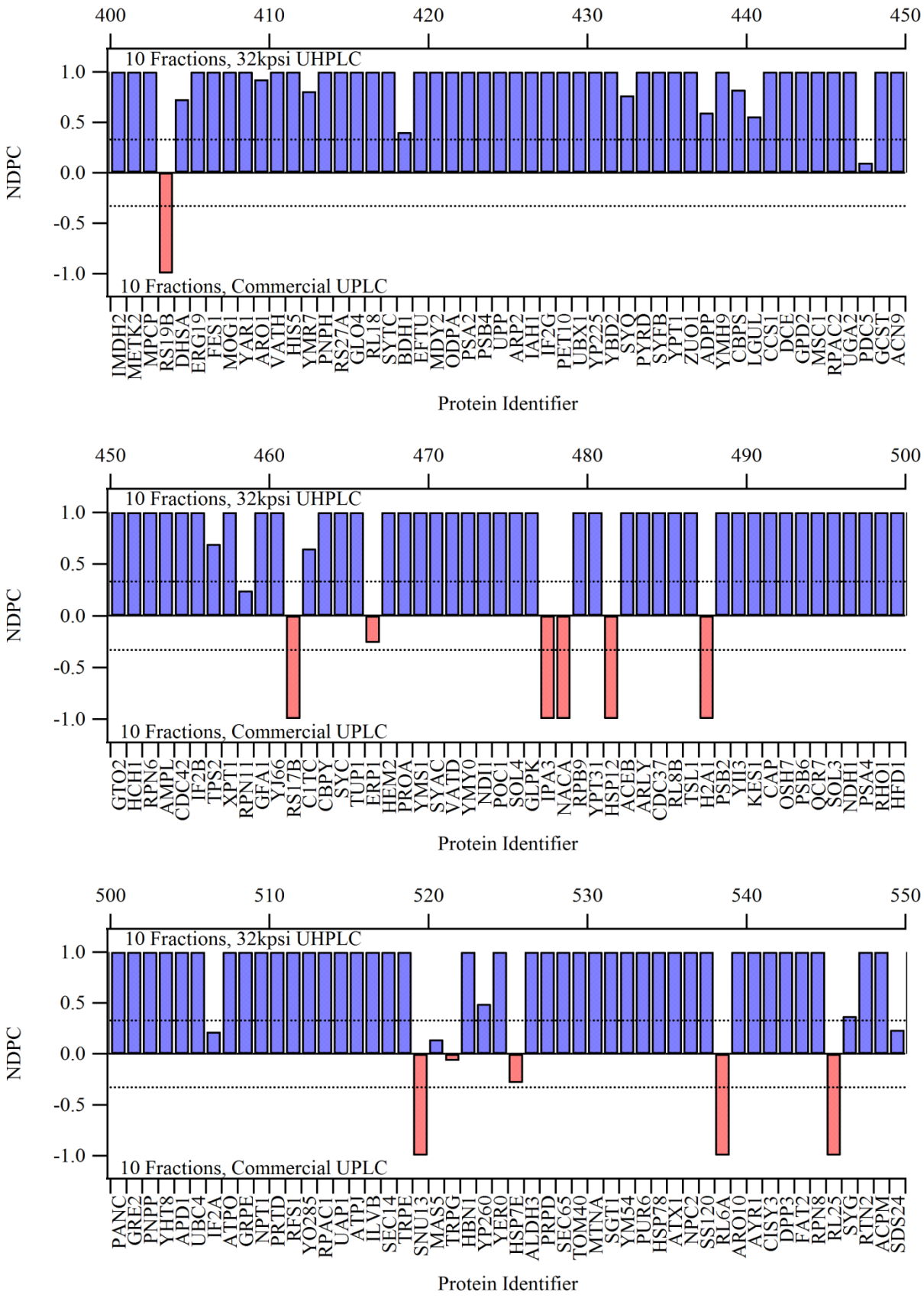

Appendix C.1. (continued)

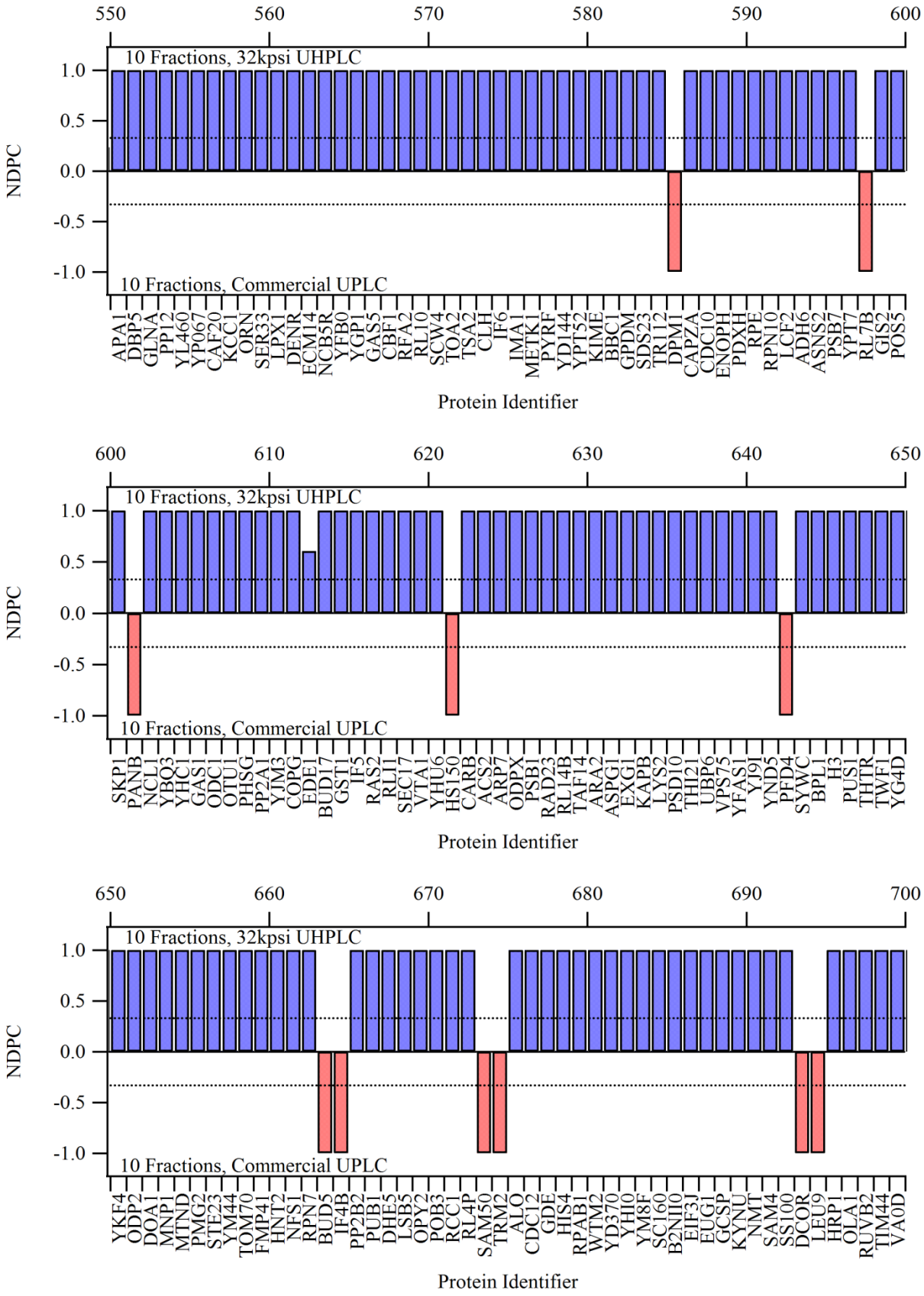

Appendix C.1. (continued)

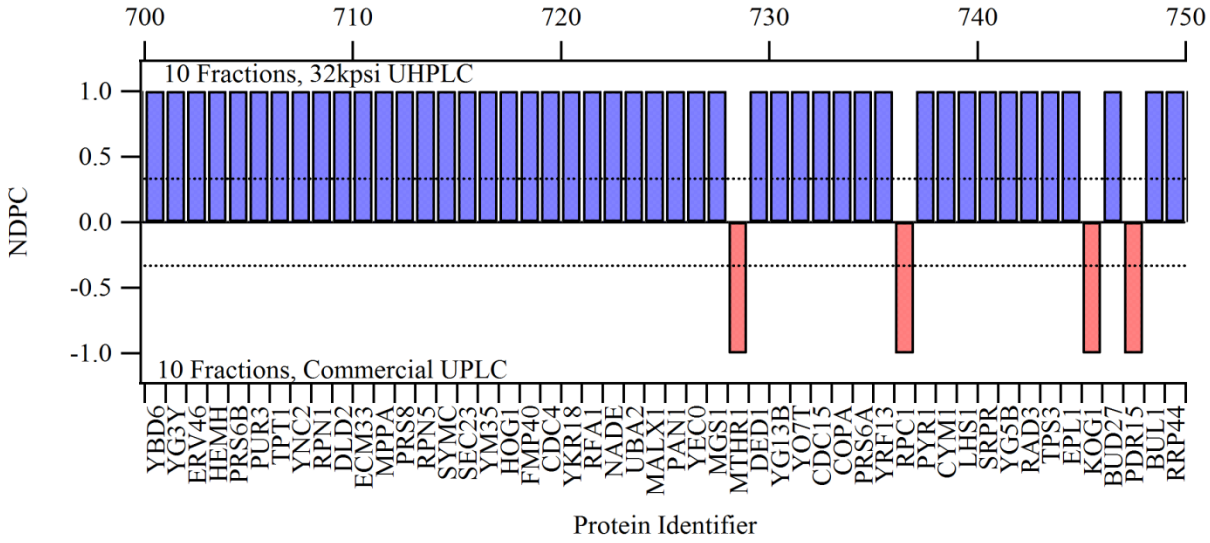

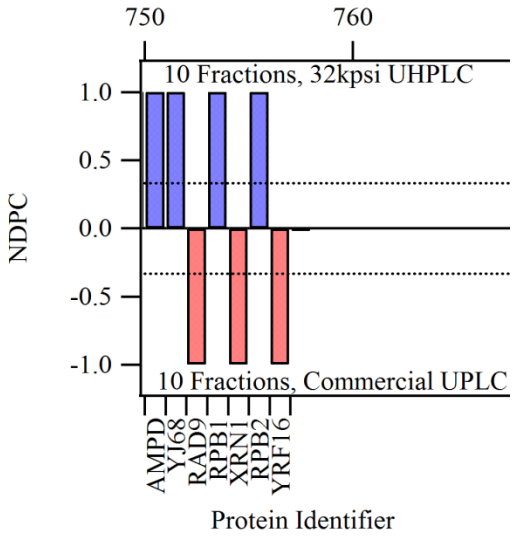

Appendix C.1. (continued)

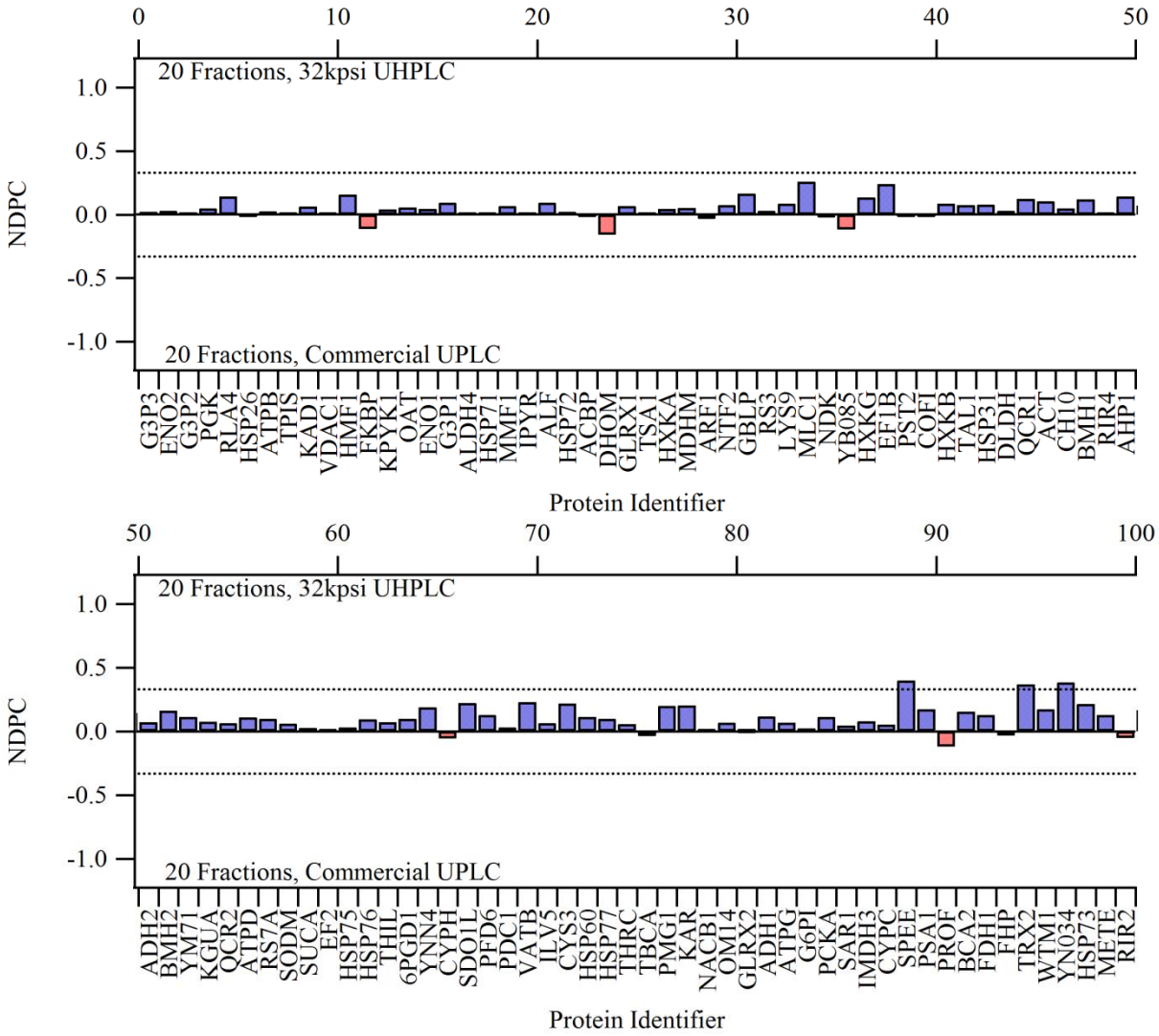

Appendix C.2. To compare the 20 fractions run on the modified system to the 20 fractions run on the standard UPLC, the NDPC is plotted with proteins with higher coverage on the left, and proteins with lower coverage on the right. If a protein was identified with higher sequence coverage when analyzed on the modified UHPLC, its NDPC value is positive (blue bars). The red bars signify higher coverage in the analysis on the standard UPLC. Differences in coverage were minimal for highly covered proteins. As protein coverage decreased, more proteins were identified with higher coverage from the analysis on the modified UHPLC. The dashed lines indicate a level of two-fold greater protein coverage. (This was a large graph and split into multiple parts.)

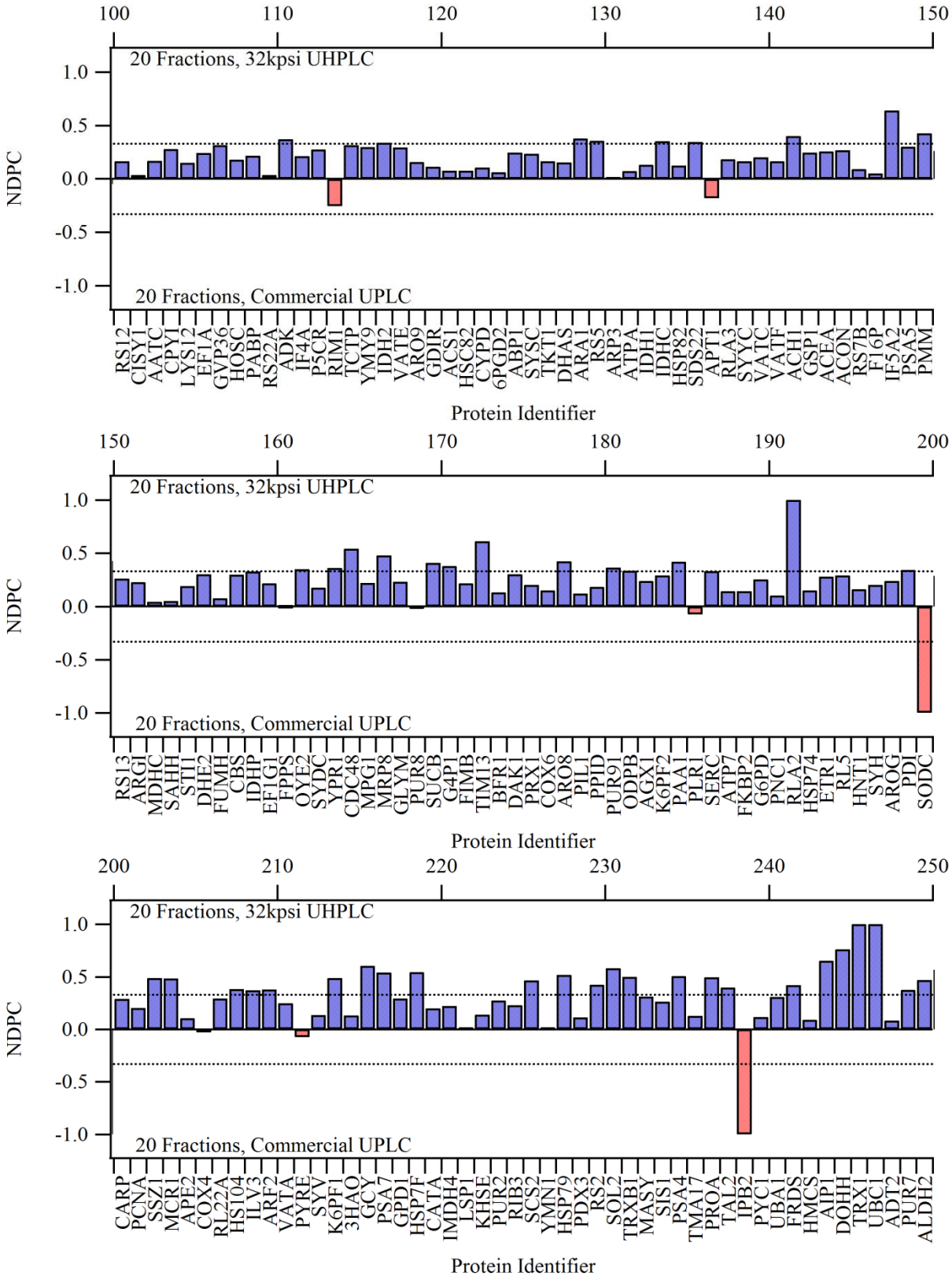

Appendix C.2. (Continued)

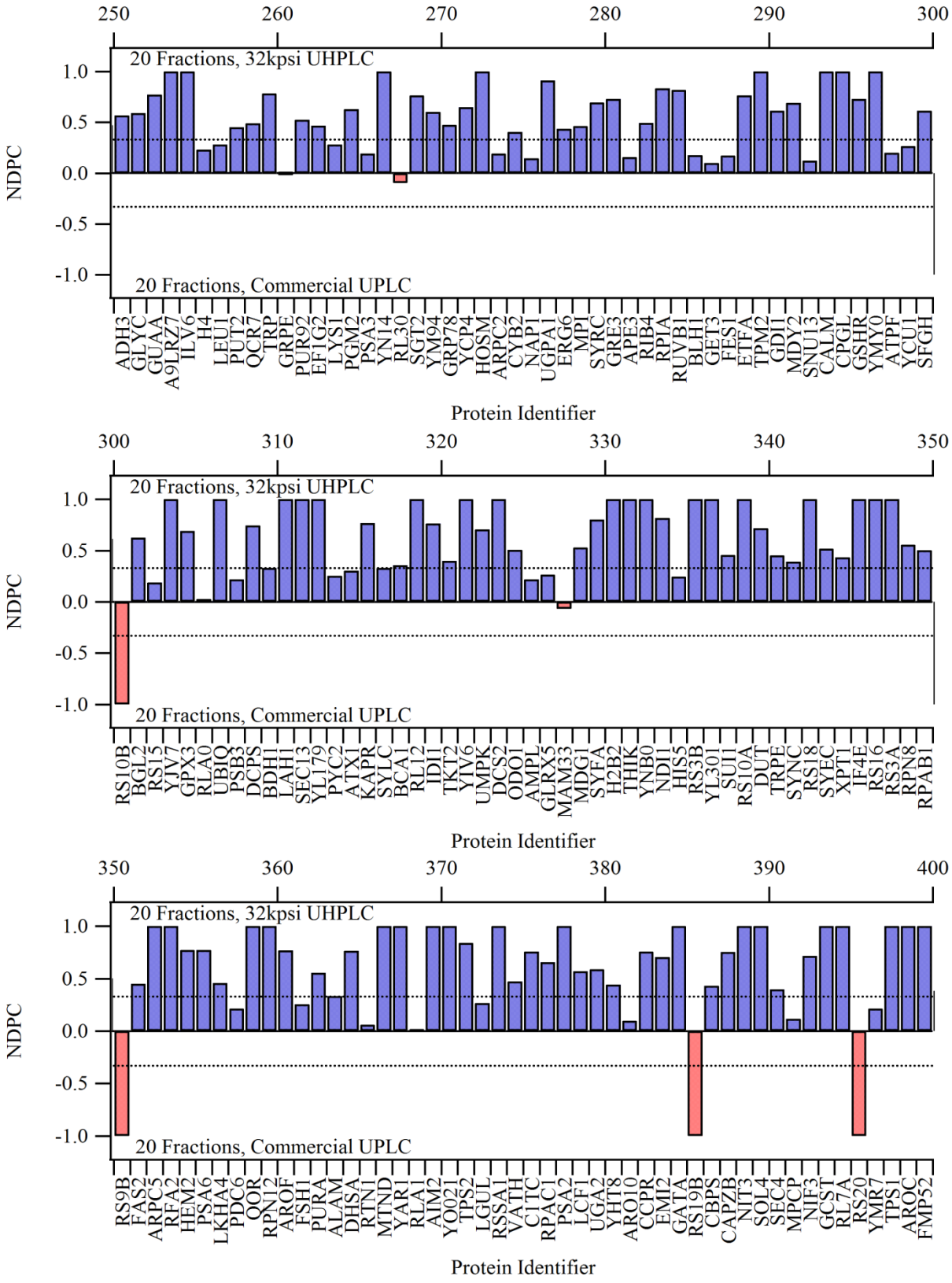

Appendix C.2. (Continued)

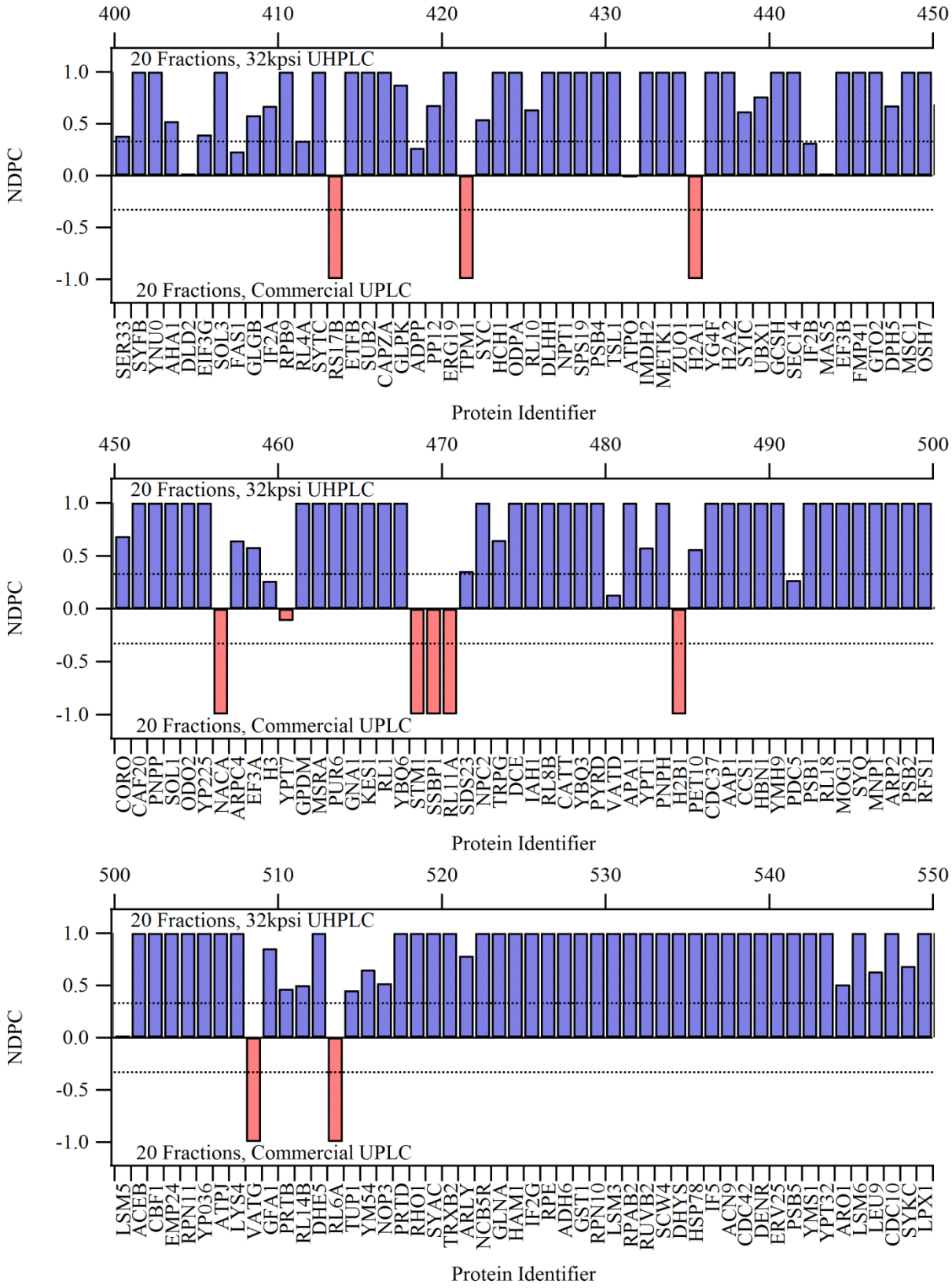

Appendix C.2. (Continued)

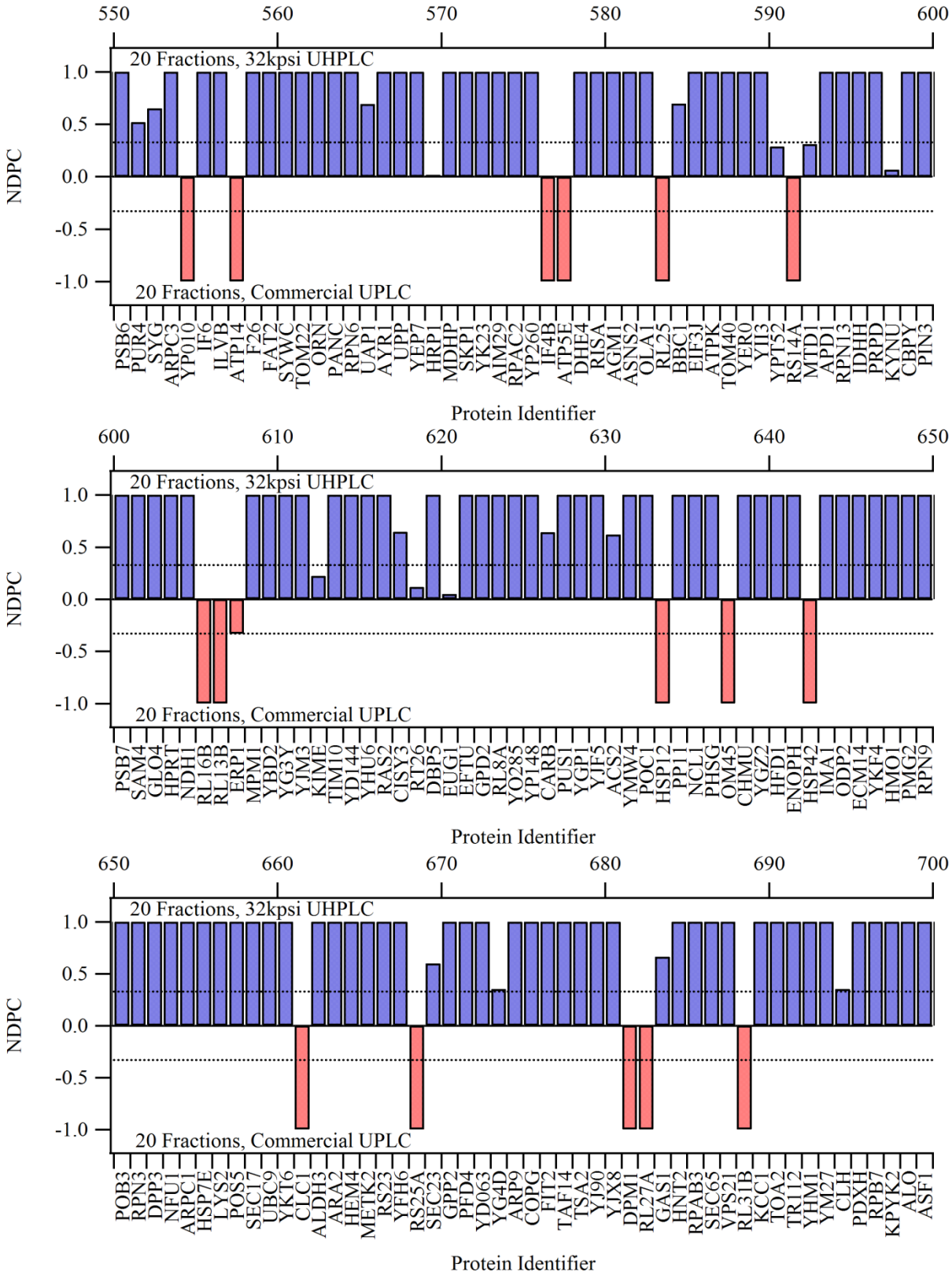

Appendix C.2. (Continued)

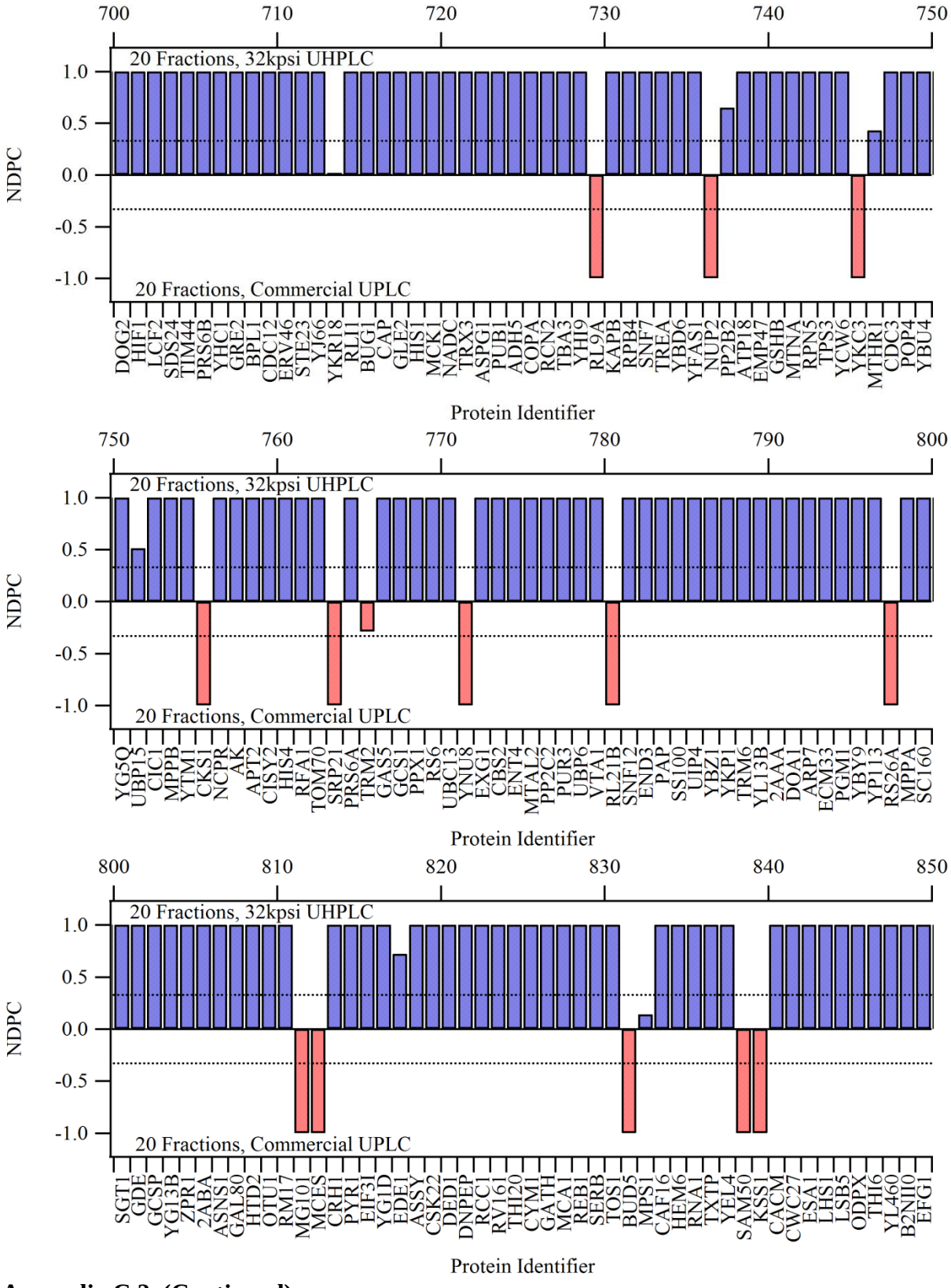

Appendix C.2. (Continued)

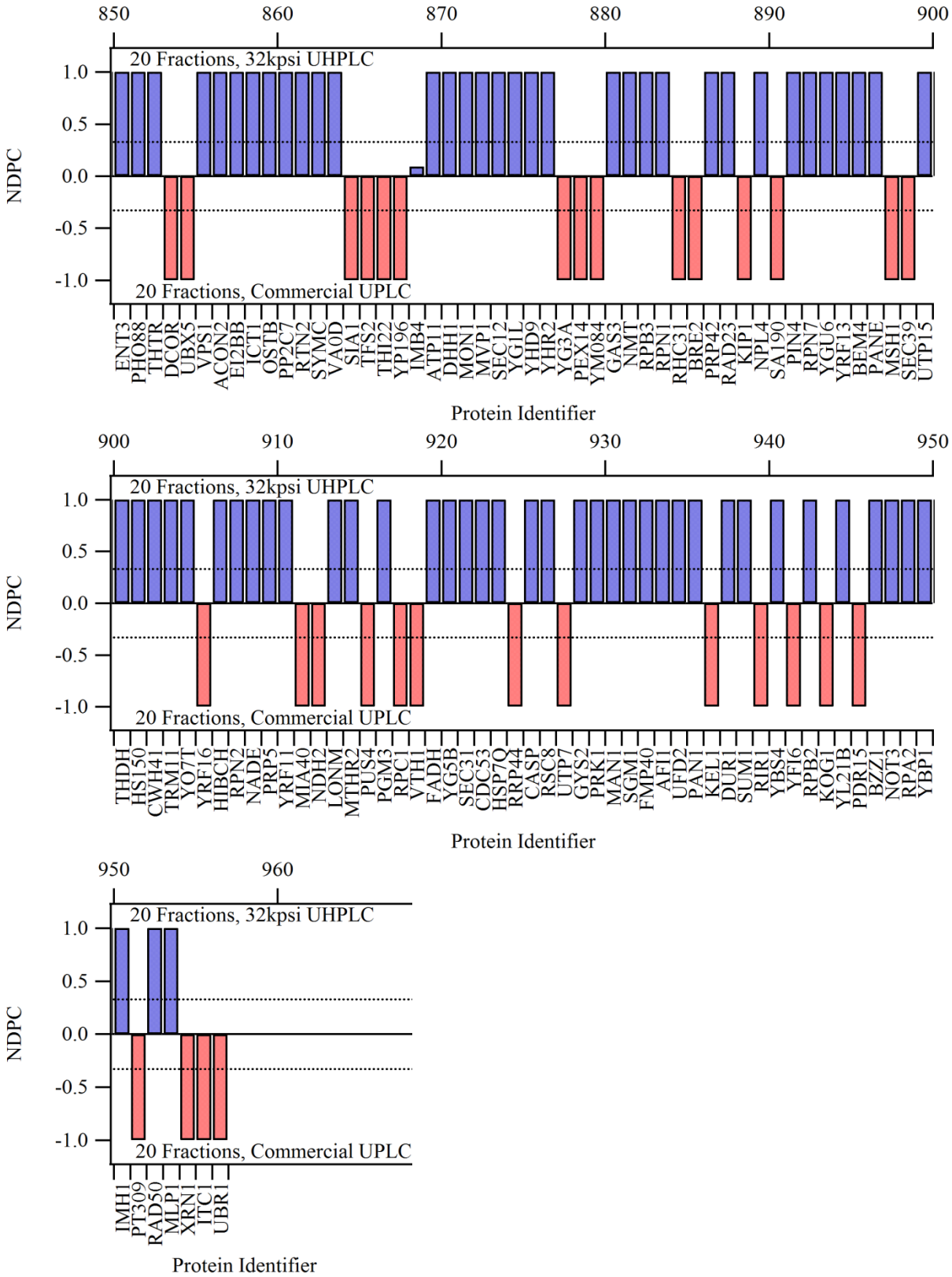

Appendix C.2. (Continued)